

University of Nottingham
UK | CHINA | MALAYSIA

Investigating the role of tumour-deposited extracellular matrix in medulloblastoma progression

James E. C. Johnson BSc

Thesis submitted to the University of Nottingham for the degree of Doctor of Philosophy

December 2022





Abstract

Introduction: The extracellular matrix (ECM) is a web of macromolecules which under normal conditions provides structural support to tissues, as well as regulating cellular differentiation, motility, migration and survival. In the past decade emerging evidence has demonstrated that tumours are able to extensively modify the composition and mechanical properties of their surrounding ECM. Tumour ECM has been shown to be pro- or anti-tumorigenic and can therefore sometimes be used to predict patient prognosis. Medulloblastoma is the most common malignant paediatric brain tumour, accounting for 10% of all cancer related deaths in children, and is the focus of this thesis. The role of tumour ECM in medulloblastoma progression is currently poorly understood. However, a recent study by our group identified ECM sub-types within the medulloblastoma molecular sub-groups, characterised by the expression of specific ECM proteins. One of these ECM sub-types was defined based on the expression of laminin in SHH and Group 4 medulloblastoma patients. High expression of laminin (*LAM*^{high}) was shown to be associated with more favourable overall survival in SHH medulloblastoma patients, whereas low laminin expression (*LAM*^{low}) was associated with poorer survival. The opposite trend was observed in Group 4 patients. Furthermore, it was shown that SHH medulloblastoma cell lines formed a sub-group specific laminin shell-like structure when grown in long-term 3D cell culture. This study aims to delineate the underlying molecular mechanisms which potentiate this pattern of survival conveyed by laminin.

Methods and Results: Differential gene expression analysis between *LAM*^{high} and *LAM*^{low} SHH and Group 4 medulloblastoma tumours in genomic patient data identified candidate 'laminin regulated genes'. However, initial validation of candidate genes by qRT-PCR analysis of SHH and Group 4 medulloblastoma cell lines grown in 2D and 3D hydrogel *in vitro* cell culture models, with and without laminin, was inconclusive.

CRISPR-Cas9 genetic editing technology was therefore utilised to create a stable laminin knockout in a SHH medulloblastoma cell line to study the effect of laminin *in vitro* more accurately. From this point onwards the focus of the study shifted towards just SHH medulloblastoma. Using this laminin knockout cell line, 3D cell culture assays were employed to assess the role of laminin in key aspects of tumour progression: migration, invasion, apoptosis evasion and therapy resistance. The findings of these assays demonstrated that laminin promotes cell migration and maintains sensitivity to apoptosis and the standard of care therapeutic vincristine in SHH medulloblastoma cells. To assess unbiased global changes in protein expression caused by laminin in SHH medulloblastoma cells, liquid chromatography-tandem mass spectrometry (LC-MS/MS) proteomic analysis was conducted on the laminin knockout SHH medulloblastoma cell line. This identified that estrogen signalling was upregulated by laminin, whereas collagen-integrin signalling was downregulated. Consultation of the literature confirmed that these pathways could underpin laminin's role in migration and maintaining apoptotic and therapeutic sensitivity, respectively.

In support of the above, integrated bioinformatics analysis of SHH medulloblastoma genomic and proteomic patient data, and subsequent immunohistochemical validation in long-term 3D cell culture models, revealed that SHH medulloblastoma cells form a multicomponent ECM shell-like structure, the components of which were all associated with a more favourable patient prognosis.

Conclusions: This study demonstrated the importance laminin in cellular migration, as well as maintaining sensitivity to apoptosis and vincristine in SHH medulloblastoma, and that these phenotypes may be mediated by the up and down regulation of estrogen and collagen-integrin signalling, respectively. Our investigations also revealed a multicomponent ECM shell-like structure in SHH medulloblastoma, the components of which could represent potential biomarkers of more favourable overall survival in patients.

COVID-19 Impact Statement

As a consequence of the COVID-19 pandemic I lost a total of 6 months in the laboratory to conduct the research for this thesis. Upon return to the laboratory, access to equipment, consumables and reagents, as well as bench space, was extremely limited due to strict social distancing measures. In addition to this, our group had only moved into the Biodiscovery Institute in January 2020, just before the first national lockdown, meaning it was already very difficult to work smoothly as the building had not been properly set up yet. Consequently, I was only able to work at roughly half capacity for another 10 months. In addition, I lost a further 3 months during the move from the Queen's Medical Centre into the Biodiscovery Institute from October-December 2019. I also spent 6 months completing laboratory rotations at the start of my PhD, as well as 3 months on my Professional Internship for PhD Students. This has meant that out of my 4 funded years I have only been able to spend 2.5 years in the laboratory, a large proportion of which was significantly hampered by COVID-19 safety measures. Although I was able to secure a 3 month extension to my PhD, the above context is important to understand some of the decisions and compromises made throughout this thesis.

Acknowledgements

This PhD is the hardest task I have ever undertaken and I quite simply would not have been able to do it without the help and support of the wonderful people in my life.

I would firstly like to thank my inspiring supervisors. Beth, your unwavering kindness, guidance and reassurance has provided me with the motivation and self-belief I have needed to get this far. Franziska, thank you for your saint-like patience and spending so much time helping me develop as a scientist.

I have been incredibly privileged to work with such amazing people over the last 4 years. To Pippa, Louisa, Michaela, Hannah, Louise, Macha, Sophie, Susie, Phoebe and Harry, thank you for being the best colleagues and friends I could have asked for. I am incredibly grateful for your constant support. I would also like to thank the rest of the CBTRC, it has been a highlight of my PhD to be a part of this amazing organisation.

To my friends Danny, Jake, Sam, Jo and Alex. You have been there for me since undergrad and I cannot imagine having done this without you.

Finally, I would like to thank my loved ones. Fliss, thank you so much for being my rock. I will forever be grateful for your love, kindness and friendship. It has meant more to me than you could ever know. To my little sisters Sophie and Catherine, thank you for the endless supply of laughs and reality checks. Lastly, Mum and Dad, I dedicate this thesis to you. I would not be here without your limitless love, support and encouragement. You are both an inspiration to me and I hope I have made you proud.

I would also like to thank the BBSRC Doctoral Training Partnership for funding this PhD.

Table of Contents

Abstract ..... **i**
COVID-19 Impact Statement ..... **iii**
Acknowledgements ..... **iv**
Table of Contents ..... **v**
List of Figures ..... **xii**
List of Tables ..... **xx**
List of Common Abbreviations ..... **xxii**

Chapter 1: Introduction **1**
1.1 Medulloblastoma overview 2
1.1.1 Epidemiology 2
1.1.2 Clinical presentation and diagnosis 2
1.1.3 Metastasis 3
1.1.4 Disease staging 4
1.1.5 Standard medulloblastoma treatment 5
1.2 Histology 5
1.2.1 Classical 6
1.2.2 Large cell/Anaplastic 6
1.2.3 Medulloblastoma with extensive nodularity 7
1.2.4 Nodular/desmoplastic 7
1.3 Medulloblastoma molecular sub-groups 8
1.3.1 WNT sub-group 10
1.3.2 SHH sub-group 11
1.3.3 Group 3 13
1.3.4 Group 4 14
1.4 Intratumoral heterogeneity within the molecular sub-groups 16
1.4.1 WNT sub-types 17
1.4.2 SHH sub-types 17
1.4.3 Group 3 sub-types 17
1.4.4 Group 4 sub-types 17
1.5 Clinical risk stratification 18
1.5.1 Low risk 18
1.5.2 Standard risk 19
1.5.3 High risk 19

1.5.4 Very high risk 19
1.6 Sub-group based therapies 19
1.6.1 WNT therapies 20
1.6.2 SHH therapies 20
1.6.3 Group 3/4 therapies 21
1.7 The tumour microenvironment 21
1.7.1 The brain extracellular matrix 22
1.7.2 The extracellular matrix and cancer 24
1.7.3 The extracellular matrix of medulloblastoma 29
1.8 Hypothesis and aims 33

Chapter 2: Materials and Methods 34
2.1 Analysis of publicly available genomic patient datasets 35
2.1.1 Analysing gene expression in groups 35
2.1.2 Gene expression-based survival analysis 35
2.1.3 Differential gene expression analysis 36
2.2 Differential gene expression analysis of mRNA sequencing data 36
2.3 Gene expression analysis of scRNAseq data 37
2.4 Identifying overlapping genes across multiple datasets 37
2.5 Standard tissue culture methods 38
2.5.1 Cell maintenance 38
2.5.2 Maintaining adherent cell lines 38
2.5.3 Maintaining suspension cell lines 38
2.5.4 Tissue culture media 41
2.5.5 Cell counting 41
2.5.6 Preparation of cell line stocks and cell storage 42
2.5.7 Recovering cell lines from frozen stocks 42
2.5.8 Preparation of cell pellets and supernatants for molecular analysis 43
2.5.9 Mycoplasma testing 43
2.6 Generation and validation of CRISPR-Cas9 knockout cell lines 44
2.6.1 Co-transfection of DAOY and ONS-76 medulloblastoma cell lines with Cas9 nuclease-EGFP mRNA and synthetic sgRNAs 44
2.6.2 Fluorescence-activated cell sorting (FACS) of transfected cell lines 45
2.6.3 DNA mismatch detection assay 46
2.6.4 Sanger Sequencing of *LAMA1* and *LAMA2* single guide RNA (sgRNA) target sites and INDEL characterisation 48
2.6.4.1 Sanger Sequencing 48

2.6.4.2 INDEL detection analysis of Sanger Sequencing data 49
2.6.5 Translating Sanger Sequencing data into an amino acid sequence and alignment to wild-type sequences 49
2.7 2D tissue culture assays 50
2.7.1 2D laminin assays 50
2.8 Transwell® migration and invasion assays 51
2.8.1 Migration assays 51
2.8.2 Invasion assays 51
2.8.3 Preparation of a standard curve 52
2.8.4 Quantifying the number of migrated and invaded cells 52
2.9 HyStem™ hyaluronan based hydrogel cell culture 52
2.9.1 Preparation of HyStem™ hydrogels 53
2.10 Spheroid culture 54
2.10.1 Neurosphere media 55
2.10.2 Spheroid generation and maintenance 55
2.10.3 Assessing spheroid dimensions 55
2.10.4 2D and 3D Spheroid CellTiter-Glo® cell viability assay 56
2.10.5 Spheroid-HyStem™ hydrogel model 56
2.10.6 Spheroid-HyStem migration assay 57
2.11 Apoptosis assays 58
2.11.1 2D and 3D Spheroid Caspase-Glo® 3/7 Apoptosis Assay 58
2.11.2 2D and 3D Spheroid CellEvent™ Caspase-3/7 Green Detection Apoptosis Assay 58
2.12 Drug Treatments 60
2.12.1 Drugs used in this study 60
2.12.2 Drug response assays and IC_{50} calculation 60
2.13 Molecular biology 61
2.13.1 RNA isolation 61
2.13.2 DNA isolation 61
2.13.3 Measuring the concentration and purity of RNA and DNA 61
2.13.4 Complementary DNA (cDNA) synthesis 62
2.13.5 Primer design 63
2.13.6 Temperature gradient optimisation of primer pairs 63
2.13.7 Agarose gel electrophoresis of DNA (with ethidium bromide) 64
2.13.8 qRT-PCR gene expression analysis 64
2.13.9 Immunoblotting 66
2.13.9.1 Cell lysis and protein isolation 66

2.13.9.2 Protein quantification by Braford assay and sample preparation 67
2.13.9.3 Preparation of SDS gels 67
2.13.9.4 SDS-PAGE 68
2.13.9.5 Protein transfer 68
2.13.9.6 Western blotting 71
2.13.9.7 Quantifying protein expression by densitometry analysis 72
2.13.10 Gelatin zymography 74
2.13.10.1 Preparation of cell line supernatants 74
2.13.10.2 Preparation of gelatin SDS gels 74
2.13.10.3 Electrophoresis of cell culture supernatants 75
2.13.10.4 Renaturing and developing the zymogram 75
2.13.10.5 Analysing the level of MMP-2/-9 secretion by densitometry analysis . 76
2.13.11 Immunohistochemistry 78
2.13.12 Immunofluorescence 80
2.14 Proteomic analysis of cell lysates by LC-MS/MS 82
2.14.1 Sample preparation and LC-MS/MS analysis 82
2.14.2 Identification of differentially expressed proteins from proteomics data 84
2.14.3 STRING analysis of differentially expressed proteins 86
2.14.4 KEGG pathway mapping analysis of differentially expressed proteins 86

Chapter 3: Identification and preliminary validation of candidate laminin regulated genes in SHH and Group 4 medulloblastoma 87
3.1 Introduction 88
3.2 Analysis of *LAMA1* and *LAMA2* expression across the medulloblastoma sub-groups 89
3.3 Identification of candidate ‘laminin regulated genes’ in SHH and Group 4 medulloblastoma 92
3.3.1 Differential gene expression analysis of a genomic medulloblastoma patient dataset (Cavalli) and a mRNA sequencing dataset of SHH medulloblastoma patient derived cell lines 94
3.3.2 Selection of candidate ‘laminin regulated genes’ for further investigation ... 96
3.4 Assessment of *LAMA1*/LAMA1 and *LAMA2*/LAMA2 expression in SHH and Group 4 medulloblastoma patient derived cell lines 104
3.5 Validating candidate ‘laminin regulated genes’ using 2D and 3D cell culture assays 109
3.5.1 Validation of candidate ‘laminin regulated genes’ using a 2D cell culture assay 110

3.5.2 Validation of candidate ‘laminin regulated genes’ using a 3D hyaluronan hydrogel cell culture assay 119
3.6 Summary points 128

Chapter 4: Creating CRISPR-Cas9 LAMA1 and LAMA2 knockouts in DAOY and ONS-76 SHH medulloblastoma cell lines 130
4.1 Introduction 131
4.2 CRISPR-Cas9 knockout workflow 133
4.3 Co-transfection and fluorescence-activated cell sorting (FACS) of DAOY and ONS-76 SHH medulloblastoma cell lines 135
4.4 DNA mismatch detection assays of *LAMA1* and *LAMA2* in total co-transfected cell populations and clonal cell lines 138
4.4.1 DNA mismatch detection assays of *LAMA1* and *LAMA2* in total co-transfected cell populations 140
4.4.2 DNA mismatch detection assays of *LAMA1* and *LAMA2* in clonal cell lines 141
4.5 Western blotting of LAMA1 and LAMA2 in DAOY KO and ONS-76 KO cell lines 144
4.6 Characterisation of INDELs in *LAMA1* and *LAMA2* by Sanger Sequencing 148
4.7 Validating that the reduction in LAMA1 and LAMA2 expression is retained in DAOY KO and ONS-76 KO cell lines 153
4.8 Analysing the LAMA1 amino acid sequence in the DAOY KO cell line 10F1C 156
4.9 Assessing differences in phenotype and viability between the DAOY non-targeting and LAMA1 knockout cell lines 158
4.10 Summary points 160

Chapter 5: Investigating the role of LAMA1 in SHH medulloblastoma progression 162
5.1 Introduction 163
5.2 Validating the formation of a laminin-111/211 shell-like structure by SHH medulloblastoma cell lines grown in a 3D spheroid model 165
5.3 Identifying additional components of the SHH medulloblastoma laminin-111/211 shell-like structure 167
5.4 Growing the DAOY LAM$^{-/-}$ cell line in a 3D spheroid model 175
5.5 Assessing the expression of ‘laminin regulated genes’ in the DAOY LAM$^{-/-}$ cell line in 2D and 3D spheroid culture 181

5.5.1 Assessing the secretion of MMP-2 and MMP-9 in the DAOY LAM$^{-/-}$ cell line in 2D and 3D spheroid culture 187
5.6 Investigating the role of LAMA1 in the migration and invasion of SHH medulloblastoma 189
5.6.1 Assessing migration of the DAOY LAM$^{-/-}$ cell line using a spheroid-hydrogel migration assay 189
5.6.2 Assessing migration and invasion of the DAOY LAM$^{-/-}$ cell line using Transwell™ assays..... 192
5.7 Investigating the role of LAMA1 in apoptosis in SHH medulloblastoma 194
5.7.1 Assessing apoptosis in the DAOY NT and DAOY LAM$^{-/-}$ cell lines 194
5.7.2 Assessing the sensitivity of the DAOY NT and DAOY LAM$^{-/-}$ cell lines to the BCL-2 small-molecule inhibitor ABT-737 199
5.8 Assessing the sensitivity of the DAOY NT and DAOY LAM$^{-/-}$ cell lines to Vincristine and Cisplatin 206
5.9 Summary points..... 212

Chapter 6: Proteomic analysis of DAOY NT and DAOY LAM$^{-/-}$ cell lines grown in 2D and spheroid culture..... 214
6.1 Introduction..... 215
6.2 Identifying LAMA1 regulated proteins in SHH medulloblastoma 218
6.3 STRING Protein-Protein interaction and KEGG pathway mapping analysis of LAMA1 regulated proteins 223
6.3.1 Analysis of proteins upregulated by LAMA1 in SHH medulloblastoma cells in 2D culture 223
6.3.2 Analysis of proteins downregulated by LAMA1 in SHH medulloblastoma cells in 2D culture 231
6.3.3 Analysis of proteins upregulated by LAMA1 in SHH medulloblastoma cells in spheroid culture 235
6.3.4 Analysis of proteins downregulated by LAMA1 in SHH medulloblastoma cells in spheroid culture 237
6.4 Identifying overlapping LAMA1 regulated proteins between 2D and spheroid culture 245
6.5 Summary points..... 250

Chapter 7: Discussion..... 252
7.1 Introduction..... 253

7.2 The composition and prognostic significance of the SHH medulloblastoma ECM shell 254
7.2.1 SHH medulloblastoma cell lines form a multicomponent ECM shell-like structure in long-term 3D culture 254
7.2.2 Expression of the SHH medulloblastoma ECM shell components correlate with more favourable patient survival 257
7.3 The role of LAMA1 in the migration and invasion of SHH medulloblastoma .. 258
7.3.1 LAMA1 has a role cellular migration in SHH medulloblastoma 259
7.3.2 The influence of LAMA1 in the invasion of SHH medulloblastoma is unclear 260
7.4 LAMA1 has conflicting roles in apoptosis between 2D and 3D spheroid-hydrogel models 263
7.5 LAMA1 increases vincristine sensitivity in SHH medulloblastoma in a 3D spheroid-hydrogel model 265
7.6 Proteomics analysis of DAOY NT and DAOY LAM$^{-/-}$ cell lines identifies pathways that may underpin LAMA1-mediated phenotypes in SHH medulloblastoma 267
7.6.1 Estrogen signalling as a mechanism of LAMA1-mediated BCL-2 and CD44 upregulation in SHH medulloblastoma 268
7.6.2 LAMA1-mediated decrease in COL1A1, COL6A1, COL6A3 and ITGB1 expression as a mechanism for increased apoptosis and drug sensitivity in SHH medulloblastoma 271
7.7 Concluding statement 278
7.8 Future work 278

References 280

Appendix 316
9.1 Appendix Figure 1 317
9.2 Appendix Figure 2 318
9.3 Appendix Figure 3 319
9.4 Appendix Figure 4 320
9.5 Appendix Figure 5 321
9.6 Appendix Figure 6 322
9.7 Appendix Figure 7 323

PhD project outputs 324

List of Figures

Figure 1.1 Illustration of leptomeningeal metastasis via the cerebrospinal fluid.. 4

Figure 1.2 The histological variants of medulloblastoma. 8

Figure 1.3 The medulloblastoma molecular sub-groups.. 9

Figure 1.4 Diagram of mutations within the WNT signalling pathway exhibited by WNT medulloblastoma patients.. 11

Figure 1.5 Diagram of mutations within the SHH signalling pathway exhibited by SHH medulloblastoma patients. 13

Figure 1.6 Intratumoral heterogeneity within the medulloblastoma molecular sub-groups.. 16

Figure 1.7 Schematic of the structure of lectican family of chondroitin sulphate proteoglycans and their interactions which hyaluronan and tenascins, in the context of the brain extracellular matrix. 24

Figure 1.8 Intracellular pathways activated in cancer by the interaction of collagen, laminin and fibronectin with cell surface ECM receptors.. 26

Figure 1.9 Structure of laminin and collagen. 28

Figure 1.10 Components of the medulloblastoma extracellular matrix signature. 30

Figure 1.11 High LAMA1/LAMA2 expression significantly correlates with overall patient survival in SHH (A) and Group 4 (B) medulloblastoma patients.. 32

Figure 2.1 Diagram illustrating the components and structure of HyStem® hydrogel compared with native extracellular matrix.. 53

Figure 2.2 Illustration of Log2 transformation and two-step normalisation of proteomics data used in in this study.. 85

Figure 3.1 LAMA1 and LAMA2 are expressed in normal cerebellum (Roth dataset) and in all 4 medulloblastoma sub-groups (Pfister and Cavalli datasets). 91

Figure 3.2 Analysis workflow for identifying ‘laminin regulated genes’ from a medulloblastoma genomic patient dataset and an mRNA sequencing dataset of patient derived SHH medulloblastoma cell lines. 93
Figure 3.3 The number of overlapping candidate ‘laminin regulated genes’ (Table 3.1) between SHH patients in the Cavalli dataset and SHH medulloblastoma cell lines in the mRNA sequencing dataset (A), as well as between SHH and Group 4 patients in the Cavalli dataset (B). 97
Figure 3.4 Differential gene expression analysis between two ECM sub-types in SHH and Group 4 medulloblastoma patient tumours, defined in the Cavalli dataset by a previous study by our group: LAMA1 and LAMA2 $(LAM)^{high}$ / Vitronectin $(VTN)^{low}$ and LAM^{low}/VTN^{low} (Linke et al., 2020; Cavalli et al. 2019). 101
Figure 3.5 Differential gene expression analysis, of mRNA sequencing data, between SHH medulloblastoma cell lines (DAOY and ONS-76) grown on top of hyaluronan hydrogels with and without laminin-111. 102
Figure 3.6 Brightfield images (4 X magnification) of the DAOY, ONS-76, CHLA-01-MED and CHLA-01-R-MED cell lines grown under their normal growth conditions.. 105
Figure 3.7 LAMA1/LAMA1 and LAMA2/LAMA2 are expressed in both SHH (DAOY and ONS-76) and Group 4 (CHLA-01 and CHLA-01-R) medulloblastoma cell lines. 108
Figure 3.8 Schematic of the 2D and 3D cell culture assays used to validate ‘laminin regulated genes’ in SHH (DAOY and ONS-76) and Group 4 (CHLA-01 and CHLA-01-R) medulloblastoma cell lines. 111
Figure 3.9 Recurrent Group 4 medulloblastoma cell line (CHLA-01-R) exhibits an adherence phenotype to laminin-111 that is absent in the primary matched pair cell line (CHLA-01)..... 112
Figure 3.10 Laminin-111 significantly alters the expression of TPPP3, NFKBIZ, MMP-2, ITGA5, RPSA and CD44 in some SHH and Group 4 medulloblastoma cell lines in a 2D cell culture assay. 116

Figure 3.11 Laminin-111 does not affect Pro-MMP-2 or MMP-9 secretion in SHH and Group 4 medulloblastoma cell lines in a 2D cell culture assay. 118
Figure 3.12 Laminin-111 does not confer an observable phenotypic change in SHH and Group 4 medulloblastoma cell lines grown in hyaluronan hydrogels. 120
Figure 3.13 Laminin-111 alters the expression of TPPP3, NFKBIZ, MMP-2 and CD44 in some SHH and Group 4 medulloblastoma cell lines in a 3D cell culture assay. . 123
Figure 3.14 Laminin-111 increases Pro-MMP-2 and MMP-9 secretion in SHH, but not Group 4 medulloblastoma cell lines in a 3D cell culture assay. 127
Figure 4.1 Workflow of creating and validating CRISPR-Cas9 knockouts of LAMA1 and LAMA2 in DAOY and ONS-76 SHH medulloblastoma cell lines..... 134
Figure 4.2 FACS analysis of DAOY and ONS-76 cells co-transfected with Cas9 nuclease-EGFP mRNA and synthetic sgRNAs identifies EGFP expression in both cell lines. 137
Figure 4.3 Diagrammatic explanation of a DNA mismatch detection assay. 139
Figure 4.4 Agarose gel electrophoresis of DNA mismatch detection assays indicates the presence of INDELs in LAMA1 and LAMA2 in EGFP positive DAOY and ONS-76 cells co-transfected with Cas9 nuclease-EGFP mRNA and LAMA1 and LAMA2 sgRNAs.. 141
Figure 4.5 Agarose gel electrophoresis of DNA mismatch detection assays indicates the presence of INDELs in LAMA1 and LAMA2 in nearly all of the clonal cell lines derived from DAOY and ONS-76 cells co-transfected with Cas9 nuclease-EGFP mRNA and LAMA1 and LAMA2 sgRNAs. 143
Figure 4.6 Western blotting of the 11 clonal cell lines, derived from DAOY cells co-transfected with Cas9 nuclease-EGFP mRNA and LAMA1 and LAMA2 sgRNAs, reveals a reduction in the expression of LAMA1 and LAMA2 relative to a non-targeting control cell line. 145
Figure 4.7 Western blotting of the 14 clonal cell lines, derived from ONS-76 cells co-transfected with Cas9 nuclease-EGFP mRNA and LAMA1 and LAMA2 sgRNAs,

reveals a reduction in the expression of LAMA1 and LAMA2 relative to a non-targeting control cell line..... 147
Figure 4.8 Workflow of LAMA1 and LAMA2 INDEL characterisation in DAOY KO and ONS-76 KO cell lines by Sanger Sequencing. 149
Figure 4.9 Western blotting of clonal cell lines, derived from DAOY and ONS-76 cells co-transfected with Cas9 nuclease-EGFP mRNA and LAMA1 and LAMA2 sgRNAs, reveals that LAMA1 and LAMA2 expression is restored to the same level as non-targeting control cell lines after 2 and 5 passages. 155
Figure 4.10 LAMA1 is truncated in the DAOY KO cell line 10F1C as a result of the identical biallelic insertion of a thymine nucleotide in the LAMA1 sgRNA target site. 157
Figure 4.11 Brightfield images (4 X magnification) demonstrate that the DAOY LAMA1 knockout cell line (10F1C) exhibits a changed phenotype compared to the DAOY non-targeting cell line. 158
Figure 4.12 The viability of the DAOY cell line is not significantly changed by the knockout of LAMA1 in 2D culture..... 159
Figure 5.1 Immunofluorescent (IF) and immunohistochemical (IHC) staining of day 1, 7, 14 and 21 DAOY and ONS-76 spheroids for laminin-111/211 reveals shell-like structure. 166
Figure 5.2 Workflow of identifying candidate ECM proteins for validation as additional components of the SHH medulloblastoma laminin-111/211 shell-like structure previously identified by our group (Linke *et al.*)..... 168
Figure 5.3 Survival analysis of 8 medulloblastoma ECM components reveals a consistent pattern of favourable overall survival correlated with high gene expression in SHH medulloblastoma patients..... 170
Figure 5.4 scRNAseq and 3D OrbiSIMS analysis of ONS-76 cells grown in a hyaluronan hydrogel, identifies COL1A1, COL6A1 and LUM for validation as additional

components of the laminin-111/211 shell structure observed in SHH medulloblastoma cell lines when grown in 3D culture..... 172
Figure 5.5 Immunofluorescent (IF) and immunohistochemical (IHC) staining of day 1 (IF) and 21 (IHC) DAOY and ONS-76 spheroids for COL1A1, COL6A1 and lumican, validates that they are part of the laminin-111/211 shell-like structure previously observed in SHH medulloblastoma cell lines grown in 3D cell culture models. 175
Figure 5.6 Growth of the DAOY LAM$^{-/-}$ cell line in a 3D spheroid model indicates that LAMA1 is essential to the formation of independent 3D cell structures in SHH medulloblastoma. 178
Figure 5.7 Growth of the DAOY LAM$^{-/-}$ cell line in a hybrid 3D spheroid-hydrogel model indicates that SHH medulloblastoma cells are able to grow as a 3D structure without LAMA1, when supported by an ECM substitute. 180
Figure 5.8 qRT-PCR gene expression analysis of the of 'laminin regulated genes' indicates that the gene expression of NFKBIZ, MMP-2, ITGAV and CLU are increased in the in the DAOY LAM$^{-/-}$ cell line in 2D and 3D spheroid culture. 183
Figure 5.9 Western blotting analysis demonstrates a reduction in CD44 and BCL-2 expression in the DAOY LAM$^{-/-}$ cell line in 2D culture and spheroids cultured for 1 day. 186
Figure 5.10 Gelatin zymography demonstrates an increase in Pro-MMP-9 and active MMP-2 secretion in DAOY LAM$^{-/-}$ cells in 2D culture. 188
Figure 5.11 A spheroid-hydrogel migration assay suggests that LAMA1 increases the migration of SHH medulloblastoma cells.. 191
Figure 5.12 Transwell™ migration and invasion assays suggest that LAMA1 increases the migration of SHH medulloblastoma cells, but not invasion. 193
Figure 5.13 Luminescent caspase-3/7 assay indicates that apoptosis is only significantly increased in the DAOY LAM$^{-/-}$ cell line compared to the DAOY NT cell line in spheroid culture. 196

Figure 5.14 Fluorescent caspase-3/7 assay indicates that apoptosis is not significantly changed between the DAOY NT and DAOY LAM$^{-/-}$ cell lines in 2D culture.. 197
Figure 5.15 Fluorescent caspase-3/7 assay indicates that apoptosis is significantly increased in the DAOY LAM$^{-/-}$ cell line compared to the DAOY NT cell line in spheroid culture. 198
Figure 5.16 The DAOY LAM$^{-/-}$ cell line is more sensitive to ABT-737 than the DAOT NT cell line in 2D culture..... 200
Figure 5.17 Apoptosis is increased in DAOY LAM$^{-/-}$ cells treated with ABT-737, compared to the DAOY NT cell line. 202
Figure 5.18 Illustration of the hybrid spheroid-hydrogel drug assay used in this study. 203
Figure 5.19 Hybrid spheroid-hydrogel drug assays demonstrate that DAOY NT spheroids are more sensitive to ABT-737 than DAOY LAM$^{-/-}$ spheroids..... 205
Figure 5.20 Vincristine and cisplatin drug response assays indicate that LAMA1 does not confer a significant difference in sensitivity to either drug. 207
Figure 5.21 Hybrid spheroid-hydrogel drug assays demonstrate that DAOY NT spheroids are more sensitive to vincristine than DAOY LAM$^{-/-}$ spheroids.. 209
Figure 5.22 Hybrid spheroid-hydrogel drug assays demonstrate that there is no difference in cisplatin sensitivity between the DAOY NT and DAOY LAM$^{-/-}$ spheroids 211
Figure 6.1 Illustration of the LC-MS/MS proteomics workflow used in this study.... 217
Figure 6.2 Illustration of the methods used to identify differentially expressed proteins in the DAOY LAM$^{-/-}$ cell line grown in 2D and spheroid culture..... 219
Figure 6.3 Differential protein expression analysis between the DAOY NT and DAOY LAM$^{-/-}$ cell lines grow in 2D and 3D spheroid culture 222
Figure 6.4 STRING Protein-Protein Interaction and KEGG pathway mapping analysis of proteins identified to be upregulated by LAMA1 in 2D culture, identify a large network of protein interaction, as well as 28 associated KEGG pathways, respectively 225

Figure 6.5 KEGG pathway mapping analysis of proteins upregulated by LAMA1 in 2D culture identifies the proteasome as an associated pathway. 228
Figure 6.6 KEGG pathway mapping analysis of proteins upregulated by LAMA1 in 2D culture, identifies estrogen signalling as an associated pathway..... 230
Figure 6.7 STRING Protein-Protein Interaction and KEGG pathway mapping analysis of proteins identified to be downregulated by LAMA1 in 2D culture, identify two interaction network of proteins, as well as 4 associated KEGG pathways, respectively. 232
Figure 6.8 KEGG pathway mapping analysis of proteins downregulated by LAMA1 in SHH medulloblastoma cells in 2D culture, identified proteoglycans in cancer (specifically collagen-integrin interaction) as an associated pathway 234
Figure 6.9 STRING Protein-Protein Interaction analysis of proteins identified to be upregulated by LAMA1 in day 1 spheroid culture, identifies one large interaction network of proteins 236
Figure 6.10 STRING Protein-Protein Interaction and KEGG pathway mapping analysis of proteins identified to be downregulated by LAMA1 in day 1 spheroid culture, identify one large interaction network of proteins, as well as 13 associated KEGG pathways, respectively 238
Figure 6.11 KEGG pathway mapping analysis of proteins downregulated by LAMA1 in spheroid culture, identifies PI3K-AKT signalling as an associated KEGG pathway 240
Figure 6.12 KEGG pathway mapping analysis of proteins downregulated by LAMA1 in spheroid culture, identifies focal adhesion signalling as an associated KEGG pathway 242
Figure 6.13 KEGG pathway mapping analysis of proteins downregulated by LAMA1 in spheroid culture, identifies protein processing in the endoplasmic reticulum as an associated KEGG pathway..... 244
Figure 6.14 LAMA1 upregulates 8 proteins and downregulates 3 in SHH medulloblastoma cells in both 2D and spheroid culture 247

Figure 6.15 Western blotting analysis of COL1A1 and COL6A1 protein expression in the DAOY NT and DAOY LAM$^{-/-}$ cell lines, suggest that they are regulated by LAMA1 in SHH medulloblastoma. 249
Figure 7.1 Hypothesised ECM shell-like structure comprised of laminin-111/211, collagens and lumican, formed by LAM^{high} SHH medulloblastoma tumours based on the findings of this study. 256
Figure 7.2 Hypothesised pathways of CD44 and BCL-2 upregulation via laminin-111 mediated ligand-independent direct genomic estrogen signalling and classical direct genomic estrogen signalling in LAM^{high} SHH medulloblastoma. 270
Figure 7.3 Hypothesised mechanisms of how type-I/type-VI collagen-ITGB1 interaction could mediate decreased drug sensitivity in DAOY LAM$^{-/-}$ spheroids. 275

List of Tables

Table 1.1 The adapted Chang's Staging System for medulloblastoma. Adapted from Chang et al., 1969. 4

Table 2.1 Medulloblastoma cell lines used in this study with clinical and cell culture information. 40

Table 2.2 Composition of cell culture media used for each cell line in this study..... 41

Table 2.3 Product code and sequence of the single guide RNAs (sgRNAs) used in this study. 45

Table 2.4 Sequence of primers used in DNA mismatch detection assays and Sanger Sequencing of LAMA1 and LAMA2 sgRNA target sites. 47

Table 2.5 Details of the drugs used in this study..... 60

Table 2.6 Sequence of primers used for qRT-PCR analysis in this study. 65

Table 2.7 Composition of buffers used in immunoblotting..... 70

Table 2.8 Components used to prepare 2 X 10% SDS gels..... 71

Table 2.9 Antibodies used in immunoblotting in this study..... 73

Table 2.10 Components used to make 2 X 10% gelatin SDS gels..... 77

Table 2.11 Composition of buffers used in zymograms. All buffers made up in dH_2O. 78

Table 2.12 Antibodies used in immunohistochemistry in this study. 80

Table 2.13 Antibodies used in immunofluorescence in this study 82

Table 2.14 Buffers used for fixing and staining protein in SDS gels for proteomic analysis 83

Table 3.1 The number of genes identified to have significantly increased or decreased expression in the LAM^{high} ECM sub-type compared to the LAM^{low} in the Cavalli dataset (SHH and Group 4 patients) and in response laminin-111 in the mRNA sequencing data (SHH patient derived cell lines)..... 95

Table 3.2 The function of the ‘laminin regulated genes’ selected for further investigation in this study, as well as their role in cancer. 99
Table 3.3 Log2 fold changes in gene expression, p-values and significance levels of all the ‘laminin regulated genes’ across the Cavalli and mRNA sequencing datasets selected for further investigation 103
Table 4.1 Sequence and position of LAMA1 and LAMA2 INDELs in DAOY KO and ONS-76 KO cell lines, as identified by analysis of Sanger Sequencing data using the online INDEL discovery tool ‘Indigo’ 152
Table 6.1 Proteins identified to exhibit differential protein expression in the DAOY $LAM^{-/-}$ cell line in 2D culture 220
Table 6.2 Proteins identified to exhibit differential protein expression in the DAOY $LAM^{-/-}$ cell line in spheroid culture 221

List of common abbreviations

ANOVA	analysis of variance	**IHC**	immunohistochemistry
BCL-2	b-cell lymphoma 2	**INDEL**	insertions and deletions
CD44	cluster of differentiation 44	**ITGB1**	integrin β1
CLU	clusterin	**KEGG**	kyoto encyclopaedia of genes and genomes
CNS	central nervous system	**KO**	knockout
COL1/6A1	collagen type-i/vi α1 chain	**LAM$^{-/-}$**	biallelic LAMA1 knockout
CRISPR-Cas9	clustered regularly interspaced short palindromic repeats and CRISPR-associated protein 9	**LAMA1/2**	laminin subunit α1/2
DMF	dimethylformamide	**LC-MS/MS**	liquid chromatography-tandem mass spectrometry
DMSO	dimethylsulfoxide	**LUM**	lumican
ECM	extracellular matrix	**MMP-2/9**	matrix metallopeptidase 2/9
EGFP	enhanced green fluorescent protein	**NT**	non-targeting
ER	estrogen receptor	**SEM**	standard error of mean
FACS	fluorescence-activated cell sorting	**SHH**	sonic hedgehog
FAK	focal adhesion kinase	**TSC**	total spectrum count
FBS	fetal bovine serum	**WNT**	wingless
FDR	false discovery rate	**mRNA**	messenger ribose nucleic acid
GFP	green fluorescent protein	**qRT-PCR**	real-time quantitative reverse transcription polymerase chain reaction
IC_{50}	half-maximal inhibitory concentration	**sgRNA**	single guide ribose nucleic acid
IF	immunofluorescence	**wt**	wild-type

Chapter 1: Introduction

1.1 Medulloblastoma overview

Medulloblastoma is the most common malignant paediatric brain tumour, accounting for 10% of all cancer-related mortalities in children (Pizer and Clifford, 2009).

1.1.1 Epidemiology

Medulloblastomas are most prevalent during the first 6-8 years of life and occur roughly 1.8 times more frequently in males than females 0-14 years of age (Ostrom *et al.*, 2017; Northcott *et al.*, 2019). Medulloblastoma is not limited to childhood or infancy, however, its rate of incidence decreases 10 fold in adulthood (Northcott *et al.*, 2019).

1.1.2 Clinical presentation and diagnosis

Medulloblastomas are a highly aggressive embryonal tumours of the posterior fossa, 75% of which arise from the cerebellar vermis and often protrude into the roof of the fourth ventricle (Pizer and Clifford, 2009; Millard and De Braganca, 2016). A smaller proportion of medulloblastomas develop in the cerebellar hemispheres, although this is generally found to be more common in older children and adults (Pizer and Clifford, 2009; Millard and De Braganca, 2016).

Due to the high rate of proliferation in these tumours, medulloblastoma patients usually develop symptoms over a period of weeks to months, including behavioural changes, nausea and vomiting, morning headaches, ataxia, anorexia and lethargy (Northcott *et al.*, 2019). These symptoms can be attributed to a combination of hydrocephalus-related increased intracranial pressure and cerebellar dysfunction caused by the tumour itself (Millard and De Braganca, 2016; Northcott *et al.*, 2019).

After the presentation of clinical symptoms, computed tomography (CT) and magnetic resonance imaging (MRI) of the brain and total spinal cord are often used to initially

diagnose medulloblastoma (Northcott *et al.*, 2019). Using CT, medulloblastoma commonly presents as a homogenous, hyperdense mass on the cerebellar vermis (Massimino *et al.*, 2016). Follow up MRI provides a more definitive diagnosis, as well as an insight into the presence or extent of metastasis. The evaluation of metastasis is also coupled with a cytological assessment of the lumbar cerebrospinal fluid (CSF) (Gerber *et al.*, 2014; Massimino *et al.*, 2016).

1.1.3 Metastasis

Metastases attached to the pia mater in the leptomeningeal space, as illustrated in Figure 1.1, are a common characteristic of medulloblastoma, with up to 30% of patients exhibiting this tumoural metastasis upon diagnosis (Wu *et al.*, 2012; Gerber *et al.*, 2014; Zapotocky *et al.*, 2017). The formation of these metastases is caused by the dissemination of the tumour via the CSF (Eberhart *et al.*, 2003; Garzia *et al.*, 2018; Van Ommeren *et al.*, 2020). Extraneural metastasis to sites such as the lung, bone, liver or lymph nodes has also been reported in medulloblastoma patients, but is rare and generally limited to patients with highly advanced disease (Rochkind *et al.*, 1991; Garzia *et al.*, 2018). Furthermore, metastatic dissemination and/or the recurrence of medulloblastoma is the most common cause of patient mortality, making it the most important clinical feature in predicting patient prognosis (Van Ommeren *et al.*, 2020).

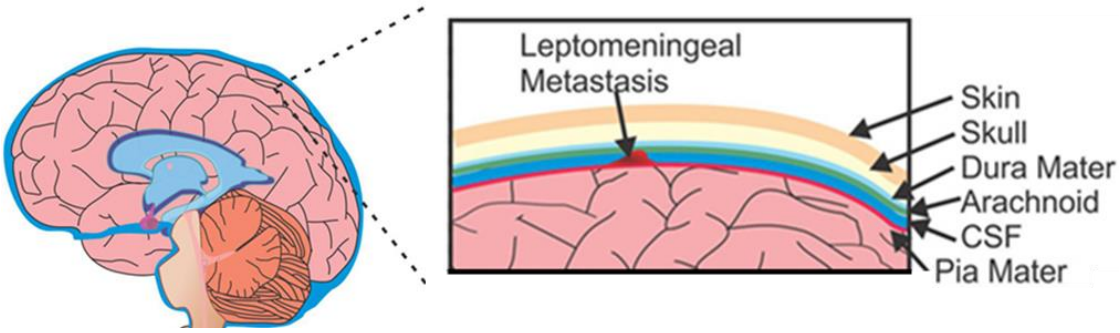


Figure 1.1 Illustration of leptomeningeal metastasis via the cerebrospinal fluid (CSF). Adapted from Singh et al. 2017.

1.1.4 Disease staging

Upon diagnosis medulloblastomas were originally classified using 'Chang's Staging System' with an adapted version still being used today (Table 1.1). This system considers both the size and location of the tumour (tumour stage – T1-4), as well as the presence and extent of metastasis (metastasis stage – M1-4) (Chang, Housepian and Herbert, 1969).

Table 1.1 The adapted Chang's Staging System for medulloblastoma. Adapted from Chang et al., 1969.

Tumour stage		Metastasis	
T1	<3 cm in diameter	**M0**	No evidence of metastasis
T2	>3 cm in diameter	**M1**	Tumour cells present in the cerebrospinal fluid
T3a	>3 cm in diameter with extension into aqueduct of Sylvius or foramen of Luschka	**M2**	Intracranial tumour beyond the primary site
T3b	>3 cm in diameter with extension into the brainstem	**M3**	Gross nodular seeding within the subarachnoid space.
T4	>3 cm in diameter with extension past the aqueduct of Sylvius and/or down past the foramen magnum	**M4**	Metastasis outside of the cerebrospinal axis (especially to bone marrow).

1.1.5 Standard medulloblastoma treatment

With modern multimodal medulloblastoma treatment patients have an overall 5-year event-free survival rate of >70% (Ramaswamy *et al.*, 2016). The first phase of medulloblastoma treatment consists of near-total neurosurgical resection of the tumour, however, the value of this has been debated as there is no conclusive evidence that near-total resection (<1.5 cm^2 residual tumour) of the tumour is actually more beneficial to patient survival than sub-total resection (>1.5 cm^2 residual tumour) (Holgado *et al.*, 2017). Surgery is typically followed by craino-spinal radiotherapy and cisplatin-cyclophosphamide-based chemotherapy (Millard and De Braganca, 2016; Ramaswamy and Taylor, 2017). Cranio-spinal radiotherapy is not conducted on infants, however, due to the overwhelming risk of critical neuro-cognitive damage in these patients (Menyhárt and Győrffy, 2020).

As a result of these intensive treatments, as well as the tissue damage caused by the tumour itself, a large proportion of medulloblastoma survivors experience significant long-term sequelae. This can include neurocognitive, neurosensory and endocrine deficits, as well as several other chronic conditions (Gerber *et al.*, 2014; Northcott *et al.*, 2019; Menyhárt and Győrffy, 2020).

1.2 Histology

The most recent World Health Organisation (WHO) classification system identified medulloblastoma as a grade IV tumour with a number of distinct histological variants: classical, nodular/desmoplastic, medulloblastoma with extensive nodularity (MBEN), large cell and anaplastic (Louis *et al.*, 2016). Most ‘large cell' tumours are comprised of a mixture of cells that exhibit phenotypes typical of either large cell or anaplastic histological variants, therefore they are commonly referred to as one combined

histological variant: large cell/anaplastic (LC/A) (Ellison, 2010). The distinctive features of the medulloblastoma histological variants are displayed in Figure 1.2.

1.2.1 Classical

Classic medulloblastoma (Figure 1.2 A) is the most common histological variant, constituting roughly 70% of all medulloblastomas, and is associated with a range of prognoses (Gilbertson and Ellison, 2008). These tumours are comprised of homologous layers of small cells with rounded or ellipsoid nuclei, a high nuclear to cytoplasmic ratio and a lack of cell molding. Homer Wright rosettes are also a common characteristic of these tumours (Louis *et al.*, 2007; McManamy *et al.*, 2007; Gilbertson and Ellison, 2008; Orr, 2020).

1.2.2 Large cell/Anaplastic

Tumours of the combined LC/A histological variant (Figure 1.2 B) make up around 17% of medulloblastomas, and are usually associated with a poor prognosis as they often exhibit high-risk molecular features, such as the amplification of the *MYC or MYCN* proto-oncogenes (McManamy *et al.*, 2007; Orr, 2020). The large cell variant is comprised of large, uniform cells with a rounded morphology, which possess especially prominent nuclei and nucleoli, 2-3 times bigger than that of the small cells of classic medulloblastoma tumours (Gilbertson and Ellison, 2008; Gibson *et al.*, 2010). The anaplastic variant consists of smaller, pleomorphic cells that are tightly packed in any gaps between the large cells. In fact, anaplastic cells are so tightly packed that they often display cell molding around the large cells. Apoptotic bodies are also a distinct feature of this histological variant (Gilbertson and Ellison, 2008; Gibson *et al.*, 2010).

1.2.3 Medulloblastoma with extensive nodularity

MBEN (Figure 1.2 C) is the rarest histological variant, accounting for only 3% of medulloblastomas, and is correlated with a more favourable outcome (McManamy *et al.*, 2007). These tumours are thought to be an atypical form of nodular/desmoplastic medulloblastoma, that arise more towards the midline of the brain and occur almost exclusively in infants (Orr, 2020). They exhibit very similar characteristics to nodular/desmoplastic tumours (i.e., differentiated neurocytic nodules surrounded by areas of high collagen/reticulin deposition) but, as implied by the name, display a much greater level of nodularity (Gilbertson and Ellison, 2008; Orr, 2020). Furthermore, MBEN nodules can be differentiated from those of the nodular/desmoplastic histological variant by their elongated, lobular architecture, and are thus often described as forming a 'stream-like' pattern (Figure 1.2 C). In addition, MBEN nodules are much more irregular and are often connected to other adjacent nodules (Louis *et al.*, 2007; Taylor *et al.*, 2012; Massimino *et al.*, 2016).

1.2.4 Nodular/desmoplastic

The nodular/desmoplastic histological variant (Figure 1.2 D) represents approximately 10% of medulloblastomas and is associated with a favourable to intermediate prognosis (Gilbertson and Ellison, 2008; Gibson *et al.*, 2010). As the name suggests, this histological variant is comprised of a nodular component and a desmoplastic component. The nodular component is made up of nodules of neurocytic differentiation, whereas the desmoplastic component consists of regions of distinctly elevated inter-cellular collagen/reticulin deposition, which is detectable by reticulin staining. The desmoplastic component surrounds the differentiated nodules, in which collagen/reticulin deposition is distinctly absent (Louis *et al.*, 2007; Gilbertson and Ellison, 2008; Massimino *et al.*, 2016; Orr, 2020).

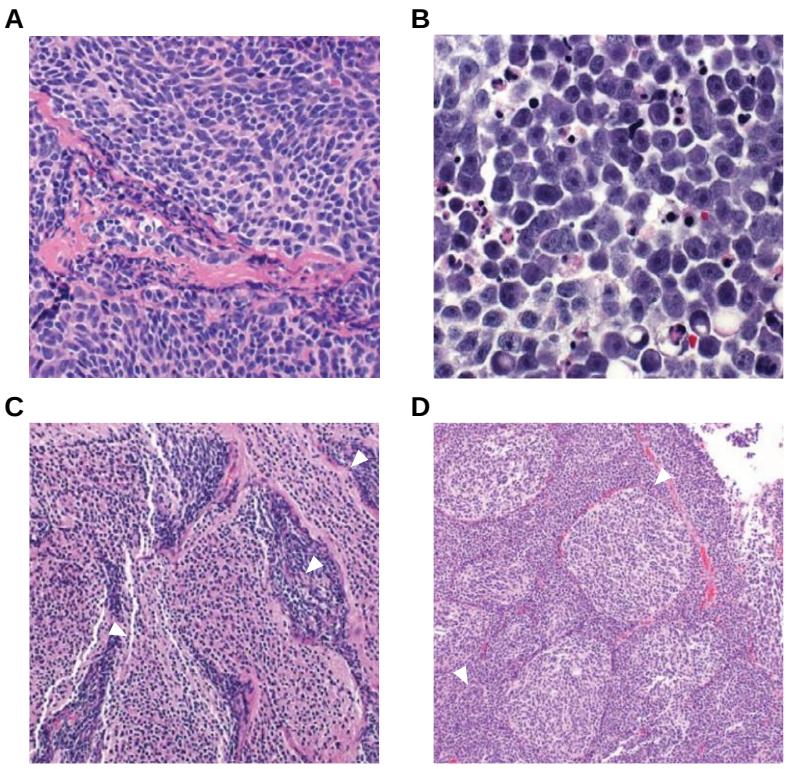


Figure 1.2 The histological variants of medulloblastoma. Medulloblastoma can be categorised into four histological variants: (**A**) classical medulloblastoma, (**B**) large cell/anaplastic medulloblastoma, (**C)** medulloblastoma with extensive nodularity (MBEN), (**D**) desmoplastic/nodular medulloblastoma. Arrows point to the distinctive features of each sub-type: small, rounded cells (classical), large uniform cells and tightly packed anaplastic cells (large cells/anaplastic), elongated reticulin-free nodules (MBEN) and elevated inter-cellular reticulin surrounding reticulin-free nodules (nodular/desmoplastic). Figure adapted from Orr *et al.* 2020.

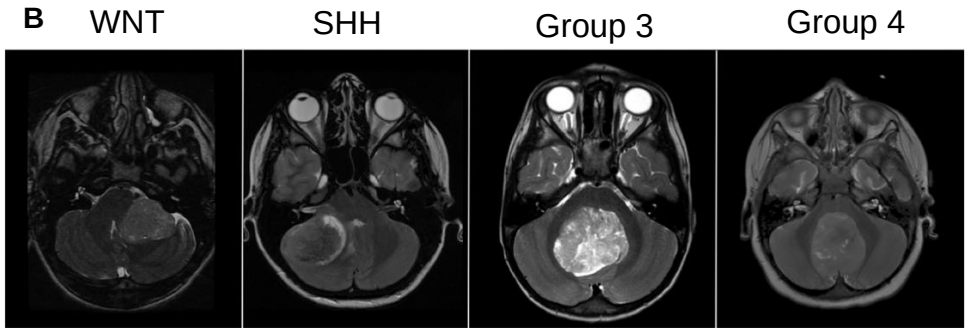
1.3 Medulloblastoma molecular sub-groups

In 2010, a conference of medulloblastoma experts was held in Boston, MA with the objective to establish definitive molecular sub-groups of medulloblastoma. Based on transcriptomic profiling of large cohorts of medulloblastoma patients it was concluded that medulloblastoma should be classified into 4 distinct sub-groups: wingless (WNT), sonic-hedgehog (SHH), Group 3 and Group 4. These four sub-groups are now regarded as discrete biological entities, characterised by differences in their genome, transcriptome, demographics, and clinical features, as summarised in Figure 1.3 A (Taylor *et al.*, 2012). MRI images of each of the medulloblastoma sub-groups, as well as their most prominent diagnostic locations are displayed in Figure 1.3 B and C.

A

		WNT	SHH	Group 3	Group 4
DEMOGRAPHICS	Age group:				
	Gender Ratio: ♂ : ♀	♂ : ♀	♂ : ♀	♂♂ : ♀	♂♂♂ : ♀
CLINICAL FEATURES	Proportion of diagnoses	10%	30%	25%	35%
	Prognosis (5-year survival rate)	>90%	75%	50%	75%
	Proportion of sub-group which are metastatic upon diagnosis	9%	15-20%	50%	35-40%
	Histology	Classical	Classical Nodular/ desmoplastic LC/A MBEN	Classical LC/A	Classical LC/A
GENETICS	Distinctive genetic and cytogenetic aberrations	*CTNNB1, DDX3X, SMARCA4, TP53* mutations Monosomy 6	*PTCH1, SMO, SUFU, TP53* mutations *MYCN* and *GLI1/2* amplification Chromosome 9q deletion	*MYC* and *OTX2* amplification. Chromosome 1q, 7, 17q gain Chromosome 10q, 11, 16q, 17p loss Presence of i(17)q	*KDM6A* mutation *SNCAIP* duplication *MYCN* and *CDK6* amplification Presence of i(17)q

B



C

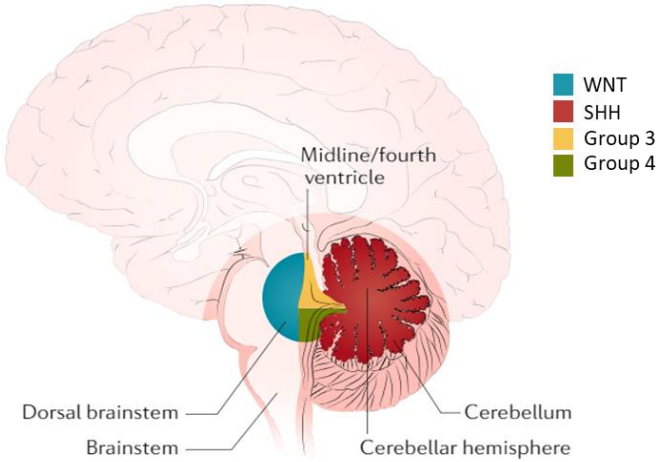


Figure 1.3 The medulloblastoma molecular sub-groups. (**A**) Table summarising the molecular and clinical features of the medulloblastoma sub-groups. Information is based on data from the following references: Taylor *et al.,* 2012 and Northcott *et al*., 2012. (**B**) Magnetic Resonance images (MRI) showing the appearance of the 4 molecular sub-groups of medulloblastoma. Adapted from Iv *et al*., 2018. (**C**) Diagrammatic illustration of a sagittal section of the cerebellum and brain stem, highlighting the most prominent diagnostic locations of medulloblastoma occurrence based on MRI. Areas have been colour coded in correspondence with the most prominent diagnostic locations of the sub-groups: wingless (WNT; blue), sonic-hedgehog (SHH; red), Group 3 (yellow), Group 4 (green). Adapted from Northcott et al., 2019.

1.3.1 WNT sub-group

WNT is the most coherently understood medulloblastoma sub-group. With current treatments, paediatric patients with WNT medulloblastoma have a 5-year survival rate of >90%, the most favourable prognosis of all the sub-groups. However, this is the rarest sub-group, accounting for only 10% of all medulloblastomas (Kool et al., 2012). WNT tumours are thought to arise from lower rhombic lip precursors and are generally located in the midline of the brain, around the fourth ventricle, infiltrating the dorsal surface of the brainstem (Figure 1.3 C) (Gibson *et al.*, 2010; Taylor *et al.*, 2012; Raybaud *et al.*, 2015). Clinical features of WNT medulloblastoma are generally uniform and include rare metastasis (9% of cases), classical histology, a roughly equal gender ratio and a peak incidence in children ≥3 years of age (Kool *et al.*, 2012; Massimino *et al.*, 2016).

The WNT sub-group is typically characterised by the upregulation of the WNT signalling pathway (Figure 1.4), which drives tumour initiation (Northcott, Jones, *et al.*, 2012). The aberrant activation of the WNT pathway is caused by somatic point mutations in exon 3 of catenin beta-1 (*CTNNB1*), which encodes β-catenin, in approximately 86% of WNT medulloblastomas (Thompson *et al.*, 2006; Northcott, Jones, *et al.*, 2012). Mutated β-catenin is resistant to cellular degradation and is localised to the nucleus where it is retained. Thus, any medulloblastoma containing cells exhibiting nuclear accumulation of β-catenin is considered to be a WNT tumour (Eberhart, Tihan and Burger, 2000; Clifford *et al.*, 2006). In the nucleus, β-catenin forms a core complex with other transcription factors and upregulates the transcription of several WNT target genes (Figure 1.4) (Mosimann, Hausmann and Basler, 2009). In addition, 8% of WNT patients exhibit germline loss of function mutations in APC regulator of WNT signalling pathway (*APC*) (Coluccia *et al.*, 2016). A diagrammatic summary of these mutations within the WNT signalling pathway is displayed in Figure 1.4. Less frequently, WNT medulloblastomas possess a heterozygous mutation of

Tumour Protein 53 (*TP53*; encodes p53 protein), however, this does not influence prognosis (Thompson *et al.*, 2006; Northcott, Jones, *et al.*, 2012). The most common cytogenetic aberration in WNT medulloblastomas is the loss of chromosome 6 (monosomy 6), which occurs in approximately 80% of WNT medulloblastomas and is nearly exclusive to this sub-group (Thompson *et al.*, 2006; Cavalli *et al.*, 2017).

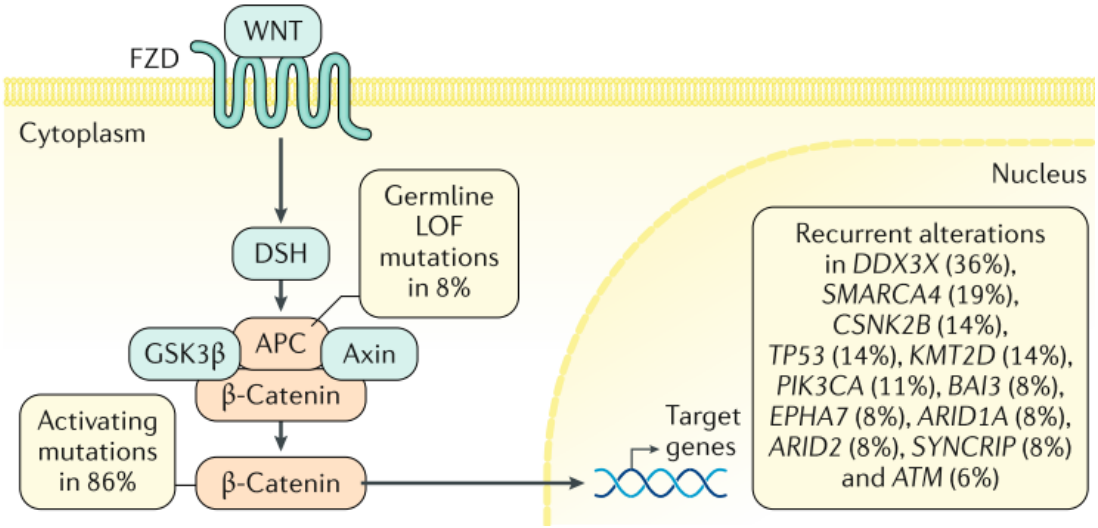


Figure 1.4 Diagram of mutations within the wingless (WNT) signalling pathway exhibited by WNT medulloblastoma patients. LOF: loss of function. Taken from Northcott *et al.,* 2019.

1.3.2 SHH sub-group

The SHH medulloblastoma sub-group represents approximately 30% of all medulloblastomas (Kool et al., 2012). Patients of this sub-group have an intermediate survival rate of approximately 75% (Northcott, Korshunov, *et al.*, 2012; Taylor *et al.*, 2012). SHH tumours most commonly arise in the cerebellar hemispheres (Figure 1.3 C), where the cell of origin is thought to be granule cell precursors (GCP) within the external granule layer (Huang *et al.*, 2016). Although medulloblastomas arising from this area of the brain are nearly exclusively predominated by the SHH sub-group, some SHH tumours have been shown to arise in the midline of the brain (Gibson *et al.*, 2010; Grammel *et al.*, 2012; Raybaud *et al.*, 2015). SHH tumours exhibit a unique bimodal pattern of incidence, with the majority of cases occurring in patients under 3

or over 16 years of age (Gajjar and Robinson, 2014). The histology of SHH tumours is also variable, in fact, this is the only medulloblastoma sub-group to exhibit all four of the medulloblastoma histological variants (Northcott, Korshunov, *et al.*, 2012; Taylor *et al.*, 2012). Furthermore, medulloblastomas with nodular/desmoplastic and MBEN histology are almost exclusive to the SHH sub-group (Kool et al., 2012). SHH tumours exhibit an equal gender ratio and have a relatively low rate of metastasis (15-20%) (Kool et al., 2012; Taylor et al., 2012).

SHH medulloblastomas are generally characterised by the aberrant activation of the SHH signalling pathway, a key pathway in cerebellar development, which is thought to drive tumour initiation (Figure 1.5). These tumours often harbour germline or somatic mutations in the components of the SHH pathway itself, which result in its activation. The most common mutations within this pathway include loss of function mutations/deletions in protein patched homologue 1 (*PTCH1*; 43% of patients) and suppressor of fused homologue (*SUFU*; 10% of patients), activating mutations in smoothened (*SMO*; 9% of patients), as well as amplification of GLI Family Zinc Finger 1 and 2 *(GLI* and *GLI2*; 9% of patients) and MYCN Proto-Oncogene (*MYCN*; 7% of patients) (Jones *et al.*, 2012; Northcott, Korshunov, *et al.*, 2012; Pugh *et al.*, 2012; Kool *et al.*, 2014). Adult and paediatric SHH medulloblastoma patients exhibit discrete patterns of these mutations: *SMO* mutations are more common in adults whereas *SUFU* mutations are nearly exclusive to infants (Coluccia *et al.*, 2016). SHH medulloblastomas also frequently exhibit a germline/somatic mutation of *TP53,* which is indicative of a poor outcome (Zhukova *et al.*, 2013). A diagrammatic summary of these mutations within the SHH signalling pathway is displayed in Figure 1.5. The most common chromosomal aberration in the SHH sub-group is the deletion of chromosome 9q, the location of the *PTCH1* locus (Coluccia *et al.*, 2016). Furthermore, the SHH medulloblastoma sub-group is associated with Gorlin syndrome in patients, a

syndrome characterised by a germline mutation of *PTCH1,* resulting in a predisposition to SHH medulloblastoma (Fujii and Miyashita, 2014).

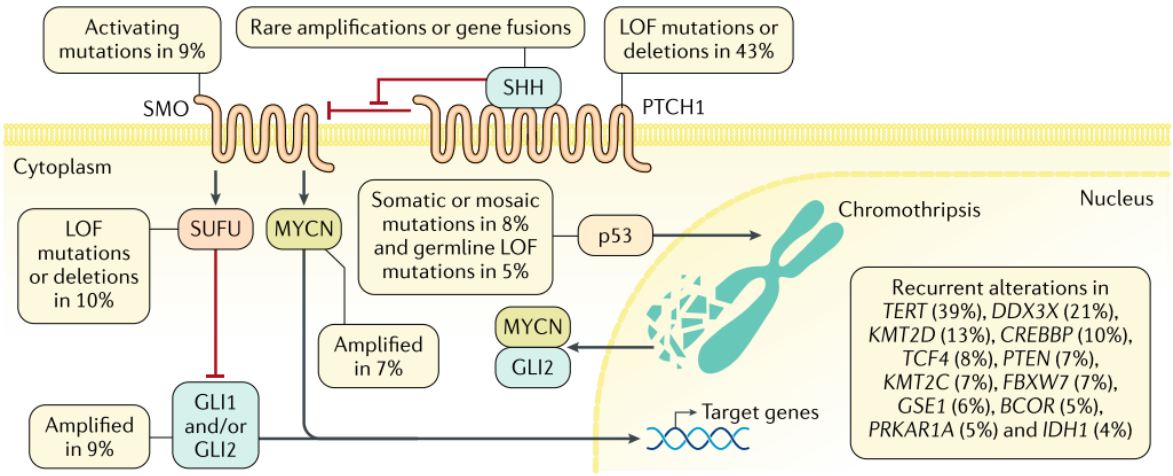


Figure 1.5 Diagram of mutations within the sonic-hedgehog (SHH) signalling pathway exhibited by SHH medulloblastoma patients. LOF: loss of function. Taken from Northcott *et al.,* 2019.

1.3.3 Group 3

Group 3 tumours constitute around 25% of all medulloblastomas and have the worst prognosis of all the sub-groups, with a 5-year survival rate of roughly 50% (Kool *et al.*, 2012). Furthermore, they are the most metastatic sub-group, with nearly 50% of cases metastasising (Kool *et al.*, 2012). Tumours of this sub-group are typically located in the fourth ventricle, touching the brainstem (Figure 1.3 C) (Kool *et al.*, 2012; Raybaud *et al.*, 2015). Both Group 3 and Group 4 tumours are thought to arise from excitatory cerebellar neurons and unipolar brush cell precursors, along the same transcriptional continuum (Williamson *et al.*, 2022). Tumours of this sub-group are very rare in adults and predominantly arise in infants and children, where they occur twice as frequently in males as they do in females (Kool *et al.*, 2012). Most Group 3 tumours have classical histology, however, a large proportion of this group exhibit LC/A histology (40%), a histological variant that is nearly exclusive to the Group 3 sub-group (Kool *et al.*, 2012).

Unlike WNT and SHH medulloblastoma, there are only a few known recurrent somatic mutations and no predisposing germline mutations in Group 3 tumours (Jones *et al.*, 2012; Taylor *et al.*, 2012; Gajjar and Robinson, 2014). The most common genetic aberration found in Group 3 medulloblastoma is the focal amplification of the proto-oncogene *MYC,* which has been identified as a somatic driver of 17% of Group 3 tumours and is associated with a low rate of survival. Furthermore, Orthodenticle homeobox 2 (*OTX2*) amplification has also been identified as another common genetic aberration in Group 3 medulloblastoma (Kool *et al.*, 2012; Ramaswamy and Taylor, 2017). However, >50% of Group 3 medulloblastomas do not possess these genetic aberrations and instead exhibit cytogenetic alterations, including the gain of chromosomes 1q, 7 and 17q as well as the deletion of chromosomes 10q, 11, 16q and 17p. Chromosome 17 aberrations are thought to be caused by the presence of an isochromosome 17 (i(17)q), which is associated with a poor outcome (Kool *et al.*, 2012; Northcott, Jones, *et al.*, 2012). Currently, the role that these chromosomal alterations play in the underpinning pathology of this sub-group is poorly understood. However, one study suggested that the chromosomal alterations may reposition active super-enhancers to the vicinity of the oncogenes Growth Factor Independent 1 Transcriptional Repressor (*GFI1*) and Growth Factor Independent 1B Transcriptional Repressor (*GFI1B*)*,* resulting in their activation, which drives tumour progression (Northcott *et al.*, 2014). This phenomenon has been termed ‘enhancer hijacking’. Furthermore, little overlap between *GFI1* or *GFI1B* activation and *MYC* amplification was observed in Group 3 tumours, suggesting that enhancer hijacking acts as a *MYC* amplification-independent mechanism in Group 3 pathogenesis (Northcott *et al.*, 2014). In addition, enhancer hijacking was also exhibited by Group 4 medulloblastomas, suggesting it may also play a role in their pathogenesis (Northcott *et al.*, 2014).

1.3.4 Group 4

Group 4 medulloblastoma is the most prevalent of all the sub-groups, accounting for 35% of all medulloblastomas and yet it is the least well understood (Kool *et al.*, 2012). The 5-year survival rate of children with Group 4 medulloblastoma is similar to that of SHH, despite metastasis occurring in roughly 35-40% of cases (Kool *et al.*, 2012; Northcott, Jones, *et al.*, 2012). Group 4 medulloblastomas are generally large tumours and located centrally in the fourth ventricle (Figure 1.3 C), often presenting with associated hydrocephalus. Histologically, Group 4 tumours are predominantly classical, but a small proportion also exhibits the LC/A histological variant (Kool *et al.*, 2012). Group 4 medulloblastomas most commonly arise in children 3-16 years of age, occurring approximately 3 times more frequently in males than females; the most unequal gender ratio of all the medulloblastoma sub-groups (Kool *et al.*, 2012; Northcott, Korshunov, *et al.*, 2012; Gajjar and Robinson, 2014).

There are currently no known predisposing germline mutations in Group 4 medulloblastoma and many of the genes that are amplified or mutated in Group 4 medulloblastoma overlap with those of Group 3 (Gajjar and Robinson, 2014). However, in contrast to Group 3 medulloblastoma, Group 4 tumours commonly exhibit preferential *MYCN* amplification over *MYC* as well as amplification of cyclin-dependent kinase 6 (*CDK6*) (Northcott *et al.*, 2011). Similarly to Group 3, the most widespread cytogenetic aberration exhibited by Group 4 medulloblastomas is i(17q), however, it occurs 40% more frequently in Group 4 medulloblastoma and holds no prognostic influence (Kool *et al.*, 2012; Shih *et al.*, 2014). Interestingly, 80% of female Group 4 medulloblastoma patients exhibit the loss of one copy of the X-chromosome, indicating that there may be tumour suppressor genes present on the chromosome (Northcott, Jones, *et al.*, 2012; Taylor *et al.*, 2012).

1.4 Intratumoral heterogeneity within the molecular sub-groups

A recent integrative study of a large DNA methylation and gene expression medulloblastoma data set by Cavalli *et al*, revealed distinct intra-sub-group heterogeneity and identified sub-types within the medulloblastoma sub-groups, as illustrated in Figure 1.6 (Cavalli *et al.*, 2017). Furthermore, the defining clinical and molecular characteristics of each of these sub-types are described below.

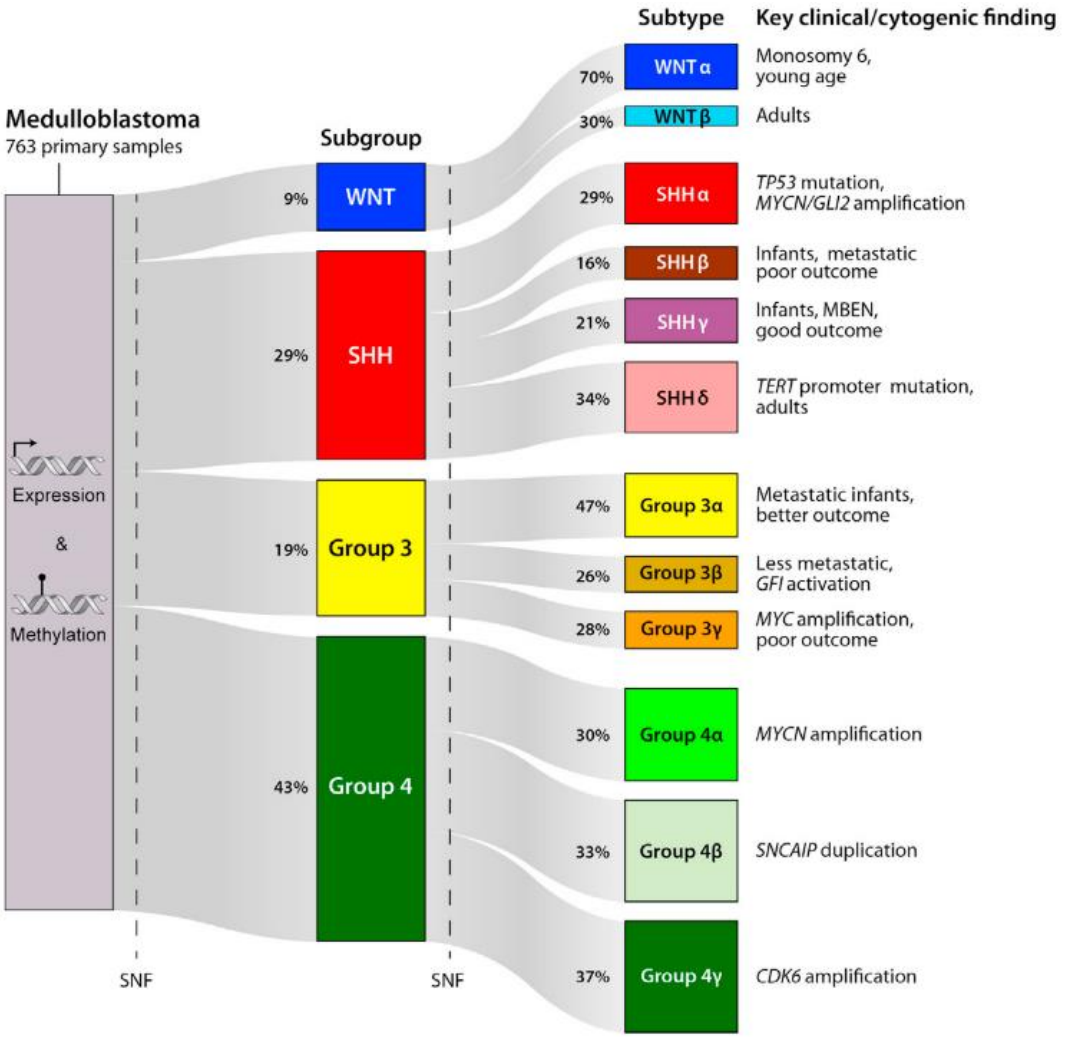


Figure 1.6 Intratumoral heterogeneity within the medulloblastoma molecular sub-groups. In a study conducted by Cavalli *et al*., integrated analysis of DNA methylation, gene expression, copy number alterations, and clinical data of 763 primary medulloblastoma samples, identified 12 sub-types within the 4 molecular sub-groups of medulloblastoma (WNT, SHH, Group 3 and Group 4). Adapted from Cavalli et al., 2017.

1.4.1 WNT sub-types

WNT medulloblastomas were shown to be comprised of at least 2 sub-types: WNTα and WNTβ, constituting 70% and 30% of WNT medulloblastomas respectively. WNTα tumours occur in children and exhibit monosomy 6 whereas the majority of WNBβ tumours occur in adults and do not exhibit monosomy 6. The 5-year survival rate for both of the WNT sub-types is nearly 100% (Cavalli *et al.*, 2017).

1.4.2 SHH sub-types

The SHH sub-group was further divided into 4 sub-types: SHHα, SHHβ, SHHγ and SHHδ. SHHα tumours possess *TP53* mutations and *MYCN* amplification. SHHβ tumours predominantly occur in infants and are frequently metastatic, so are consequently associated with a poor outcome. SHHγ tumours have a balanced genome and are associated with good outcomes. Finally, the SHHδ sub-type mainly arises in adults and almost exclusively exhibits MBEN histology (Cavalli *et al*., 2017).

1.4.3 Group 3 sub-types

Three sub-types of Group 3 medulloblastoma have now been identified: Group 3α, Group 3β and Group 3γ. The Group 3α sub-type most frequently arises in infants and often metastasises. Group 3β tumours exhibit high levels of *OTX2* amplification as well as *GFI1* oncogene activation. Lastly, Group 3γ is characterised by *MYC* amplification and a high rate of metastasis; this sub-type has the worst outcome of all medulloblastomas (Cavalli *et al*., 2017).

1.4.4 Group 4 sub-types

Similarly to Group 3, Group 4 medulloblastoma was divided into three sub-types: Group 4α, Group 4β and Group 4γ. Both Group 4α and Group 4γ exhibit chromosome 7q gain, chromosome 8p loss and focal amplification of *CDK6*. *MYCN* amplification is also present Group 4α and is what differentiates the sub-type from Group 4γ. Group

4β medulloblastoma exhibits synuclein alpha interacting protein (*SNCAIP*) duplication (Cavalli *et al*., 2017).

More recently, another integrative study by Sharma *et al* combined 3 DNA methylation and gene expression medulloblastoma datasets from previous studies (including the Cavalli dataset), in order to define subtypes more robustly within Group 3 and Group 4 tumours, the molecular drivers of which are largely unknown (Sharma *et al.*, 2019). The study identified 8 Group 3/4 medulloblastoma sub-types (sub-type I-VIII) with distinct demographics, as well as clinical and molecular features. Notably, sub-type III was found to have the worst survival of the all the sub-types of less than 40%, likely due to its increased occurrence of *MYC*/*MYCN* amplification (Sharma *et al.*, 2019). The enhanced understanding of medulloblastoma sub-group heterogeneity provided by these studies may allow for more effective, sub-type specific therapeutic targets to be identified more easily in the future. However, further work is still required to fully delineate the genomic landscape of medulloblastoma.

1.5 Clinical risk stratification

In the 1990s, a medulloblastoma patient risk stratification tool was established and is still used today to determine the intensity of the course of treatment required. The tool broadly stratifies medulloblastoma patients over 3 years of age (all patients ≤3 years of age are automatically classed as high risk) into two groups: high-risk and average-risk. (Packer and Vezina, 2008; Ramaswamy *et al.*, 2016). These risk groups are mainly based on two key clinical features: the occurrence of leptomeningeal metastasis and the size of post-operative residual tumour. If a patient exhibits leptomeningeal metastasis at the time of diagnosis or has a post-operative residual tumour ≥1.5 cm² in size, they are considered to be ‘high-risk'. If a patient does not possess either of these features then they are considered to be ‘average-risk' (Millard

and De Braganca, 2016). However, a refined patient stratification system, based on the medulloblastoma molecular sub-groups and their pathology, has recently been proposed by Ramaswamy *et al*. The intention of this system is to provide a basis to more accurately identify very high-risk patients, who may benefit from more intense treatment regimens, and for which the development of novel targeted therapies should be prioritised to improve outcome (Ramaswamy *et al.*, 2016). In this system patients are categorised into 4 groups with differing rates of survival: low risk, standard risk, high risk and very high risk, as described below.

1.5.1 Low risk

Non-metastatic WNT tumours (in patients under 16 years of age) and Group 4 medulloblastomas, that exhibit the entire gain of chromosome 17 or loss of chromosome 11, are considered to be 'low risk' tumours. These patients typically have a survival rate of >90% with current standard treatment protocols (Ramaswamy *et al.*, 2016).

1.5.2 Standard risk

Non-metastatic, SHH tumours (apart from *TP53* mutated patients), Group 3 tumours (without *MYC* amplification) and Group 4 tumours (without chromosome 11 loss) are categorised as standard risk and are associated with a survival rate of 75-90% with current standard treatment protocols (Ramaswamy *et al.*, 2016).

1.5.3 High risk

MYCN-amplified and/or metastatic wild-type *TP53* SHH medulloblastomas are regarded as high-risk tumours, as well as metastatic Group 4 medulloblastomas. These patients are associated with a 50-75% survival rate with current high-risk treatment protocols (Ramaswamy *et al.*, 2016).

1.5.4 Very high risk

Medulloblastomas that are considered to be very high risk include metastatic Group 3 patients (particularly *MYC* amplified) and SHH tumours with a germline *TP53* mutation. Very high-risk medulloblastoma patients have the worst survival rate of <50%. These patients may benefit from more intense chemo/radiotherapy and should be prioritised for novel therapeutic strategies (Ramaswamy *et al.*, 2016).

1.6 Sub-group based therapies

Our vastly improved understanding of the molecular basis of medulloblastoma, specifically the identification of some of its drivers, has prompted the development of several sub-group-specific treatments. However, the recent identification of the sub-types within the medulloblastoma sub-groups may alter our approach to the development of these therapies in the future (Wang *et al.*, 2018).

1.6.1 WNT therapies

As the 5-year survival of WNT medulloblastoma patients is so high (>90%) WNT-specific treatments are centred around the de-escalation of CSRT and the accompanying chemotherapy (Gajjar and Robinson, 2014). The main objective of this approach is to reduce the long-term sequelae associated with this form of treatment while maintaining the exceptional survival rate (Gajjar and Robinson, 2014; Coluccia *et al.*, 2016; Remke and Ramaswamy, 2022). However, although studies are ongoing, several recent reports have indicated that a reduction in these therapies results in an unacceptable number of treatment failures (Cohen *et al.*, 2019; Gupta *et al.*, 2022; Remke and Ramaswamy, 2022). Ongoing research is also investigating less toxic treatments for this sub-group (Gajjar and Robinson, 2014).

1.6.2 SHH therapies

Following the identification of *SMO* mutations as a driver of SHH medulloblastomas, SMO inhibitors (such as vismodegib and sonidegib) were evaluated in preclinical, as well as clinical trials, as a potential targeted therapy for SHH tumours (Wang *et al.*, 2018). This was the first example of a targeted therapy for medulloblastoma. SMO inhibitors have received a significant level of interest from the pharmaceutical industry as they have the potential to be applied to several types of cancers with aberrantly activated SHH pathways (Lin and Matsui, 2012). However, since there are several mutations which can drive SHH medulloblastoma, SMO inhibitors are only effective against tumours which possess a mutation upstream of *SMO,* rendering them ineffective as a monotherapy against all SHH medulloblastomas (Kool *et al.*, 2014). Furthermore, sustained exposure to these drugs can cause a *SMO* mutation, altering the structure of the protein to a sufficient degree that binding of the drug is inhibited, making the tumour resistant *SMO* inhibitors (Yauch *et al.*, 2009).

1.6.3 Group 3/4 therapies

The large overlap between the molecular profiles of Group 3 and Group 4 medulloblastomas suggests that treatments effective against Group 3 medulloblastoma may also target Group 4 medulloblastoma (Gajjar and Robinson, 2014; Coluccia *et al.*, 2016). *MYC* amplification, which often occurs in Group 3 and Group 4 medulloblastoma, is epigenetically regulated by the Bromodomain and Extra-Terminal motif (BET) protein which is able to bind to acetylated lysine residues via its bromodomain, permitting the recruitment of transcription factors and maintaining MYC transcription (Filippakopoulos and Knapp, 2012). Thus, BET bromodomain inhibitors have been investigated as a potential treatment of medulloblastoma and have been shown to reduce cell viability, induce apoptosis and prolong the survival of xenograft models in MYC-driven medulloblastomas (Bandopadhayay *et al.*, 2014). Unfortunately, specific cyclin-dependant kinases (CDKs) are able to promote MYC

stabilisation in tumour cells however more recently it has been shown that the combination of BET bromodomain inhibitor and CDK2 inhibitor can work synergistically to cause cell cycle arrest and tumoural apoptosis in MYC-driven Group 3 medulloblastoma tumours (Bolin *et al.*, 2018). In addition, a study by Cook Sanger *et al* demonstrated that the CDK4/6 inhibitor palbociclib caused the regression of *MYC*-amplified Group 3 tumours in patient derived xenograft (PDX) mouse models, suggesting that it represents a suitable targeted therapy for these very high-risk tumours (Cook Sangar *et al.*, 2017).

1.7 The tumour microenvironment

The tumour microenvironment (TME) is a dynamic and complex system consisting of the resident cells and extracellular matrix (ECM) that surrounds the tumour. It has been shown that the TME has a significant influence in the formation, progression and therapy response of cancers, including medulloblastoma, and that tumours are able to distinctly modify its composition (Wang, Tong and Yang, 2014; van Bree and Wilhelm, 2022). The TME of brain tumours (and thus that of medulloblastoma), is one of the most complex and unique, owing to its distinctive ECM and the specific combination of resident cell-types including neurons, microglia and astrocytes, that are only found in the brain (Quail and Joyce, 2017). Research regarding the TME has primarily focused on how the cellular components, such as immune cells, may enhance cancer progression. However, in the past decade numerous studies have demonstrated that the non-cellular part of the TME, the ECM, also plays a major role in tumour progression and therapy response (Lu, Weaver and Werb, 2012; Henke, Nandigama and Ergün, 2020). The role of ECM in the progression of medulloblastoma is the focus of this study.

1.7.1 The brain extracellular matrix

The ECM was initially viewed as a static, stable structure which primarily functioned as a cellular scaffold, providing physical support to tissues, helping them to maintain their morphology and mechanical integrity. However, it is actually a highly dynamic matrix and conducts several essential biological functions (Frantz, Stewart and Weaver, 2010). In non-disease conditions these functions include regulating cellular differentiation, motility, migration, survival and development and are mediated by ECM-cell adhesion via specific cellular receptors and the regulation of cytokines and growth factor concentration gradients (Pickup, Mouw and Weaver, 2014). Additionally, the ECM plays a vital role in maintaining water retention and the pH of the local microenvironment in tissues (Mammoto and Ingber, 2010).

Each tissue type has its own highly heterogeneous ECM which is continuously remodelled and tailored to the function of the tissue (Pickup, Mouw and Weaver, 2014). The brain has an especially unique ECM, as the skull provides a lot of the structural support that is usually supplied by the ECM in most other tissues (Rauch, 2004). Non-CNS ECMs usually consists of an interconnected web of macromolecules such as collagen and laminins, whereas the brain ECM is primarily composed of glycoproteins, proteoglycans (depicted in Figure 1.7) giving it unique mechanical properties (Ruoslahti, 1996).

Hyaluronan (hyaluronic acid) is the primary component of brain ECM and forms the backbone of the matrix. It is a long non-sulphated glycosaminoglycan (GAG) composed of repeating disaccharide units of glucuronate and *N*-acetylglucosamine (Novak and Kaye, 2000; Rauch, 2004; Necas *et al.*, 2008; Nicholson and Hrabětová, 2017). Hyaluronan is able to aggregate aggrecan, versican, neurocan and brevican, all of which are chondroitin sulphate proteoglycans (CSPG) and together form the lectican family of CSPGs (Yamaguchi, 2000). These aggregates form ‘lamp-brush’ like structures which extend outwards from the hyaluronan chain (Mörgelin *et al.*, 1994).

All of the lecticans share a similar structure consisting of a globular N-terminal hyaluronan-binding domain and a globular C-terminal lectin-containing domain, separated by a highly glycosylated central region (Rauch, 2004). Among the lecticans, aggrecan is the most heavily modified with chondroitin sulphate (Mörgelin *et al.*, 1994). The globular C-terminus of the lecticans is able to bind numerous glycoproteins and glycolipids. Specific lecticans are able to interact with the oligomeric glycoproteins tenascin-C and tenascin-R (Yamaguchi, 2000). This interaction cross-links the lecticans between different hyaluronan chains, creating an interconnected 3D matrix structure. Additionally, the dimeric glycoprotein fibulin-2 is able to specifically cross-link versican molecules (Olin *et al.*, 2001). During the maturation of the brain, it is thought the components of the ECM are replaced, but by homologous proteins of the same family, allowing the overall structure to be maintained (Bandtlow and Zimmermann, 2000). For example, in the mouse brain, it has been observed that the versican V1 splice variant neurocan and tenascin-C are prominent in the developing brain, but in the adult brain, their homologues versican splice variant V2 brevican and tenascin-R are much more prevalent (Rauch, 2004).

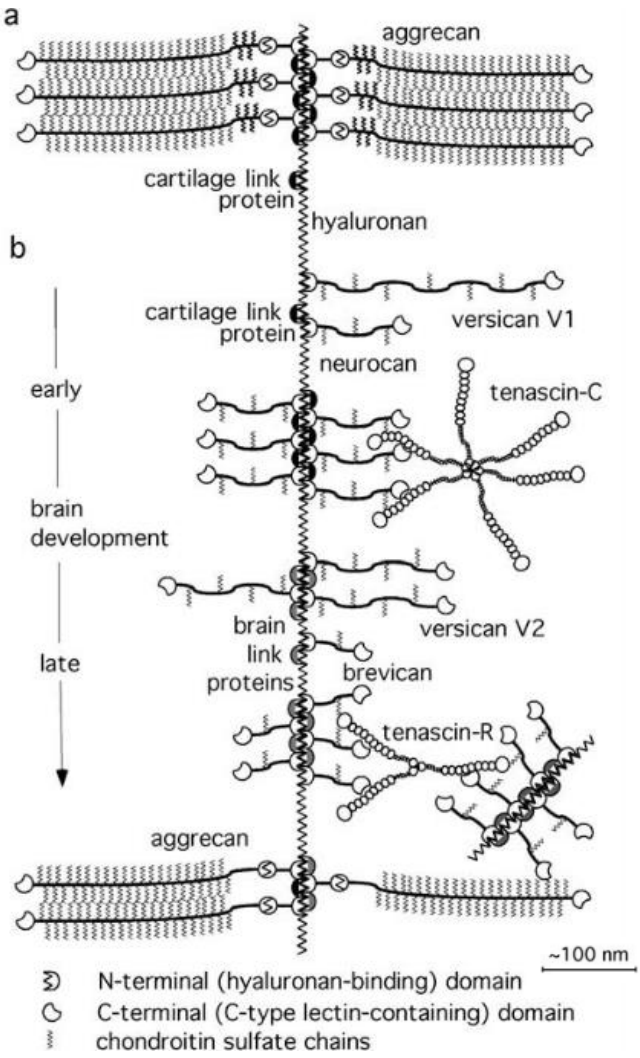


Figure 1.7 Schematic of the structure of lectican family of chondroitin sulphate proteoglycans and their interactions which hyaluronan and tenascins, in the context of the brain extracellular matrix (ECM). Arrow indicates the components of the developing brain in the top half of the schematic and the altered ECM components of the mature brain in the bottom half. Adapted from Rauch, 2004.

1.7.2 The extracellular matrix and cancer

A multitude of clinical and molecular studies have demonstrated that many types of solid tumours are able to drastically reorganise and modify the composition and mechanical properties of their surrounding ECM, via the deposition of ECM proteins by tumour cells themselves and cancer-associated fibroblasts (CAFs), or astrocytes in brain cancers (Wiese, Karus and Faissner, 2012; Cheng *et al.*, 2020; J. Huang *et al.*, 2021; Allnoch *et al.*, 2022; Popova and Jücker, 2022). In cancer in general, it has been

reported that tumour ECM can constitute up to 60% of tumour mass and thus represents an important area of cancer biology (Casey *et al.*, 2009; Pickup, Mouw and Weaver, 2014). It has been demonstrated that the tumour ECM can be pro- or anti-tumorigenic and that the specific ECM signature of tumours can be used to predict patient outcome in some cancers (Conklin *et al.*, 2011; Jiang *et al.*, 2019; Paolillo and Schinelli, 2019; Martins Cavaco *et al.*, 2020; Rousselle and Scoazec, 2020; Winkler *et al.*, 2020; Cox, 2021; Karamanos *et al.*, 2021).

The tumour ECM is able to influence tumour progression through the direct activation of intracellular pathways within cancer cells. For example, the adhesion of cancer cells to the ECM proteins collagens, laminins and fibronectin (among the most commonly dysregulated in cancers) via cell surface receptors such as integrins, can directly activate many key intracellular signalling pathways, such as extracellular signal-regulated kinase (ERK), phosphatidylinositol-3 kinase-AKT serine/threonine kinase 1 (PI3K-AKT) and focal adhesion kinase (FAK) (Levental *et al.*, 2009; Pickup, Mouw and Weaver, 2014; Henke, Nandigama and Ergün, 2020). The upregulation of these pathways can then aid tumour progression, by promoting hallmarks of cancer such as apoptosis evasion, cell proliferation and insensitivity to growth inhibitors, as illustrated in Figure 1.8. Furthermore, increased cellular adhesion to the ECM has also been shown to mechanically enhance tumour migration and invasion and thereby metastasis (Paolillo and Schinelli, 2019).

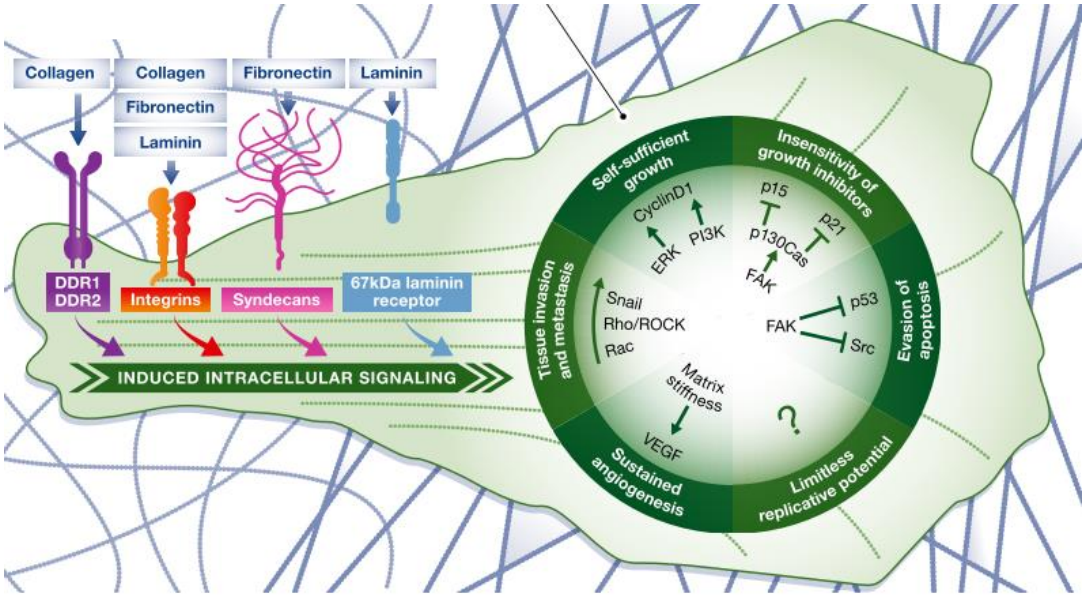


Figure 1.8 Intracellular pathways activated in cancer by the interaction of collagen, laminin and fibronectin with cell surface ECM receptors. Adapted from Pickup and Weaver *et al.,* 2014.

The overexpression of ECM proteins can also distinctly enhance tumour progression through increasing the stiffness of the tumour ECM (Schwartz, 2010; Grasset *et al.*, 2018). Increased tumour ECM stiffness is commonly associated with poor clinical outcome and has been shown to contribute to uncontrolled proliferation, invasion and metastasis, angiogenesis, therapy resistance, genome instability, and immunosuppression in tumours, through a combination of intracellular pathway activation and altered physical properties of a stiffer ECM (Huang *et al.*, 2021). This increase in tumour ECM stiffness is often attributed to an overabundance of collagens and hyaluronan in tumours (Kalluri, 2003; Giussani *et al.*, 2015; Insua-Rodríguez and Oskarsson, 2016). Increased collagen deposition has been shown to specifically increase the stiffness of the periphery of the tumour, where its resistance to tensile stress means it becomes stiffer when it is stretched as the tumour grows (Conklin *et al.*, 2011; Stylianopoulos *et al.*, 2012; Gkretsi and Stylianopoulos, 2018). In addition, excessive cross-linking of collagens by lysyl oxidase (LOX), an enzyme which is frequently overexpressed in cancers, has also been shown to significantly contribute to increased stiffness of the tumour periphery (Levental *et al.*, 2009). Conversely,

hyaluronan is thought to specifically increase the stiffness of the tumour core, which counteracts the compressive force exerted by periphery of the tumour (Stylianopoulos *et al.*, 2012, 2013).

As mentioned above, laminins and collagens are two of the most frequently dysregulated ECM proteins in cancer and are specifically relevant to this study. An explanation of their structure is therefore described as follows. Laminins are glycoproteins that form a key structural component of the ECM, mainly in basement membranes, and also have a role in the stimulation of cellular growth and differentiation, mediating cell communication and the stimulation of neurite out-growth (Beck, Hunter and Engel, 1990). They are heterotrimeric in structure and are composed of α, β and γ subunits, wound together into a cruciform structure (Sasaki, Fässler and Hohenester, 2004; Aumailley, 2013). In humans, there are five α (α1–α5), four β (β1–β4) and three γ (γ1–γ3) subunits of laminin (Aumailley, 2013). Each isoform is named in accordance with the three subunits from which it is composed. For example, laminin-111 is a heterotrimer of α1, β1 and γ1 subunits (Aumailley *et al.*, 2005). Collagens are fibrous proteins that are crucial parts of the ECM, forming large networks which provide structural support in basement membranes (where they bind to laminins), tissues and bone, as well as directing fibroblasts in tissue repair (Shoulders and Raines, 2009; Neel *et al.*, 2013). Collagens are hetero or homotrimers, composed of 1, 2 or 3 different α chains and are defined by the type of α chain from which they are comprised (Shoulders and Raines, 2009; Popova and Jücker, 2022). For example, the most common type of collagen (type-I) is composed of 2 type-I collagen alpha chain 1 (COL1A1) chains and 1 type-I collagen alpha chain 2 (COL2A1) chain. The structure of both of these protein is displayed in Figure 1.9.

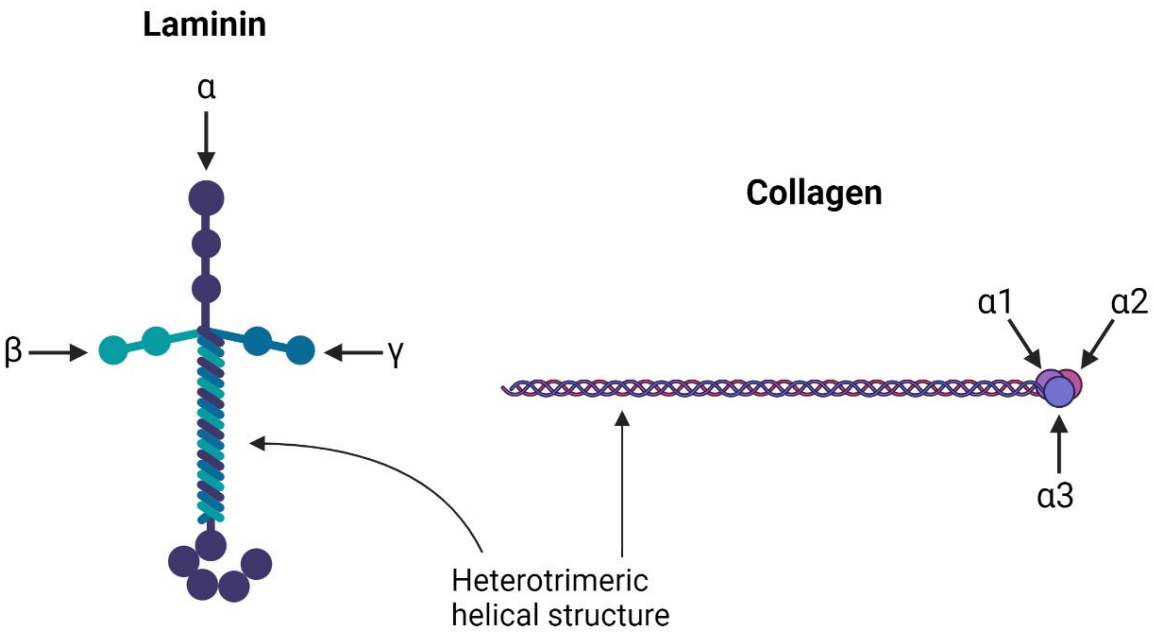


Figure 1.9 Structure of laminin and collagen. Laminin is comprised of an α, β and γ subunit, whereas collagen is comprised of 3 α subunits.

Although the ECM can support tumours, it is often degraded as part of several aspects of tumour progression, including migration and invasion into local tissues, angiogenesis induction and cell proliferation (via the release of growth factors from the ECM) (Bauvois, 2012; Bonnans, Chou and Werb, 2014; Najafi, Farhood and Mortezaee, 2019). The process of ECM degradation is mediated by ECM degrading enzymes, the most prominent of which are matrix metalloproteinases (MMPs). MMPs are a family of 23 zinc-containing, calcium dependant endopeptidases that are able to degrade all ECM proteins, although they most commonly degrade collagens, laminins, gelatin and fibronectin (Isaacson *et al.*, 2017). They are secreted from cells as zymogens which are then subsequently activated by proteolytic cleavage of their pro sequence or oxidation (Bonnans, Chou and Werb, 2014). MMPs exhibit a low level of activity in normal conditions, but are commonly overexpressed in tumours, where they are generally correlated with tumour invasion and metastasis and are thus indicative of poor patient outcome (Bonnans, Chou and Werb, 2014). Among the MMPs, the

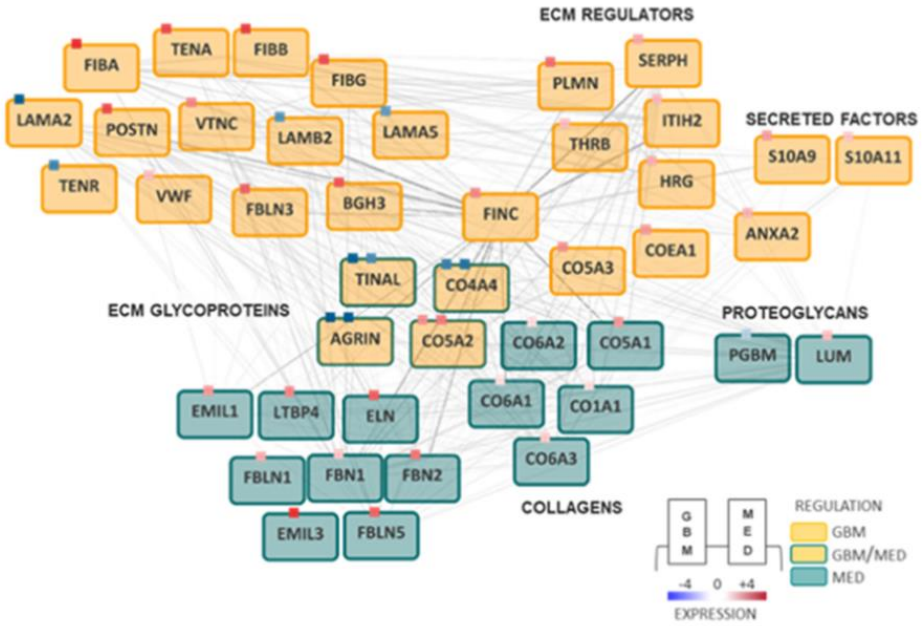
roles of MMP-2 and MMP-9 in cancer progression are best characterised (Bauvois, 2012; Najafi, Farhood and Mortezaee, 2019).

1.7.3 The extracellular matrix of medulloblastoma

Our current understating of the ECM composition of brain tumours is limited, with it only being to focus of a few studies to date (Quail and Joyce, 2017; van Bree and Wilhelm, 2022). However, a recent study by Trombetta-Lima *et al.,* was the first to establish the ECM signatures of medulloblastoma and glioblastoma, by comparing the proteome of decellularised patient tumours to normal cerebellum and isocortexes, respectively (Trombetta-Lima *et al.*, 2021). Both malignancies exhibited distinct ECM signatures compared to their respective control tissues, as well as to each other, indicating that the tumour ECM is highly relevant in brain tumours (Figure 1.10 A).

The medulloblastoma ECM signature was shown to consist of 19 differentially regulated ECM proteins (15 upregulated and 4 downregulated). Of the 15 ECM proteins identified to be upregulated in medulloblastoma, 5 were collagens, 8 were ECM glycoproteins and 2 were proteoglycans, as summarised in Figure 1.10 B. These findings were then validated by immunohistochemical staining of patient tissue microarrays (TMAs) and analysis of genomic medulloblastoma patient data (Cavalli dataset) (Cavalli *et al.*, 2017). The latter demonstrated that the expression of several of the medulloblastoma ECM signature proteins was especially enriched in the WNT and SHH medulloblastoma sub-groups, indicating that the tumour ECM may be particularly important in the progression of tumours from these sub-groups.

A



B

ECM protein type	ECM protein
Collagens	Type-I collagen alpha 1 chain (COL1A1)
	Type-V collagen alpha 1 chain (COL5A1)
	Type-V collagen alpha 2 chain (COL5A2)
	Type-VI collagen alpha 1 chain (COL6A1)
	Type-VI collagen alpha 2 chain (COL6A2)
	Type-VI collagen alpha 3 chain (COL6A3)
Proteoglycans	Lumican (LUM)
Glycoproteins	Elastin Microfibril Interfacer 1 (EMIL1)
	Latent-Transforming Growth Factor Beta-Binding Protein 4 (LTBP4)
	Elastin (ELN)
	Fibulin (FBLN1)
	Fibrillin 1 (FBN1)
	Fibrillin 2 (FBN2)
	Elastin Microfibril Interfacer 3 (EMIL3)
	Fibulin 5 (FBLN5)

Figure 1.10 Components of the medulloblastoma extracellular matrix signature. (**A**) Network analysis of proteins differentially regulated in medulloblastoma vs cerebellum (green boxes) and glioblastoma vs isocortexes (orange boxes). Proteins differentially regulated in both comparisons are in orange boxes with green borders. Red and blue boxes indicate if the proteins are up or down regulated compared to control tissue, respectively. Taken from Trombetta-Lima *et al.* (**B**) Table of the extracellular matrix proteins identified to be upregulated in medulloblastoma tumours by Trombetta-Lima *et al*.,. MED: medulloblastoma. GBM: glioblastoma.

Although the Trombetta-Lima study has greatly enhanced our understanding of the medulloblastoma ECM, there are limitations to these findings. Firstly, the ECMs of only 5 patient tumours were analysed in the study and their sub-groups were not reported, meaning that the full spectrum of medulloblastoma ECM components, as well as inter-/intra-sub-group heterogeneity, was not identified. In addition, no association between the expressions of the medulloblastoma ECM signature proteins and patient outcome was made, leaving the role of the tumour ECM in medulloblastoma progression unclear. A recent study by our group, however, examined the gene and protein expression of ECM components in medulloblastoma, by analysing genomic patient data (the same dataset analysed in the Trombetta-Lima study) and patient TMAs (comprising >40 patients) respectively (Linke *et al.*, 2020). From this analysis, the Linke study identified ECM sub-types within the medulloblastoma sub-groups, defined by the expression of specific ECM components. Furthermore, these sub-types were shown to be predictive of patient prognosis in SHH, Group 3 and Group 4 medulloblastoma (Linke *et al.*, 2020).

Two of these sub-types were defined by either high or low expression of both the laminin α1 (*LAMA1*) and α2 (*LAMA2*) subunits, in addition to the decreased expression of vitronectin (*VTN*), in SHH and Group 4 medulloblastoma; these ECM sub-types were termed LAM^{high}/VTN^{low} and LAM^{low}/VTN^{low}. In the SHH sub-group, LAM^{high}/VTN^{low} patients were found to have a more favourable overall survival, whereas the LAM^{low}/VTN^{low} patients had a much poorer overall survival, as displayed in Figure 1.11. Conversely, Group 4 patients exhibited the opposite trend in survival; LAM^{high}/VTN^{low} patients had a poorer overall survival, whereas LAM^{low}/VTN^{low} patients had a much better overall survival. LAM^{high}/VTN^{high} and LAM^{low}/VTN^{high} ECM sub-types were also identified in the Group 4 patients (Figure 1.10). However, the expression of vitronectin negated the differential effect of *LAMA1* and *LAMA2* expression on patient survival. In the SHH sub-group all tumours were identified as VTN^{low}. Therefore, for simplicity, the

LAM^{high}/*VTN*^{low} and *LAM*^{low}/*VTN*^{low} medulloblastoma ECM sub-types are referred to as *LAM*^{high} and *LAM*^{low} respectively throughout this study. These findings demonstrated the importance of the specific composition of the tumour ECM on the survival of SHH and Group 4 medulloblastoma patients. The aim of this thesis is to further elucidate the molecular mechanisms underpinning this finding.

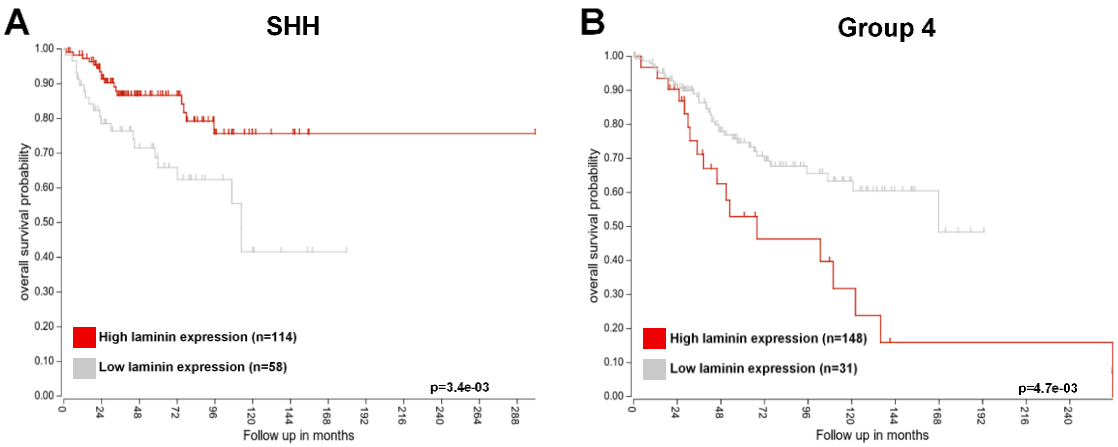


Figure 1.11 High Laminin Subunit α1 (*LAMA1*) / Laminin Subunit α2 (*LAMA2*) expression significantly correlates with overall patient survival in SHH (A) and Group 4 (B) medulloblastoma patients. Adapted from *Linke* et al., 2020.

1.8 Hypothesis and aims

As discussed, high *LAMA1*/*LAMA2* expression has been shown to significantly correlate with a more favourable overall survival in SHH medulloblastoma patients and worse overall survival in Group 4 patients. However, the molecular mechanisms which potentiate this effect remain unknown.

We hypothesised that the expression of *LAMA1/LAMA2* differentially modulates molecular mechanisms in SHH and Group 4 medulloblastoma, which convey a less aggressive phenotype in the former and a more aggressive phenotype in the latter.

The aims of this study were to:

1) Identify molecular drivers of *LAM*^{high} SHH and Group 4 medulloblastoma through the analysis of a large scale genomic medulloblastoma dataset (Cavalli dataset) and validate these *in vitro*.

2) Create a LAMA1/LAMA2 knockout in SHH and Group 4 medulloblastoma cell lines, to assess if aspects of tumour progression, such as cellular migration, invasion, apoptosis evasion and therapy resistance, are affected by LAMA1/LAMA2 expression, using 3D cell culture models.

3) Unravel LAMA1/LAMA2's effect on global protein expression in SHH and Group 4 medulloblastoma by conducting proteomic analysis of knockout cell lines in 2D and 3D culture models.

Chapter 2: Materials and Methods

2.1 Analysis of publicly available genomic patient datasets

In this study three publicly available gene expression array datasets (Cavalli and Pfister (medulloblastoma) and Roth (normal cerebellum)) were accessed and analysed using the R2: Genomics Analysis and Visualisation Platform (http://r2.amc.nl) (R2) (Roth *et al.*, 2006; Cavalli *et al.*, 2017; Northcott *et al.*, 2017).

2.1.1 Analysing gene expression in groups

In order to analyse the expression of genes in groups within a dataset (e.g. the medulloblastoma sub-groups) the 'View a Gene in Groups' function was used in R2. To assess gene expression in groups between datasets the R2:MegaSampler tool was also used. All data was then exported to GraphPad Prism® (version 9.4.1), where significant differences in gene expression between groups was calculated using a Kruskal-Wallis test with Dunn's multiple comparisons.

2.1.2 Gene expression-based survival analysis

To conduct gene expression-based survival analysis on the Cavalli dataset, Kaplan-Meier curves, based on the expression of a gene of interest, were initially generated using the R2:KaplanScan tool. The R2:KaplanScan tool determines the most statistically significant cut-off for survival analysis based on gene expression data. This is achieved by splitting the dataset into two groups (minimum of 8 samples per group) based on the expression of a gene of interest ('high' and 'low' expression groups). Starting with the 8 samples with the lowest level of gene expression versus the rest of the samples in the dataset, the R2:KaplanScan then uses every increasing expression value as a new cut-off to create two groups and determine the statistical significance of the difference in survival between them in a logrank (Mantel–Cox) test. The two

groups which yield the most significant p-value are then returned with a Kaplan Meier curve.

2.1.3 Differential gene expression analysis

To conduct differential gene expression analysis on the Cavalli dataset, the results of the R2:KaplanScan (described above) were used to create a 'track' via the 'save as track' function, whereby each patient is labelled as having 'high' or 'low' gene expression, depending on the group in which they were placed by the R2:KaplanScan. Differential gene expression analysis was then conducted between patients with 'high' and 'low' expression of the gene of interest using the 'Differential Expression Between Two Groups' tool in R2. The statistical test used in the analysis was a One-Way ANOVA (after the data had undergone a Log2 transformation) with an uncorrected p-value and a q-value (a p-value adjusted using the Benjamini-Hochberg False Discovery Rate (FDR) approach) to correct for multiple testing.

For Table 3.1 and Figure 3.4 the tracks defined in a previous study by our lab (LAM^{high}/VTN^{low} and LAM^{low}/VTN^{low}) were used for differential gene expression analysis within the SHH (LAM^{high}/VTN^{low}: n=114; LAM^{low}/VTN^{low}: n=58) and Group 4 (LAM^{high}/VTN^{low}: n =31; LAM^{low}/VTN^{low}: n=148) sub-groups (Linke *et al.*, 2020). For all other analyses only patients from SHH sub-group (n=223) were used to create 'tracks' and conduct differential gene expression analysis.

2.2 Differential gene expression analysis of mRNA sequencing data

Analysis of an mRNA sequencing dataset of SHH patient derived cell lines (DAOY and ONS-76) grown on top of hyaluronan hydrogels with and without laminin (laminin-111),

was used in this study. Differential gene expression analysis between the laminin conditions for each cell line was achieved by initially calculating Log2 fold changes in gene expression between conditions. Significant differences in gene expression were then calculated by a One-Way ANOVA with an uncorrected p-value and a q-value (p-values adjusted utilising the Benjamini-Hochberg False Discovery Rate (FDR) approach). All data was collected and analysed by Dr Franziska Linke, a previous post-doctoral researcher in Dr Coyle's group.

2.3 Gene expression analysis of scRNAseq data

Single cell RNA sequencing (scRNAseq) data of ONS-76 SHH medulloblastoma cells grown in a hyaluronan hydrogel was analysed in this study using Loupe Browser 5 (https://www.10xgenomics.com/products/loupe-browser). In order to identify the number of cells which expressed a gene of interest, a filter for each gene of interest, with a threshold of expression of > 0, was generated. The number of cells which were identified to express the gene was then divided by the total number of cells in the dataset to calculate the percentage of cells which expressed the gene.

2.4 Identifying overlapping genes across multiple datasets

In order to identify genes present in multiple (up to 4) datasets the online using the online bioinformatics software Venny 2.1 (https://bioinfogp.cnb.csic.es/tools/venny/) was used. Lists of genes were pasted into 'List' boxes within the software and a Venn diagram was generated. Overlapping genes were then identified by clicking on the overlapping section of the Venn diagram.

2.5 Standard tissue culture methods

2.5.1 Cell maintenance

Four medulloblastoma cell lines were utilised in this study. Their clinical information and specific culture methods are listed in Table 2.1. All cell lines were cultured at 37°C and 5% CO_2 in a humidified incubator (New Brunswick, Galaxy 170R). Cell lines were passaged at 70-80% confluence.

2.5.2 Maintaining adherent cell lines

Adherent cell lines were passaged by aspirating media off the cells and washing them once with Hank's Balanced Salt Solution (HBSS; Gibco, 14170). The cells were subsequently detached by incubating with 2 mL 1 X Trypsin-etheylenediaminetetraacetic acid (EDTA) in the T75 flask (Sigma, LH-SIG2044) for 5 minutes at 37°C. Trypsin was then inactivated by the addition of double the volume of appropriate growth media. Detached cells were then removed from the flask and centrifuged at 123 x g for 5 minutes in a 50 mL tube. After discarding the supernatant, the cell pellet was resuspended in appropriate growth media and split at a ratio of 1:2-1:30 (depending on the doubling time of the cell line) into a standard treated T-75 tissue culture flask (Corning, 430641U), containing the appropriate pre-warmed growth media.

2.5.3 Maintaining suspension cell lines

Suspension cell lines (CHLA-01 and CHLA-01-R) were subcultured in non-treated T-75 tissue culture flasks (Eppendorf; 0030711025) by aspirating certain volumes of cell suspension (e.g. half or a third) and replacing it with appropriate fresh growth media.

Aspirated cell suspension was either discarded or used to expand the cell lines into more flasks. Once a week the entire cell suspension was centrifuged in a 50 mL tube at 123 x g. Two thirds of the supernatant was removed and replaced with appropriate growth media. The cell suspension was then decanted into a new non-treated tissue culture flask (Eppendorf; 0030 710.029).

Table 2.1 Medulloblastoma cell lines used in this study with clinical and cell culture information.

Cell Line	Sub-group	Sub-type	Metastatic stage	Clinical information	Growth type	Flask Type	Source	Reference
DAOY	**SHH**	Putative SHH α	Non-metastatic (M0)	4-year-old male. *TP53* mutated cerebellar medulloblastoma of posterior fossa.	Adherent	Cell culture treated	ATCC®HTB-186™	Jacobsen *et al*., 1985
ONS-76		Putative SHH β	Metastatic tumours present at the right prepontine cistern (M2)	2-year-old female. Large midline cerebellar medulloblastoma.	Adherent	Cell culture treated	Annette Künkele (Charité Universitätsmedizin, Berlin)	Tamura *et al*., 1985
CHLA-01-MED	**Group 4**	n/a	Non-metastatic primary tumour (M0)	8-year-old male. Cerebellar tumour with leptomeningeal dissemination.	Suspension	Non-treated	Professor Geoff Pilkington (University of Portsmouth, UK)	Xu *et al*., 2015
CHLA-01-R-MED		n/a	Metastatic recurrence 8 months after diagnosis (M3)	Matched pair to CHLA-01. Recurrent metastatic cells from pleural fluid.	Suspension	Non-treated		

2.5.4 Tissue culture media

Information regarding the culturing media for each of the cell lines used in this study can be found in Table 2.2 below.

Table 2.2 Composition of cell culture media used for each cell line in this study

Cell Line	Media
DAOY	Dulbecco's Modified Eagle Medium (DMEM) + 10% FBS
ONS-76	Roswell Park Memorial Institute (RPMI) 1640 Medium + 10% FBS
CHLA-01-MED	DMEM-F12 + B27 (Gibco 17504044) + 20 ng/mL recombinant human basic fibroblast growth factor (FGF; Gibco, PHG0266) + 20 ng/mL recombinant human epidermal growth factor (EGF; Gibco, PHG0315)
CHLA-01-R-MED	

2.5.5 Cell counting

To count adherent cell lines, cells were detached and decanted into a 50 mL tube as previously described. 10 µL of the cell suspension was removed and mixed at a 1:1 ratio with Trypan Blue (Sigma-Aldich T8154). 10 µL of this solution was then applied on to a Neubauer Counting Chamber (VWR; 718605) with an affixed coverslip. Viable (clear) cells on each corner square were counted. This number was then used to calculate the number of viable cells/mL within the cell suspension, using the below equation:

Cells per mL= (Average cells per square) x (Dilution factor: 2) x (1×10^4)

To count suspension cells, 3 – 5 mL of cell suspension was decanted into a 50 mL tube and centrifuged at 123 x g for 5 minutes. The supernatant was removed and resultant pellet was resuspended in 1 mL of accutase (Sigma; A6964) and incubated for 10 minutes at room temperature, in order to disaggregate cells. Cells were then pipetted up and down several times to ensure that cells were fully disaggregated, before being counted as described above. The calculated cells/mL was then divided by the number of mL of cell suspension taken from the original flask.

2.5.6 Preparation of cell line stocks and cell storage

To store stocks of cells for long periods of time, cells were detached from a confluent flask as previously described and centrifuged at 123 x g for 5 minutes. Cell lines were then resuspended in CELLBANKER® 2 cryopreservation media (AMS Biotechnology Ltd., 11891) at a concentration of 1 x 10^6 cells/mL. The cell suspension was then aliquoted into 0.5 mL FluidX tubes (Brooks Life Sciences, 68-0703) and transferred to the -80 °C freezer. The cryovials were subsequently transferred into liquid nitrogen for long-term storage (Brooks; BioStore™III cell storage system).

2.5.7 Recovering cell lines from frozen stocks

To recover cells from frozen stocks, cryovials containing cell suspension were placed into a 37 °C water bath and closely monitored until they had thawed. They were then immediately removed from the cryovials and added to a 50 mL tube containing 10 mL of warmed media. The cell suspension was then centrifuged at 123 x g for 5 minutes. The supernatant was discarded, and the cell pellet was resuspended in 12 mL of warmed media, which was then transferred into a cell culture treated T-75 cell culture flask. Suspension cell lines were resuspended in 5 mL of warmed media and placed into a non-treated T-25 flask.

2.5.8 Preparation of cell pellets and supernatants for molecular analysis

To form cell pellets for molecular analysis, cells were detached as previously described and centrifuged at 200 x g for 5 minutes. The supernatant was removed, and the pellet was resuspended in 1 mL HBSS in order to remove any remaining fetal bovine serum (FBS). The cell suspension was then transferred into a 1.5 mL microcentrifuge tube and centrifuged again at 200 x g for 5 minutes. The supernatant was again removed, and the remaining cell pellet was then snap frozen in a dewar of liquid nitrogen. The cell pellets were then removed from liquid nitrogen and placed into -80 °C storage.

Supernatants for zymography analysis were harvested from either cells seeded into 6 well plates or pooled from cells seeded into 3D hydrogels/spheroids of the same condition and placed into a 1.5 mL microcentrifuge tube. Supernatants were centrifuged at 1000 x g to remove any remaining cells or cellular debris. The supernatant was then decanted into a fresh 1.5 mL microcentrifuge tube which was split into 30 µL aliquots before being snap frozen in liquid nitrogen as previously described.

2.5.9 Mycoplasma testing

All cell lines in this study were tested for the presence of mycoplasma after recovery and then once a month post-recovery. To detect mycoplasma contamination, media that had been in contact with the cell lines for a minimum of 3 days was tested using the MycoAlert Mycoplasma Detection Kit (Lonza, LT07-118), following the manufacturer's instructions.

2.6 Generation and validation of CRISPR-Cas9 knockout cell lines

The Horizon Discovery® Cas9 nuclease mRNA and Edit-R predesigned synthetic single guide RNA (sgRNA) system was used generate stable CRISPR-Cas9 knockout SHH medulloblastoma cell lines. In this system cells are co-transfected with a Cas9 nuclease mRNA that is fused to a fluorescent reporter gene, as well as 1 or more synthetic sgRNAs. After co-transfection, cells expressing the reporter gene are then identified and isolated by fluorescence-activated cell sorting (FACS). Clonal cell lines are then propagated from individual or multiple fluorescent cells. Gene knockouts are then validated in these cell lines by DNA mismatch detections assays and Sanger Sequencing of the sgRNA(s) target site, as well as western blotting of the protein(s) of interest.

2.6.1 Co-transfection of DAOY and ONS-76 medulloblastoma cell lines with Cas9 nuclease-EGFP mRNA and synthetic sgRNAs

DAOY and ONS-76 SHH medulloblastoma cell lines were co-transfected with a Cas9 nuclease-EGFP mRNA (Horizon; CAS11860), as well either both *LAMA1* and *LAMA2* Edit-R® predesigned synthetic sgRNAs (Horizon; SG-012118-01-0002 and SG-011070-01-0002, respectively) or a non-targeting Edit-R® synthetic sgRNA (Horizon; U-009501-01-02). The sequence of each sgRNA can be found in Table 2.3.

Preceding co-transfection, the Cas9 nuclease-EGFP mRNA was thawed on ice and the synthetic sgRNAs were resuspended 10 µL of 10 mM Tris-HCL buffer pH 7.4 (Horizon; B-006000-100). Co-transfection of cell lines was then conducted using a Nucleofector® II Device (Lonza; AAB-1001) with the corresponding Cell Line Nucleofector™ Kit V (Lonza; VCA-1003), following the manufacturer's instructions. 1 x 10^6 cells were used in each co-transfection, in which the Nucleofector® II

electroporation programme X-001 was used. Prior to the electroporation stage of the protocol, both the Cas9 nuclease-EGFP mRNA and sgRNAs were added to cells suspended in electroporation buffer, to a final concentration of 0.05 µg/µL and 5 µM, respectively. After co-transfection, cells were immediately seeded into a T-25 cell culture flask containing pre-warmed medium and incubated overnight.

Table 2.3 Product code and sequence of the single guide RNAs (sgRNAs) used in this study.

Single guide RNA (sgRNA)	Product code	Sequence
LAMA1	SG-012118-01-0002	ACTGGCTCCCAAGTACTACT
LAMA2	SG-011070-01-0002	AGTCACAGAGATTGCAGCGA
Non-targeting	U-009501-01-02	GATACGTCGGTACCGGACCG

2.6.2 Fluorescence-activated cell sorting (FACS) of transfected cell lines

The day after cells had been co-transfected with Cas9 nuclease-EGFP mRNA and sgRNAs (as described in the previous section), fluorescent cells expressing EGFP were identified and isolated by FACS. To achieve this, co-transfected cells, as well as untransfected negative control cells, were initially detached by trypsinisation and centrifuged at 123 x g (as previously described), before being resuspended in 1 mL of appropriate cell culture medium. Cells were then transported to the University of Nottingham Flow Cytometry Facility in a 1.5 mL tube, where FACS was conducted using a Beckman Coulter Astrios EQ cell sorter (Beckman Coulter). Untransfected negative control cells initially underwent FACS in order to establish the threshold of autofluorescence for each cell line. Using these thresholds, EGFP positive co-transfected cells were then identified and isolated, before being seeded into a 96 well plate (at a 1 or 10 cells/well seeding density) or back into a 1.5 mL tube (these cells were used to make cell stocks of the whole co-transfected cell populations).

All FACS and related analyses was conducted by Dr David Onion or Nicola Croxall, staff at the University of Nottingham Flow Cytometry Facility.

2.6.3 DNA mismatch detection assay

In order to rapidly detect insertion/ deletion mutations (INDELs) at the *LAMA1* and *LAMA2* sgRNA targets sites in co-transfected cells, DNA mismatch detection assays were conducted using a T7 Endonuclease I Assay Kit (GeneCopeia™; IC006). A detailed explanation of how a DNA mismatch detection assay works can be found in section 4.4.1. The first step of the DNA mismatch detection assay was to amplify the sgRNA target site of interest by polymerase chain reaction (PCR) from genomic DNA (gDNA) isolated from either total co-transfected cell populations or clonal cell lines (details of gDNA isolation methodology can be found in section 2.12.2). PCR reactions were conducted in a 0.2 mL PCR tube and comprised 17 µL iQ™ SYBR® master mix (Bio-Rad; 1708880), 1.5 µM of forward and reverse primer (Eurofins), 50 ng of gDNA and nuclease-free H_2O to a final volume of 20 µL. The PCR was then conducted in a Techne TC-512 Thermocycler using the following programme: 5 minutes at 94 °C, 35 cycles of: 30 seconds at 94 °C, 30 seconds at 60 °C and 1 minute at 72 °C, and then finally 72 °C for 5 minutes. The *LAMA1* and *LAMA2* primer pairs used in these reactions were specifically designed so that sgRNA target site was offset from the centre of the PCR product by approximately 100 bp, this was to ensure that different sized fragments were formed if the PCR product was cleaved by T7 endonuclease and could therefore be observed on an agarose gel. The sequence of these primers can be found in Table 2.4. Positive control DNA (containing two different mismatched sequences and therefore guaranteed to be cleaved by T7 endonuclease I) was also amplified using the same PCR protocol outlined above. This PCR product was used in the downstream steps of the protocol, to ensure that the assay had worked correctly. Positive control DNA and the corresponding primers were provided in the T7

Endonuclease I Assay Kit. Once the sgRNA target site had been amplified, the PCR products were briefly mixed and then heated for 5 minutes at 95 °C, before being cooled to room temperature for 10 minutes. Then, 1 µL of 2 U/µL T7 Endonuclease I was added to each PCR product, which were then incubated at 37 °C for 45 minutes. In order to assess if T7 Endonuclease I cleavage had occurred, and therefore INDELs were present, 10 µL of the enzyme treated PCR products was analysed by agarose gel electrophoresis (details of agarose gel electrophoresis methodology can be found in section 2.12.6). If three DNA bands, instead of one, were detected then this indicated that there were INDELs present at sgRNA target site of the gene of interest.

Table 2.4 Sequence of primers used in DNA mismatch detection assays and Sanger Sequencing of Laminin Subunit α1 (*LAMA1*) and Laminin Subunit α2 (*LAMA2*) single guide (sgRNA) target sites.

Primer	Forward/Reverse	Sequence (5' to 3')
LAMA1 DNA mismatch detection	Forward	AAGCAGGGGGCAACGAAGAA
	Reverse	TCACCAAACACACTGCTCAGGA
LAMA2 DNA mismatch detection	Forward	TGTCAGCAGCACATACCTTACAAGT
	Reverse	AAAAACCCATACCCAGCCCCTC
LAMA1 amplification for Sanger Sequencing	Forward	AAGCAGGGGGCAACGAAGAA
	Reverse	TCACCAAACACACTGCTCAGGA
LAMA2 amplification for Sanger Sequencing	Forward	CACCCCTCCCAGATTGTCCT
	Reverse	TACCCAGCCCCTCTCTACCT
LAMA1 Sanger Sequencing (nested)	Forward	AGGGTCATGAGGTTCAGC
LAMA2 Sanger Sequencing (nested)	Forward	GCAGTGTTTATCGGTATG

2.6.4 Sanger Sequencing of *LAMA1* and *LAMA2* single guide RNA (sgRNA) target sites and INDEL characterisation

The *LAMA1* and *LAMA2* sgRNA targets sites in clonal cell lines were Sanger Sequenced and analysed, in order to fully characterise the INDELs present.

2.6.4.1 Sanger Sequencing

LAMA1 and *LAMA2* sgRNA targets sites were initially amplified by PCR from gDNA of clonal cell lines. Reactions for each sample were conducted in a 0.2 mL PCR tube and comprised 17 µL iQ™ SYBR® master mix (Bio-Rad; 1708880), 1.5 µM of forward and reverse primer (Eurofins), 50 ng of gDNA and nuclease-free H_2O to a final volume of 20 µL. The PCR was then conducted in a Techne TC-512 Thermocycler using the following programme: 5 minutes at 94 °C, 35 cycles of: 30 seconds at 94 °C, 30 seconds at 60 °C and 1 minute at 72 °C, and then finally 72 °C for 5 minutes. The primers used in this reaction flanked the sgRNA target site by at least 200 base pairs (bp) and were designed following the protocol outlined in a paper by Xie, Ma and Liu (Xie, Ma and Liu, 2019). The sequence of these primers can be found in Table 2.4.

Once the sgRNA targets sites had been amplified, the PCR products were then purified using the ExoSAP-IT™ Express PCR Product Cleanup kit (ThermoFisher; 75002), following the manufactures instructions. The purified PCR products were then taken to the University of Nottingham Deep Seq facility for Sanger Sequencing, using a 3130xl ABI PRISM Genetic Analyser (Life Technologies). The sequence of the nested forward primers used for Sanger Sequencing of *LAMA1* and *LAMA2* are also displayed in Table 2.4. These primers were designed to be between 150 and 300 bp upstream of the sgRNA target site and were also designed using the protocol outlined protocol outlined in the paper by Xie, Ma and Liu (Xie, Ma and Liu, 2019).

All Sanger Sequencing was conducted by Matthew Carlile, a staff member at the University of Nottingham Deep Seq facility.

2.6.4.2 INDEL detection analysis of Sanger Sequencing data

To identify the position and sequence of INDELs in each allele of *LAMA1* and *LAMA2* in each clonal cell line, Sanger Sequencing chromatograms were analysed using the online INDEL discovery tool 'Indigo' (https://www.gear-genomics.com/indigo/). The *LAMA1* and *LAMA2 c*hromatograms were uploaded individually to Indigo using the 'Chromatogram file upload' function. The corresponding wild-type chromatogram was also uploaded using the 'Align to' function. The analysis was then run by clicking the 'Launch Analysis' button. All results were then exported to a PDF file, which was then manually assessed for INDELs.

2.6.5 Translating Sanger Sequencing data into an amino acid sequence and alignment to wild-type sequences

The effect of INDELs on the amino acid sequence of LAMA1 and LAMA2 was determined by initially translating the *LAMA1* or *LAMA2* nucleotide sequences, obtained from Sanger Sequencing of the clonal cell lines, into amino acid sequences, using the Expasy online DNA/RNA translation tool (https://web.expasy.org/translate/). This was achieved by copy and pasting the nucleotide sequence into the translation tool and clicking the 'TRANSLATE!' button. The results of this were then exported to a Microsoft Word document. Amino acid sequences were then aligned to the corresponding wild-type amino acid sequence, using the online multiple sequence alignment tool, Clustal Omega (https://www.ebi.ac.uk/Tools/msa/clustalo/). To do this, the clonal cell line and wild-type LAMA1 or LAMA2 amino acid sequences were both copy and pasted both into the alignment tool, separated by a line, and the 'Submit'

button was pressed. The results of this analysis were then also exported to a Microsoft Word document, where they were then manually assessed.

2.7 2D tissue culture assays

2.7.1 2D laminin assays

In the 2D laminin assays, cell lines were seeded onto uncoated and laminin-coated wells of a 6 well plate (Greiner; 657160). After being incubated for 48 hours both the cell pellet and supernatant were harvested for molecular analysis. In order to coat the wells of a 6-well plate with laminin, a 10 µg/mL laminin solution was created by adding 10 µL of a 1 mg/mL laminin-111 (Sigma®, L4544) stock to 1 mL of HBSS (with Ca^{2+} and Mg^{2+} to promote laminin adhesion) (Gibco®, 14025092). The laminin solution was then added to the appropriate wells of the plate, which was then sealed and incubated at 4 °C overnight. The next day the laminin solution was removed, and the laminin-coated wells were washed twice with 1 mL of standard HBSS.

To seed the cells into the plate they were detached and counted as previously described. The quantity of cells required (100,000 cells per well for adherent cell lines and 500,000 cells per well for suspension cell lines) was centrifuged in a 50 mL tube for 5 minutes at 123 x g. The cell pellet was then resuspended in 2 mL of the appropriate media and added to the well. After 48 hours the supernatant and cell pellet were harvested as previously described.

2.8 Transwell® migration and invasion assays

The migration and invasion of cell lines was assessed using modified Boyden chamber assays in 24 well plates (previously optimised by Dr Macha Aldighieri, a former PhD student in Dr Beth Coyle's lab).

2.8.1 Migration assays

In the migration assays, cells were initially starved in 2% FBS media overnight. The next day, 1 x 10^5 cells were seeded into uncoated polycarbonate Transwell™ inserts with a pore diameter of 8 µm (Greiner Bio-One Thincert, 662638) in 100 µL of 0% FBS media. 600 µL of 10% FBS media was then added to the well below to create an FBS gradient to encourage cellular migration. The assay was then incubated for 48 hours at 37°C, 5% CO_2. Subsequently, the number of migrated cells in the bottom chamber of the assay was quantified relative to a standard curve (section 2.8.4) using PrestoBlue (ThermoFisher; A13262).

2.8.2 Invasion assays

The same method as the migration assay was used for the invasion assays apart from the insert was coated with Collagen IV (Cultrex 3410-010-01) diluted to 10 µg/mL in 50 µl of H_2O overnight prior to the assay. The purpose of this coating was to replicate the basement membranes that are present *in vivo* which brain tumours invade through. The inserts are also usually coated with laminin-111 (the other main ECM component of basement membranes), however, this step was omitted since the purpose of the assay was to determine how laminin produced by SHH cells affects their ability to invade.

2.8.3 Preparation of a standard curve

A standard curve of a known number of cells (ranging from 0 to 1 x 10^6) was prepared in triplicate for each biological replicate to quantify the number of migrated/invaded cells. Cells were resuspended in 1 X cell disassociation solution (CDS) (AMSBIO, 3455-096-05) and seeded into a 96 well black-walled plate (Greiner Bio-One, 655090). PrestoBlue was then added to each of the wells at a concentration of 1:10 and incubated for 1 hour at 37°C, 5% CO_2 after which the excitation of each well was measured at 586 nm in a Fluorostar Omega plate reader.

2.8.4 Quantifying the number of migrated and invaded cells

After incubating the migration and invasion assays for 48 hours, the non-migrated cells were removed from the top of the insert using a cotton swab. The media in the bottom well was then aspirated and replaced with 300 µL of 1 X CDS with PrestoBlue (ThermoFisher; A13262) diluted 1:10. This was then incubated for one hour at 37°C, 5% CO_2. Subsequently, the CDS/PrestoBlue solution was transferred to a 96 well black-walled plate (Greiner Bio-One, 655090) in triplicate (100 µL in 3 wells per insert). The excitation of each well was measured at 586 nm in a Fluorostar Omega plate reader. All readings were exported to Microsoft Excel and were used to calculate the number of migrated/invaded cells against the standard curve.

2.9 HyStem™ hyaluronan based hydrogel cell culture

In this study, cells were seeded within HyStem™ hyaluronic acid based hydrogels (Advanced BioMatrix, GS310) to specifically recapitulate the brain ECM and stiffness (optimised by Dr Franziska Linke, Postdoctoral research fellow in Dr Beth Coyle's group). HyStem™ hydrogels are composed of two components: thiol modified

hyaluronan (Glycosil®) and a thiol reactive cross linker (Extralinker®). When mixed, the crosslinker facilitates the gelification of the hyaluronan solution (Figure 2.1).

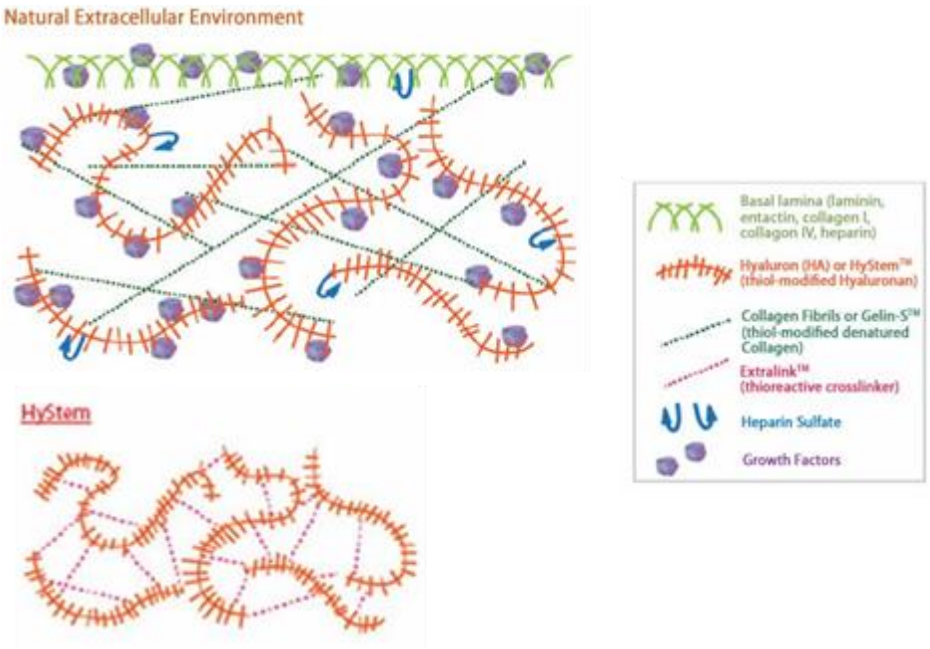


Figure 2.1 Diagram illustrating the components and structure of HyStem® hydrogel compared with native extracellular matrix. In the *in vivo* extracellular matrix , hyaluronan is interconnected by collagen fibrils and bound by heparin sulfate as well as growth factors. In the Hystem hydrogel, hyaluronan forms a similar matrix, but is interconnected by Extralink™ instead of collagen.

2.9.1 Preparation of HyStem™ hydrogels

To prepare the hydrogels, degassed water, lyophilised Glycosil® and lyophilised Extralinker® were initially removed from -20 °C storage and thawed at room temperature for 1 hour. Using a 1 mL syringe and needle, 1 mL of degassed water was then added to the lyophilised Glycosil® and put on a Stuart Tube Roller (Stuart, LAB123) in a 50 mL tube at room temperature for 30 minutes, to allow it to fully dissolve. Meanwhile, also using a syringe, 0.25 mL of degassed water was added to the lyophilised Extralinker® and inverted several times to dissolve. The Glycosil® and Extralinker® solutions were then removed from their respective vials and decanted into separate microcentrifuge tubes to make a stock of each solution.

To then embed cells within the hydrogel, a 100 µL hydrogel was formed in three stages in a well of a 96 well plate: the bottom gel (30 µL), the middle gel with encapsulated cells (40 µL) and the top gel (30 µL). To form each section of the hydrogel, Extralinker® and Glycosil® were mixed at a ratio of 1:5 respectively to make gelling solution that was pipetted into the 96 well plate. This method formed hydrogel with Glycosil® and Extralinker® concentrations of 1% and 2% respectively, resulting in a matrix stiffness of 1.5-2 kPa, similar to that of brain tissue. At this stage, recombinant laminin-111 (Sigma®) was also added to some of the gels at a concentration of 1:60. After pipetting each section of the hydrogel into the wells, the plate was centrifuged at 1500 rpm for 1 minute, to ensure that each section of the gels was level, and was then allowed to set for at least 30 minutes in a 37 °C incubator. To seed the cells into the middle layer they were detached and counted as previously described. The quantity of cells required (10,000 cells per gel for adherent cell lines and 50,000 cells per gel for suspension cell lines) was then collected and centrifuged in a microcentrifuge tube for 5 minutes at 123 x g. The cell pellet was then resuspended in the appropriate volume of Glycosil® solution and mixed with Extralinker®, before being pipetted into the 96 well plate, on top of the bottom layer of hydrogel. Once the top layer had set, 100 µL of appropriate media was added to each of the wells. 200 µL of HBSS was also pipetted into the outermost wells of the plate to reduce evaporation of medium throughout the plate. To maintain cells every 2/3 days half of the media was aspirated and replaced with fresh growth medium.

2.10 Spheroid culture

All spheroid culture, assays and analysis methodologies were previously optimised by Dr Sophie Roper, a former PhD student in Dr Beth Coyle's lab (Roper and Coyle, 2022).

2.10.1 Neurosphere media

All spheroids were cultured in Neurosphere medium, which was composed of DMEM/F-12, 2% B-27 supplement, 1% N-2 supplement (Gibco, 17502048), 2 µg/mL Heparin (Stem Cell Technologies, 07980), 20 ng/mL epidermal growth factor (EGF), and 10 ng/mL basic fibroblast factor (bFGF). Fresh neurosphere medium stored for up to 3 days at 4 °C.

2.10.2 Spheroid generation and maintenance

Only the SHH medulloblastoma DAOY and ONS-76 cell lines were used in the spheroid assays in this study. In order to generate spheroids, cells were grown under standard tissue culture conditions until they reached approximately 70% confluency. Cells were then detached, as previously described, and centrifuged at 123 x g for 5 mins, before being resuspended in 3 mL of neurosphere medium. Cells were then counted and seeded into a 96 well Ultra Low Attachment (ULA) plate (Corning, 7007) in a total volume of 200 µL of neurosphere medium. The DAOY cell line was seeded at a concentration of 250 cells/well and the ONS-76 cell line was seeded at a concentration of 200 cells/well. 200 µL of HBSS was pipetted into the outermost wells of the plate to reduce evaporation of medium throughout the plate. To maintain the spheroids, half of the media was aspirated and replaced with fresh growth medium every 3/4 days.

2.10.3 Assessing spheroid dimensions

To assess spheroid growth, images of the spheroids were captured using a Brunel Multiple Interface camera attached to a brightfield inverted microscope at 10 X magnification. The scale of the captured images was determined using a calibration slide. To measure the size of the spheroids a macro (developed by Ivanov et al., 2014)

for the software ImageJ was used. The macro automatically outlined the spheroid and from this calculated its area. If the macro was unable to accurately identify the outline of the spheroid it was instead done manually. This data was then exported to Microsoft Excel and was used to calculate the below dimensions of the spheroids:

Radius (r) = $\sqrt{A/\pi}$ **Diameter (d) = 2r** **Volume (v) =$4/3\pi r^3$**

2.10.4 2D and 3D Spheroid CellTiter-Glo® cell viability assay

To assess the viability of cells grown in 2D or spheroid cell culture, the CellTiter-Glo® 3D cell viability assay (Promega, G9683) was used. This is a luciferase based assay whereby cells are lysed and a luminescent signal is produced proportional to the amount of adenosine triphosphate (ATP) present in the sample; this is used as an indication of cell viability. To conduct the assay in 2D culture, cells were grown in a clear bottomed, black-walled 96-well plate (Greiner Bio-One, 655090) in 200 µL of media. At the relevant time point half of the media was aspirated and replaced with 100 µL of CellTiter-Glo® 3D cell viability reagent. In spheroid culture, the spheroids were firstly transferred from the ultra-low attachment plate (in which they were generated) into a black-walled 96-well plate (Greiner Bio-One, 655090) in 100 µL of media. 100 µL of CellTiter-Glo® 3D cell viability reagent was then added to the spheroids in each well. Both spheroid and 2D plates were then covered and incubated at room temperature for 30 minutes after which luminescence was measured using a FLUOstar Omega plate reader (BMG Labtech Ltd). All readings were then exported to Microsoft Excel where they were normalised to a blank (media) control.

2.10.5 Spheroid-HyStem™ hydrogel model

In spheroid-HyStem™ hydrogel experiments, spheroids were initially generated as outlined in 2.5.2 and cultured overnight. The next day, as much media as possible was then removed from each of the wells containing the spheroids in the 96 well ULA plate. The appropriate volume of HyStem™ hydrogel was then prepared as described in 2.4.1 and 50 µL was pipetted on top of the spheroids in order to embed them. The plate was then incubated at 37°C for 30 minutes to facilitate the setting of the gel. 100 µL of fresh neurosphere media was then added on top of each hydrogel. The volume and relative outgrowth of the embedded spheroids was then measured daily over a 4 day period by manual imaging. For some experiments in this study, this model was adapted in order to assess how different drugs affected the growth of spheroids. In these cases, the day after spheroids were embedded with the hydrogel (day 1) the spheroids were treated with 5 different concentrations of each drug, as well as a vehicle control. The relative outgrowth of the spheroids treated with drugs was then compared to those treated with the vehicle control in order to assess how the drug had affected the growth of the spheroids.

2.10.6 Spheroid-HyStem migration assay

In spheroid-HyStem™ migration assays spheroids were initially generated as outlined in 2.5.2 and cultured overnight. The next day 50 µL of hydrogel was pipetted into the wells of a cell culture treated 96 well plate, which was then incubated at 37 °C for 30 minutes to facilitate the setting of the hydrogel. Spheroids were then removed from ULA 96 well plate in which they were generated in 100 µL of media, which was then pipetted on top of the set hydrogel. Subsequently, another 100 µL of media was added to each of the wells. The migration (area) of the spheroids across the hydrogel was then measured daily over a 3 day period by manual imaging using a Brunel Multiple Interface camera attached to a brightfield inverted microscope at 10 X magnification.

2.11 Apoptosis assays

In order to assess the level of apoptosis in cells in standard cell culture conditions, or when cells had been treated with the BCL-2 small-molecular inhibitor ABT-737, a luminescent and a fluorescent apoptosis assay were used.

2.11.1 2D and 3D Spheroid Caspase-Glo® 3/7 Apoptosis Assay

To measure the level of apoptosis of cells grown in 2D and spheroid culture, the Caspase-Glo® 3/7 Apoptosis Assay (Promega, G8981) was used. This is a luciferase based assay whereby the Caspase-Glo® 3/7 Apoptosis Assay reagent, which contains a luminogenic caspase-3/7 substrate in lysis buffer, is added to cells. The lysis buffer lyses the cells and the luminogenic caspase-3/7 substrate is cleaved by caspase-3/7 activity in cells, producing a luminescent signal indicative of the level of apoptosis. The methodology of this assay is identical to that of the CellTiter-Glo® 3D cell viability assay (2.10.4) for both 2D and spheroid culture, except that 100 µL of Caspase-Glo® 3/7 Apoptosis Assay (Promega, G8981) reagent was added to 2D and spheroid cultures instead of CellTiter-Glo® 3D cell viability reagent. All readings were exported to Microsoft Excel where they were normalised to a blank (media) control and in drug assays readings were also normalised to a vehicle control.

2.11.2 2D and 3D Spheroid CellEvent™ Caspase-3/7 Green Detection Apoptosis Assay

To capture caspase-3/7 activity in live cells grown in 2D and spheroid cell culture, the CellEvent™ Caspase-3/7 Green Detection Apoptosis Assay was used (ThermoFisher, C10423). This is a fluorogenic assay whereby a DNA-binding dye, which is inactivated by a DEVD-peptide, is added to cells. The DEVD peptide is then specifically cleaved

by caspase-3/7 activity in apoptotic cells. The cleavage of the peptide then allows the dye to bind to DNA resulting in a bright, fluorescent emission (~520 nm) in the nuclei of apoptotic cells, which can then be imaged using fluorescent microscopy.

To conduct the assay in 2D culture, cells were grown in a black-walled 96-well plate (Greiner Bio-One, 655090) in 100 µL of media. At the relevant time point all media was aspirated and replaced with 100 µL of phosphate buffered saline (PBS) with 5% FBS, mixed with the CellEvent™ Caspase-3/7 Green Detection reagent to a final concentration of 6 µM. In spheroid culture, as much media as possible was removed from the wells of the ultra-low attachment plate in which the spheroids were generated and also replaced with 100 µL of PBS with 5% FBS mixed with the CellEvent™ Caspase-3/7 Green Detection reagent to final concentration of 6 µM. The plates were then incubated at 37 °C for 45 minutes before being imaged using the GFP channel (470/525 nm) of an EVOS M7000 fluorescent microscope (ThermoFisher). The number of apoptotic nuclei were then counted and used as an indication of the level of apoptosis. In drug-based assays the number of apoptotic nuclei was normalised to a vehicle control.

2.12 Drug Treatments

2.12.1 Drugs used in this study

Information regarding the drugs used in this study is displayed in Table 2.5.

Table 2.5 Details of the drugs used in this study

Drug	Stock Concentration	Vehicle	Product Details
Vincristine	100 µM	DMSO	Selleckchem, S1241
Cisplatin	10 mM	DMF	Selleckchem, S1166
ABT-737	10 mM	DMSO	Selleckchem, S1002

2.12.2 Drug response assays and IC_{50} calculation

Drug response assays were used in this study to assess the sensitivity of DAOY cells to vincristine, cisplatin and the small molecule BCL-2 inhibitor ABT-737 (Table 2.5). In these assays, 10,000 cells were seeded into the wells of clear bottomed, black walled 96 well plate (Greiner; 655096) in 100 µL of complete media and incubated at 37 °C and 5% CO_2 for 16 hours. Cells were then treated with a range of concentrations of the selected drug, as well as the highest concentration of the vehicle (in which the drug was dissolved), and incubated at 37 °C and 5% CO_2 for 3 days. CellTiter-Glo® (Promega; G9683) was then used to measure the viability of the treated cells, by adding 100 µL of CellTiter-Glo® reagent to each well and incubating at room temperature for 30 minutes as previously described, after which luminescence was measured using a FLUOstar Omega plate reader (BMG Labtech Ltd). All readings were then exported to Microsoft Excel.

These values were then used to calculate the half maximal inhibitory concentration (IC_{50}) of the drug. To achieve this, cell viability values were initially normalised to the blank (media) control, after which they were calculated as a percentage relative to cells treated with the vehicle control and exported to GraphPad Prism 8. After log

transformation, these values were then used to generate dose-response curves, and thus IC_{50} values, using non-linear regression analysis with a four-parameter dose-response equation. The IC_{50} values were used as an indication of how sensitive the cells were to the drug.

2.13 Molecular biology

2.13.1 RNA isolation

RNA was extracted from cell pellets as well as pooled spheroids and hydrogels that had been snap frozen (as previously described in section 2.1), using the NuceloSpin® RNA kit (Machery-Nagel) following the manufacturer's instructions. The concentration of the eluted RNA was then measured using a Nanodrop2000 spectrophotometer (Thermo Scientific) before being stored at -80 °C.

2.13.2 DNA isolation

DNA was extracted from cell pellets that had been snap frozen (as previously described in section 2.1) using the NuceloSpin® DNA kit (Machery-Nagel) following the manufacturer's instructions. The concentration of the eluted DNA was then measured using a Nanodrop2000 spectrophotometer (Thermo Scientific) before being stored at -20 °C.

2.13.3 Measuring the concentration and purity of RNA and DNA

The concentration and purity or RNA and DNA was measured using a Nanodrop2000 spectrophotometer. All samples were analysed by pipetting 2 µL of RNA/DNA on to

the lower pedestal and closing the sampling arm. The concentration of samples was then calculated from the absorbance of the sample at 260 nm. The 260/280 nm ratio of absorbance was used as an indication of RNA/DNA 'purity' (DNA ~1.8 / RNA ~2.0). Before use and between each sample read, the upper and lower pedestals were cleaned with nuclease free water. In order to remove background from readings elution buffer was read as a blank, prior to the analysis of RNA/DNA samples.

2.13.4 Complementary DNA (cDNA) synthesis

RNA, isolated from cell pellets as described in section 2.9.1, was converted to complementary DNA (cDNA) by cDNA synthesis for real-time quantitative reverse transcription PCR (qRT-PCR) analysis. To do this 2 µg of RNA from each sample was added to a 0.2 mL nuclease free PCR tube with nuclease-free water (Stratech Science; PCR-258L-JEN) to a final volume of 11 µl. 1 µl of deoxynuleoside triphosphates (dNTPs) mix (25 mM; Thermo Scientific; R1121) and 1 µl of random primers (3 µg/µL; Invitrogen; 48190011) was then added to each sample, which were subsequently incubated at 65 °C for 5 minutes and then on ice for 1 minute. After incubation, 1 µL of 0.1 M dithiothreitol (DTT) (0.1M; Invitrogen; 1080-044), 4 µl of 5 X First Strand Buffer (Invitrogen; 1080-044), 1 µl of RNaseOUT (Invitrogen; 10154652) and 1 µl Superscript III reverse transcriptase (Invitrogen; 1080-044), or 1 µl of dH_2O in the no reverse transcriptase control, was then added to each sample, to make a final volume of 20 µl. The reaction mix was then placed into a Techne TC-512 Thermocycler which ran the following programme: 25 °C for 5 minutes, 50 °C for 60 minutes, 70 °C for 15 minutes. After the programme had elapsed the newly formed cDNA was then stored at -20 °C.

2.13.5 Primer design

All primers used in this study were designed using NCBI primer blast (https://www.ncbi.nlm.nih.gov/tools/primer-blast/). The online tools OligoAnalzer (https://eu.idtdna.com/pages/tools/oligoanalyzer) and Oligonucleotide Properties Calculator (http://OligoCalc.com) were then used to determine the primers least likely to form hairpin structures.

2.13.6 Temperature gradient optimisation of primer pairs

To validate the specificity and optimise the annealing temperature of primer pairs a temperature gradient PCR (a PCR reaction where several different annealing temperatures are used) was conducted on control cDNA. Reactions for each annealing temperature were conducted in a 0.2 mL PCR tube and comprised 7.5 µL iQ SYBR master mix, 1.5 µM of forward and reverse primers (Eurofins), 50 ng of cDNA template and nuclease-free H_2O to a final volume of 15 µL. The PCR was then conducted in a Techne TC-512 Thermocycler with the following programme: 3 minutes at 95 °C, 40 cycles of 30 seconds at 94 °C then 1 minute at a range of annealing temperatures and finally 5 minutes at 72 °C. In order to determine the optimal annealing temperature of primers the PCR reactions were analysed by agarose gel electrophoresis (with ethidium bromide; section 2.13.7). From this it was ascertained which annealing temperature yielded the most product and was therefore the optimal annealing temperature for the primer pair. If, at any of the temperatures, products were present that were not at the predicted molecular weight, a different annealing temperature was used or the primers were redesigned. After the optimum annealing temperature had been identified the efficiency of the primer pair was assessed by a qRT-PCR (section 2.13.8) of a concentration gradient (ranging from 0.3125 to 5 ng/µL) of cDNA. The efficiency of the primer pair was then calculated using the Bio-Rad® CFX Maestro software.

2.13.7 Agarose gel electrophoresis of DNA (with ethidium bromide)

To separate and visualise PCR products, 4 µL of each reaction was mixed with 2 µL of loading dye (New England BioLabs), before being pipetted into the wells of a 2% w/v agarose gel (with ethidium bromide), alongside 1 µL of DNA ladder with an appropriate range and electrophoresed at 120 V for 45 minutes. Automated imaging of the gel was then conducted using a Gel Dock™ (Bio-Rad®).

2.13.8 qRT-PCR gene expression analysis

In order to measure relative gene expression within samples, qRT-PCR, using SYBR-green chemistry, was utilised. All qRT-PCR reactions were conducted in 384 well plate in technical triplicates. Each reaction mix comprised of 10-20 ng of cDNA (made up to 2 µl in nuclease free water), 1.5 µl of forward primer (150 nM), 1.5 µl of reverse primer (150 nM) and 5 µl of iQ SYBR Green Supermix (Bio-Rad®) in a final volume of 10 µl. For each cDNA sample, a separate no transcript control reaction mix was also made (as previously described), which contained nuclease free water in place of the cDNA. The plate was then placed into Bio-Rad C1000 CFX96 RT-PCR machine detection system where the following programme was run: 3 minutes at 94 °C, 40 cycles of 30 seconds at 94 °C and 60 seconds at the optimised annealing temperature of the primer pair and finally 5 minutes at 72 °C. After the programme had elapsed a melt curve was generated (by heating the reaction at increments of 0.5 °C increased every 5 seconds from 65-95 °C) to ensure the specificity of the product generated. The sequences of all the primers used for qRT-PCR analysis in this study can be found in Table 2.6.

Table 2.6 Sequence of primers used for qRT-PCR analysis in this study.

Primer	Forward/Reverse	Sequence (5' to 3')	Optimised annealing temperature (°C)
LAMA1	Forward	TGACGGAAGCGGATATGCAG	60
	Reverse	TCCACTTTGGCAGTGCTGAT	
LAMA2	Forward	CAACGCTGAGAAACTTGAGTATGA	60
	Reverse	CCAGGGAACATCCTTTGGTAAC	
TPPP3	Forward	CAGGGGATAATACGGCGGAG	60
	Reverse	TTCGGAAGGACAGAACGACG	
NFKBIZ	Forward	AGCCTGGGAGCATGATTGTG	60
	Reverse	AAGTAGCTCAGGTTGAGCGG	
CD44	Forward	CTCTCTCCCTCCACTTCAC	60
	Reverse	GCCTAATGTCCAGTTTCTTTCA	
MMP-2	Forward	GCCTTTAACTGGAGCAAAAACAA	60
	Reverse	TCCATTTTCTTCTTCACTCATTG	
ITGA5	Forward	TGCCGAGTTCACCAAGACTG	60
	Reverse	TGCAATCTGCTCCTGAGTGG	
ITGB3	Forward	CATCACCATCCACGACCGAA	60
	Reverse	GGTTGTTGGCTGTGTCCCAT	
RPSA	Forward	TGTTGCCATTGAAAACCCTGC	60
	Reverse	CTTCAGCACAGCCCTCTGG	
CLU	Forward	TGTGAGCTGATCGCTTGGAG	60
	Reverse	TCACTGGTATGACAGTCCCT	
TTYH1	Forward	AGCCTGCACAAGGACTATGG	60
	Reverse	CCTGAGGGTTGAAAGGGTCG	
TWIST1	Forward	CAAGCTGAGCAAGATTCAGACCC	60
	Reverse	AGACCGAGAAGGCGTAGCTGA	
YBX1	Forward	AAGAAGGTCATCGCAACGAAG	61
	Reverse	CTCCTACACTGCGAAGGTACT	
GAPDH	Forward	ATGTTCGTCATGGGTGTGAA	61
	Reverse	CTCTTCTGGGTGGCAGTGAT	

qRT-PCR results were analysed using either the ΔCt or ΔΔCt method (Ct represents the cycle number where the fluorescence generated by the PCR reaction is distinguishable from background noise). In this method, the level of gene expression is first normalised to the housekeeper gene glyceraldehyde-3-phosphate dehydrogenase (GAPDH) using the below equation:

$$\Delta Ct = \text{average } \Delta Ct \text{ (gene of interest)} - \text{average } \Delta Ct \text{ (GAPDH)}$$

$$\text{Relative gene expression} = 2^{-\Delta Ct}$$

In some cases, this value was then used to calculate the relative change in gene expression between two samples, using the below equation:

$$\Delta\Delta Ct = \text{average } \Delta Ct \text{ (treated sample)} - \text{average } \Delta Ct \text{ (untreated sample)}$$

$$\text{Relative fold change in change expression} = 2^{-\Delta\Delta Ct}$$

2.13.9 Immunoblotting

In order to assess the presence and relative quantity of specific proteins expressed in cell lines immunoblotting was utilised.

2.13.9.1 Cell lysis and protein isolation

To create cell lysates for immunoblotting, washed cell pellets or pooled spheroids were thawed on ice before being resuspended in 20-50 µL of NP-40 lysis buffer (Table 2.7) containing 1 X cOmplete® protease inhibitor cocktail (Roche; 11836170001). Cell

lysates were then vortexed three times, to ensure complete lysis of the cells, with 10 minute intervals in which they were incubated on ice. Next, the cell lysates were centrifuged at 14,000 x g for 15 minutes at 4 °C in order to remove any cellular debris. The supernatants from each cell lysate were then transferred to new 1.5 mL tube.

2.13.9.2 Protein quantification by Braford assay and sample preparation

A Bradford assay with a standard curve of known protein concentrations was used to determine the quantity of protein in cell lysates. Firstly, 1:40 dilutions of cell lysates in ddH_2O were prepared in triplicate alongside standard curve dilutions of Bovine Serum Albumin (BSA) (Sigma Aldrich; A3311) ranging from 0 to 100 µg/mL. 50 µL of each dilution (cell lysates and standard curve) was then pipetted into a clear bottomed 96 well plate. 200 µL of 1 X Bio-Rad Protein Assay Dye (Bio-Rad; 5000001) was then added to each dilution and incubated for 5 minutes. The plate was then placed into an Omega FLUOstar plate reader and absorbance at 595 nm was assessed. From this the standard curve was used to calculate the concentration of protein in each cell lysate. Cell lysates were then diluted to a concentration of 1 µg/µL in NP-40 lysis buffer and 4 X sample buffer (with β-mercaptoethanol; Table 2.3) and incubated at 95 °C for 10 minutes. Samples were then either stored at -20 °C or used immediately in a sodium dodecyl sulfate polyacrylamide gel electrophoresis (SDS-PAGE).

2.13.9.3 Preparation of SDS gels

10% sodium dodecyl sulfate (SDS) gels were chosen for the analysis of all target proteins in this study. Before the preparation of gels, 1.5 mm spacer plates and short plates were cleaned with 70% industrial methylated spirit (IMS) and assembled with gel casting frames, which were placed into gel casting stands. The components of the resolving gel (Table 2.8) were then mixed and pipetted between the casting plate and

the short plate. The gel was then overlaid with 70% IMS to ensure level setting, promote polymerisation and to remove air bubbles. After the gel had polymerised, the IMS was removed and the components of the stacking gel (Table 2.8) were mixed together and pipetted on top of the resolving gel. A 10-/15-well 1.5 mm comb was then immediately placed into the gel, which was then allowed to polymerise for 1 hour. Once set, the gel was either used immediately in a SDS-PAGE or stored in damp tissue wrapped in foil for up to a week.

2.13.9.4 SDS-PAGE

In order to separate the proteins in each cell lysate by molecular weight, discontinuous SDS polyacrylamide gel electrophoresis (SDS-PAGE) was conducted. First, polyacrylamide gels were placed into a running modulate which was then placed into an electrophoresis tank. The tank was then filled with running buffer (Table 2.7). Next, 10-50 ng of protein from each cell lysate was added into the wells of the polyacrylamide gel using a Hamilton syringe, depending on how highly the protein of interest was expressed in the cell lines from which the cell lysates were derived. To determine the size of detected proteins, 5 µL of Amersham Rainbow Ladder™ (Merck; GERPN800E) was also added to the first well of the gels. Gels were then electrophoresed at 40 mA, until the samples had reached the resolving gel, at which point the current was increased to 80 mA. Once the samples had reached the bottom of the resolving gel, the gels were removed from the gel electrophoresis tank and running module.

2.13.9.5 Protein transfer

To transfer proteins from a polyacrylamide gel to a Hybond® polyvinylidene fluoride (PVDF) membrane (Amersham; GE10600023) on which they could be detected and quantified, the membranes were first activated by incubation in methanol for 30

seconds, ddH_2O for 3 minutes and in transfer buffer for 15 minutes. Electrophoresed gels were then carefully removed from their casting plates and the stacking gel was discarded. Gels were then added to a transfer stack in a gel holder cassette. The order of components in the transfer stack were: black side of cassette, sponge, filter paper, gel, activated PVDF membrane, filter paper, sponge, clear side of cassette. A roller was used to remove any air bubbles between the gel and the membrane. The transfer cassette was then closed and placed into the transfer cell, which was placed into a gel electrophoresis tank and filled with transfer buffer (Table 2.7) that had been cooled to 4 °C. The tank was then placed into a 4 °C fridge, where it was run at 100 V constantly for two hours. After the transfer was complete, the power pack was switched off and the membranes were removed from the transfer cassettes.

Table 2.7 Composition of buffers used in immunoblotting. All buffers made up in dH_2O.

Buffer	Materials
NP-40 Lysis Buffer	150 mM NaCl 0.5% NP-40 50 mM Tris pH 7.4 1 mM EDTA
4 X SDS Sample Buffer	40% Glycerol (Courtner and Warner) 240 mM Tris/HCl pH 6.8 8% SDS 0.04% Bromophenol blue (Fisher) + 5% β-Mercaptoethanol (Sigma) added fresh.
10 X Running Buffer	250 mM Tris base 1.9 M Glycine 4% SDS
10 X Transfer Buffer	250 mM Tris base 1.9 M Glycine
1 X Transfer Buffer	100 mL 10 X transfer buffer 200 mL Methanol 700 mL ddH2O
10 X TBS	20 mM Tris Base pH 7.6 1.5 M NaCl
1 X TBS-T	100 mL 10 x TBS 1 mL Tween-20 (Sigma) 899 mL ddH2O

Table 2.8 Components used to prepare 2 X 10% SDS gels

Material	Resolving gel	Stacking gel
1 M Tris pH 8.8	3.9 mL	n/a
1 M Tris pH 6.8	n/a	0.65 mL
ddH_2O	2.5 mL	3.58 mL
30% Acrylamide/bis solution (Sigma)	3.4 mL	0.67 mL
10% SDS (Sigma)	0.1 mL	0.05 mL
10% Ammonium Persulphate (APS; Sigma)	0.1 mL	0.05 mL
N,N,N′,N′-Tetramethylethylenediamine (TEMED; Sigma)	0.01 mL	0.005 mL

2.13.9.6 Western blotting

To blot for target proteins, post transfer-membranes were initially blocked with either 5% BSA (Sigma Aldrich; A3311) or 5% milk (Marvel) in Tris-Buffered Saline, 0.1% Tween® (TSB-T) (depending on the recommended blocking buffer on the primary antibody) for one hour at room temperature. The blocking buffer was removed and the primary antibody (Table 2.9) was then added to the membrane at an appropriate dilution in blocking buffer. This was then incubated at 4 °C overnight. The next day, the primary antibody was removed and the membrane was washed three times with TBS-T for 10 minutes. The secondary antibody was then added to the membrane at a dilution of 1:2000 in blocking buffer and incubated at room temperature for one hour. The secondary antibody was removed and the membrane was again washed three times with TBS-T for 10 minutes.

Protein bands were then visualised on membranes by chemiluminescence. This was achieved by incubating membranes with Pierce™ enhanced chemiluminescence (ECL) Western Blotting Substrate (ThermoFisher Scientific; 32106) for 2-5 minutes,

depending on the level of expression of the target protein. For proteins that had a low level of expression or were difficult to visualise the ECL Signal Fire solution (Cell Signalling; 6883S) was used instead. Protein bands were then imaged in a LI-COR Odyssey® XF Imaging System at 700 nm for 30 seconds to 5 minutes, also depending on the level of expression of the target protein. Membranes were also imaged at 500 nm for 30 seconds in order to capture a fluorescent image of the protein ladder to determine the size of imaged proteins.

In order to blot for further target proteins, membranes were initially washed twice in TBS-T for two minutes and then incubated with ReBlot Plus Mild Antibody Stripping Solution (10 X; Merck; 2502) for 15 minutes at room temperature. The stripping solution was then removed and the membranes were again washed twice in TBS-T for two minutes, after which the blotting and visualisation process was repeated from the blocking step.

2.13.9.7 Quantifying protein expression by densitometry analysis

Visualised protein bands were quantified by densitometry analysis using the LI-COR Image Studio Lite® software. Images of the blots were loaded into the software and the ‘Analysis’ tab was selected. Rectangles were then drawn around each protein band and their density was automatically determined. The relative density of each protein was calculated using the housekeeping protein GAPDH, which was visualised with every blot as a loading control. Significant differences in relative protein density were calculated using an unpaired t-test, a One-Way ANOVA or a Two-Way ANOVA.

Table 2.9 Antibodies used in immunoblotting in this study

Antibody	Primary/Secondary	Host Species	Dilution	Source
LAMA1	Primary	Mouse	1:1000	Fisher (CL3087)
LAMA2	Primary	Rabbit	1:1000	Abcam (ab140482)
CD44	Primary	Rabbit	1:1000	Abcam (ab157107)
MMP-2	Primary	Rabbit	1:1000	Cell Signalling Technology (4022)
CLU	Primary	Rabbit	1:1000	Abcam (ab92548)
BCL-2	Primary	Rabbit	1:1000	Cell Signalling Technology (2876)
COL-I	Primary	Rabbit	1:1000	Abcam (ab7463)
COL-VI	Primary	Rabbit	1:1000	Abcam (ab45139)
GAPDH	Primary	Rabbit	1:1000	Cell Signalling Technology (2118S)
Anti-Rabbit IgG, HRP linked	Secondary	Goat	1:2000	Cell Signalling Technology (7074S)
Anti-Mouse IgG, HRP linked	Secondary	Goat	1:2000	Cell Signalling Technology (7076S)

2.13.10 Gelatin zymography

In order to analyse the quantity of MMP-2 and MMP-9 secreted by cells, gelatin zymography was utilised (Heussen and Dowdle, 1980).

2.13.10.1 Preparation of cell line supernatants

Snap frozen cell line supernatants (media conditioned by cell lines) were thawed on ice and then directly mixed 1:4 with 4 X β-mercaptoethanol-free sample buffer (Table 2.7) and vortexed for 5 seconds before being added directly to the gel.

2.13.10.2 Preparation of gelatin SDS gels

Before preparing the gels, a 3 mg/mL gelatin solution was made by dissolving the appropriate quantity of gelatin powder (Sigma; MFCD00081638) in distilled water. This solution was then placed into a 37 °C water bath and incubated for at least 2 hours to ensure that the gelatin had fully dissolved. Subsequently, the gelatin solution was passed through a sterile filter and cooled at 4 °C. 1 mm spacer plates and short plates were then cleaned with 70% IMS and assembled with gel casting frames which were placed into gel casting stands. The materials to make a 10% gelatin SDS resolving gel (Table 2.10) were then mixed together and pipetted between the casting plate and the short plate. 70% IMS was then layered on top of the gel to ensure that it stayed level while setting. Once the resolving gel had fully polymerised the IMS was removed and the materials required to form the stacking gel (Table 2.10) were mixed before being pipetted on top of the gelatin resolving gel. A 10-well 1 mm comb was then immediately inserted into the gel which was then allowed to polymerise for 1 hour. Once formed, the gel was either used immediately or stored in damp tissue wrapped in foil for up to a week.

2.13.10.3 Electrophoresis of cell culture supernatants

Gelatin SDS gels were placed into an electrophoresis tank in running modules and the combs were carefully removed. The gels were then submerged in running buffer (Table 2.10). 20 µl of prepared samples and media that the cells were cultured in (to account for the MMPs present in FBS), as well as recombinant MMP-2 as a positive control, were then added to each of the wells of the gels using a Hamilton syringe (any empty wells were filled with 4 X sample buffer mixed 1:4 with dH_2O). Gels were then run at a constant 125 V until the sample buffer had reached the bottom of the gels. To ensure that the MMPs had migrated an adequate distance through the gels, they were run at 125 V for a further 30 minutes.

2.13.10.4 Renaturing and developing the zymogram

Once electrophoresis was complete the gels were removed from the running apparatus and carefully placed into a container that had been prefilled with 30 mL of renaturing buffer (Table 2.11) and incubated for one hour at room temperature with gentle agitated on a rocker. The renaturing buffer was then removed from the container and replaced with 30 mL of developing buffer (Table 2.11) and incubated with the gels for 60 minutes, also at room temperature on the rocker. The developing buffer was then removed and replaced with a further 30 mL of developing buffer and incubated with gels overnight at 37 °C. The next day the developing buffer was removed and replaced with H_2O and incubated for 5 minutes at room temperature on the rocker, in order to rinse the gels. This process was repeated three times to ensure that all the developing buffer had been removed from the gels. After the last rinse, 30 mL of staining solution (Table 2.11) was then added to the gels and incubated at room temperature for 15 minutes on the rocker. The staining solution was then removed and the replaced with 30 mL of de-staining solution and incubated for two hours or until white bands started to appear on the gels. Then, the de-staining solution was removed

and replaced with 30 mL of fixation buffer (Table 2.11) and incubated for 30 minutes on the rocker. The gels were then removed from the container, mounted into a plastic wallet and sealed with tape.

2.13.10.5 Analysing the level of MMP-2/-9 secretion by densitometry analysis

After fixation and mounting the zymograms were then photographed and the intensity of the MMP bands were evaluated by densitometry analysis using the LI-COR Image Studio Lite® software, to obtain an indication of the level of MMP-2 and MMP-9 secreted by cell lines. Images of the zymograms were loaded into the software and the 'Analysis' tab was selected. Rectangles were then drawn around each MMP band and their density was automatically determined. The density of the MMP bands from the corresponding control medium, which was run on the same zymogram, was subtracted from all cell line supernatants to account for MMPs present in FBS. However, the control medium used in the zymograms in section 3.5 was fresh, rather than medium of the same age as used during cell seeding. We have therefore decided that the media controls were not representative of the quantity of MMPs that would have actually been present in the media after incubation in the assays at 37 °C. Consequently, in the densitometry analysis of these zymograms we have not subtracted the media control from the cell line supernatants, as we are still able to use this to compare MMP secretion between cell lines, as well as treated and untreated conditions.

Table 2.10 Components used to make 2 X 10% gelatin sodium dodecyl sulfate (SDS) gels

Material	Resolving gel	Stacking gel
3 mg/mL gelatin solution	5 mL	n/a
1.5 M Tris/HCl pH 8.8	3.8 mL	n/a
0.5 M Tris/HCL pH 6.8	n/a	0.32 mL
Distilled H_2O	1 mL	3.9 mL
10% SDS	0.15 mL	0.05 mL
Acrylamide/bis solution (30%)	5 mL	0.75 mL
10% APS	0.15 mL	0.08 mL
N,N,N′,N′-Tetramethylethylenediamine (TEMED; Sigma)	0.015 mL	0.005 mL

Table 2.11 Composition of buffers used in zymograms. All buffers made up in dH_2O.

Buffer	Materials
4 X Sample Buffer	62.5 mM Tris-HCl pH 6.8 25% glycerol 4% SDS 0.01% bromophenol blue
10 X Running Buffer	25 mM Tris Base 192 mM Glycine 0.1% SDS
10 X Developing Buffer	Ready-made 10 X Developing buffer (BioRad, #161076)
Renaturing Buffer	2.5% Triton-X-100 (Sigma, T8787)
Staining Solution	40% Methanol 10% Glacial acetic acid 0.5% Coomassie blue R-250
De-staining Solution	40% Methanol 10% Glacial acetic acid 50% Deionised water
Fixation Buffer	5% Glycerine 30% methanol

2.13.11 Immunohistochemistry

Immunohistochemistry (IHC) was used to stain target proteins in formalin-fixed paraffin embedded (FFPE) spheroids (previously generated and processed by Dr Sophie Roper). To achieve this, the Pierce™ Peroxidase IHC Detection Kit (ThermoFisher; 36000) was used. Samples, mounted on slides, were firstly incubated at 60 °C overnight, in order to melt the paraffin in which they were embedded. The next day

any remaining paraffin was removed from samples by submerging them in xylene for 15 minutes. Samples were then rehydrated by submerging them in a series of increasingly dilute ethanol baths (100%, 95%, 80% and 70% ethanol) for 5 minutes each, before washing them in water for approximately 30 seconds. Heat or enzymatic induced antigen retrieval was then conducted on samples. In heat-induced antigen retrieval, samples were steamed with sodium citrate buffer (pH 6.0) for 40 minutes. In enzymatic-induced antigen retrieval, samples were incubated with pepsin solution for 10 minutes in a humidified box at room temperature (Abcam; ab64201). The type of antigen retrieval used was determined by the recommendation of the manufactures of the primary antibody (Table 2.12). After antigen retrieval, samples were washed in PBS twice for 2 minutes in coplin jars. To quench the activity of endogenous peroxidases, samples were then incubated with peroxidase suppressor for 30 minutes in a humidified box at room temperature, before being washed in PBS twice for 2 minutes. Next samples were incubated with blocking buffer for 30 minutes, also in a humidified box at room temperature. Primary antibodies, diluted in blocking buffer, were then added to samples (the dilutions of each primary antibody can be found in Table 2.12) and incubated for 1 hour at room temperature in a humidified box. Samples were then washed in PBS 3 times for 2 minutes. Next, the corresponding secondary antibody, also diluted in blocking buffer, was added to samples and incubated for 1 hour at room temperature in a humidified box (the dilutions of each secondary antibody can be found in Table 2.12). Samples were then washed in PBS 3 times for 2 minutes. Following this wash step, samples were then incubated with a 1 X 3,3′-diaminobenzidine (DAB) solution (diluted in stable peroxidase buffer from a 10 X solution included in Pierce™ Peroxidase IHC Detection Kit) for approximately 5-10 minutes at room temperature in a humidified box. Samples were then washed in PBS 3 times for 2 minutes, before also being washed once in water. Harris Modified Haematoxylin (included in Pierce™ Peroxidase IHC Detection Kit) was then added to samples, in order to counter stain them, and incubated for approximately 30 seconds

at room temperature. Samples were then briefly washed 3 times in water and then rinsed under running water until the water turned clear. Samples were then dehydrated by submerging them in the same ethanol dilutions mentioned above, but in the reverse order, and then xylene. Samples were then removed from the xylene and dried. To mount samples, 1-2 drops of mounting medium (included in Pierce™ Peroxidase IHC Detection Kit) was then added to samples, upon which a 24 x 50 mm coverslip was then carefully placed. Mounted samples were then allowed to dry overnight. Once dried, samples were imaged on an EVOS M7000 microscope (ThermoFisher) using the brightfield channel and 4 X magnification.

Table 2.12 Antibodies used in immunohistochemistry in this study.

Antibody	Primary/Secondary	Host Species	Dilution	Source	Antigen retrieval
LAMA1+A2	Primary	Rabbit	1:100	Acbcam (ab7463)	Heat
COL-I	Primary	Rabbit	1:100	Abcam (ab7463)	Heat
COL-VI	Primary	Rabbit	1:100	Abcam (ab45139)	Heat
LUM	Primary	Donkey	1:10	R and D systems (AF2846)	Enzymatic
Anti-Rabbit IgG, HRP linked	Secondary	Goat	Stock is pre-diluted	Abcam (ab92548)	n/a
Anti-Donkey IgG, HRP linked	Secondary	Goat	1:1000	Abcam (ab6885)	n/a

2.13.12 Immunofluorescence

Immunofluorescence (IF) was used to stain target proteins in spheroids that had been cultured for 1 day. To achieve this, 10-20 spheroids were initially pooled in a 1.5 mL microcentrifuge tube and centrifuged at 120 x g for 1 minute (the same centrifugal x g and time were used throughout this methodology), to ensure all spheroids were at the bottom of the tube. The neurosphere media in which the spheroids had been collected

in was then carefully removed from the tube. To fix the spheroids, 150 µL of 4% paraformaldehyde (PFA) was added to the pooled spheroids, which were then incubated at room temperature for 15 minutes. Spheroids were then centrifuged and as much PFA as possible was removed. The spheroids were then washed twice in 150 µL of PBS, centrifuging between each wash. In order to permeabilise the cells within the spheroids, PBX (0.1% Triton X-11 in PBS) was then added to the tube and incubated for 30 minutes at room temperature, after which the spheroids were centrifuged and as much PBX as possible was removed. The spheroids were then washed twice with PBS as before. Next, 150 µL of 10% goat serum (Vector Laboratories; S1000) diluted in PBS (blocking buffer) was added to the spheroids, which were then incubated for 1 hour at room temperature. Spheroids were then centrifuged and as much of the blocking buffer as possible was removed. Next, 150 µL of the primary antibody, diluted in blocking buffer, was added to the spheroids (dilutions of primary antibodies can be found in Table 2.13), before incubating at room temperature for 1 hour. Spheroids were then centrifuged and as much primary antibody as possible was removed. The spheroids were washed 3 times in PBT (0.1% Tween-20 in PBS) for 5, 10 and 15 minutes at room temperature, centrifuging between in each step. 150 µL of the corresponding secondary antibody was then added to spheroids, before incubating at room temperature for 1 hour in a darkened chamber. Spheroids were then centrifuged and as much secondary antibody as possible was removed. The spheroids were then again washed 3 times in PBT, as described above, centrifuging between in each step. The spheroids were then briefly equilibrated in PBS. To then stain the nuclei of the individual cells within the spheroids, 150 µL of a diluted 4′,6-diamidino-2-phenylindole (DAPI) (Invitrogen; D1306) solution (5 mg/mL in PBS) was added to the spheroids, which were then incubated for 5 minutes at room temperature in a darkened chamber. The spheroids were then centrifuged and as much of the DAPI solution as possible was removed from the spheroids. The spheroids were then washed 3 times in PBS, centrifuging between in each step. Spheroids were

pipetted into one of the wells of a clear bottomed 96 well plate and immediately imaged using a Leica SPEII Confocal Microscope with a 10 X air lens. 30 image z-stacks of the protein of interest and DAPI were captured, starting from the bottom of each spheroid. The middle 10 images were then overlaid using ImageJ software. Composite z-stack images of the protein of interest and DAPI were also made using ImageJ software.

Table 2.13 Antibodies used in immunofluorescence in this study

Antibody	Primary/Secondary	Host Species	Dilution	Source
LAMA1+A2	Primary	Rabbit	1:100	Abcam (ab7463)
COL-I	Primary	Rabbit	1:100	Abcam (ab7463)
COL-VI	Primary	Rabbit	1:100	Abcam (ab45139)
Alexa-Fluor 488 Anti-Rabbit	Secondary	Goat	1:100	Invitrogen (A21244)

2.14 Proteomic analysis of cell lysates by LC-MS/MS

In order to identify proteins differentially expressed between control and LAMA1 knockout DAOY SHH medulloblastoma cells, cell lysates were analysed by liquid chromatography-tandem mass spectrometry (LC-MS/MS) proteomic analysis.

2.14.1 Sample preparation and LC-MS/MS analysis

To prepare samples for LC-MS/MS analysis, protein was initially isolated from biological triplicates of cell pellets and pooled spheroids. Isolated protein was then quantified as previously described and cell lysates were then diluted to a concentration

of 0.375 µg/µL in NP-40 lysis buffer and 4 X sample buffer (with β-mercaptoethanol; Table 2.7) and incubated at 95 °C for 10 minutes. 7.5 µg (20 µL) of protein from each sample was then loaded into the wells of a 10% SDS-page gel and electrophoresed at 40 mA (as previously described) until the samples had just reached the resolving gel. The gels were then removed from the electrophoresis apparatus and the stacking gel was discarded. The protein samples within the gels were then fixed and stained by first incubating the gel in staining solution (Table 2.14) in a covered tray for 1 hour, with gentle agitation on a rocker. The staining solution was then discarded and replaced with de-staining solution (Table 2.14) in which the gels were incubated for 1 hour. The de-staining solution was then removed and replaced with fresh de-staining solution, in which the gels were incubated in overnight. The next day, the gels were removed from the destaining solution and the stained protein samples were then cut out of the gel using a scalpel and placed into individual, labelled microcentrifuge tubes containing 200 µL of distilled water. The tubes containing the protein samples were then sent to the University of Cambridge Centre for Proteomics, at room temperature, where they were trypsin digested into peptides before being analysed using label free LC-MS/MS using a Dionex Ultimate 3000 RSLC nanoUPLC (Thermo Fisher Scientific Inc, Waltham, MA, USA) system interfacing with a Orbitrap Lumos mass spectrometer (Thermo Fisher Scientific Inc, Waltham, MA, USA).

Table 2.14 Buffers used for fixing and staining protein in SDS gels for proteomic analysis. Buffers made up in dH_2O

Buffer	Materials
Staining Solution	0.1% Coomassie blue R-250 10% Methanol 10% Glacial acetic acid
De-staining Solution	10% Methanol 10% Glacial acetic acid

2.14.2 Identification of differentially expressed proteins from proteomics data

Proteomic data was initially accessed in the software Scaffold 5 (https://www.proteomesoftware.com/products/scaffold-5), where the data was filtered using with the following parameters: 99% protein threshold, minimum 2 peptides and 95% peptide threshold. The data was then exported to Microsoft Excel, where any proteins with accession number containing 'cRAP' were omitted, since these are regarded as common proteomic contaminants. Next, 4 different methods of differential protein expression analysis were used to identify target proteins, which were determined by the number of biological replicates which contained Total Spectrum Count (TSC) values ≥2 for each protein, in each cell line. TSC values represent the sum of the total numbers of peptide reads for a given protein (Hawkridge, 2014).

Firstly, when there were TSC values in 3 biological replicates in one cell line, but none in the other, these were considered target proteins (Method 1). Secondly, when there were TSC values in all 3 biological replicates in one cell line, but only in 1 in the other, target proteins were identified as those where the TSC value of the 1 biological replicate was ≥1 less than the mean of the 3 biological replicates (Method 2). The remaining 2 methods (Methods 3 and 4) were used when there were either TSC values in 3 biological replicates in one cell line, and 2 in the other, or when there were TSC values in all biological replicates in both cell lines. In circumstances where there were TSC values in 3 biological replicates in one cell line, and 2 in the other, the missing value was replaced with a 0 in order to represent the limit of detection (also known as Deterministic Minimum Imputation). Methods 3 and 4 utilised a statistical analysis methodology described by Aguilan et al., where LC-MS/MS proteomics data was analysed using statistical analysis plug-in packages for Microsoft Excel (Aguilan, Kulej and Sidoli, 2020). In this method, the proteomics data was firstly Log2 transformed, before undergoing a two-step normalisation. In the first step of normalisation, the mean

expression of all proteins within a sample was subtracted from the expression of each individual protein within the same sample. In the second step, the correlation slope between the mean expression of each protein in all samples with the mean expression of each protein in the individual samples was initially calculated. The transformed and once normalised values in each sample were then divided by their corresponding correlation slope value. This transformation and two-step normalisation process is illustrated in Figure 2.2. After the transformation and normalisation of data, proteins with significantly different expression between the cell lines were identified using either a heteroscedastic t-test or a homoscedastic t-test, depending on if the variances between the two sets of biological replicates were significantly different (as determined by an F-test). Differentially expressed proteins were determined as those where $p<0.05$. These differential expression analysis methods are illustrated in Figure 6.2.

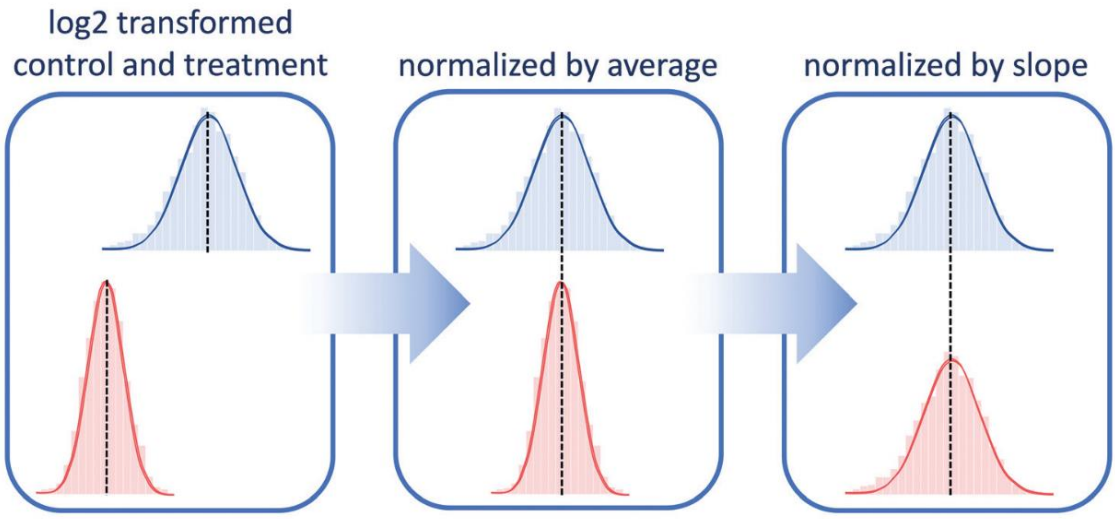


Figure 2.2 Illustration of Log2 transformation and two-step normalisation of proteomics data used in in this study. Adapted from Aguilan *et al.* 2020.

2.14.3 STRING analysis of differentially expressed proteins

In order to generate Protein-Protein Interaction Networks using sets of differentially expressed target proteins, the publicly available online software STRING was used (https://string-db.org/). To do this, proteins were uploaded to the 'Multiple Proteins' function. Interaction networks were then generated using all active interaction sources, which consist of curated databases, experimentally determined, gene neighbourhood, gene fusions, gene co-occurrence, textmining, co-expression, protein homology. For proteins lists larger than 100 proteins a confidence score of 0.7 (high) was used, for those below 100 proteins a medium confidence score of 0.4 (medium was used).

2.14.4 KEGG pathway mapping analysis of differentially expressed proteins

To associate sets of differentially expressed proteins with known molecular pathways, Kyoto Encyclopaedia of Genes and Genomes (KEGG) pathway mapping analysis was used (Kanehisa and Goto, 2000). This was achieved by uploading protein lists to the publicly online bioinformatics tool DAVID (https://david.ncifcrf.gov/tools.jsp), via the 'Upload' function in 'Analysis Wizard'. Analysis was then conducted using the 'Functional Annotation Tool', from which 'KEGG_PATHWAY' was selected. This produced a chart detailing the p-value of association (calculated using modified version of Fisher's Exact test for gene-enrichment analysis) for each identified pathway and the number and name of the proteins used to identify them. Significantly associated pathways were considered those where $p<0.05$. This chart also provided links to diagrams of the identified KEGG pathways, which highlighted the proteins used to identify them.

Chapter 3: Identification and preliminary validation of candidate laminin regulated genes in SHH and Group 4 medulloblastoma

3.1 Introduction

A study by our group recently identified that *LAMA1* and *LAMA2* expression has prognostic significance in SHH and Group 4 medulloblastoma (Linke *et al.*, 2020). However, the molecular mechanisms underlying this pattern of survival remain unknown. We believe that elucidating these mechanisms will have two-fold applications. Firstly, it will allow for the drivers of tumour progression in the sub-types with poor overall survival to be identified (LAM^{low} SHH and LAM^{high} Group 4 medulloblastomas), and therefore targets for pharmaceutical approaches. Secondly, it will help to establish further biomarkers of the sub-types with a more favourable overall survival (LAM^{high} SHH and LAM^{low} Group 4 medulloblastomas), which will facilitate enhanced patient risk stratification. We therefore sought to identify and validate candidate molecular drivers of these LAM^{high} and LAM^{low} ECM sub-types in SHH and Group 4 medulloblastoma, through the analysis of genomic patient data and *in vitro* cell culture models respectively.

The aims of this chapter were to:

A) Establish the level of *LAMA1* and *LAMA2* expression across the medulloblastoma sub-groups by analysing large scale genomic patient datasets.
B) Establish a set of candidate 'laminin regulated genes' in SHH and Group 4 medulloblastoma by conducting integrated differential gene expression analysis of a large-scale genomic patient dataset and mRNA sequencing data of SHH medulloblastoma cell lines.
C) Validate the selected 'laminin regulated genes' using SHH and Group 4 medulloblastoma cell lines in 2D and 3D hydrogel cell culture assays, whereby the cell lines are stimulated with exogenous laminin-111.

3.2 Analysis of *LAMA1* and *LAMA2* expression across the medulloblastoma sub-groups

Prior to identifying candidate 'laminin regulated genes' in SHH and Group 4 medulloblastoma, we sought to first identify if the level of *LAMA1* and *LAMA2* gene expression significantly differs between the medulloblastoma sub-groups, as well as normal cerebellum. To achieve this we analysed two publicly available genomic medulloblastoma patient datasets: Pfister (n=223; Northcott *et al.*, 2017) and Cavalli (n=763; Cavalli *et al.*, 2017), as well as a normal cerebellum dataset: Roth (n=9; Roth *et al.*, 2006).

Analysis of the datasets was performed using the R2: Genomics Analysis and Visualisation Platform (R2), with significant differences in gene expression being calculated using the Kruskal-Wallis test with Dunn's multiple comparisons. Since the Pfister (medulloblastoma) and Roth (normal cerebellum) datasets were generated using the same expression array, we were able to directly compare the expression of *LAMA1* and *LAMA2* between the medulloblastoma sub-groups and normal cerebellum using the R2:MegaSampler tool (Figure 3.1 A and C). The Cavalli dataset was generated on a different expression array, so was analysed separately (Figure 3.1 B and D).

In the Roth and Pfister datasets *LAMA1* expression was significantly lower in the SHH, Group 3 and Group 4 sub-groups than in normal cerebellum ($p<0.01$ for all comparisons; Figure 3.1 A). However, there was no significant difference in *LAMA1* expression between the sub-groups (Figure 3.1 A). Conversely, analysis of the Cavalli dataset showed that *LAMA1* expression was significantly different between all the sub-groups ($p<0.01$ for all comparisons; Figure 3.1 B). Furthermore, expression was found to be highest in the SHH sub-group and lowest in the WNT sub-group (Figure 3.1 B).

In the Roth and Pfister datasets *LAMA2* expression was significantly higher in the SHH sub-group than in normal cerebellum, whereas in the rest of the sub-groups it was unchanged ($p \leq 0.001$; Figure 3.1 C). Furthermore, the expression of *LAMA2* was significantly different between all sub-groups apart from between Group 3 and Group 4 ($p<0.001$ for all comparisons; Figure 3.1 C). The SHH sub-group exhibited the highest level of expression, while the WNT sub-group exhibited the lowest (Figure 3.1 C). In line with these findings, *LAMA2* expression was also found to be significantly different between all sub-groups apart from Group 3 and Group 4 in the Cavalli dataset (Figure 3.1 D). In addition, *LAMA2* was also most highly expressed in the SHH sub-group and least expressed in the WNT sub-group ($p<0.0001$ for all comparisons; Figure 3.1 D). Interestingly, this pattern of expression is similar to that of *LAMA1*, which was also found to be most highly expressed in the SHH sub-group and least expressed in the WNT sub-group in the Cavalli dataset.

In summary, these findings indicated that *LAMA1* and *LAMA2* are often expressed at different levels across the medulloblastoma sub-groups. In addition, the SHH sub-group most frequently exhibits the greatest level of expression, whereas the WTN sub-group exhibits the lowest.

It is worth noting that the validity of the comparison of *LAMA1* and *LAMA2* expression between the medulloblastoma sub-groups and normal cerebellum may be limited due to the relatively small sample size of the Roth dataset (n=9). In addition, the difference in the pattern of *LAMA1* expression across the medulloblastoma sub-groups between the Pfister and Cavalli datasets, can potentially be explained by the differing number of *LAMA1* probes in the gene arrays used to generate them. In the Pfister dataset, the gene array used only had 22 probes for *LAMA1*, whereas there were 80 probes in the one used to generate the Cavalli dataset. This may mean that the gene array used in the Cavalli dataset was more sensitive to *LAMA1* than the one used in the Pfister dataset and was therefore more reliable in its detection. Conversely, the gene arrays

have a more similar number of *LAMA2* probes (Pfister: 44 and Cavalli: 67), which could be the reason why the pattern of *LAMA2* expression across the sub-groups is more alike between the datasets. Furthermore, it also worth considering that since the Cavalli dataset contains a much larger number of medulloblastoma patients (n=763) than the Pfister dataset (n=223), it may therefore be more robust in the identification of the level *LAMA1* and *LAMA2* gene expression in the medulloblastoma sub-groups.

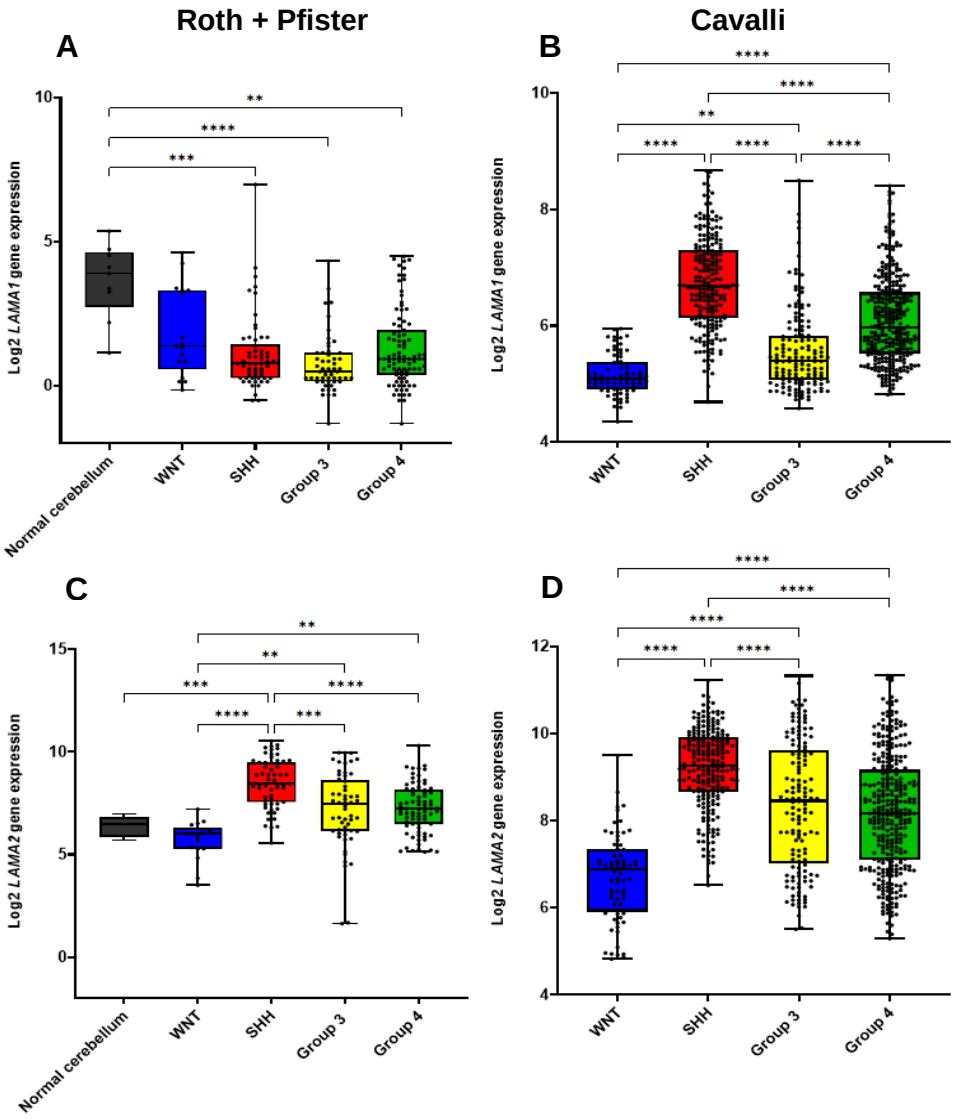


Figure 3.1 Laminin Subunit α1 (*LAMA1*) and Laminin Subunit α2 (*LAMA2*) are expressed in normal cerebellum (Roth dataset) and in all 4 medulloblastoma sub-groups (Pfister and Cavalli datasets). *LAMA1* and *LAMA2* gene expression (Log2) was assessed in the Roth (n = 9) and Pfister (WNT: n=17, SHH: n=59, Group 3: n=56, Group 4: n=91) datasets together (**A** and **C**) and just in the Cavalli dataset (WNT: n=70, SHH: n=223, Group 3: n=144, Group 4: n=326) (**B** and **D**) using the R2: Genomics Analysis and Visualization platform. Box and whisker plots indicate the interquartile range as well as the median value of each group. Error bars show the smallest and largest value in each group. Significant differences in gene expression between groups were calculated using a Kruskal-Wallis test with Dunn's multiple comparisons post-hoc test; **p≤0.01, ***p≤0.001, ****p≤0.0001.

3.3 Identification of candidate ‘laminin regulated genes’ in SHH and Group 4 medulloblastoma

In order to better understand why *LAM*^{high} SHH medulloblastomas have a favourable overall survival, whereas *LAM*^{high} Group 4 tumours have a poor overall survival, we sought to identify genes that are regulated by LAMA1 and LAMA2 in these sub-groups (‘laminin regulated genes’).

To achieve this, integrated differential gene expression analysis was conducted on two datasets: the aforementioned genomic patient dataset (Cavalli dataset) and mRNA sequencing data of SHH medulloblastoma cell lines (DAOY and ONS-76) grown on top of hyaluronan hydrogels with and without laminin-111. The mRNA sequencing dataset was obtained and analysed by Dr Franziska Linke, a previous post-doctoral researcher in Dr Coyle’s lab. To establish the most conserved ‘laminin regulated genes’, the candidate genes that overlapped in both datasets or sub-groups (Cavalli) were identified. These candidates were then screened in the literature to establish their function in non-disease conditions, as well as if they had any previously identified roles in cancer. From the genes with an already established role in cancer, 8 were selected for further investigation and validation in 2D and 3D *in vitro* cell culture assays. The workflow of this selection process is illustrated in Figure 3.2.

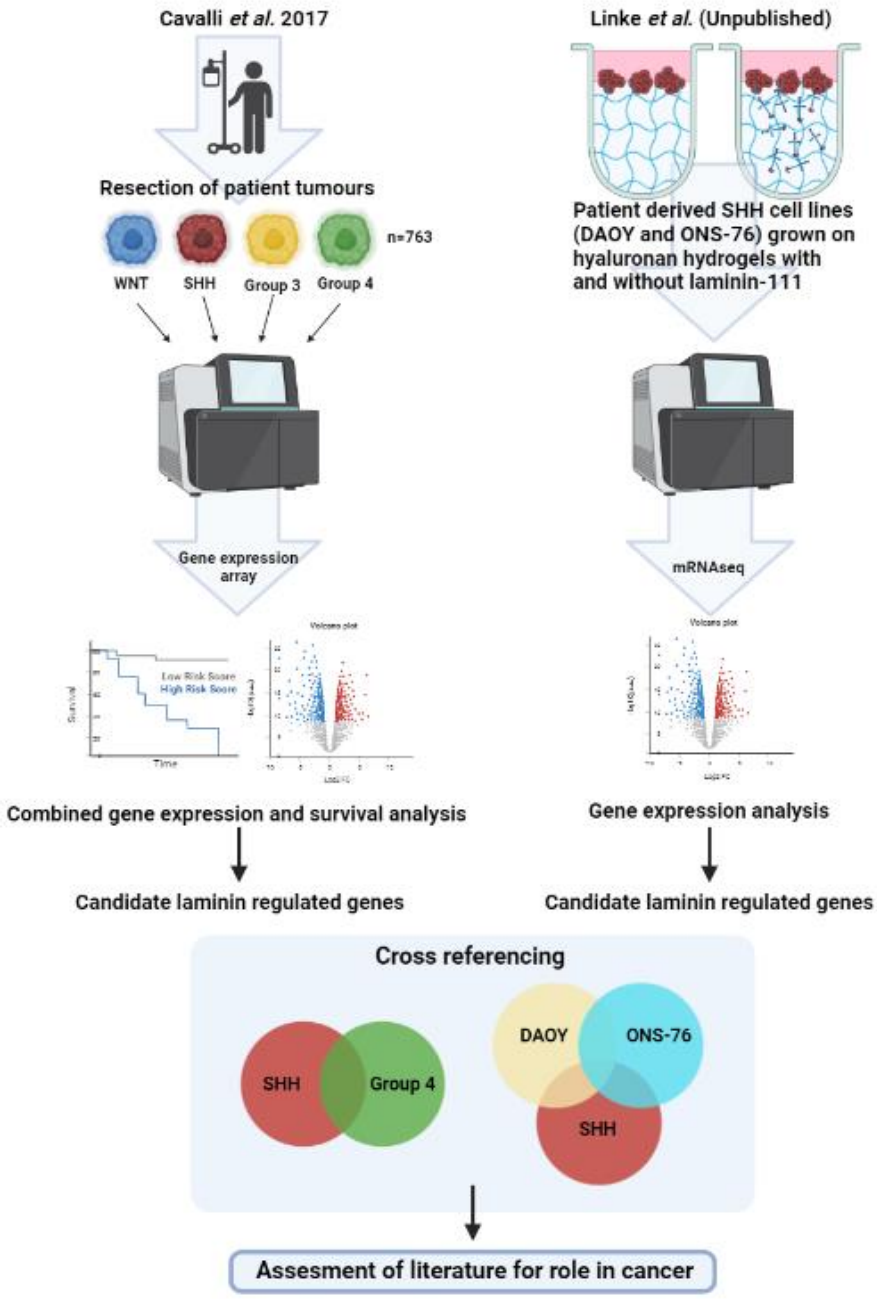


Figure 3.2 Analysis workflow for identifying 'laminin regulated genes' from a medulloblastoma genomic patient dataset and an mRNA sequencing dataset of patient derived SHH medulloblastoma cell lines. Candidate 'laminin regulated genes' were initially identified by differential gene expression analysis of both the Cavalli dataset (patient samples) and mRNA sequencing data of SHH medulloblastoma patient derived cell lines (DAOY and ONS-76) grown on top of hyaluronan hydrogels with and without laminin-111. The candidate 'laminin regulated genes' identified from both analyses, as well as between sub-groups (Cavalli), were then cross reference to create a list of conserved candidate genes. The literature was then assessed to identify the function of these genes in normal conditions as well as any previously identified roles in cancer. This was then used to select 'laminin regulated genes' for further investigation.

3.3.1 Differential gene expression analysis of a genomic medulloblastoma patient dataset (Cavalli) and a mRNA sequencing dataset of SHH medulloblastoma patient derived cell lines

Differential gene expression analysis was conducted on both the Cavalli dataset and the mRNA sequencing dataset of SHH medulloblastoma cell lines, in order to establish an initial set of candidate 'laminin regulated genes'. Details of the methodology used to conduct the differential gene expression analysis can be found in section 2.1.3.

The number of genes which were found to have significantly increased or decreased expression in the *LAM*^{high} ECM sub-type compared to the *LAM*^{low} in the Cavalli dataset (SHH and Group 4 patients) and in response laminin-111 in the mRNA sequencing dataset (SHH patient derived cell lines) are displayed in Table 3.1. Although the number of genes with significantly increased expression in response to laminin-111 in the ONS-76 cell line was low compared to the DAOY cell line, a similar number of genes overall were identified in both cell lines in the RNAseq data.

Table 3.1 The number of genes identified to have significantly increased or decreased expression in the *LAM*^{high} ECM sub-type compared to the *LAM*^{low} in the Cavalli dataset (SHH and Group 4 patients) and in response laminin-111 in the mRNA sequencing data (SHH patient derived cell lines).

Dataset	Sub-group / Cell line	Number of genes with increased expression	Number of genes with decreased expression
Cavalli	SHH	734	711
	Group 4	1094	826
mRNA sequencing	DAOY	420	1481
	ONS-76	6	299

3.3.2 Selection of candidate 'laminin regulated genes' for further investigation

The number and identity of the candidate 'laminin regulated genes' which were identified in the differential gene expression analysis of both the SHH sub-group patients in the Cavalli dataset and the SHH medulloblastoma cell lines in the mRNA sequencing dataset, were determined using the online bioinformatics software Venny 2.1. Furthermore, candidate genes which appeared in the differential gene expression analysis of both the SHH and Group 4 patients in the Cavalli dataset, were also identified by the same process. Both sets of analyses are displayed in Figure 3.3.

Four candidate 'laminin regulated genes', with previously established roles in tumour progression, were selected for further investigation from the genes overlapping between the analysis of the SHH sub-group patient tumours and both the SHH medulloblastoma cell lines (Figure 3.3 A). These genes were: Tubulin Polymerization Protein 3 (*TPPP3*), NF-κB inhibitor zeta (*NFKBIZ*), Clusterin (*CLU*) and Integrin Subunit B 3 (*ITGB3*) (Figure 3.4 A). Matrix Metalloproteinase 2 (*MMP-2*) was also identified from this analysis, but from genes overlapping between SHH patients and just the DAOY SHH medulloblastoma cell line (Figure 3.4 A). MMP-2 is a target of particular interest as it is part of a family of ECM-degrading enzymes with an established role in medulloblastoma progression (Vince *et al.*, 2001; Bhoopathi *et al.*, 2011). Furthermore, *NFKBIZ*, *CLU* and *MMP-2* were also identified from the candidate genes overlapping between SHH and Group 4 patients in the Cavalli dataset (Figure 3.4 B). Similarly, Integrin Subunit αV (*ITGAV*) was also identified from this overlap.

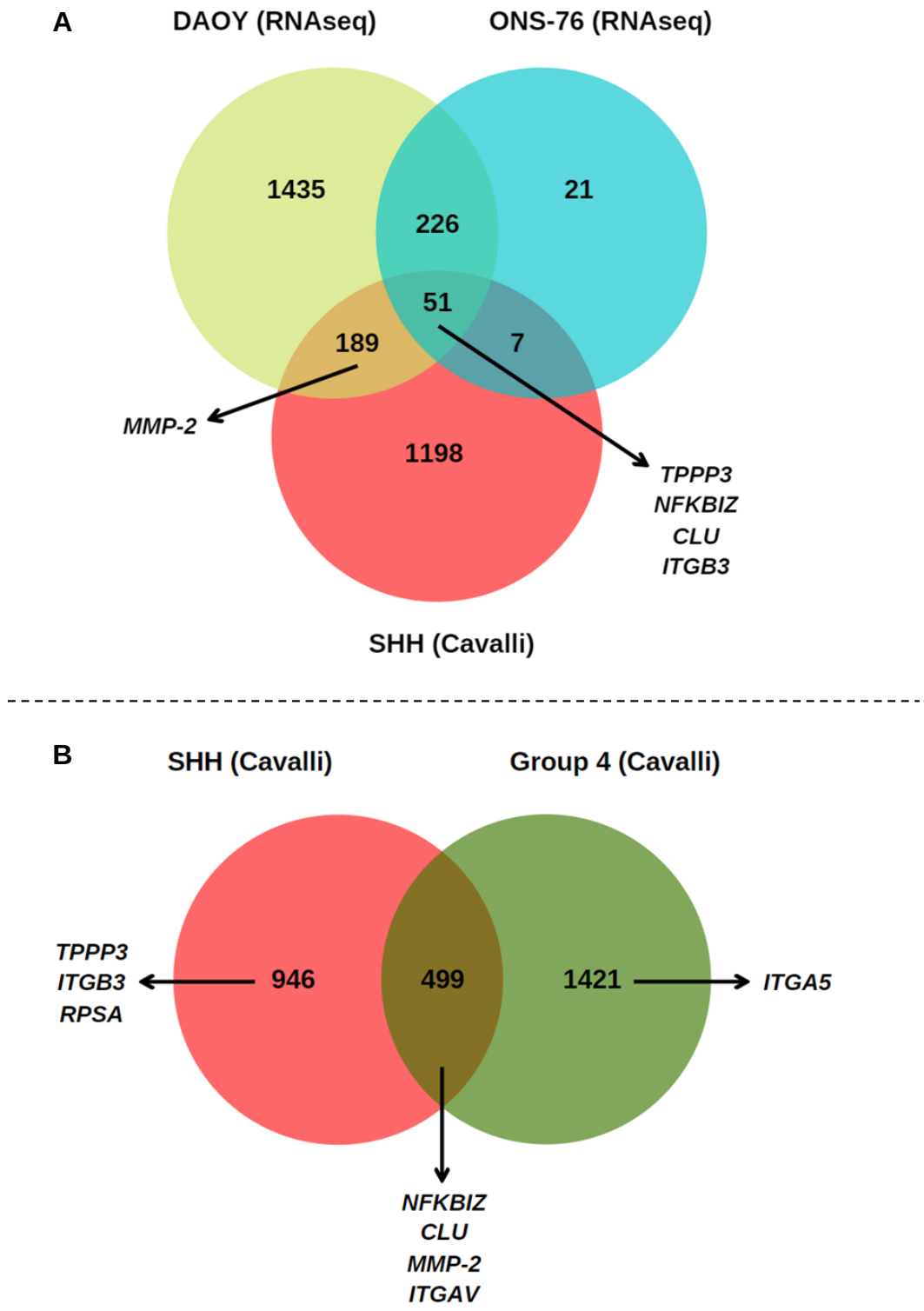


Figure 3.3 The number of overlapping candidate 'laminin regulated genes' (Table 3.1) between SHH patients in the Cavalli dataset and SHH medulloblastoma cell lines in the mRNA sequencing dataset (A), as well as between SHH and Group 4 patients in the Cavalli dataset (B). The number and identity of overlapping genes was established using the online bioinformatics software Venny 2.1.

Since cellular response to laminin is mediated by a range integrin and non-integrin cell-surface receptors, it is important to understand the specific laminin receptors expressed by a tumour, as these receptors facilitate the activation of different cellular pathways and functions associated with tumour progression (Digiacomo and Meruelo, 2016; Su *et al.*, 2020). We therefore decided to also include the laminin receptors Integrin Subunit α5 (*ITGA5*) and Ribosomal Protein SA (*RPSA*) for further investigation, although they were only identified from the analysis of SHH and Group 4 tumours respectively (Figure 3.3). This difference in the expression of laminin receptors between the two sub-groups may be especially important as it could play a role in their different clinical outcomes in response to high levels of LAMA1 and LAMA2 expression.

Finally, *CD44* was also selected as a target for further validation, despite not being identified from the analyses of either the Cavalli or mRNA sequencing datasets. This is because, in addition to having many previous links to tumour progression, CD44 is the primary cell surface receptor for hyaluronan, which forms the backbone of the brain ECM and the *in vitro* hydrogel used in this study. In addition, CD44 can also interact with other ECM components including laminins and collagens (Radotra and McCormick, 1997; Goodison, Urquidi and Tarin, 1999; Okamoto *et al.*, 2002; Necas *et al.*, 2008; Chetty *et al.*, 2012; Mooney *et al.*, 2016; Yamakawa *et al.*, 2017; Ma, Dong and Chang, 2019; Thorne *et al.*, 2020; Xu *et al.*, 2020; Medrano-González *et al.*, 2021). Furthermore, it has been shown by our group to be highly expressed by SHH medulloblastoma cells grown in a 3D hydrogel model (Linke *et al.*, 2020). It therefore merits investigation in the context of medulloblastoma interaction with laminin.

The function of all the candidate ‘laminin regulated genes’ selected for further validation, in normal and disease conditions is shown in Table 3.2.

Table 3.2 The function of the 'laminin regulated genes' selected for further investigation in this study, as well as their role in cancer.

Gene	Function	Role in cancer
TPPP3 (Tubulin Polymerization Promoting Protein Family Member 3)	Regulates microtubule dynamics and has microtubule bundling activity (Zhou *et al.*, 2009)	Tumour proliferation and invasion, metastasis and immune infiltration (Li and Yu, 2017; Li *et al.*, 2018; Z. Yang *et al.*, 2020)
NFKBIZ (NF-κB Inhibitor Zeta)	Positive and negative transcriptional regulator of NF-κB and STAT3 (Motoyama *et al.*, 2005; Trinh *et al.*, 2008)	Modulation of tumour apoptosis induction (Totzke *et al.*, 2006; Li *et al.*, 2018)
MMP-2 (Matrix Metalloproteinase 2)	Zinc endopeptidase involved in the breakdown of the extracellular matrix and tissue remodelling (Bauvois, 2012; Jiang and Li, 2021)	Tumour invasion and metastasis (Egeblad and Werb, 2000 Mook, Frederiks and Van Noorden, 2004)
CLU (Clusterin)	Stress induced molecular chaperone with a role in apoptosis, tissue remodelling and adhesion (Jones and Jomary, 2002; Oh *et al.*, 2019)	Metastasis, regulation of MMP-2 and MMP-9 secretion as well as apoptosis evasion (Zhang *et al.*, 2005; Shapiro *et al.*, 2015; Bonacini *et al.*, 2019)
ITGA5 (Integrin Subunit A 5)	Forms heterodimers with integrin β family members to form cell receptors to fibronectin and osteopontin (Martino *et al.*, 2009; Barczyk, Carracedo and Gullberg, 2010)	Tumour migration and metastasis (Erdogan *et al.*, 2017; Gao *et al.*, 2019)
ITGAV (Integrin Subunit A V)	Forms heterodimers with integrin β family members to form cell receptors to laminin, fibronectin, vitronectin and fibrinogen (Barczyk, Carracedo and Gullberg, 2010; Wong *et al.*, 2010)	Tumour invasion and formation of pre-metastasis niche (Hoshino *et al.*, 2015; Attieh *et al.*, 2017)
ITGB3 (Integrin Subunit B 3)	Forms heterodimers with integrin α family members to form cell receptors to fibronectin, vitronectin and fibrinogen (Barczyk, Carracedo and Gullberg, 2010)	Promotion of EMT and tumour invasion (Attieh *et al.*, 2017; Wen *et al.*, 2019)
RPSA (Ribosomal Protein SA)	Non-integrin laminin receptor that enables cellular adhesion to basement membranes (Tohgo *et al.*, 1994; Digiacomo and Meruelo, 2016)	Promotes tumour invasion and metastasis through increased cellular adhesion (Martignone *et al.*, 1993; Carbone *et al.*, 1995)
CD44 (Cluster of differentiation 44)	Transmembrane adhesion glycoprotein (with several splice variants) that primarily associates with hyaluronan (HA), as well as several other ECM components (Aruffo *et al.*, 1990; Ponta, Sherman and Herrlich, 2003)	Tumour invasion, proliferation and apoptosis evasion (Chetty *et al.*, 2012; Mooney *et al.*, 2016; Yamakawa *et al.*, 2017; Ma, Dong and Chang, 2019)

The direction in which the expression of the selected ‘laminin regulated genes’ are altered in either the *LAM*^{high} ECM sub-type in SHH and Group 4 patient tumours or by the presence of laminin-111 in SHH medulloblastoma cell lines (DAOY and ONS-76), can be observed in Figures 3.4 and 3.5 respectively, where both datasets have been visualised in the form of volcano plots. Furthermore, the exact Log2 fold changes in gene expression, p-values and level of significance of all the selected candidate genes are displayed in Table 3.3. *CLU, NFKBIZ* and *ITGB3* represent the most promising targets as their differential regulation by *LAMA1* and *LAMA2*/laminin-111 is maintained across both datasets in all sub-groups and cell lines.

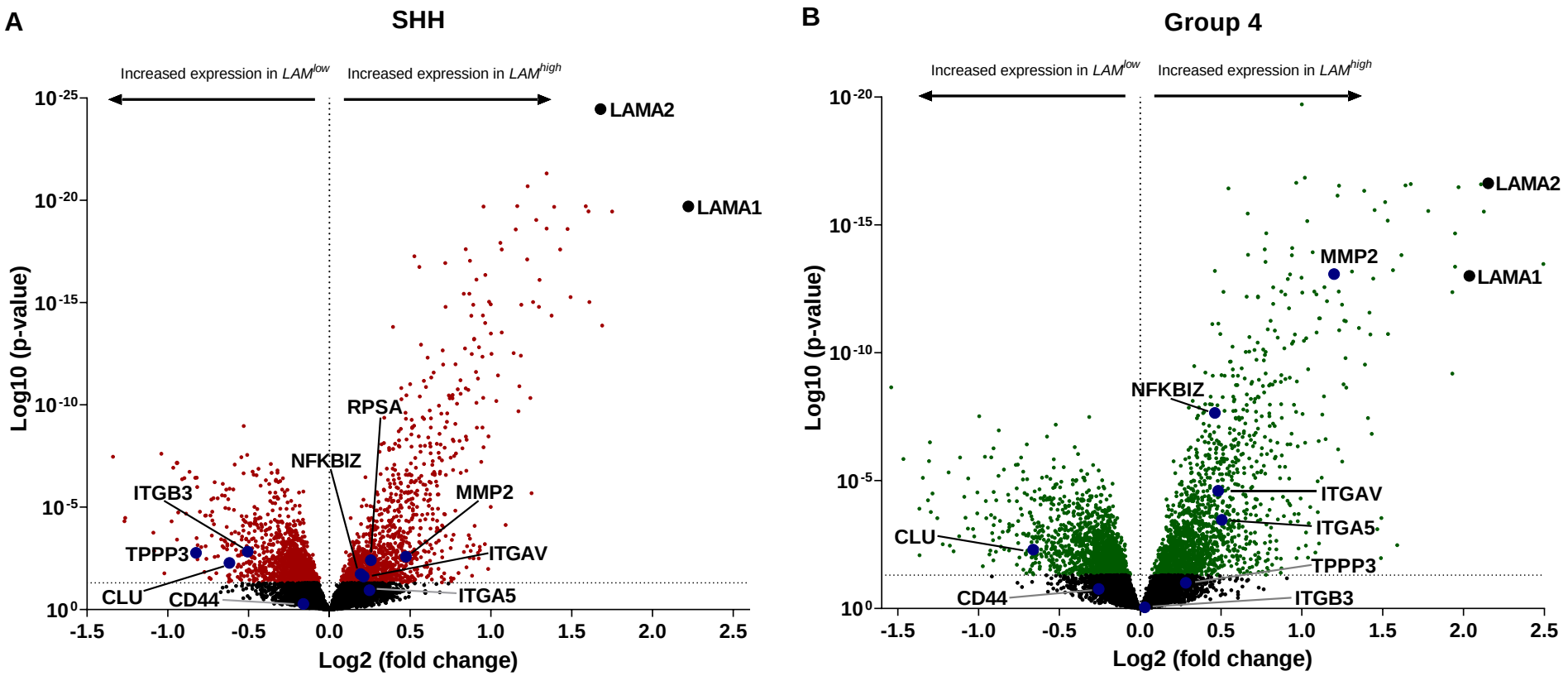


Figure 3.4 Differential gene expression analysis between two ECM sub-types in SHH and Group 4 medulloblastoma patient tumours, defined in the Cavalli dataset by a previous study by our group: Laminin Subunit α1 (*LAMA1*) and Laminin Subunit α2 (*LAMA2*) *(LAM)*^{high} / Vitronectin *(VTN)*^{low} and *LAM*^{low}*/VTN*^{low} (Linke *et al*., 2020; Cavalli *et al*. 2019). This analysis was used to identify candidate 'laminin regulated genes' in the SHH (**A**) and Group 4 (**B**) medulloblastoma sub-groups. Each dot represents one gene, coloured dots above the dotted line represent significant genes (p-value cut off <0.05). For the SHH sub-group, LAM^{high}/VTN^{low}: n=114 and LAM^{low}/VTN^{low}: n=58. For Group 4, LAM^{high}/VTN^{low}: n=31 and LAM^{low}/VTN^{low}: n=40. Significance was determined using One-Way ANOVA analyses (after the data had undergone a Log2 transformation) with an uncorrected p-value and a q-value determined using the Benjamini-Hochberg False Discovery Rate (FDR) approach to correct for multiple testing. The Log2 fold change indicates the mean expression level for each gene. 'Laminin regulated genes' selected for further investigation are labelled and represented by enlarged blue dots. *LAMA1* and *LAMA2* are also enlarged and labelled as they are the genes which define the '*LAM*^{high}' ECM sub-type.

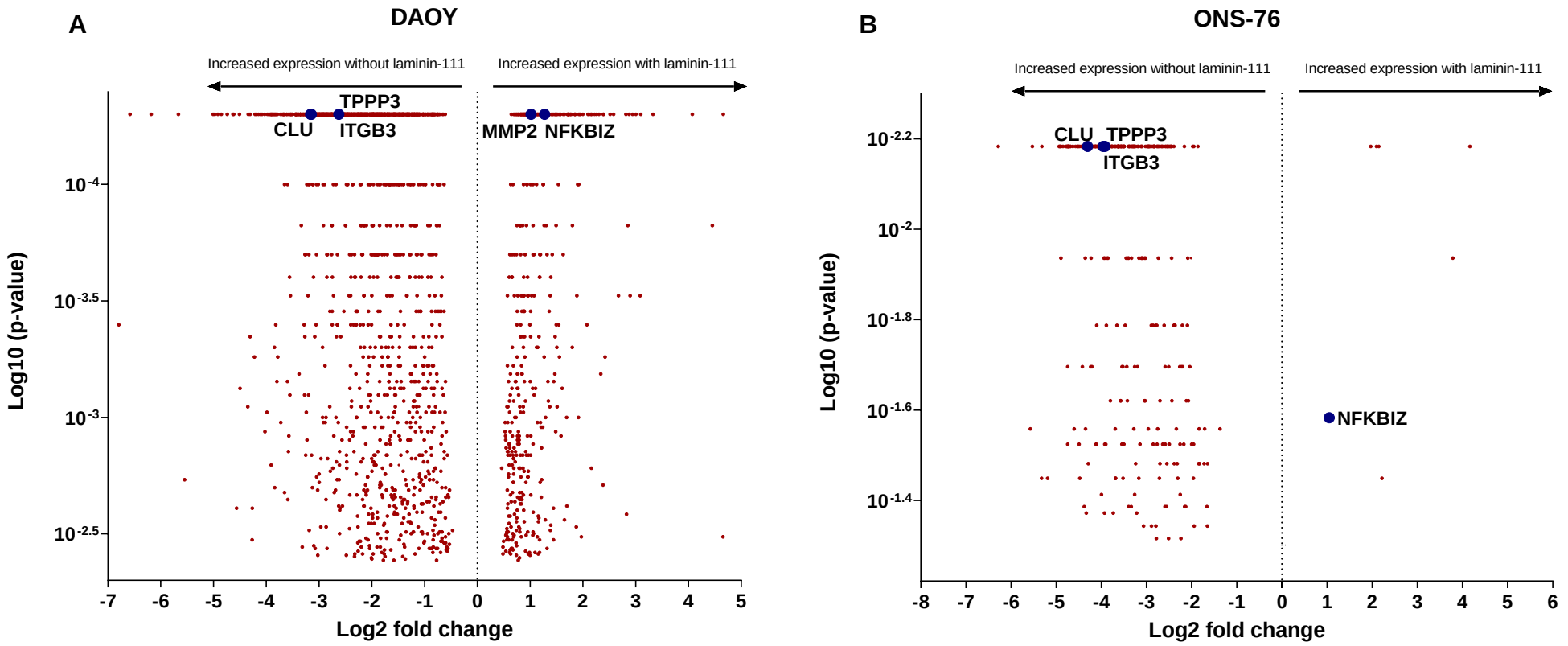


Figure 3.5 Differential gene expression analysis, of mRNA sequencing data, between SHH medulloblastoma cell lines (DAOY and ONS-76) grown on top of hyaluronan hydrogels with and without laminin-111. This analysis was used to identify candidate 'laminin regulated genes' from both the DAOY (**A**) and ONS-76 (**B**) SHH medulloblastoma cell lines. Each dot represents one gene, with all genes being significant (p-value cut off <0.05). Significance was determined using One-Way ANOVA analyses with an uncorrected p-value and a q-value determined utilising the Benjamini-Hochberg False Discovery Rate (FDR) approach to correct for multiple testing. The Log2 fold change indicates the mean expression level for each gene (n=3). 'Laminin regulated genes' selected for further investigation are labelled and represented by enlarged blue dots.

Table 3.3 Log2 fold changes in gene expression, p-values and significance levels of all the 'laminin regulated genes' across the Cavalli and mRNA sequencing datasets selected for further investigation. Boxes shaded blue indicate a decrease in gene expression in response to high Laminin Subunit α1 (*LAMA1*) and Laminin Subunit α2 (*LAMA2*) expression/laminin-111, whereas orange indicates an increase. p*<0.05, **p≤0.01, ***p≤0.001, ****p≤0.0001

Gene	Cavalli SHH			RNAseq DAOY (SHH)			RNAseq ONS-76 (SHH)			Cavalli Group 4		
	Log2 Fold change	p-value	Significance	Log2 Fold change	p-value	Significance	Log2 Fold change	p-value	Significance	Log2 Fold change	p-value	Significance
TPPP3	-0.823	0.00168	**	-2.623	0.00142	**	-4.532	0.00655	**	0.282	0.0991	ns
NFKBIZ	0.212	0.0242	*	1.273	0.00142	**	1.050	0.0261	*	0.461	2.25E-08	****
MMP2	0.474	0.00259	**	1.019	0.00142	**	0.36906	0.547	ns	1.199	8.39E-14	****
CLU	-0.619	0.00529	**	-3.160	0.00142	**	-4.307	0.00655	**	-0.663	0.005	**
ITGA5	0.249	0.113	ns	-0.125	0.895	ns	0.0619	0.887	ns	0.505	0.0003	***
ITGAV	0.193	0.0184	*	0.211	0.858	ns	0.698	0.207	ns	0.482	2.49E-05	****
ITGB3	-0.506	0.00147	**	-3.147	5.0E-04	****	-3.963	0.00655	**	0.0292	0.898	ns
RPSA	0.257	0.00388	**	0.257	0.378	ns	0.0676	0.999	ns	-0.0818	0.353	ns
CD44	-0.16046	0.527	ns	0.299	0.534	ns	0.00344	0.994	ns	-0.257	0.173	ns

3.4 Assessment of *LAMA1*/LAMA1 and *LAMA2*/LAMA2 expression in SHH and Group 4 medulloblastoma patient derived cell lines

To further investigate the candidate 'laminin regulated genes', patient derived medulloblastoma cell lines from the SHH and Group 4 sub-groups were selected for cell culture validation assays. For the SHH sub-group the DAOY and ONS-76 cell lines were selected, these were the same cell lines that were used to generate the mRNA sequencing dataset. For Group 4, the CHLA-01-MED (CHLA-01) and CHLA-01-R-MED (CHLA-01-R) cell lines were chosen; a matched pair cell line where CHLA-01 was derived from the primary tumour and CHLA-01-R was derived from a malignant pleural effusion from the same patient. Clinical and cell culture information regarding these cell lines can be found in Table 2.1. Furthermore, images of all cell lines under normal growth conditions can be observed in Figure 3.6.

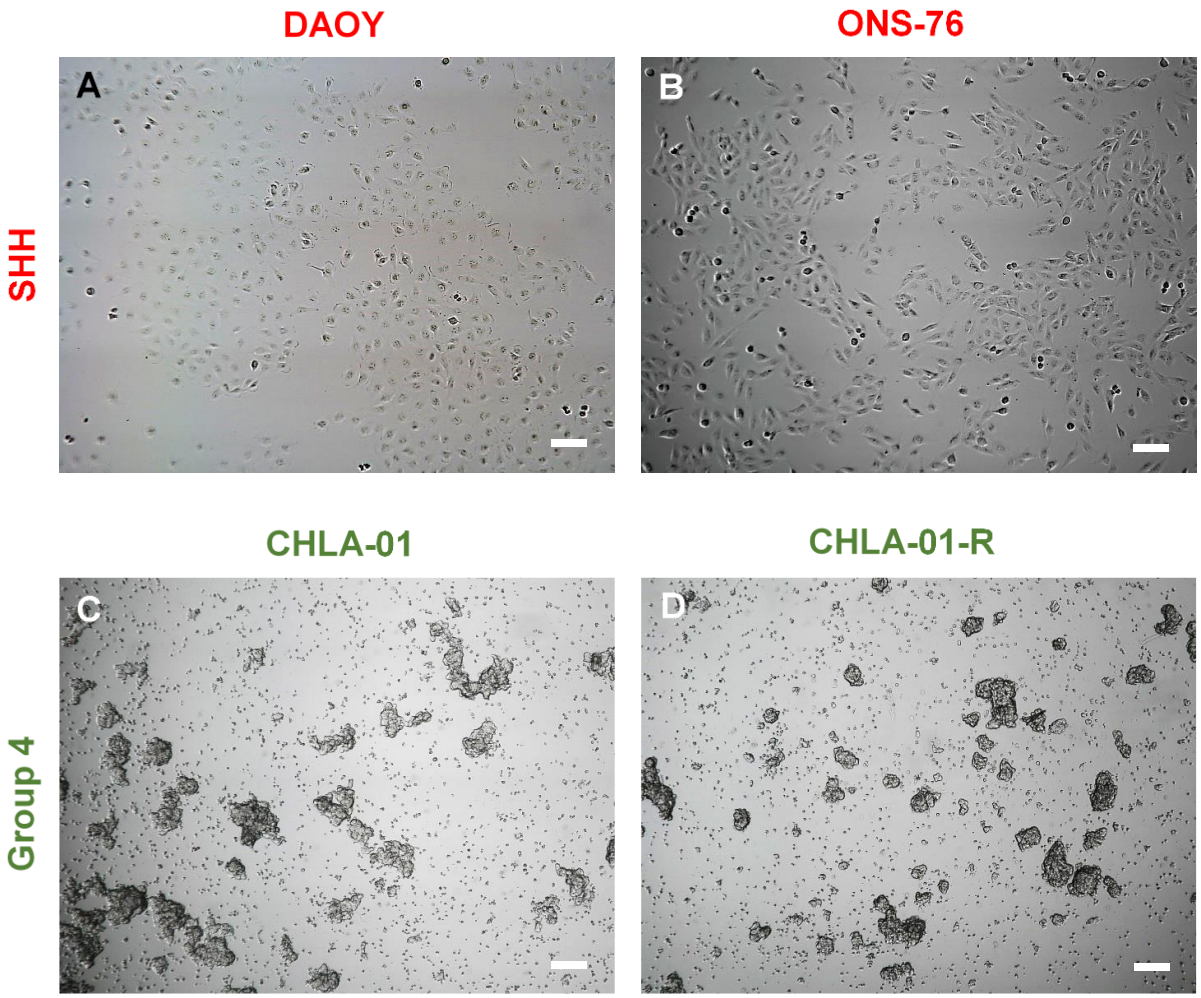


Figure 3.6 Brightfield images (4 X magnification) of the DAOY, ONS-76, CHLA-01-MED and CHLA-01-R-MED cell lines grown under their normal growth conditions. The DAOY (**A**) and ONS-76 (**B**) cell lines grow as an adherent monolayer in DMEM + 10% FBS and RPMI +10% FBS respectively, whereas as both the CHLA-01 (**C**) and CHLA-01-R (**D**) cell lines grow in suspension in DMEM F12 + B27 + 20 ng/mL bFGF and EGF. Scale bar 100 µm.

Prior to using these cell lines in cell culture models their level of *LAMA1*/LAMA1 and *LAMA2*/LAMA2 expression was assessed, to confirm that they synthesise these subunits of laminin and were therefore representative models to be used in further studies (Figure 3.7). *LAMA1* and *LAMA2* gene expression was analysed by qRT-PCR analysis (Figure 3.7 A and B), whereas their level of protein expression was determined by western blotting (Figure 3.7 C-F). In both gene and protein expression analyses, significant differences in expression between the CHLA-01 and CHLA-01-R cell lines were determined by both a One-Way ANOVA, that included the SHH cell lines, as well as an unpaired t-test that compared them directly; this is of interest since they represent the primary and metastatic disease of the same patient.

qRT-PCR analysis demonstrated that *LAMA1* is expressed at a detectable level across both the SHH and Group 4 cell lines (Figure 3.7 A). This analysis also showed that *LAMA1* gene expression is significantly higher in both Group 4 cell lines compared to the SHH cell lines ($p<0.05$ for all comparisons; Figure 3.7 A). Western blotting analysis also showed that LAMA1 is expressed across all of the cell lines of interest, supporting the findings of the qRT-PCR analysis. However, it also demonstrated that LAMA1 protein expression is in fact significantly higher in the both the SHH cell lines compared to the CHLA-01 Group 4 cell line, but not the CHLA-01-R ($p<0.05$; Figure 3.7 C and E).

qRT-PCR analysis of *LAMA2* demonstrated that it is also expressed across both the SHH and Group 4 cell lines (Figure 3.7 B). This analysis also showed that the ONS-76 SHH cell line has a significantly greater level of *LAMA2* expression than the other SHH cell line (DAOY), as well as both Group 4 cell lines ($p<0.05$ for all comparisons; Figure 3.7 B). Western blotting analysis also demonstrated that LAMA2 is expressed across all of the cell lines of interest, corroborating the findings from the qRT-PCR analysis (Figure 3.7 D). However, this analysis also indicated that although the level of LAMA2 protein expression is still higher in the ONS-76 cell line compared with the

DAOY cell line, it is not significant (Figure 3.7 F). Furthermore, contrary to the gene expression analysis, both the Group 4 cell lines have a significantly higher level of LAMA2 protein expression than the SHH cell lines ($p<0.01$ for all comparisons; Figure 3.7 D and F).

In summary, *LAMA1* gene expression is higher in the Group 4 cell lines than the SHH cell lines, whereas LAMA1 protein expression is higher in both SHH cell lines than in the primary Group 4 cell line (CHLA-01) (Figure 3.7 A, C and E). Furthermore, *LAMA2* gene expression is higher in one SHH cell line (ONS-76) than the other (DAOY), as well as both Group 4 cell lines, while LAMA2 protein expression is higher in both Group 4 cell lines compared to both SHH cell lines (Figure 3.7 B, D and F).

In addition to these findings, the primary Group 4 cell line (CHLA-01) was shown to exhibit a significantly higher level of *LAMA1* gene expression than its recurrent counterpart (CHLA-01-R) when compared directly by a t-test (Figure 3.7 A). However, the inverse is true with regards to LAMA1 protein expression which was found to be significantly greater in the CHLA-01-R cell line compared to the CHLA-01 ($p<0.05$; Figure 3.7 C and E). This is especially interesting as it suggests that LAMA1 has a more prominent role Group 4 metastases than the primary tumour. In contrast, neither qRT-PCR nor western blotting analysis indicated a significant difference in the expression of *LAMA2*/LAMA2 between the CHLA-01 and CHLA-01-R cell lines (Figure 3.7 D and F).

The differences between gene and protein expression throughout these analyses could perhaps be attributed to unexplained differences in translational regulation of *LAMA1* and *LAMA2* in the cell lines.

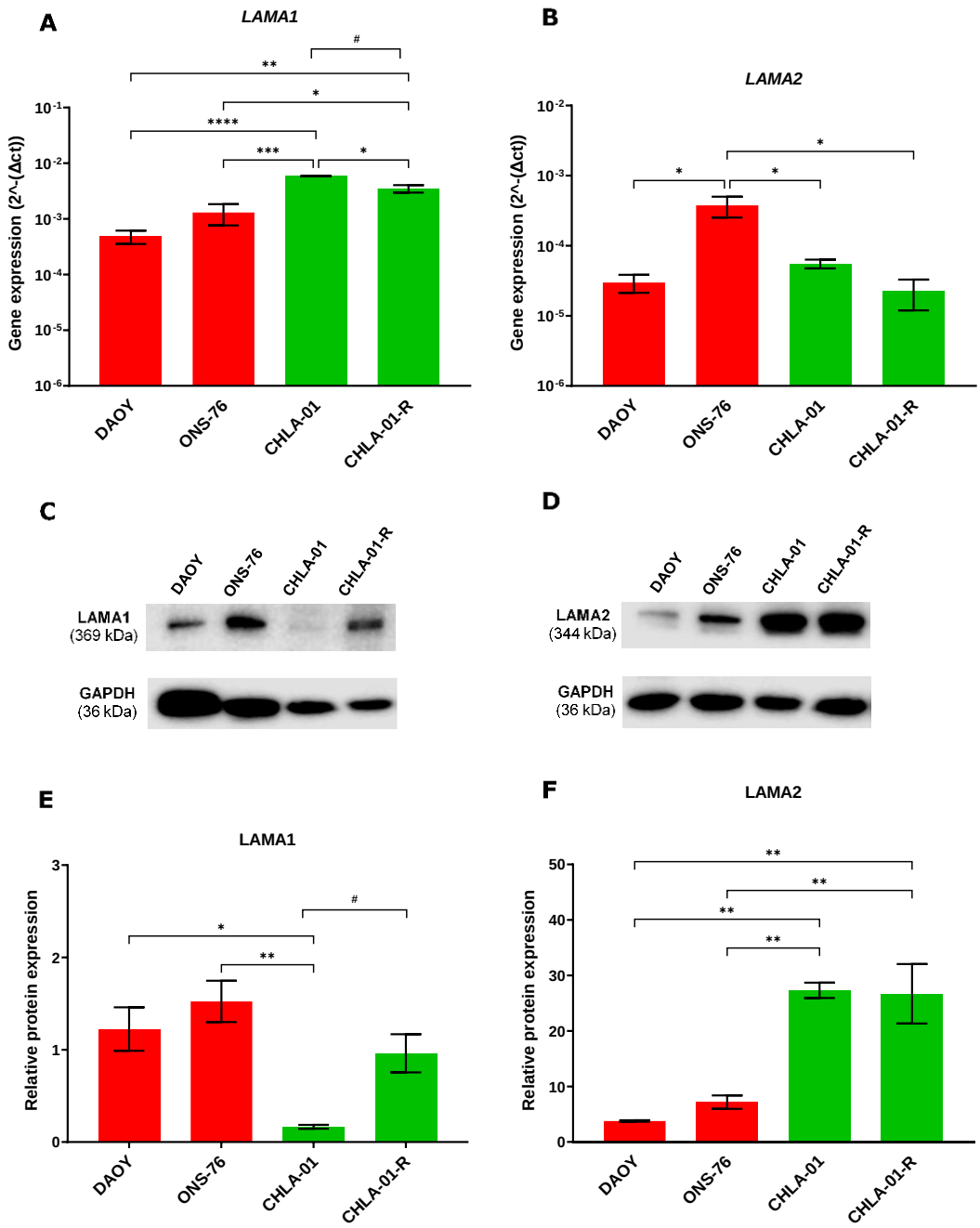


Figure 3.7 Laminin Subunit α1 (*LAMA1*/LAMA1) and Laminin Subunit α2 (*LAMA2*/LAMA2) are expressed in both SHH (DAOY and ONS-76) and Group 4 (CHLA-01 and CHLA-01-R) medulloblastoma cell lines. qRT-PCR analysis demonstrated that *LAMA1* (**A**) and *LAMA2* (**B**) are expressed in both SHH (red) and Group 4 (green) medulloblastoma cell lines. This finding was corroborated by western blotting and densitometry analysis of LAMA1 (**C** and **E**) and LAMA2 (**D** and **F**) expression in the same cell lines. Both qRT-PCR and western blotting analyses were normalised to *GAPDH*/GAPDH as a loading control. Representative blots are shown. Full length, exemplar blots of the antibodies used here can be overserved in Appendix Figure 1. Mean ± SEM plotted; n=3. Significance was assessed using One-Way ANOVA analyses with Tukey's multiple comparisons test; *p<0.05, **p≤0.01, ***0.001, ****p<0.0001. Since the CHLA-01 and CHLA-01-R are a matched pair of cell lines, significance was also calculated directly between them using an unpaired t-test; #p<0.05. All significant comparisons are highlighted, otherwise comparisons are not significant.

3.5 Validating candidate 'laminin regulated genes' using 2D and 3D cell culture assays

Once we had selected the candidate 'laminin regulated genes' for further investigation (as outlined in section 3.3) we sought to validate them in both 2D and 3D *in vitro* cell culture assays, whereby the cell lines were exposed to exogenous laminin-111 (Figure 3.8). This is the same isoform of laminin that was used to stimulate the SHH medulloblastoma cell lines in the RNAseq dataset, which identified relevant genes overlapping with the patient dataset (Figure 3.3).

In the 2D assay, cell lines were seeded into a 6 well plate with and without laminin-111 coating and incubated for 48 hours, whereas in the 3D assay, cell lines were grown in hyaluronan hydrogels with and without laminin-111 for 21 days. Hyaluronan is the main component of the brain ECM, making the 3D assay a brain-specific model (Novak and Kaye, 2000). Details of the methods for the 2D and 3D assays can be found in sections 2.6.1 and 2.8.2 respectively.

In these assays the effect of laminin-111 was studied by assessing changes in the phenotype of the cell lines, the expression of the selected 'laminin regulated genes' and the secretion of MMP-2 (as one of the 'laminin regulated genes' is MMP-2). Firstly, in order to assess any phenotypic changes in response to laminin-111, brightfield microscope images of the cell lines were captured at different time points throughout both the 2D (24 and 48 hours) and 3D (every 3 days) assays. Next, to assess if laminin-111 stimulated any changes in the expression of the selected 'laminin regulated genes', RNA was extracted from the cell lines in both assays and used in qRT-PCR analysis. Finally, in order to assess changes in MMP-2 secretion, the supernatant from each cell line (i.e. the media in which the cells were being grown) was collected at the end of the 2D assay and every 2-3 days in the 3D assay, and a gelatin zymography was conducted. Gelatin zymography is a form of gel electrophoresis which detects the

activity of the gelatinases MMP-2 and Matrix Metalloproteinase 9 (MMP-9) (as well as their zymogen forms Pro-MMP-2 and Pro-MMP-9) in cell line supernatants, via enzymatic digestion of gelatin within the polyacrylamide gel. Densitometry analysis of the digestion bands is then conducted to calculate the level of MMP-2/-9 present in the sample. Although MMP-9 was not identified as a 'laminin regulated gene', it is also a gelatinase that is detected by gelatin zymography. MMP-9 also has a role in medulloblastoma progression and tumour metastasis, therefore throughout this study the level of MMP-9 secretion has also been assessed (Yu and Stamenkovic, 1999; Mook, Frederiks and Van Noorden, 2004; Özen *et al.*, 2004; Annabi *et al.*, 2010). An overview of these assays and analyses is shown in Figure 3.8.

3.5.1 Validation of candidate 'laminin regulated genes' using a 2D cell culture assay

In order to validate the selected 'laminin regulated genes' the previously described 2D cell culture assay was conducted using the SHH (DAOY and ONS-76) and Group 4 (CHLA-01 and CHLA-01-R) medulloblastoma cell lines.

Firstly, any phenotypic effects of laminin-111 on the cell lines were assessed from brightfield microscope images taken after 48 hours incubation. Representative images can be observed in Figure 3.9. In the SHH cell lines, laminin-111 had no obvious phenotypic effect (Figure 3.9 A). However, the recurrent Group 4 cell line (CHLA-01-R), exhibited a distinct adherence phenotype, which was absent in the primary cell line (CHLA-01), suggesting that Group 4 metastases may interact with laminin-111 in a different manner to that of the primary tumour (Figure 3.9 B).

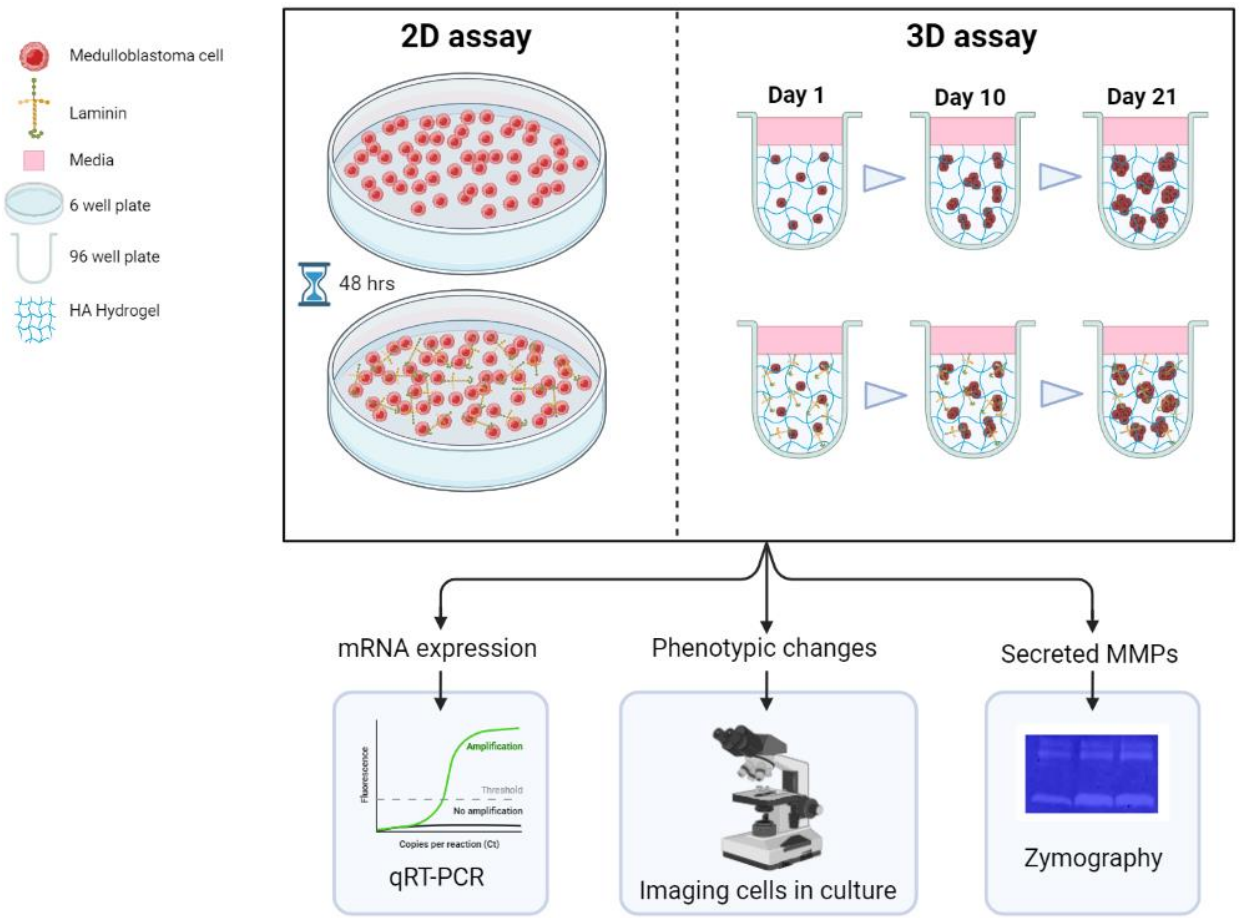


Figure 3.8 Schematic of the 2D and 3D cell culture assays used to validate 'laminin regulated genes' in SHH (DAOY and ONS-76) and Group 4 (CHLA-01 and CHLA-01-R) medulloblastoma cell lines. In the 2D assay, cell lines were seeded into a 6 well plate with and without laminin-111 and incubated for 48 hours. In the 3D assays cell lines were grown in 3D hyaluronan hydrogels with and without laminin-111 for 21 days. In both of the assays the cell lines were imaged using a light microscope in order to assess any phenotypic changes in response to laminin-111. At the end of the 2D assay and every 2/3 days in the 3D assay the supernatant was collected and at the end of both assays the cells were harvested. A zymography was then conducted on the supernatant in order to assess changes in Matrix Metalloproteinase 2 (MMP-2) secretion, while the cells were used to conduct qRT-PCR analysis of the selected 'laminin regulated genes'.

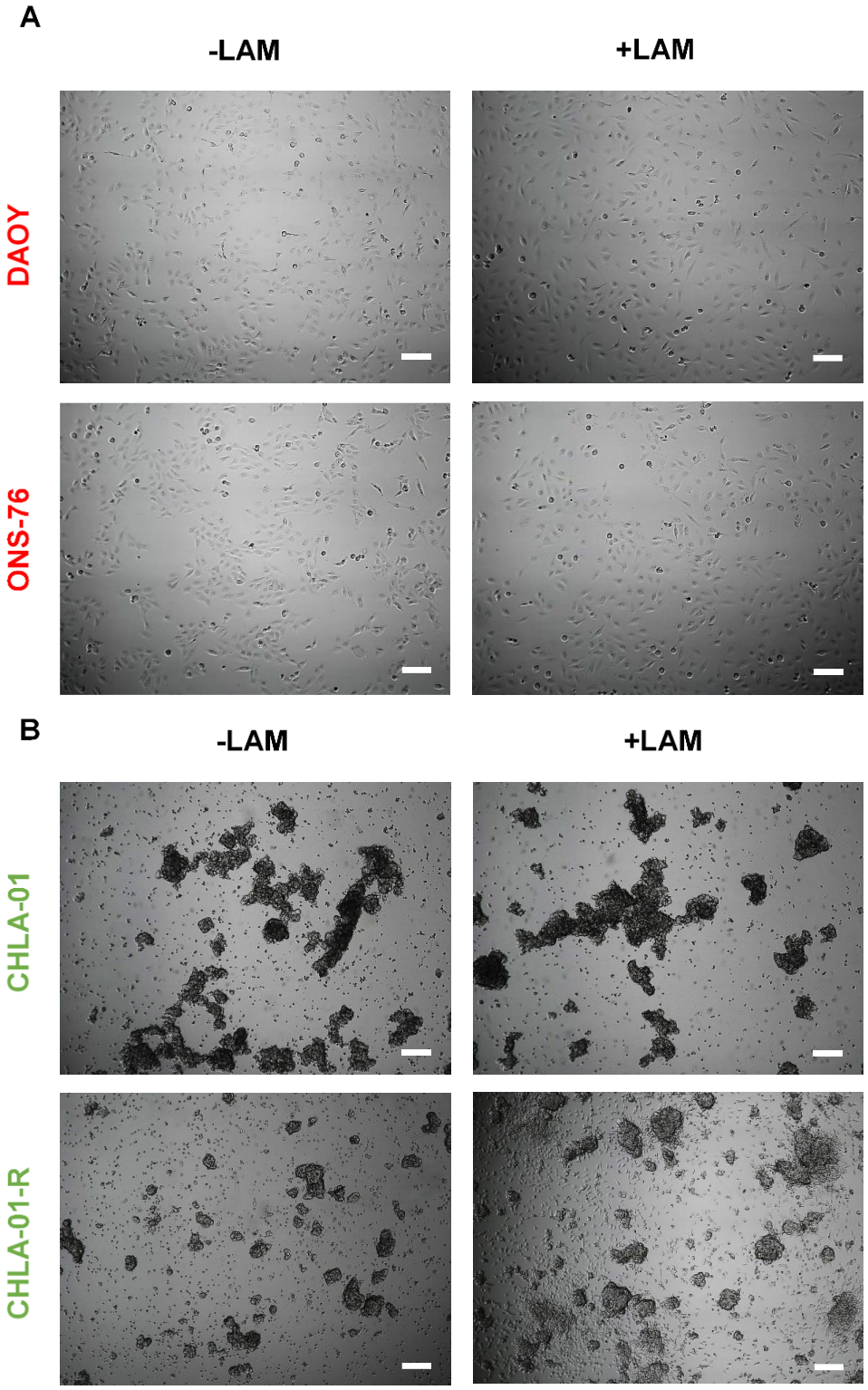


Figure 3.9 Recurrent Group 4 medulloblastoma cell line (CHLA-01-R) exhibits an adherence phenotype to laminin-111 that is absent in the primary matched pair cell line (CHLA-01). Brightfield images (4 X magnification) of SHH (DAOY and ONS-76) (**A**) and Group 4 (CHLA-01 and CHLA-01-R) (**B**) medulloblastoma cell lines after 48 hours incubation in a 6 well plate with (+LAM) and without (-LAM) laminin-111 coating. SHH cell lines remain phenotypically unchanged, whereas the recurrent Group 4 cell line (CHLA-01-R) exhibits an adherence phenotype that is absent in its primary counterpart (CHLA-01). Representative images are shown (n=3). Scale bar 100 µm.

Next, qRT-PCR analysis of the selected 'laminin regulated genes' (Table 3.2) demonstrated that *TPPP3*, *NFKBIZ, MMP-2*, *ITGA5*, *RPSA* and *CD44* were the only genes to exhibit significantly altered expression in response to laminin-111 in any of the SHH or Group 4 medulloblastoma cell lines (Figure 3.10 A, B, C, E, H and I). However, the direction in which the expression of these genes was altered by laminin-111 did not always align with the genomic analysis of patient tumours (Cavalli) and SHH medulloblastoma cell lines (mRNA sequencing) from which they were identified (section 3.3).

The expression of *TPPP3* was found to be significantly increased by laminin-111 in the ONS-76 SHH cell line as well as the recurrent Group 4 cell line (CHLA-01-R) ($p<0.05$ for all comparisons; Figure 3.10 A). Whereas, in both the mRNA sequencing and genomic patient data, *TPPP3* expression was downregulated in response to laminin-111 in the SHH cell lines and in LAM^{high} SHH tumours respectively (Table 3.3). Furthermore, *TPPP3* expression was unaltered in the LAM^{high} ECM sub-type in Group 4 tumours (Table 3.3).

NKFBIZ expression was found to be significantly increased by laminin-111 in just the CHLA-01-R cell line ($p\leq0.0001$; Figure 3.10 B). This finding was corroborated by the genomic patient data, which indicated that *NFKBIZ* expression was also significantly increased in LAM^{high} Group 4 tumours (Table 3.3).

The expression of *MMP-2* was found to be significantly increased in the DAOY SHH cell line and decreased in the recurrent Group 4 cell line (CHLA-01-R), in response to laminin-111 ($p<0.05$ for all comparisons; Figure 3.10 C). In line with this, *MMP-2* expression was also found to also be increased in response to laminin-111 in the DAOY SHH cell line in the mRNA sequencing data and in LAM^{high} SHH tumours in the genomic patient data (Table 3.3). In contrast to these findings however, *MMP-2*

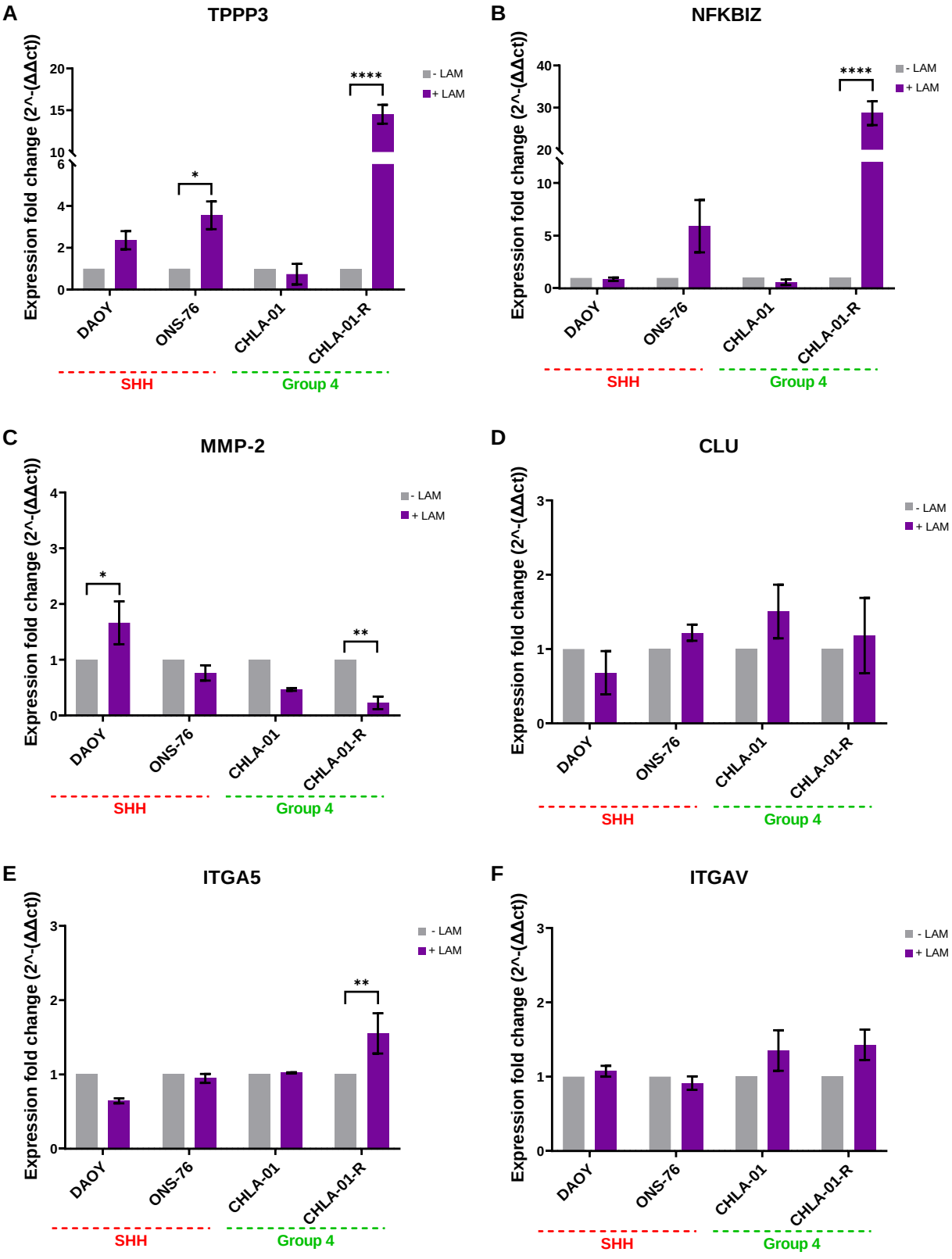
expression was found to be significantly increased in *LAM*^{high} Group 4 tumours in the genomic patient data (Table 3.3).

The expression of *ITGA5* was found to be significantly increased by laminin-111 in the recurrent Group 4 cell line (CHLA-01-R) ($p \leq 0.01$; Figure 3.10 E). In corroboration of this finding, *ITGA5* expression was also upregulated in *LAM*^{high} Group 4 tumours in the genomic patient data (Table 3.3).

RPSA expression was found to be significantly increased in the primary Group 4 cell line (CHLA-01) in response to laminin-111 ($p < 0.05$; Figure 3.10 H). However, the expression of *RPSA* was unaltered in *LAM*^{high} Group 4 tumours in the genomic patient data (Table 3.3).

Lastly, the expression of *CD44* was shown to be significantly increased in the recurrent Group 4 cell line (CHLA-01-R; $p \leq 0.0001$), despite not being identified from the genomic analyses of medulloblastoma cell lines or patient tumours.

Interestingly, the cell line which exhibited significantly altered expression of the most 'laminin regulated genes' (markedly so in the case of *NFKBIZ, TPPP3* and *CD44*) in response to laminin-111 was the recurrent Group 4 cell line (CHLA-01-R), the same cell line which exhibited a distinct adherence phenotype to laminin-111 (Figure 3.9 B). This suggests that the expression of these genes may be altered as a consequence of the unique interaction with laminin-111 exhibited by this cell line.


A
TPPP3
Expression fold change (2^-(ΔΔct))
- LAM
+ LAM
****
*
DAOY
ONS-76
CHLA-01
CHLA-01-R
SHH
Group 4
B
NFKBIZ
Expression fold change (2^-(ΔΔct))
- LAM
+ LAM
****
DAOY
ONS-76
CHLA-01
CHLA-01-R
SHH
Group 4
C
MMP-2
Expression fold change (2^-(ΔΔct))
- LAM
+ LAM
*
**
DAOY
ONS-76
CHLA-01
CHLA-01-R
SHH
Group 4
D
CLU
Expression fold change (2^-(ΔΔct))
- LAM
+ LAM
DAOY
ONS-76
CHLA-01
CHLA-01-R
SHH
Group 4
E
ITGA5
Expression fold change (2^-(ΔΔct))
- LAM
+ LAM
**
DAOY
ONS-76
CHLA-01
CHLA-01-R
SHH
Group 4
F
ITGAV
Expression fold change (2^-(ΔΔct))
- LAM
+ LAM
DAOY
ONS-76
CHLA-01
CHLA-01-R
SHH
Group 4

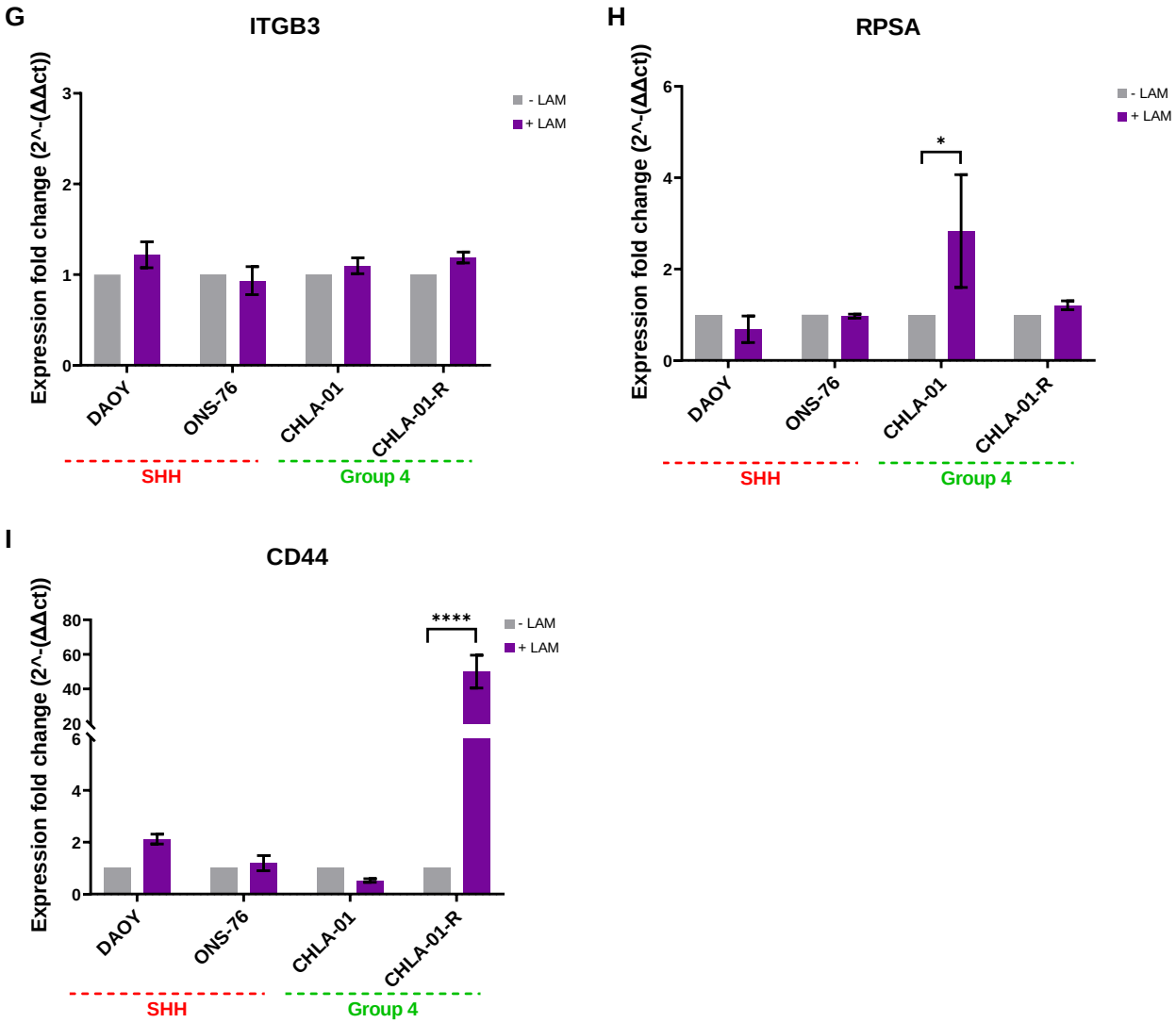


Figure 3.10 Laminin-111 significantly alters the expression of Tubulin Polymerization Promoting Protein Family Member 3 (*TPPP3*), NF-κB Inhibitor Zeta (*NFKBIZ*), Matrix Metalloproteinase 2 (*MMP-2*), Integrin Subunit A 5 (*ITGA5*), Ribosomal Protein SA (*RPSA*) and Cluster of Differentiation 44 (*CD44*) in some SHH and Group 4 medulloblastoma cell lines in a 2D cell culture assay. (**A** – **I**) qRT-PCR analysis of the selected 'laminin regulated genes' (section 3.3) in SHH and Group 4 medulloblastoma cell lines in a 2D cell culture assay whereby cells were seeded into a 6 well plate with and without a laminin-111 coating and incubated for 48 hours. Only the expression of *TPPP3, NFKBIZ, MMP-2, ITGA5, RPSA* and *CD44* were significantly altered by laminin-111 in any of the cell lines. All qRT-PCR analysis was conducted relative to *GAPDH*. Relative changes in gene expression between cells incubated in uncoated and laminin-111 coated wells was calculated using the ΔΔCt method (section 2.12.7). Mean ± SEM plotted; n=3. Significance was assessed using Two-Way ANOVA analyses with Sidak's multiple comparisons post-hoc test; *p<0.05, **p≤0.01, ****p≤0.0001. All significant comparisons are highlighted, otherwise comparisons are not significant.

Finally, gelatin zymography analysis was conducted on the supernatant collected from both the SHH and Group 4 cell lines in the 2D assay. The raw and relative values of the densitometry analysis of Pro-MMP-2 and MMP-9 can be observed in Figure 3.11.

Pro-MMP-2 secretion was specifically assessed as it was the form of MMP-2 that was detected in every cell line. The raw values were used to compare Pro-MMP-2/MMP-9 secretion between the cell lines and the relative values were used to compare between the laminin-111 conditions within cell lines. Relative values were calculated by dividing the laminin-111 coated condition (+LAM) by the uncoated condition (-LAM).

This analysis indicated that laminin-111 did not significantly alter Pro-MMP-2 secretion in any of the SHH or Group 4 cell lines in the 2D assay (Figure 3.11 A-C). However, a decrease in Pro-MMP-2 secretion in response to laminin-111 was indicated in the primary Group 4 cell line (CHLA-01), although it was not significant (Figure 3.11 C). This supports the same trend identified by the qRT-PCR analysis of *MMP-2* in the CHLA-01 cell line (Figure 3.10 C). Furthermore, by comparing the raw Pro-MMP-2 band intensity values of just the uncoated control conditions, it is possible to assess the differences in Pro-MMP-2 secretion between cell lines in normal growth conditions (Figure 3.11 B). The ONS-76 SHH cell line secreted the highest level of Pro-MMP-2 out of all the cell lines. The DAOY SHH cell line and the metastatic Group 4 cell line (CHLA-01-R) secreted a similar level of Pro-MMP-2, while the primary Group 4 cell line secreted the least (Figure 3.11 A and B). It is particularly interesting that the recurrent Group 4 cell line seemingly secretes more Pro-MMP-2 than its primary counterpart, as MMP-2 secretion has been highly linked with metastasis in a variety of cancers (Mook, Frederiks and Van Noorden, 2004; Jezierska and Motyl, 2009; Wang *et al.*, 2014). However, direct comparisons of Pro-MMP-2/MMP-9 secretion between the cell lines are limited as some of the supernatants were analysed on different zymograms and, unlike qRT-PCR and western blotting analyses, MMP-2/-9 secretion is not normalised to a housekeeping gene.

Finally, MMP-9 secretion was only detected in the SHH cell lines, which exhibited a similar level of secretion. However, stimulation with laminin-111 did not affect the level of MMP-9 secretion in either of the SHH cell lines (Figure 3.11 A, D and E).

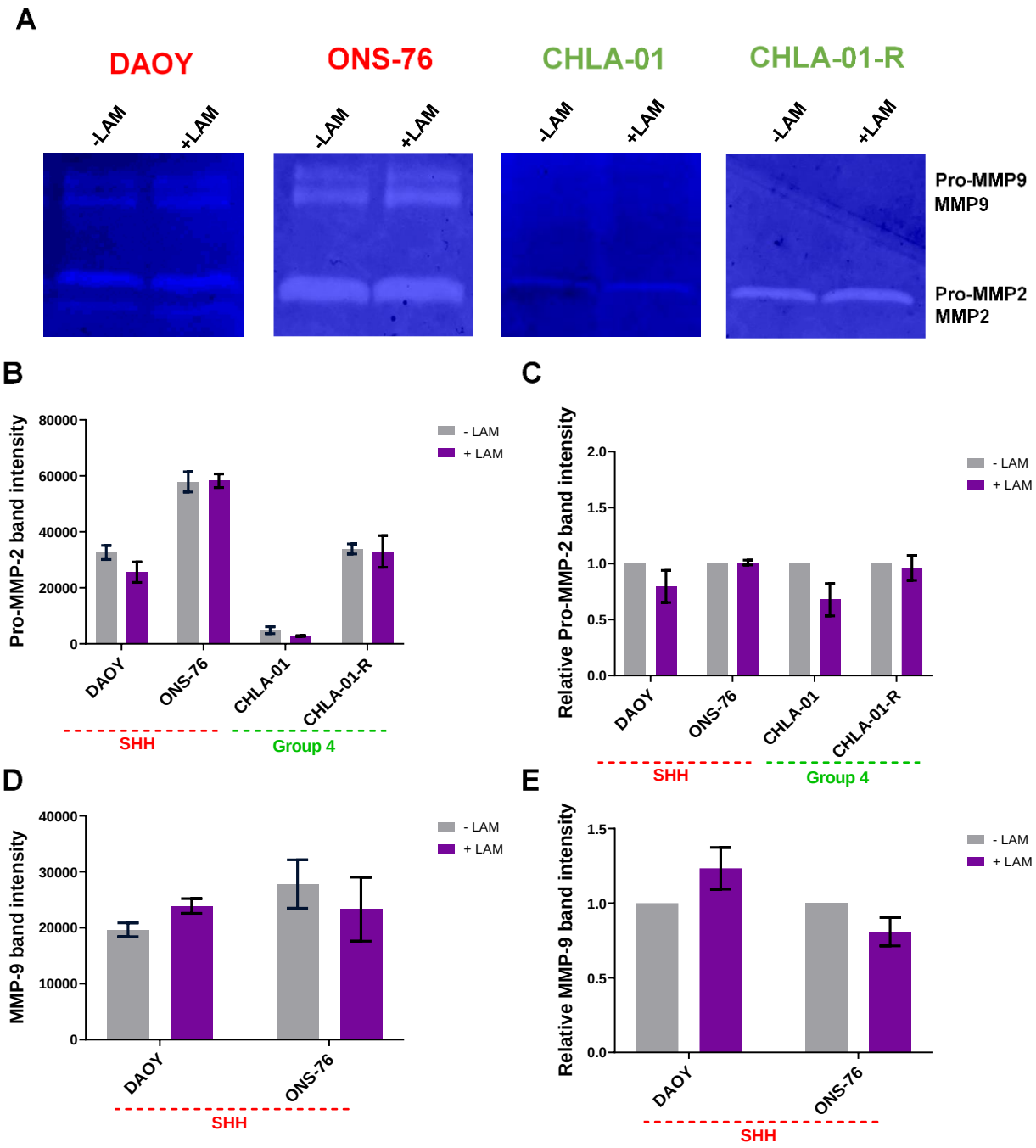


Figure 3.11 Laminin-111 does not affect Pro-Matrix Metalloproteinase 2 (Pro-MMP-2) or Pro-Matrix Metalloproteinase 9 (MMP-9) secretion in SHH and Group 4 medulloblastoma cell lines in a 2D cell culture assay. Gelatin zymography was used to detect Pro-MMP-2/MMP-9 in the supernatant of medulloblastoma cell lines in 2D cell culture assays whereby cells were seeded into a 6 well plate with and without laminin-111 coating and incubated for 48 hours (**A**). Pro-MMP-2/MMP-9 mediated proteolysis of the zymogram was detected as a white band, which was then analysed by densitometry analysis in order to determine the quantity of Pro-MMP-2/MMP-9 secretion. The results of this analysis are displayed as raw values (**B**: Pro-MMP-2 and **D**: MMP-9) as well values that have been normalised to the uncoated wells for each cell line (**C**: Pro-MMP-2 and **E**: MMP-9). Representative zymograms are shown. Recombinant MMP-2 was added to the first lane of each zymogram as a positive control. Mean ± SEM plotted; n=3. Significance was assessed using Two-Way ANOVA analyses with Sidak's multiple comparisons post-hoc test. All significant comparisons are highlighted, otherwise comparisons are not significant.

3.5.2 Validation of candidate ‘laminin regulated genes’ using a 3D hyaluronan hydrogel cell culture assay

The previously described 3D cell culture assay was also conducted using the SHH (DAOY and ONS-76) and Group 4 (CHLA-01 and CHLA-01-R) medulloblastoma cell lines, in order to validate the selected ‘laminin regulated genes’, as well as identify any differences in the response of the cell lines to laminin-111 between 2D and 3D culture.

As in the 2D assay, any phenotypic effects of laminin-111 were assessed from brightfield microscope images taken of the cell lines throughout the 21 days of the assay (images were captured every 3 days). Representative images of the SHH and Group 4 cell lines growing within the hyaluronan hydrogels with and without laminin-111 (at time points 16 hours, 8 days and 21 days), can be observed in Figure 3.12. Unlike the 2D assay, laminin-111 did not confer a change in phenotype in any of SHH or Group 4 medulloblastoma cell lines (Figure 3.12).

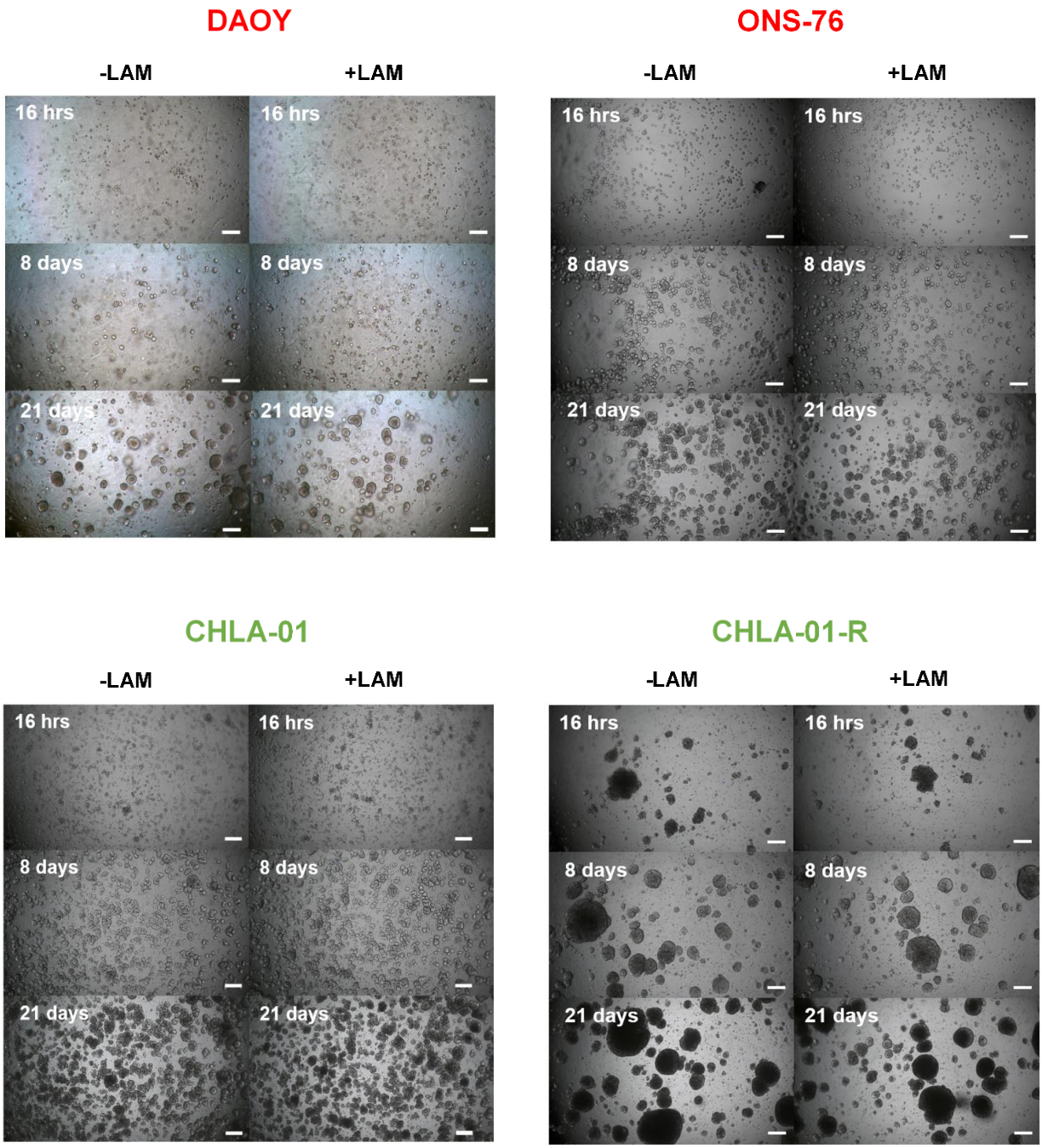


Figure 3.12 Laminin-111 does not confer an observable phenotypic change in SHH and Group 4 medulloblastoma cell lines grown in hyaluronan hydrogels. Brightfield images (4 X magnification) of SHH (DAOY (**A**) and ONS-76 (**B**)) and Group 4 (CHLA-01 (**C**) and CHLA-01-R (**D**)) medulloblastoma cell lines after 16 hours, 8 days and 21 days growth in hyaluronan hydrogels with (+LAM) and without (-LAM) laminin-111, indicate that both SHH and Group 4 cell lines remain phenotypically unchanged at all time points. Representative images shown (n=2). Scale bar 100 µm.

The RNA yield from the medulloblastoma cell lines in the 3D assay was very low due to the hydrogel interfering with RNA extraction. Consequently, only enough RNA to analyse the expression of 4 of the 'laminin regulated genes' was obtained from the hydrogels. Therefore, only the expression of *TPPP3, NFKBIZ, MMP-2* and *CD44* were analysed by qRT-PCR analysis, as these were the genes which exhibited the most response to laminin-111 in the 2D assay (Figure 3.10). Furthermore, the COVID-19 pandemic began just after the second replicate of this experiment had been obtained. After returning to the lab, we encountered difficulties accessing the hyaluronan hydrogels as well batch issues. This meant that we were only able to obtain two replicates of this experiment. Therefore, the significance of the changes in gene expression were not calculated and so inferences regarding the expression of the 'laminin regulated genes', in response to laminin-111, have been made based on the direction and variability of the two replicates.

This analysis demonstrated that many of laminin-111 induced changes in gene expression identified across the SHH and Group 4 medulloblastoma cell lines in the 2D assay were lost or altered in the 3D assay (Figure 3.13). Furthermore, as in the 2D assay, the direction in which the expression of these genes was altered by laminin-111 did not always align with the genomic analysis of patient tumours or SHH medulloblastoma cell lines from which they were identified (section 3.3).

Firstly, in the 3D assay, the expression of *TPPP3* was found to be increased in both of the SHH cell lines (DAOY and ONS-76) but remained unchanged in the Group 4 cell lines (CHLA-01 and CHLA-01-R) (Figure 3.13 A). Whereas, in the 2D assay *TPPP3* expression was found to be significantly increased by laminin-111 in just the recurrent Group 4 cell line (CHLA-01-R) (Figure 3.10 A). Additionally, *TPPP3* expression was found to be decreased, rather than increased, in the LAM^{high} ECM sub-type in SHH tumours in the genomic patient data, as well as in response to laminin-111 in the mRNA sequencing data of the SHH cell lines (Table 3.3).

Secondly, *NFKBIZ* expression was decreased by laminin-111 in the primary Group 4 cell line (CHLA-01) and both SHH cell lines but was slightly increased in the recurrent Group 4 cell line (CHLA-01-R) in the 3D assay (Figure 3.13 B). However, in the 2D assay, the expression of *NFKBIZ* was only found to be significantly altered by laminin-111 in the recurrent Group 4 cell line (CHLA-01-R), where it was increased (Figure 3.10 B). Moreover, *NFKBIZ* expression was found to be increased in the *LAM*^{high} ECM sub-type in both SHH and Group 4 tumours in the genomic patient data, as well as in response to laminin-111 in both SHH cell lines in the mRNA sequencing data (Table 3.3). This corroborates the finding of increased *TPPP3* expression in the recurrent Group 4 cell line in response to laminin-111 in the 3D assay but contradicts that of decreased expression in the primary Group 4 and both SHH cell lines.

Additionally, *MMP-2* expression was unchanged by laminin-111 in all of the cell lines in the 3D assay, apart from the primary Group 4 cell line (CHLA-01) where expression was reduced (Figure 3.13 C). Similarly, in the 2D assay, *MMP-2* expression was also found to be reduced in the primary Group 4 cell line, however, it was also reduced in the recurrent Group 4 cell line (CHLA-10-R), which was not observed in the 3D assay (Figure 3.10 C). In contrast to the findings of both the 2D and 3D assays, *MMP-2* expression was found to be increased in the *LAM*^{high} ECM sub-type in Group 4 tumours in the genomic patient data (Table 3.3).

Finally, in the 3D assay the expression of *CD44* was found to be increased by laminin-111 in the ONS-76 SHH cell line and the recurrent Group 4 cell line (CHLA-01-R), as well as decreased in the primary Group 4 cell line (CHLA-01), in response to laminin-111 (Figure 3.13 D). Likewise, in the 2D assay *CD44* expression was also decreased in the primary Group 4 cell line (CHLA-01) and increased in the recurrent cell line (CHLA-01-R) (Figure 3.10 I). However, *CD44* expression was increased in the DAOY SHH cell line, not the ONS-76 (Figure 3.10 I). These changes in expression are

particularly interesting as *CD44* was not identified from either of the genomic analysis of patient tumours or SHH cell lines.

The discrepancies in the expression of the ‘laminin regulated genes’ between the 2D and 3D laminin assays could possibly be due the distinct biological differences between cells grown in a 3D hydrogel and as a monolayer in 2D culture. In 3D hydrogel culture there are oxygen and nutrient diffusion gradients between the periphery and centre of nodules, which are absent in 2D culture, as well as increased cell to cell interaction compared to 2D culture (Worthington, Pochan and Langhans, 2015; Nazari, 2020). These factors can distinctly alter global gene expression in cells and could have therefore caused the differences in the expression of the ‘laminin regulated genes’ between the 2D and 3D laminin assays (Worthington, Pochan and Langhans, 2015; Roper *et al.*, 2021). In addition, the hyaluronan backbone of the hydrogel used in the 3D laminin assay can activate different intracellular pathways, via its interaction with cell surface receptors, which may have also contributed to changes in global gene expression compared to the 2D laminin assay (Laurent and Fraser, 1992; Necas *et al.*, 2008).

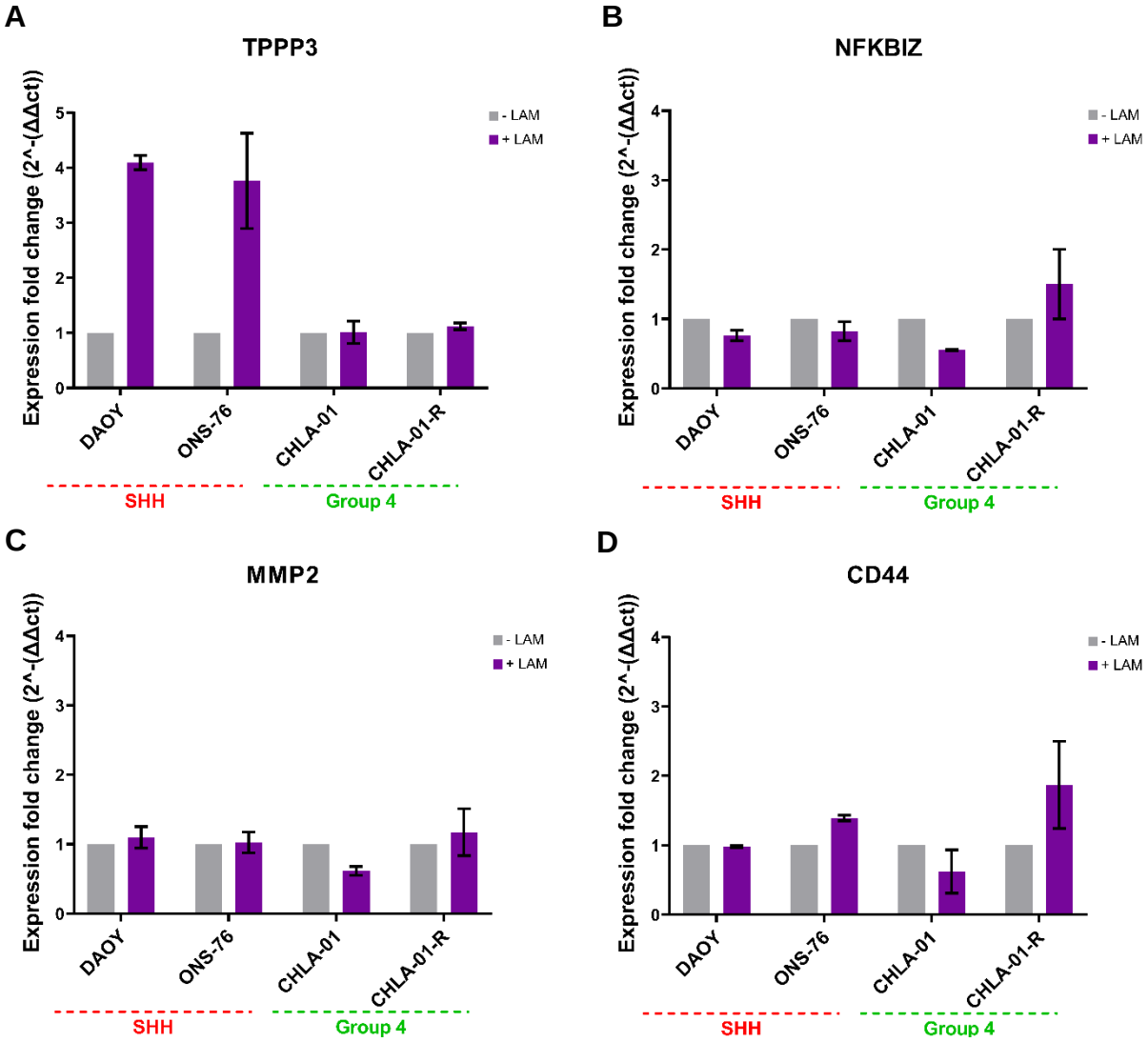


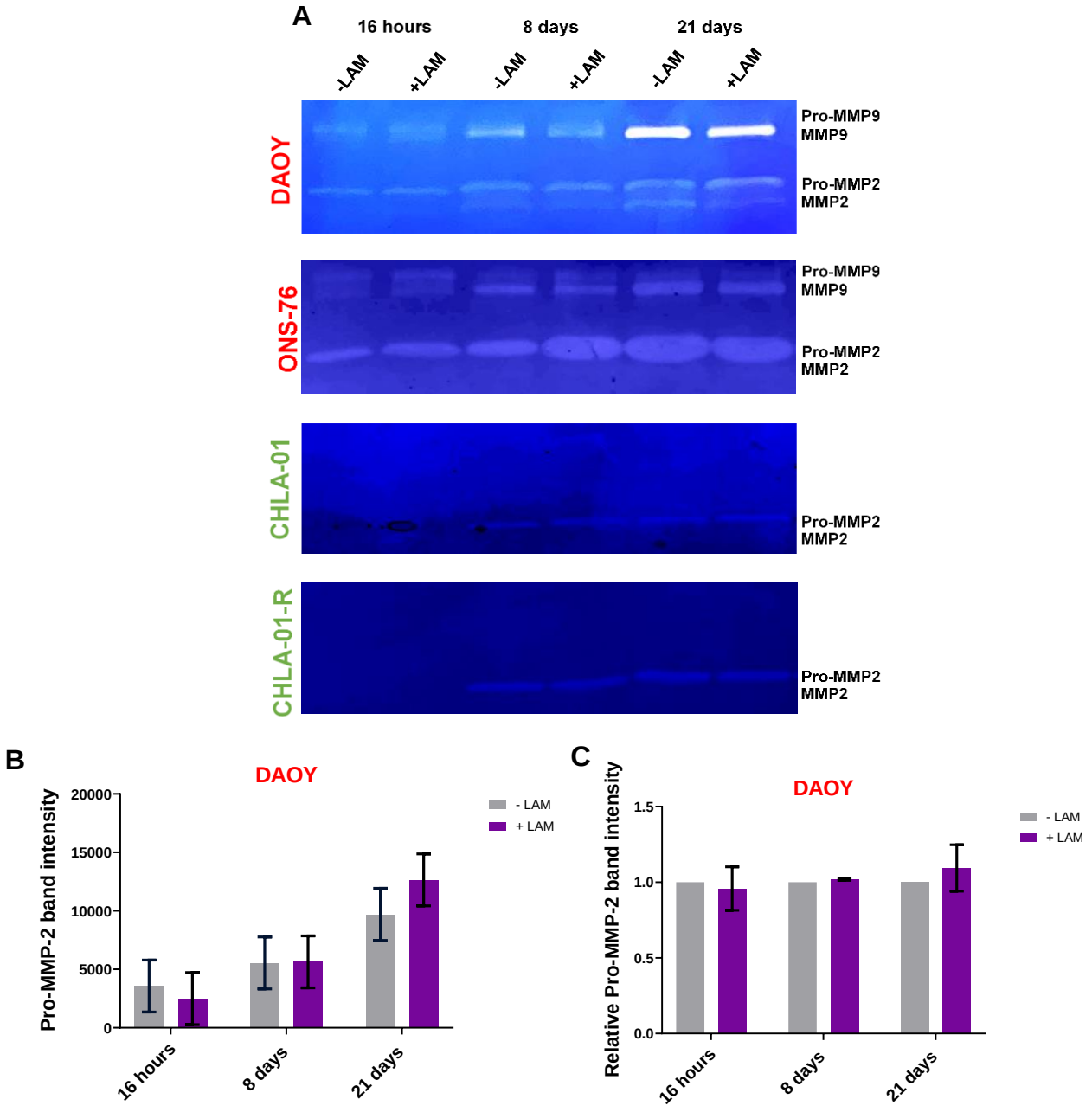
Figure 3.13 Laminin-111 alters the expression of Tubulin Polymerization Promoting Protein Family Member 3 (*TPPP3*), NF-κB Inhibitor Zeta (*NFKBIZ*), Matrix Metalloproteinase 2 (*MMP-2*) and Cluster of differentiation 44 (*CD44*) in some SHH and Group 4 medulloblastoma cell lines in a 3D cell culture assay. (**A** – **D**) qRT-PCR analysis of *TPPP3, NFKBIZ, MMP-2* and *CD44* expression in SHH and Group 4 medulloblastoma cell lines in a 3D cell culture assay whereby cells were seeded into hyaluronan hydrogels with and without laminin-111 and grown for 21 days. All qRT-PCR analysis was conducted relative to *GAPDH* as a loading control. Relative changes in gene expression between cells grown with and without laminin-111 was calculated using the ΔΔCt method (section 2.12.7). Mean ± SEM plotted; n=2.

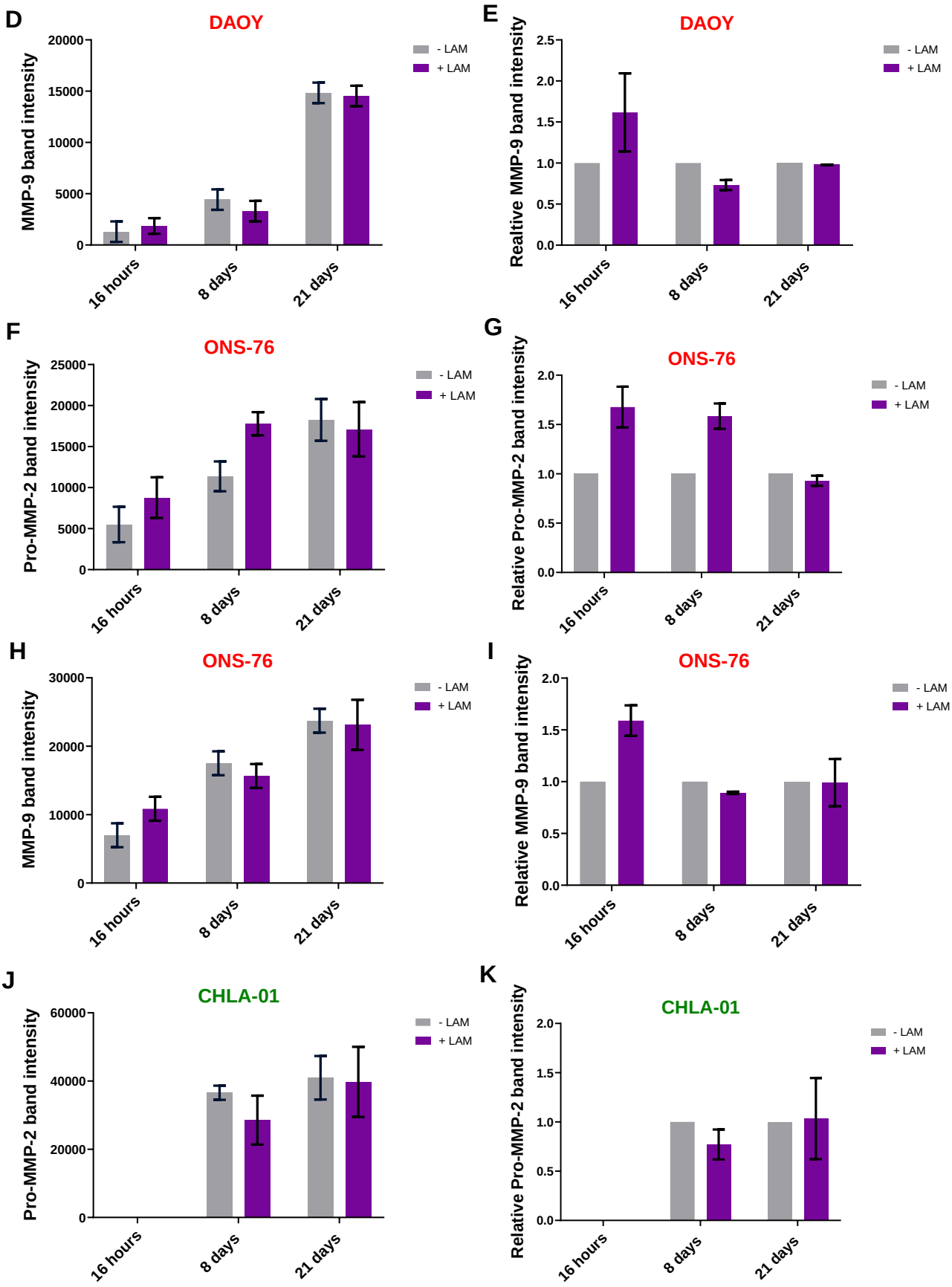
Gelatin zymography analysis was also conducted on the supernatants collected from both the SHH and Group 4 cell lines in the 3D assay. However, supernatants from several different time points were used (16 hours, 8 days and 21 days), instead of just the end point, in order to assess how Pro-MMP-2/MMP-9 secretion changed in

response to laminin-111 over the time course of the assay. The raw and relative values of the densitometry analysis of Pro-MMP-2/MMP-9 can be observed in Figure 3.14. The raw values were used to assess changes in Pro-MMP-2/MMP-9 secretion over the time course of the assay and the relative values were used to compare between laminin-111 conditions. In the 2D assay the raw values of the densitometry analysis, in the non-laminin-111 conditions, were used to compare the level of Pro-MMP-2/MMP-9 secretion between the cell lines in normal growth conditions. However, because the supernatants from each cell line were analysed on their own zymogram in the 3D assay this comparison was not made. Once again, the significance between conditions was not calculated as only two replicates of this assay were obtained, therefore, inferences regarding Pro-MMP-2/MMP-9 secretion in response to laminin-111 have been made based on the direction and variability of the two replicates.

This analysis demonstrated that in the 3D assay laminin-111 caused an increase in Pro-MMP-2 secretion in the ONS-76 SHH cell line at the 16 hour and 8 day time points, suggesting that laminin-111 upregulates Pro-MMP-2 secretion in SHH medulloblastoma (Figure 3.14 A and E). However, this effect was lost at 21 days (Figure 3.14 A and E). This finding was corroborated by the genomic analysis of patient tumours and SHH cell lines, which showed that *MMP-2* expression was also increased in the *LAM*^{high} SHH tumours as well as in response to laminin-111 in the DAOY SHH cell line (Table 3.3). In the rest of the cell lines, laminin-111 did not seem to have an effect on the secretion of Pro-MMP-2 (Figure 3.14 A). However, a single replicate of a 7 day 3D assay was conducted on the Group 4 cell lines, which revealed that there was an observable increase in Pro-MMP-2 secretion in response to laminin-111 in the CHLA-01-R cell line (Appendix Figure 2). This suggests that this phenotype is also lost at the later time points of the 21 days assay, as it was in the ONS-76 cell line. The RNA yield from the 7 day assay was too low to conduct qRT-PCR analysis, however, and was therefore not expanded to the SHH cell lines. Additionally, there was also an

observable increase in MMP-9 secretion in response to laminin-111 in both the SHH cell lines (DAOY and ONS-76), but only at the initial 16 hour time point (Figure 3.14 E and G). Furthermore, both the SHH and Group 4 cell lines exhibited an increase in Pro-MMP-2 secretion over the time course of the 3D assay (Figure 3.14 A, B, F, J and L). Likewise, in the SHH cell lines MMP-9 secretion also increased over time throughout the assay (Figure 3.14 D and H). Both of these findings are likely due to the growth of the cell lines throughout the assay causing an increase in of Pro-MMP-2/-9 secretion in proportion to the increased cell number.




D
DAOY
MMP-9 band intensity
20000
15000
10000
5000
0
16 hours
8 days
21 days
- LAM
+ LAM
E
DAOY
Realtive MMP-9 band intensity
2.5
2.0
1.5
1.0
0.5
0.0
16 hours
8 days
21 days
- LAM
+ LAM
F
ONS-76
Pro-MMP-2 band intensity
25000
20000
15000
10000
5000
0
16 hours
8 days
21 days
- LAM
+ LAM
G
ONS-76
Relative Pro-MMP-2 band intensity
2.0
1.5
1.0
0.5
0.0
16 hours
8 days
21 days
- LAM
+ LAM
H
ONS-76
MMP-9 band intensity
30000
20000
10000
0
16 hours
8 days
21 days
- LAM
+ LAM
I
ONS-76
Relative MMP-9 band intensity
2.0
1.5
1.0
0.5
0.0
16 hours
8 days
21 days
- LAM
+ LAM
J
CHLA-01
Pro-MMP-2 band intensity
60000
40000
20000
0
16 hours
8 days
21 days
- LAM
+ LAM
K
CHLA-01
Relative Pro-MMP-2 band intensity
2.0
1.5
1.0
0.5
0.0
16 hours
8 days
21 days
- LAM
+ LAM

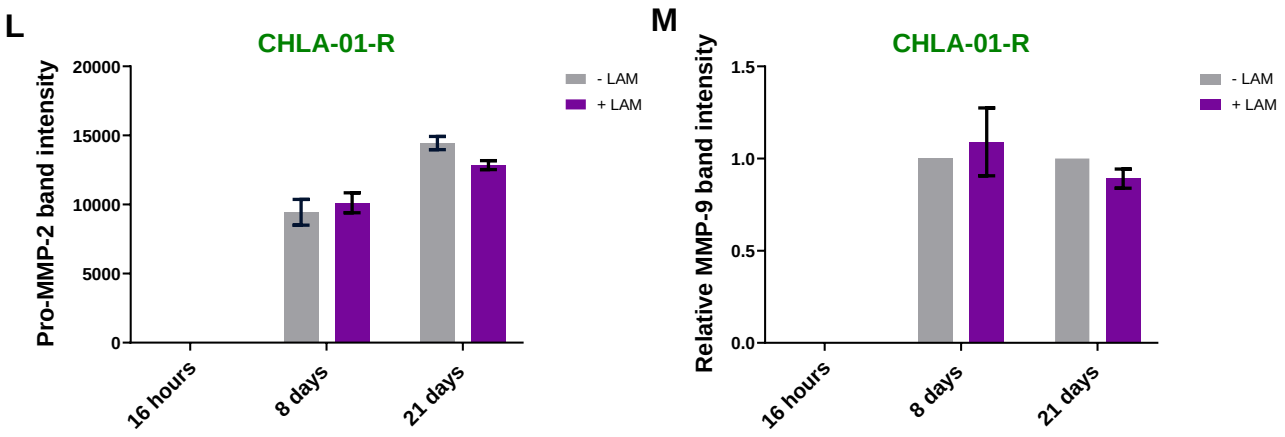


Figure 3.14 Laminin-111 increases Pro Matrix Metalloproteinase 2 (Pro-MMP-2) and Pro Matrix Metalloproteinase 9 (MMP-9) secretion in SHH, but not Group 4 medulloblastoma cell lines in a 3D cell culture assay. Gelatin zymography was used to detect Pro-MMP-2/MMP-9 in the supernatant of SHH and Group 4 medulloblastoma cell lines that had been grown in a 3D cell culture assay, whereby cells were seeded into hyaluronan hydrogels with and without laminin-111 grown for 21 days (**A**). Supernatants from the time points 16 hours, 8 days and 21 days were analysed in the zymograms. Pro-MMP-2/MMP-9 mediated proteolysis of the zymogram was detected as a white band, which was then analysed by densitometry analysis in order to determine the quantity of Pro-MMP-2/MMP-9 secretion of each cell line. The results of this analysis are displayed as raw values as well values that have been normalised to the non-laminin-111 condition for each cell line (DAOY: **B**-**E**, ONS-76: **F**-**I**, CHLA-01: **J** and **K**, CHLA-01-R: **L** and **M**). Representative zymograms are shown. Recombinant MMP-2 was added to the first lane of each zymogram as a positive control. Mean ± SEM plotted; n=2.

As demonstrated in section 3.4 both the SHH and Group 4 medulloblastoma cell lines synthesise LAMA1 (the α subunit of laminin-111) and LAMA2 (the α subunit of laminin-211). Furthermore, in the previously mentioned study by our group it was shown that the SHH cell lines deposit a laminin-111/211 shell-like structure when grown in long-term hyaluronan based hydrogels (Linke *et al.*, 2020). It is therefore possible that the endogenous laminin-111/laminin-211 produced by these cell lines masks the effect of the exogenous laminin-111 in the assays described in this study, especially so in the long term 3D assay. This may explain why the observable laminin-111 mediated increase in Pro-MMP-2/MMP-9 secretion in the SHH cell lines was lost at the later time points of the 3D assay (Figure 3.14). It may also explain some of the discrepancies between the qRT-PCR analysis of the 'laminin regulated genes' in the 2D and 3D assays (Figure 3.10 and Figure 3.13). Therefore, in order to more accurately study the effect of LAMA1/LAMA2 on SHH and Group 4 medulloblastoma, a LAMA1 and LAMA2 cell line knockdown/knockout model is required.

3.6 Summary points

- Analysis of *LAMA1* and *LAMA2* expression in large scale genomic medulloblastoma patient datasets demonstrated that they are expressed across the medulloblastoma sub-groups.

- In the largest available genomic medulloblastoma patient dataset, *LAMA1* and *LAMA2* are both most highly expressed in the SHH sub-group.

- Eight candidate 'laminin regulated genes' were selected from integrated differential gene expression analysis between *LAM*^{high} and *LAM*^{low} ECM sub-types in SHH and Group 4 patient tumours (Cavalli genomic patient dataset) and SHH cell lines grown on hyaluronan hydrogels with and without laminin-111 (mRNA sequencing dataset), for further investigation in 2D and 3D cell culture validation assays.

- *CD44* was also selected for further investigation in validation assays, despite not being identified from either of the genomic analyses, due to its significant interaction with hyaluronan, the backbone of the brain ECM and the hydrogel used in this study, as well as laminins (Underhill, 1992; Merzak, Koocheckpour and Pilkington, 1994; Goodison, Urquidi and Tarin, 1999).

- qRT-PCR and western blotting analyses demonstrated that the SHH (DAOY and ONS-76) and Group 4 (CHLA-01 and CHLA-01-R) cell lines selected to be used in cell culture validation assays, both express *LAMA1*/LAMA1 and *LAMA2*/LAMA2.

- A 2D cell culture validation assay showed that the recurrent Group 4 cell line (CHLA-01-R) exhibited an adherence phenotype when seeded onto laminin-111, that was absent in its primary counterpart cell line (CHLA-01).

- Although qRT-PCR analysis of the 2D and 3D cell culture validation assays demonstrated that exogenous laminin-111 altered the gene expression of several candidate 'laminin regulated genes' (*TPPP3, NKFBIZ, MMP-2, ITGA5, RPSA* and *CD44),* the direction of these changes in gene expression were mostly contradictory to the genomic analyses from which they were identified.

- Gelatin zymography of cell line supernatants from the 3D assay demonstrated that laminin-111 increased Pro-MMP-2 secretion in the ONS-76 SHH cell line after 16 hours and 8 days in the assay, suggesting that Pro-MMP-2 secretion is upregulated by laminin-111 in SHH medulloblastoma. However, this phenotype was lost at 21 days suggesting that the endogenous laminin-111 (LAMA1) produced by the cells may mask any effect of the exogenous laminin-111 in the 3D, and possibly the 2D, assay.

- To study the effect of LAMA1/LAMA2 on SHH and Group 4 medulloblastoma more accurately, a LAMA1/LAMA2 knockdown/knockout cell line model is required.

Chapter 4: Creating CRISPR-Cas9 LAMA1 and LAMA2 knockouts in DAOY and ONS-76 SHH medulloblastoma cell lines

4.1 Introduction

To more accurately study the effect of LAMA1 and LAMA2 on SHH and Group 4 medulloblastoma, a LAMA1/LAMA2 knockdown or knockout cell line model was required.

This part of the project was to be conducted on return to the laboratory after the first national lockdown when laboratory access, equipment and consumables were extremely limited. Therefore, it was necessary to focus on the role of LAMA1 and LAMA2 in either the SHH or Group 4 medulloblastoma sub-group. The SHH sub-group was chosen for 3 main reasons. Firstly, as previously discussed, a recent study by our group identified that *LAM*^{high} SHH medulloblastoma patients have a much better overall survival than *LAM*^{low} (Linke *et al.*, 2020). Hence, deciphering how LAMA1 and LAMA2 confer better survival in this sub-group represented a realistic route to fully establishing them as biomarkers for lower-risk SHH medulloblastoma patients. Secondly, in the same study it was identified by immunohistochemical (IHC) staining that SHH cell lines form a laminin-111/211 shell-like structure when grown in long-term hyaluronan hydrogels, whereas Group 4 cell lines exhibit more diffuse expression (Linke *et al.*, 2020). This led us to hypothesise that this sub-group specific structure may mechanically inhibit the growth of *LAM*^{high} SHH tumours and could therefore be one of the reasons that these patients have a better overall survival, thus meriting investigation. Finally, the DAOY and ONS-76 SHH cell lines grow as an adherent monolayer, whereas the CHLA-01 and CHLA-01-R Group 4 cell lines grow in suspension. Adherent cell lines are generally much more amenable to transfection than suspension cell lines, a technique commonly employed in gene knockout/knockdown protocols (Basiouni, Fuhrmann and Schumann, 2012). Therefore, it was more likely that successful knockouts/knockdowns would be achieved in the adherent SHH medulloblastoma cell lines.

A variety of different knockdown and knockout technologies exist, however, we decided that a stable knockout would be the most appropriate method to employ, since we would be growing the cell lines in long-term 3D assays. We therefore chose to use a stable clustered regularly interspaced short palindromic repeats and CRISPR-associated protein 9 (CRISPR-Cas9) knockout method, since it allows for the generation of precise and stable knockouts.

To achieve this, we selected the Horizon Discovery® Cas9 nuclease mRNA and Edit-R predesigned synthetic single guide RNA (sgRNA) system. This specific system was chosen for several reasons. Firstly, it allows for the transient expression of the Cas9 nuclease, without incorporating exogenous DNA into the host cell's genome. Secondly, multiple sgRNAs, against different targets (i.e., *LAMA1* and *LAMA2*) can be used. Finally, the workflow for this system is relatively simple, only requiring one co-transfection of cells with pre-designed reagents. This factor was particularly important due to the previously mentioned laboratory access limitations.

The aims of this chapter were to:

A) Co-transfect DAOY and ONS-76 SHH medulloblastoma cells with Cas9 nuclease mRNA, as well as *LAMA1* and *LAMA2* synthetic sgRNAs.
B) Isolate clonal cell lines from co-transfected DAOY and ONS-76 cells.
C) Validate LAMA1 and LAMA2 knockouts in the clonal DAOY and ONS-76 cell lines.

4.2 CRISPR-Cas9 knockout workflow

The CRISPR-Cas9 workflow used in this study was as follows. DAOY and ONS-76 SHH medulloblastoma cell lines were initially co-transfected with a Cas9 nuclease-enhanced green fluorescent protein (EGFP) mRNA (which consists of a single mRNA strand that is translated into two separate proteins: the Cas9 nuclease protein and EGFP as a reporter gene), as well as both *LAMA1* and *LAMA2* Edit-R® predesigned synthetic sgRNAs. Co-transfected cells expressing EGFP, and therefore the Cas9 nuclease, were then isolated using fluorescence-activated cell sorting (FACS). An initial DNA mismatch detection assay was then conducted on genomic DNA (gDNA) isolated from all EGFP positive cells, to identify if insertion or deletion mutations (INDELs) were present at the *LAMA1* and *LAMA2* sgRNA target sites. After the presence of INDELs in the EGFP positive cells had been confirmed, clonal cell lines were then propagated from either 1 or 10 parent cells in a 96 well plate. Once the clonal cell lines became confluent within the 96 well plate, they were seeded into a 6 well plate and then into a T25 cell culture flask. At this point, stocks and pellets (for knockout validation) of the clonal cell lines were harvested. LAMA1 and LAMA2 knockouts were then validated in each of the clonal cell lines using three techniques. Firstly, a DNA mismatch detection assay of the *LAMA1* and *LAMA2* sgRNA target sites was conducted to confirm the presence of INDELs. Secondly, western blotting of LAMA1 and LAMA2 was used to identify protein loss. Finally, Sanger Sequencing of the *LAMA1* and *LAMA2* sgRNA target sites was used to establish the position and sequence of INDELs. The clonal cell lines which exhibited the greatest level of reduction in protein expression were then selected to be used in further experiments. A diagrammatic overview of this workflow can be observed in Figure 4.1.

This entire process was conducted in parallel with DAOY and ONS-76 cells that had been co-transfected with a non-targeting Edit-R® synthetic sgRNA as a negative

control for the CRISPR-Cas9 knockout workflow, as well as to create non-targeting control cell lines for subsequent experiments.

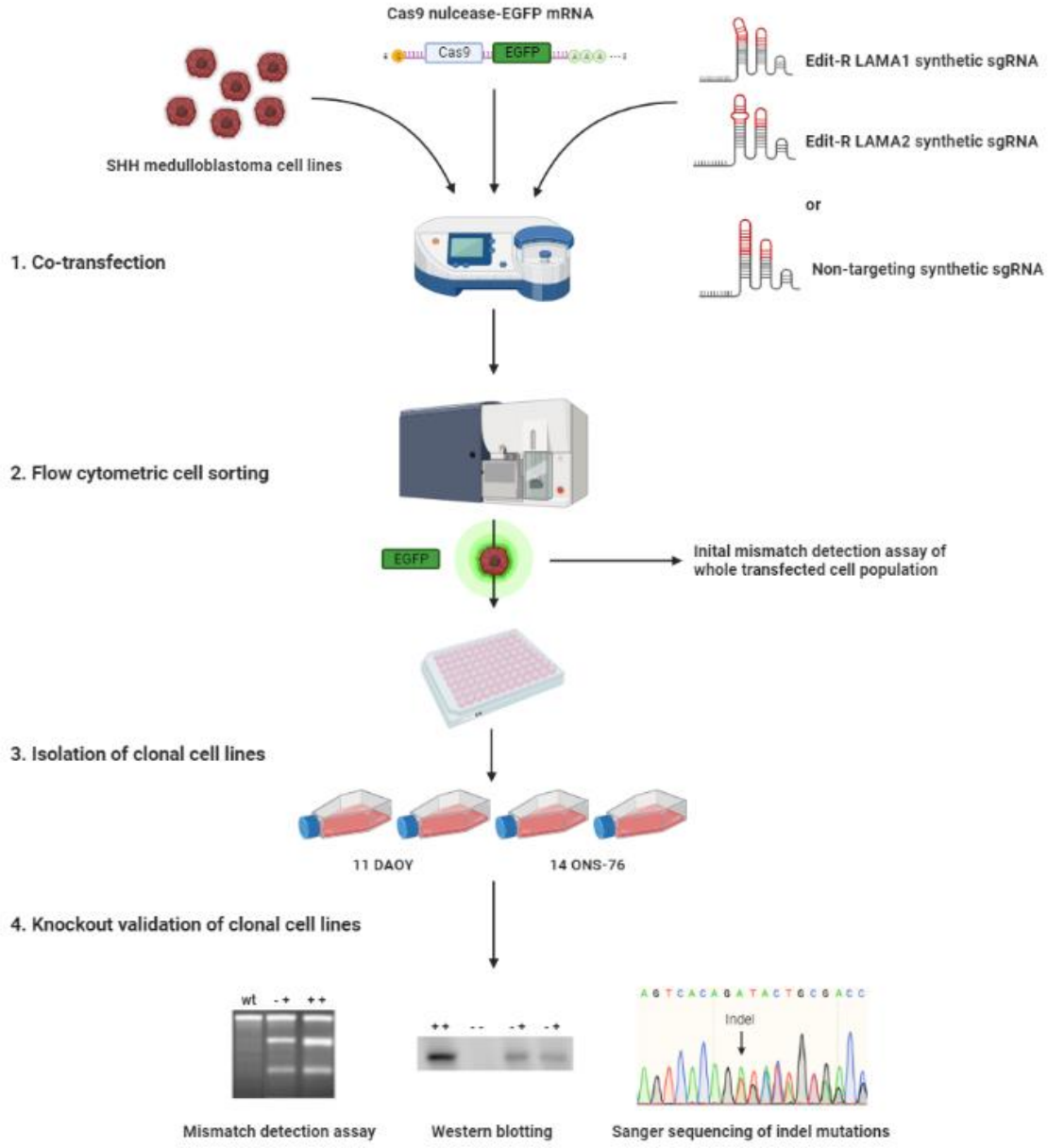


Figure 4.1 Workflow of creating and validating CRISPR-Cas9 knockouts of Laminin Subunit α1 (LAMA1) and Laminin Subunit α2 (LAMA2) in DAOY and ONS-76 SHH medulloblastoma cell lines. DAOY and ONS-76 SHH medulloblastoma cell lines were co-transfected with Cas9 nuclease mRNA, which was fused to enhanced green fluorescent protein (EGFP) as a reporter gene, as well as *LAMA1* and *LAMA2* synthetic single guide (sgRNAs). Cell lines were also separately co-transfected with a non-targeting synthetic sgRNA as a negative control. EGFP positive cells were then isolated by fluorescence-activated cell sorting (FACS). An initial DNA mismatch detection assay was then conducted on genomic DNA (gDNA) isolated from the EGFP positive cells to confirm the presence of insertion or deletion mutations (INDELs). Clonal cell lines were then propagated from the EGFP positive cells from either 1 or 10 parent cells. LAMA1 and LAMA2 knockouts were then validated in each of the clonal cell lines using a DNA mismatch detection assay and Sanger Sequencing of the *LAMA1* and *LAMA2* sgRNA target sites, as well as western blotting of LAMA1 and LAMA2.

4.3 Co-transfection and fluorescence-activated cell sorting (FACS) of DAOY and ONS-76 SHH medulloblastoma cell lines

DAOY and ONS-76 cells were co-transfected with Cas9 nuclease-EGFP mRNA and either *LAMA1* and *LAMA2* sgRNAs or a non-targeting sgRNA. Once the cells had been co-transfected, they were seeded into a T25 cell culture flask and incubated overnight. This allowed for the Cas9 nuclease (and EGFP) to be expressed and complex with the *LAMA1* or *LAMA2* sgRNAs, so that directed double stranded DNA breaks could occur. For simplicity, 'co-transfection' henceforth implies the transfection of the Cas9 nuclease-EGFP mRNA as well as the specified sgRNA.

The next day, FACS was used to identify and isolate the co-transfected cells which expressed EGFP, and therefore Cas9 nuclease. Initially, untransfected negative control cells underwent FACS to determine the threshold of autofluorescence of the DAOY and ONS-76 cell lines (Figure 4.2 A and D). These thresholds were then used to identify and quantify the number of co-transfected cells which expressed EGFP, therefore allowing for the transfection efficiency to be calculated (Figure 4.2). In the DAOY cell line, cells co-transfected with the non-targeting sgRNA exhibited a transfection efficiency of 45%, whereas cells co-transfected with *LAMA1* and *LAMA2* sgRNAs had a transfection efficiency of 82%. (Figure 4.2 B and C). Furthermore, in the ONS-76 cell line, cells co-transfected with the non-targeting sgRNA had a low transfection efficiency of only 17%, therefore the cell population was enriched by FACS to 57% EGFP positive cells (Figure 4.2 E). Finally, the ONS-76 cells co-transfected with *LAMA1* and *LAMA2* sgRNAs were found to have a transfection efficiency of 60% (Figure 4.2 F).

Cell sorting was then used to seed either 1 or 10 EGFP positive cells into each well of a 96 well plate for the propagation of clonal cell lines. All the remaining EGFP positive cells were seeded back into cell culture flasks and used to make cell stocks of each

co-transfection. However, all the cells seeded into 96 well plates for clonal isolation became contaminated. Therefore, the cell stocks of the remaining EGFP positive cells from both cell lines and sgRNAs were thawed and used to seed 1 or 10 cells manually into a 96 well plate by serial dilution, in order to propagate clonal cell lines.

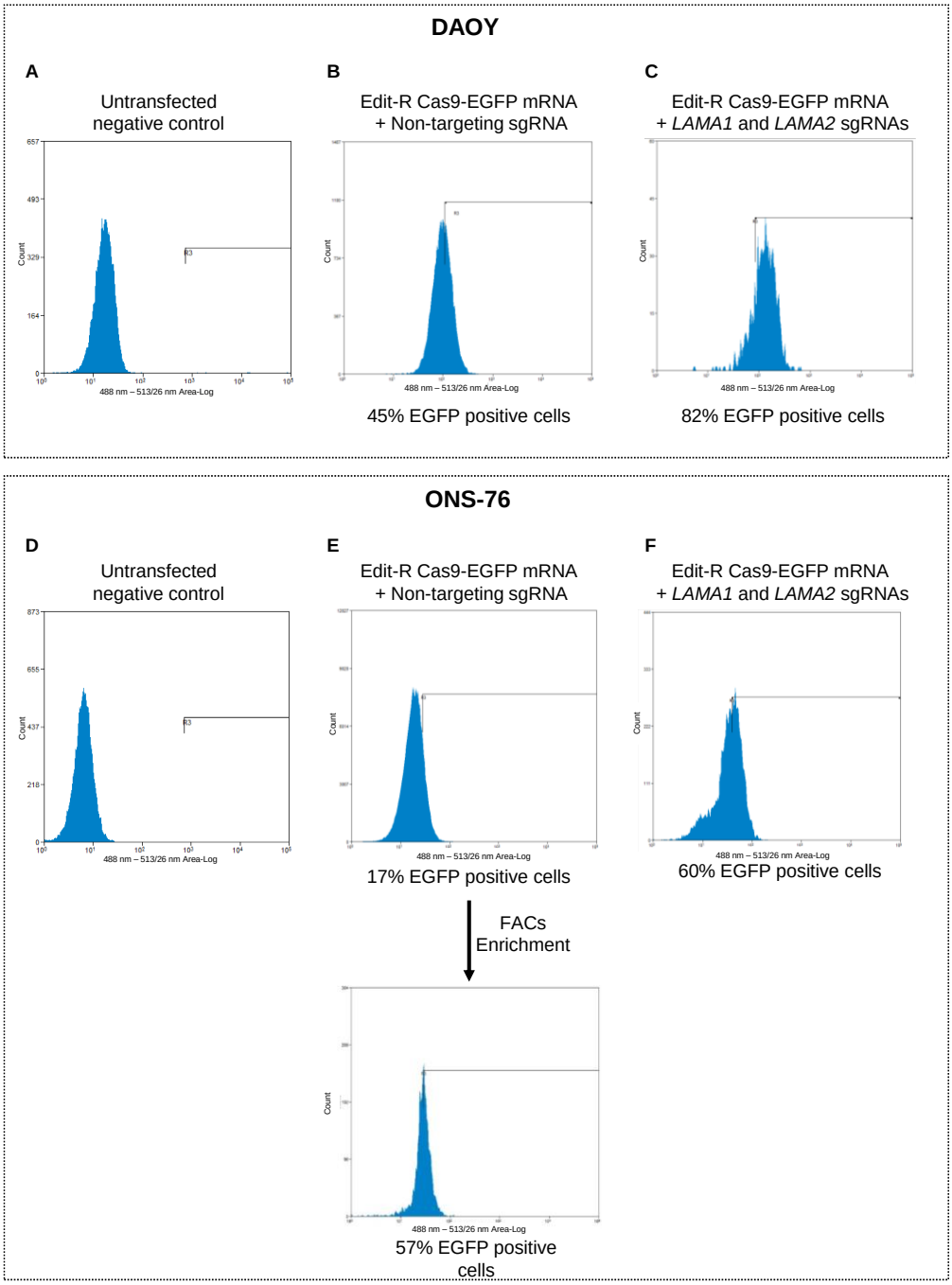


Figure 4.2 Fluorescence-activated cell sorting (FACS) analysis of DAOY and ONS-76 cells co-transfected with Cas9 nuclease-enhanced green fluorescent protein (EGFP) mRNA and synthetic single guide RNAs (sgRNAs) identifies EGFP expression in both cell lines. FACS analysis of untransfected negative control cells was initially used to determine the threshold of autofluorescence of each cell line (**A** and **D**). These thresholds were then used to identify EGFP expressing cells in the respective cell lines. DAOY cells co-transfected with the non-targeting sgRNA had a transfection efficiency of 45% (**B**). DAOY cells co-transfected with Laminin Subunit α1 (*LAMA1*) and Laminin Subunit α2 (*LAMA2*) sgRNAs had a transfection efficiency of 82% (**C**). ONS-76 cells co-transfected with the non-targeting sgRNA had a low transfection efficiency of 17%, the cell population was therefore enriched using FACS to 57% EGFP positive cells (**E**). ONS-76 cells co-transfected with *LAMA1* and *LAMA2* sgRNAs had transfection efficiency of 60% (**F**). All FACS data is displayed as histograms. In B, C, E and F, the vertical black line on the histogram denotes the threshold of autofluorescence as determined using the untransfected cells. 'Co-transfection' implies the transfection of the Cas9 nuclease-EGFP mRNA as well as the specified sgRNA.

4.4 DNA mismatch detection assays of *LAMA1* and *LAMA2* in total co-transfected cell populations and clonal cell lines

In order to detect INDELs at the sgRNA target site of *LAMA1* and *LAMA2* in the DAOY and ONS-76 cell lines, DNA mismatch detection assays were conducted on gDNA isolated from the total co-transfected cell populations and the derived clonal cell lines.

A DNA mismatch detection assay (also known as a T7 endonuclease detection assay) is a PCR based assay, whereby specifically designed primers are initially used to amplify the sgRNA target site of the gene of interest from gDNA. The PCR product is then denatured by heating and then renatured by cooling. If there is a monoallelic INDEL or different biallelic INDELs present, then a mixture of heteroduplexes (between the mismatched sequences caused by the INDELs) and homoduplexes are formed when the PCR product is renatured. T7 endonuclease I is then incubated with the renatured PCR product and specifically cleaves any heteroduplexes. If there are INDELs present, then this results in formation of three different sized DNA fragments; one larger fragment where DNA from the same allele has renatured together into a homoduplex and has therefore not been cleaved, as well as two smaller fragments where DNA from different alleles has renatured together into a heteroduplex, which has then been cleaved in two by T7 endonuclease I. In order to assess if this has occurred, the enzyme treated PCR product is then electrophoresed on an agarose gel and imaged. The presence of 3 DNA bands, instead of 1, indicates that there are INDELs present at sgRNA target site of the gene of interest. A diagrammatic explanation of this assay can be found in Figure 4.3.

One limitation of a DNA mismatch detection assay is that it is unable to detect the presence of the same biallelic INDELs. This is because when this PCR product is

renatured only homoduplexes would be formed and T7 endonuclease I would be unable to cleave the product, therefore meaning only 1 DNA band would be detected.

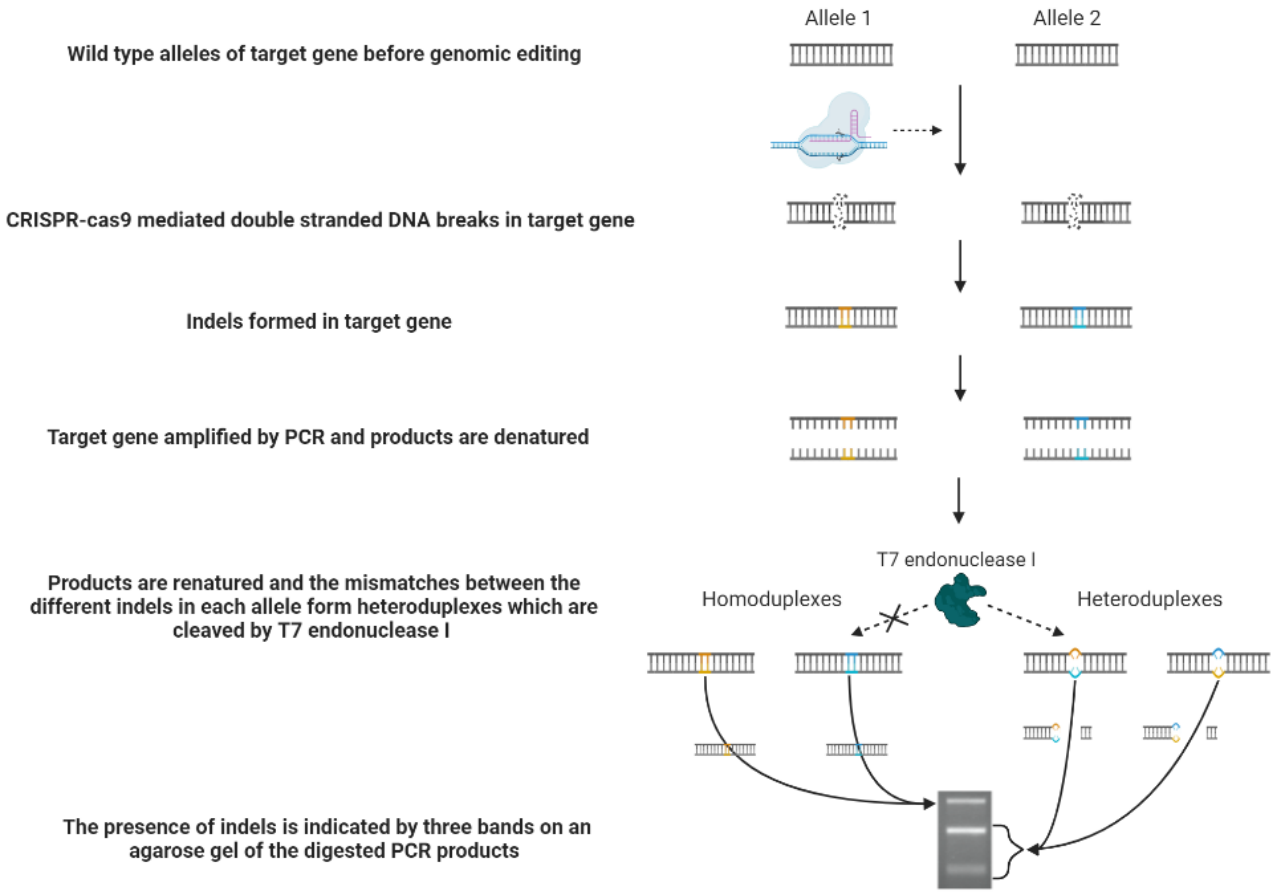


Figure 4.3 Diagrammatic explanation of a DNA mismatch detection assay. In a DNA mismatch detection assay the single guide (sgRNA) target site of the gene of interest is amplified by PCR. The product is then denatured by heating, before cooling to renature. The presence of monoallelic or different biallelic insertion or deletion mutations (INDELs) causes the formation of heteroduplexes when the product is renatured. T7 endonuclease I is then added to the renatured PCR product and specifically cleaves any heteroduplexes. The enzyme treated PCR product is then electrophoresed on an agarose gel and imaged. The presence of 3 DNA bands indicates that there are INDELs present at the sgRNA target site of the gene of interest.

4.4.1 DNA mismatch detection assays of *LAMA1* and *LAMA2* in total co-transfected cell populations

An initial DNA mismatch detection assay for *LAMA1* and *LAMA2* was conducted using gDNA isolated from the total EGFP positive DAOY and ONS-76 cells co-transfected with either *LAMA1* and *LAMA2* sgRNAs or the non-targeting sgRNA. This was to confirm that site directed mutagenesis of *LAMA1* and *LAMA2* had occurred in the total co-transfected cell populations, before clonal cell lines were propagated.

The results of the DNA mismatch detection assays are displayed in Figure 4.4. The presence of 3 DNA bands in just the EGFP positive DAOY and ONS-76 cells co-transfected with *LAMA1* and *LAMA2* sgRNAs (referred to as DAOY KO and ONS-76 KO cells henceforth) indicated the presence of INDELs at the *LAMA1* (Figure 4.4 A) and *LAMA2* (Figure 4.4 B) sgRNA target sites. This finding confirmed that site directed mutagenesis of *LAMA1* and *LAMA2* had occurred in these cells and therefore the propagation of clonal cell lines should be conducted.

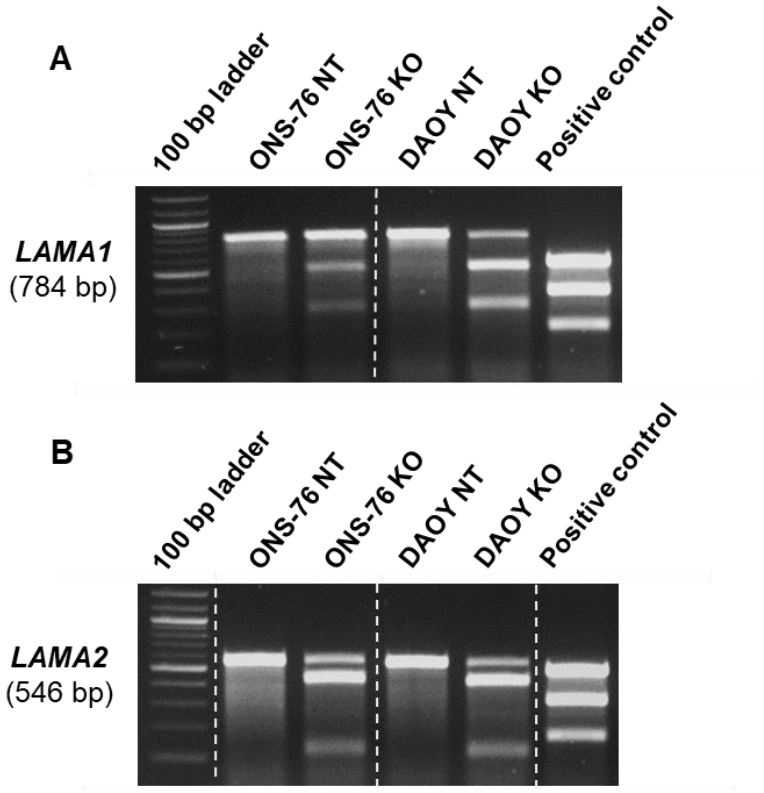


Figure 4.4 Agarose gel electrophoresis of DNA mismatch detection assays indicates the presence of insertion or deletion mutations (INDELs) in Laminin Subunit α1 (*LAMA1*) and Laminin Subunit α2 (*LAMA2*) in enhanced green fluorescent protein (EGFP) positive DAOY and ONS-76 cells co-transfected with Cas9 nuclease-EGFP mRNA and *LAMA1* and *LAMA2* single guide RNAs (sgRNAs). The presence of 3 DNA bands in the EGFP positive DAOY and ONS-76 cells co-transfected with *LAMA1* and *LAMA2* sgRNAs (DAOY KO and ONS-76 KO respectively) indicates the presence of INDELs at the *LAMA1* (**A**) and *LAMA2* (**B**) sgRNA target sites. The positive control is an INDEL containing DNA sequence provided by the manufacture. White dashed lines indicate where the gel image has been cropped as to only display the relevant bands for simplicity. The uncropped gels for A and B can be observed in Appendix Figure 3.

4.4.2 DNA mismatch detection assays of *LAMA1* and *LAMA2* in clonal cell lines

Genomic DNA (gDNA) was isolated from each of the clonal cell lines established from the DAOY KO and ONS-76 KO cells (11 and 14 cell lines respectively; Figure 4.1). This was then used to conduct DNA mismatch detection assays for *LAMA1* and *LAMA2*, the results of which can be observed in Figure 4.5. For reference, the clonal

cell lines were named in accordance with the position of the well within the 96 well plate in which they were propagated and the number of parent cells seeded into that well. For example, a clonal cell line named ‘9G1C’ will have been grown in well ‘9G’ in which 1 cell (‘1C’) will have been seeded.

In all of the 11 DAOY KO cell lines, there were 3 bands detected in the DNA mismatch detection assays for both *LAMA1* and *LAMA2*, apart from in *LAMA1* in the cell line 10F1C (Figure 4.5 A). Furthermore, there were also 3 bands detected for both *LAMA1* and *LAMA2* in all of the 14 ONS-76 KO cell lines, apart from *LAMA1* in the cell line 8F1C (Figure 4.5 B). Now that it had been confirmed that INDELs were present in the DAOY and ONS-76 KO cell lines, we next wanted to assess whether they conferred a reduction in protein expression by western blotting.

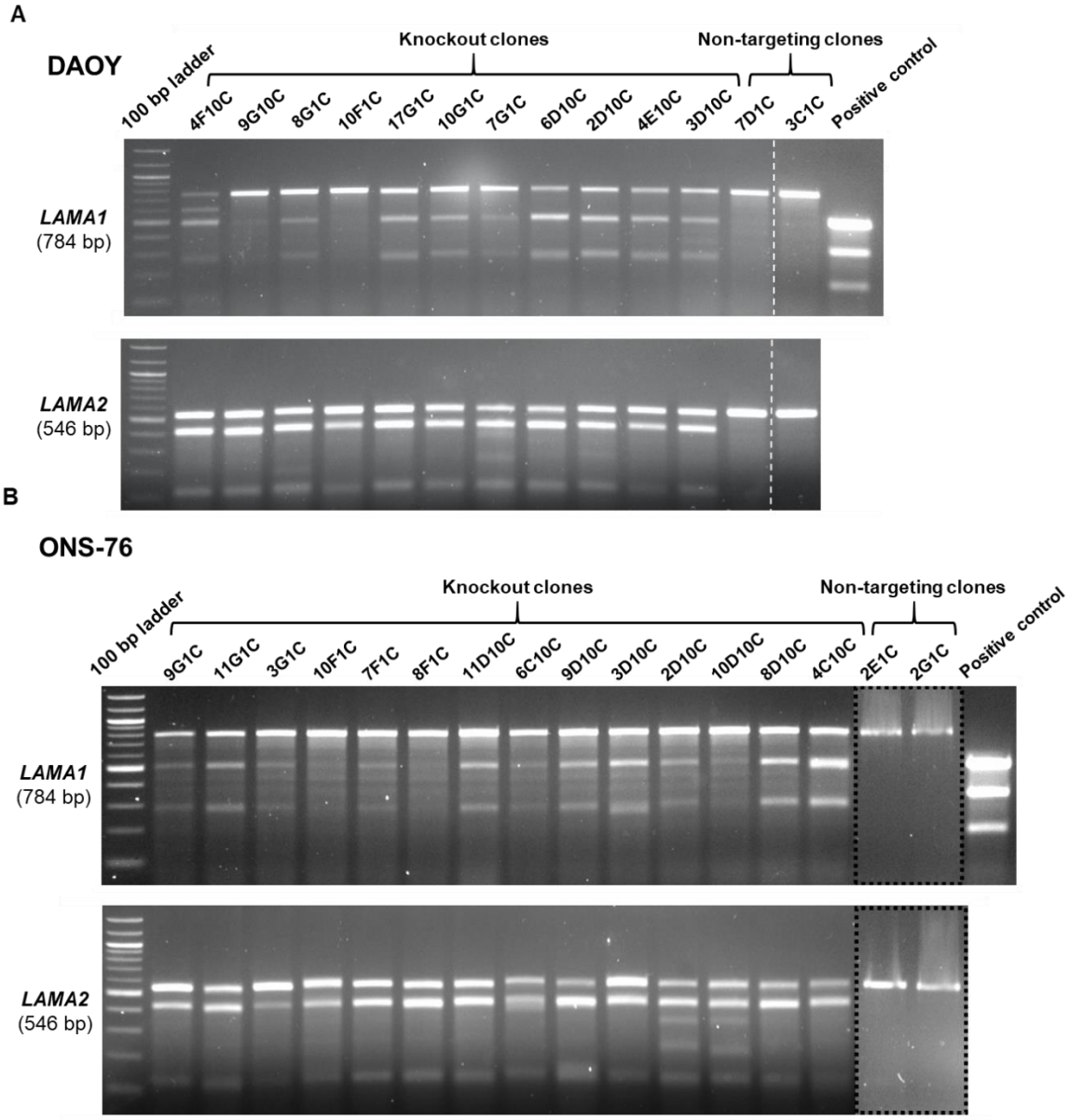


Figure 4.5 Agarose gel electrophoresis of DNA mismatch detection assays indicates the presence of insertion or deletion mutations (INDELs) in Laminin Subunit α1 (*LAMA1*) and Laminin Subunit α2 (*LAMA2*) in nearly all of the clonal cell lines derived from DAOY and ONS-76 cells co-transfected with Cas9 nuclease-enhanced green fluorescent protein (EGFP) mRNA and *LAMA1* and *LAMA2* single guide RNAs (sgRNAs). The presence of 3 DNA bands in the clonal cell lines derived from DAOY (**A**) and ONS-76 (**B**) cells co-transfected with *LAMA1* and *LAMA2* sgRNAs, indicates the presence of INDELs at the *LAMA1* and *LAMA2* sgRNA target sites. Clonal cell lines were named in accordance with the position of the well within the 96 well plate in which they were grown, and the number of parent cells seeded into that well. For example, a clonal cell line named '9G1C' will have been grown in well '9G' in which a single cell ('1C') will have been seeded. The positive control is an INDEL containing DNA sequence provided by the manufacture. White dashed lines indicate where the gel image has been cropped as to only display the relevant bands for simplicity. Black dotted boxes indicate where DNA has been electrophoresed on a separate agarose gel but has been displayed together with the main gel, also for simplicity. Uncropped gels for A and B can be observed in Appendix Figure 3.

4.5 Western blotting of LAMA1 and LAMA2 in DAOY KO and ONS-76 KO cell lines

Western blotting was conducted on protein isolated from each of the KO cell lines (Figures 4.6 and 4.7). The level of LAMA1 and LAMA2 expression in the KO cell lines was calculated as a percentage relative to the non-targeting control cell lines which exhibited the most similar level of LAMA1 and LAMA2 expression to the wild-type. These were the DAOY non-targeting cell line 7D1C and the ONS-76 non-targeting cell line 2G1C.

As can be observed in Figure 4.6 A and C, the expression of LAMA1 was reduced in all the DAOY KO cell lines, apart from in 17G1C. The DAOY KO cell lines 8G1C, 6D10C and 3D10C exhibited the highest level of reduction of 74%, 97% and 88% respectively (Figure 4.6 C). Additionally, LAMA1 protein expression was completely lost in the DAOY KO cell line 10F1C (Figure 4.6 A and C), despite the fact that only a single band was identified in the DNA mismatch detection assay for *LAMA1* in this cell line (Figure 4.5 A). This suggested that the INDELs present in *LAMA1* in 10F1C were identical and were therefore not detected by the DNA mismatch detection assay. Furthermore, LAMA2 expression was also reduced in all of the DAOY KO cell lines, apart from in 2D10C (Figure 4.6 B and D). However, none of the DAOY KO cell lines exhibited complete LAMA2 protein loss. The KO cell lines 8G1C, 10F1C and 3D10C displayed the greatest level of reduction in LAMA2 expression of 79%, 74% and 60% respectively.

From this analysis, the DAOY KO cell lines 10F1C, 8G1C and 3D10C were chosen for expansion into cell stocks, since they exhibited the highest level of reduction in the expression of both LAMA1 and LAMA2.

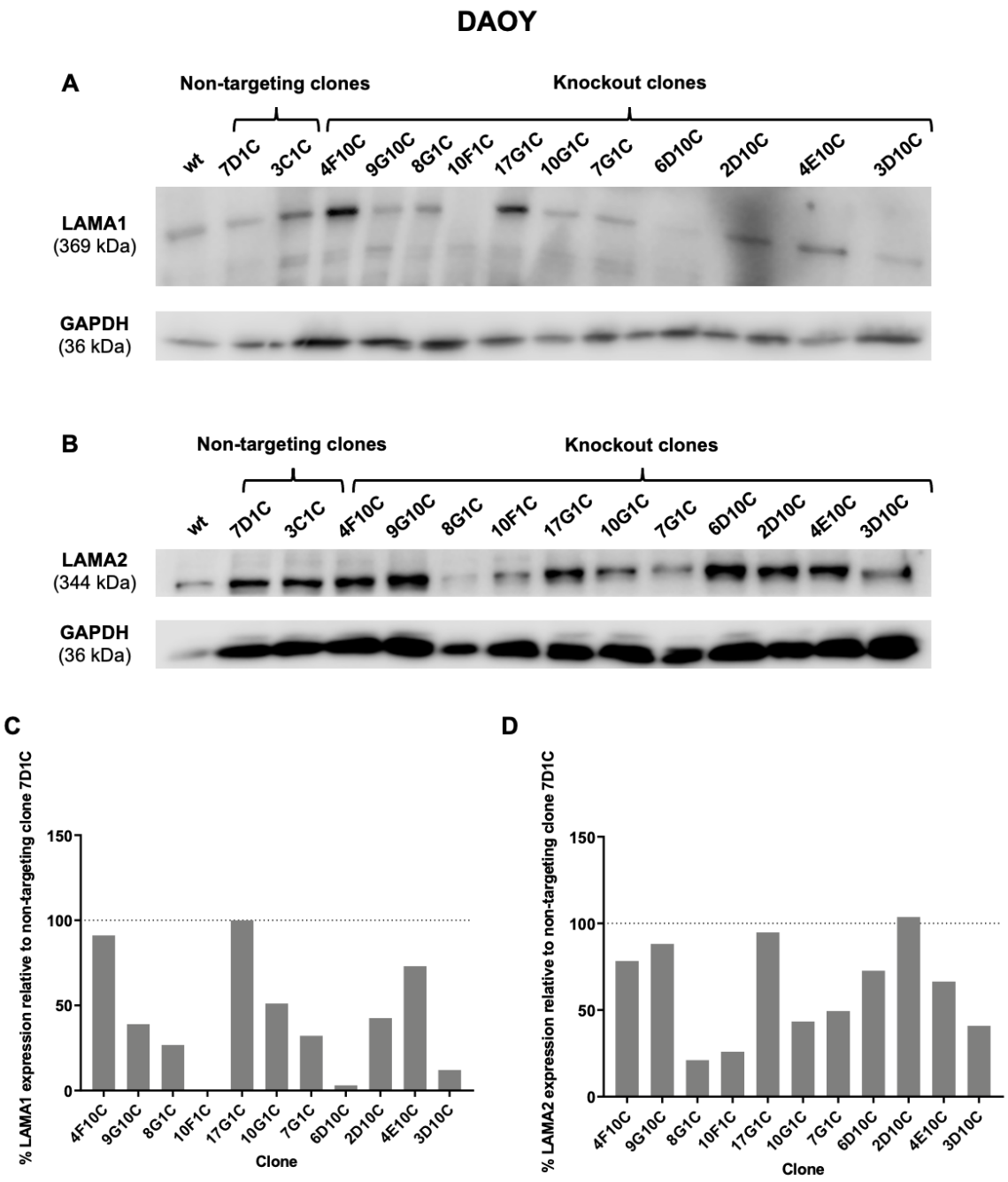


Figure 4.6 Western blotting of the 11 clonal cell lines, derived from DAOY cells co-transfected with Cas9 nuclease-enhanced green fluorescent protein (EGFP) mRNA and Laminin Subunit α1 (*LAMA1*) and Laminin Subunit α2 (*LAMA2*) single guide RNAs (sgRNAs), reveals a reduction in the expression of LAMA1 and LAMA2 relative to a non-targeting control cell line. The relative expression of LAMA1 (**A** and **C)** and LAMA2 (**B** and **D**) was reduced in all the DAOY KO cell lines, apart from in 17G1C (LAMA1) and 2D10C (LAMA2). LAMA1 protein expression was completely lost in the DAOY KO cell line 10F1C, however, none of the cell lines exhibited complete LAMA2 protein loss. Western blotting analyses were conducted relative to GAPDH as a loading control. The normalised expression of LAMA1 and LAMA2 in the DAOY KO cell lines was then calculated as a percentage relative to the non-targeting control cell line 7D1C. The dotted line in C and D represents 100% LAMA1 and LAMA2 expression. Full length, exemplar blots of the antibodies used here can be observed in Appendix Figure 1.

As displayed in Figure 4.7 A and C, the expression of LAMA1 was reduced in the majority of the 14 ONS-76 KO cell lines. However, the KO cell lines 9G1C, 7F1C, 8F1C and 11D10C, did not exhibit any reduction in LAMA1 expression (Figure 4.7 A and C). Conversely, the KO cell lines 9D10C, 8D10C and 4C10C showed the greatest the level of reduction in LAMA1 expression of 79%, 82% and 73% respectively (Figure 4.7 A and C). However, none of the ONS-76 KO cell lines exhibited complete LAMA1 protein loss. Furthermore, LAMA2 expression was also reduced in most of the ONS-76 KO cell lines, apart from 3G1C, 8F1C, 9D10C and 10D10C, which did not exhibit any reduction in LAMA2 expression (Figure 4.7 B and D). The cell lines 6C10C, 8D10C and 4C10C displayed the highest level of reduction in the expression of LAMA2 of 77%, 78% and 82% respectively (Figure 4.7 B and D). None of the ONS-76 KO cell lines exhibited complete LAMA2 protein loss.

From this analysis, the ONS-76 KO cell lines 4C10C, 6C10C and 8D10C were chosen for expansion into cell stocks, since they exhibited the highest level of reduction in the expression of both LAMA1 and LAMA2.

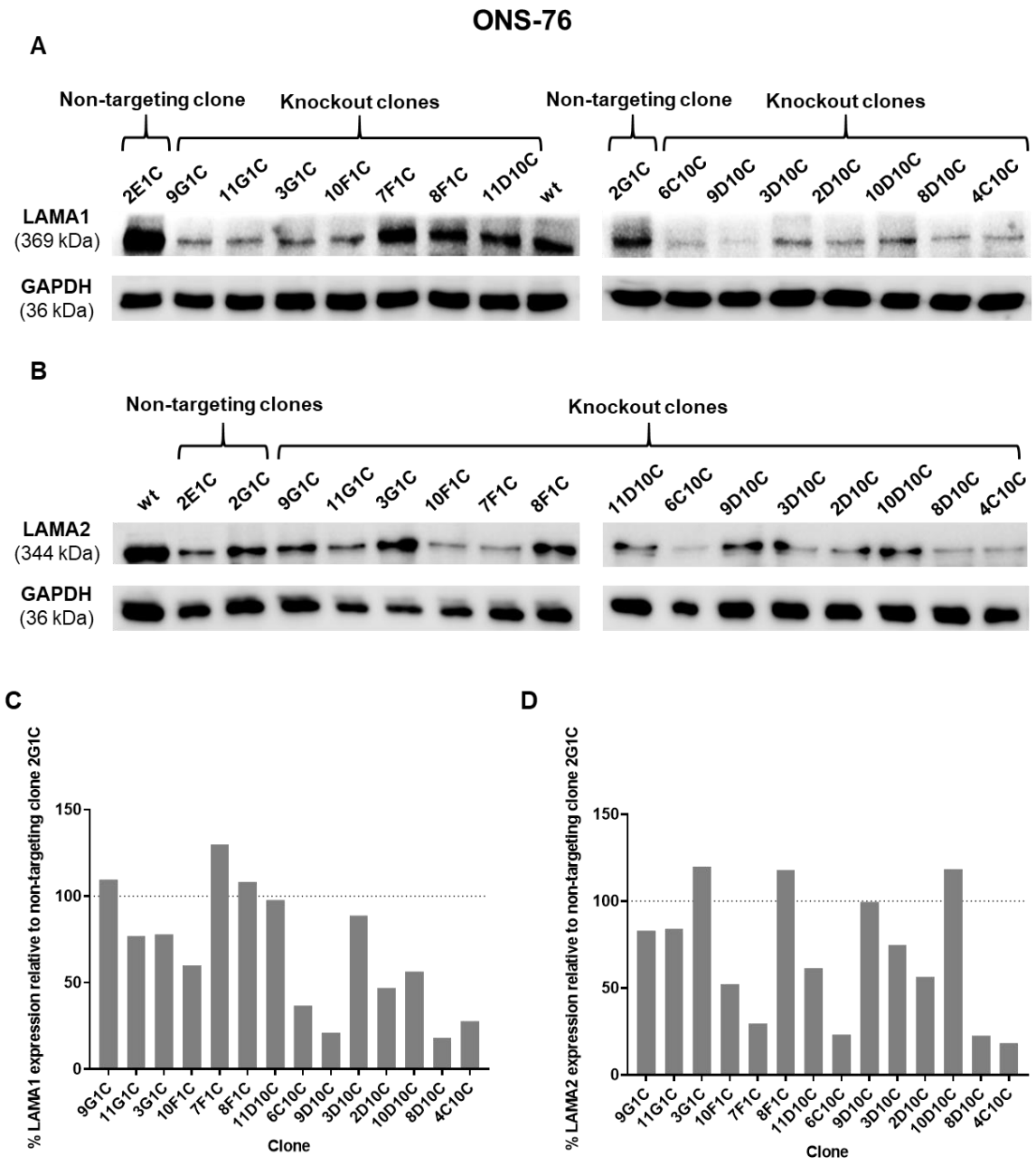


Figure 4.7 Western blotting of the 14 clonal cell lines, derived from ONS-76 cells co-transfected with Cas9 nuclease-enhanced green fluorescent protein (EGFP) mRNA and Laminin Subunit α1 (*LAMA1*) and Laminin Subunit α2 (*LAMA2*) single guide RNAs (sgRNAs), reveals a reduction in the expression of LAMA1 and LAMA2 relative to a non-targeting control cell line. The relative expression of LAMA1 (**A** and **C)** and LAMA2 (**B** and **D**) was reduced in the majority of the ONS-76 KO cell lines. However, the KO cell lines 9G1C, 7F1C, 8F1C and 11D10C did not exhibit any reduction in LAMA1 expression. Furthermore, the KO cell lines 3G1C, 8F1C, 9D10C and 10D10C did not display any reduction in LAMA2 expression. None of the KO cell lines exhibited complete loss of LAMA1 or LAMA2 expression. Western blotting analyses were normalised to GAPDH. The normalised expression of LAMA1 and LAMA2 in the ONS-76 KO cell lines was then calculated as a percentage relative to the non-targeting control cell line 2G1C. The dotted line in C and D represents 100% LAMA1 and LAMA2 expression. Full length, exemplar blots of the antibodies used here can be overserved in Appendix Figure 1.

4.6 Characterisation of INDELs in *LAMA1* and *LAMA2* by Sanger Sequencing

Once we had identified which of the DAOY and ONS-76 KO cell lines which exhibited the greatest reduction in LAMA1 and LAMA2 protein expression, we next sought to fully characterise the INDELs present in these cell lines. To do this, gDNA isolated from each of the selected KO cell lines was firstly amplified by PCR using specifically designed primers for the *LAMA1* and *LAMA2* sgRNA target sites. The PCR products were then purified and Sanger Sequenced at the University of Nottingham Deep Seq facility. Subsequent chromatograms of both the *LAMA1* and *LAMA2* sgRNA target sites were then analysed using the online INDEL discovery tool 'Indigo' (https://www.gear-genomics.com/indigo/), in order to identify the position and sequence of INDELs. A diagrammatic illustration of this process can be observed in Figure 4.8.

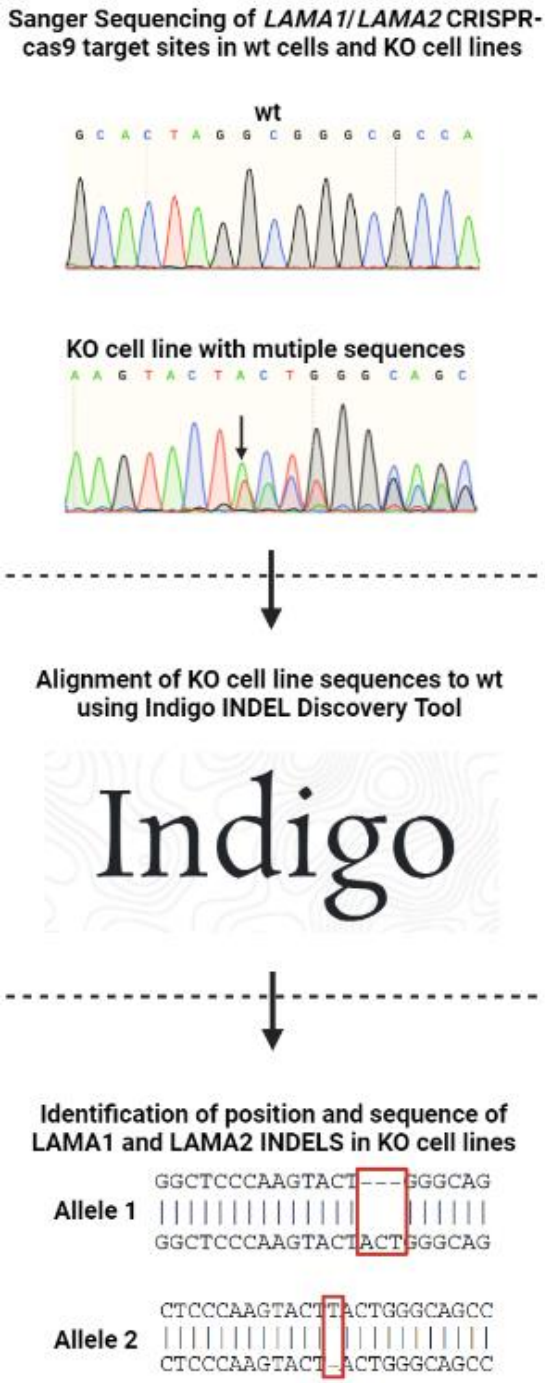


Figure 4.8 Workflow of Laminin Subunit α1 (*LAMA1*) and Laminin Subunit α2 (*LAMA2*) insertion or deletion mutation (INDEL) characterisation in DAOY KO and ONS-76 KO cell lines by Sanger Sequencing. Genomic DNA (gDNA) isolated from each of the KO cell lines was amplified by PCR using primers for the *LAMA1* and *LAMA2* single guide RNA (sgRNA) target sites. The PCR products were then Sanger Sequenced. Chromatograms of the *LAMA1* and *LAMA2* sgRNA target sites were then analysed using the online INDEL discovery tool 'Indigo'. This tool works by separating the superimposed signal peaks in chromatograms (beginning from the sgRNA target site), caused by the presence of monoallelic or biallelic INDELs, and aligning them to the corresponding wild-type sequence; a process known as degenerate sequence decoding (DSD). This then identified the position and sequence of INDELs.

The INDEL characterisation of the *LAMA1* and *LAMA2* sgRNA target sites in the selected DAOY KO and ONS-76 KO cell lines is displayed in Table 4.1. In some of the KO cell lines there were more than 2 different sequences for *LAMA1* or *LAMA2* identified from chromatograms. This could be due to some of the cell lines being derived from multiple parent cells, i.e., those that were derived from 10 parent cells or as a result of a seeding error in cell lines that were supposed to be derived from a single cell. In these circumstances, each of the cells that survived the seeding process may have possessed different mono or biallelic INDELs, therefore meaning that multiple sequences were then detected in the whole cell line population. Another reason for this may be the ploidy of the cell lines. According to the American Type Culture Collection (ATCC), the DAOY cell line can often contain cells which are either tetraploid or hypertetraploid (ATCC, 2023). Furthermore, the karyotype of the ONS-76 cell line has not been established. This could have meant that the some of the cells within the cell lines contained more than 2 alleles for *LAMA1* and *LAMA2,* which may have resulted in the formation of more than 2 different *LAMA1* and *LAMA2* INDELs within these cells, and thus more than 2 different sequences for each gene would have been detected in the whole cell line population, even in KO cell lines derived from a single cell. The Indigo INDEL discovery tool is only able to analyse two different sequences, therefore, in the cell lines where more than two sequences were detected for *LAMA1* or *LAMA2*, it was not possible to characterise the INDELs.

In the selected DAOY KO cell lines, a variety of different INDELs were identified in the *LAMA1* and *LAMA2* sgRNA target sites (Table 4.1). Firstly, in the KO cell line 10F1C, there was an insertion of a thymine nucleotide in the same position in both alleles of *LAMA1*. The same INDEL in the same position of *LAMA1* was anticipated for this cell line, due to only a single band being detected in the DNA mismatch detection assay for *LAMA1* in 10F1C (Figure 4.5). 10F1C also possessed an 18 nucleotide deletion in one allele of *LAMA2*. In the cell line 8G1C there was a monoallelic insertion of a

thymine nucleotide in *LAMA1* and two different 4 and 5 nucleotide deletions in the alleles of *LAMA2*. Finally, in the cell line 3D10C there was a monoallelic insertion of a single thymine nucleotide in *LAMA1*, in the same position as in 10F1C. However, it was not possible to characterise *LAMA2* INDELs in this cell line, as there were more than two different *LAMA2* sequences identified from the chromatogram. The reason that only two sequences were detected for *LAMA1* in the same cell line, may be that out of the parent cells which survived the seeding process, only one of them possessed a *LAMA1* indel. Therefore, this was then the only *LAMA1* INDEL present in the whole cell line population, meaning that only two *LAMA1* sequences were detected. This is applicable to the rest of the cell lines where this is the case.

A range of different INDELs were also detected in *LAMA1* and *LAMA2* in the selected ONS-76 KO cell lines (Table 4.1). Firstly, in the KO cell line 4C10C, a monoallelic 33 nucleotide deletion was identified in *LAMA1* and a 3 nucleotide insertion was detected in *LAMA2*. Additionally, in the cell line 6C10C, there was monoallelic insertion of a single thymine nucleotide in *LAMA1*. However, there were more than two sequences detected for *LAMA2,* so INDEL characterisation could not be conducted. Lastly, in the cell line 8D10C, there were too many different sequences for *LAMA1* detected for INDEL characterisation to be conducted. However, a monoallelic insertion of a single thymine nucleotide was identified in *LAMA2*.

Table 4.1 Sequence and position of Laminin Subunit α1 (*LAMA1*) and Laminin Subunit α2 (*LAMA2*) insertion or deletion mutations (INDELs) in DAOY KO and ONS-76 KO cell lines, as identified by analysis of Sanger Sequencing data using the online INDEL discovery tool 'Indigo'. 'Too many sequences' refers to when more than 2 different sequences for *LAMA1*/*LAMA2* were detected by Sanger Sequencing and the Indigo tool was therefore unable to analyse them. Nucleotides highlighted in green illustrate where they have been inserted and ones highlighted in red illustrate where they have been deleted from the wild-type *LAMA1*/*LAMA2* single guide RNA target site sequences.

	ID	No. parent cells	LAMA1				LAMA2			
			No. alleles mutated	Indel 1	Indel 2	Position of Indel	No. alleles mutated	Indel 1	Indel 2	Position of Indel
DAOY	10F	1	2	Insertion (T)	Insertion (T)	**Indel 1:** ACTGGCTCCCAAGTACTTACTGGG **Indel 2:** ACTGGCTCCCAAGTACTTACTGGG	1	Deletion (18 nt)	n/a	**Indel 1:** AGTCACAGAGATTGCAGCGAGGGTAGTTC
DAOY	8G	1	1	Insertion (G)	n/a	**Indel 1:** ACTGGCTCCCAAGTACTGACT	2	Deletion (4 nt)	Deletion (5 nt)	**Indel 1:** AGTCACAGAGATTGCAGCGAGGGG Indel 2: AGTCACAGAGATT GCAGGGAGGGTAGTTC
DAOY	3D	10	2	Insertion (T)	n/a	**Indel 1:** ACTGGCTCCCAAGTACTTACT	Too many sequences	n/a	n/a	n/a
ONS-76	4C	10	1	Deletion (33 nt)	n/a	**Indel 1:** ACCGCGGTCATGCAGAGACTGGCTCCCAAGTACTACTGG	1	Insertion (3 nt)	n/a	**Indel 1:** AGTCACAGAGATTGCAGACACGAGGG
ONS-76	6C	10	1	Insertion (T)	n/a	**Indel 1:** ACTGGCTCCCAAGTACTTACT	Too many sequences	n/a	n/a	n/a
ONS-76	8D	10	Too many sequences	n/a	n/a	n/a	2	Insertion (T)	n/a	**Indel 1:** AGTCACAGAGATTGCAGTCGAGGG

4.7 Validating that the reduction in LAMA1 and LAMA2 expression is retained in DAOY KO and ONS-76 KO cell lines

To ensure that the reduction of LAMA1 and LAMA2 expression exhibited by the selected KO cell lines was retained over multiple passages, western blotting of LAMA1 and LAMA2 was conducted on protein isolated from the KO cell lines that had been passaged 2 and 5 times. This was important to determine so that the KO cell lines could be used in subsequent long-term experiments. Both the western blots and densitometry analysis can be observed in Figure 4.9. Once again, LAMA1 and LAMA2 expression in the KO cell lines was calculated as a percentage relative to the non-targeting control cell lines.

Both LAMA1 and LAMA2 expression was found to have been restored to the same level (or above) as the respective non-targeting cell lines after 2 and 5 passages in all of the DAOY KO (apart from 10F1C) and ONS-76 KO cell lines (Figure 4.9 A-D). However, the complete loss of LAMA1 expression exhibited by the DAOY KO cell line 10F1C, was retained after both 2 and 5 passages. Conversely, its initial reduction in LAMA2 expression (Figure 4.6 B and D) was restored to same level as the non-targeting control cell line after passaging (Figure 4.9 A-D). This cell line was therefore expanded into more cell stocks.

One potential reason for the restoration of LAMA1 and LAMA2 expression in the majority of the DAOY KO and ONS-76 KO cell lines, could be that some of the cells seeded, for cell lines derived from multiple cells, possessed no INDELs in *LAMA1* or *LAMA2*. This would have resulted in a mixed population of cells, which either expressed both LAMA1 and LAMA2, only one of them, or neither of them. Expressing LAMA1 and LAMA2 could have then given cells a selection advantage, allowing them to outcompete cells which only expressed one or neither of them, meaning that the cell line population then became predominately LAMA1 and LAMA2 expressing cells over

passages. Another reason could be due to some of KO cell lines only possessing monoallelic INDELs for *LAMA1* or *LAMA2*, as shown in Table 4.1. Consequently, cells may have been able to express LAMA1 and LAMA2 to the same level as the non-targeting cell lines from only one wild-type allele.

Due to restricted lab access after the first national lockdown in 2020, as well as significantly delayed delivery times of reagents and limited laboratory consumables, also as a consequence of the COVID-19 pandemic, the work detailed in this chapter took approximately a year to complete. As a consequence (and because we did not know if there would be another national lockdown) we decided that instead of repeating the knockout process, we would continue with downstream experiments focusing on the role of LAMA1 in SHH medulloblastoma, using the DAOY KO cell line 10F1C, which exhibited a stable and complete loss of LAMA1 protein expression. However, if the knockout process was to be repeated 2 factors would be changed. Firstly, all the KO cell lines would be derived from a single cell (as previously mentioned), to ensure that all cells within each KO cell line possess the same INDEL(s). Secondly, more KO cell lines would be established to increase the likelihood of obtaining complete LAMA1/LAMA2 knockouts.

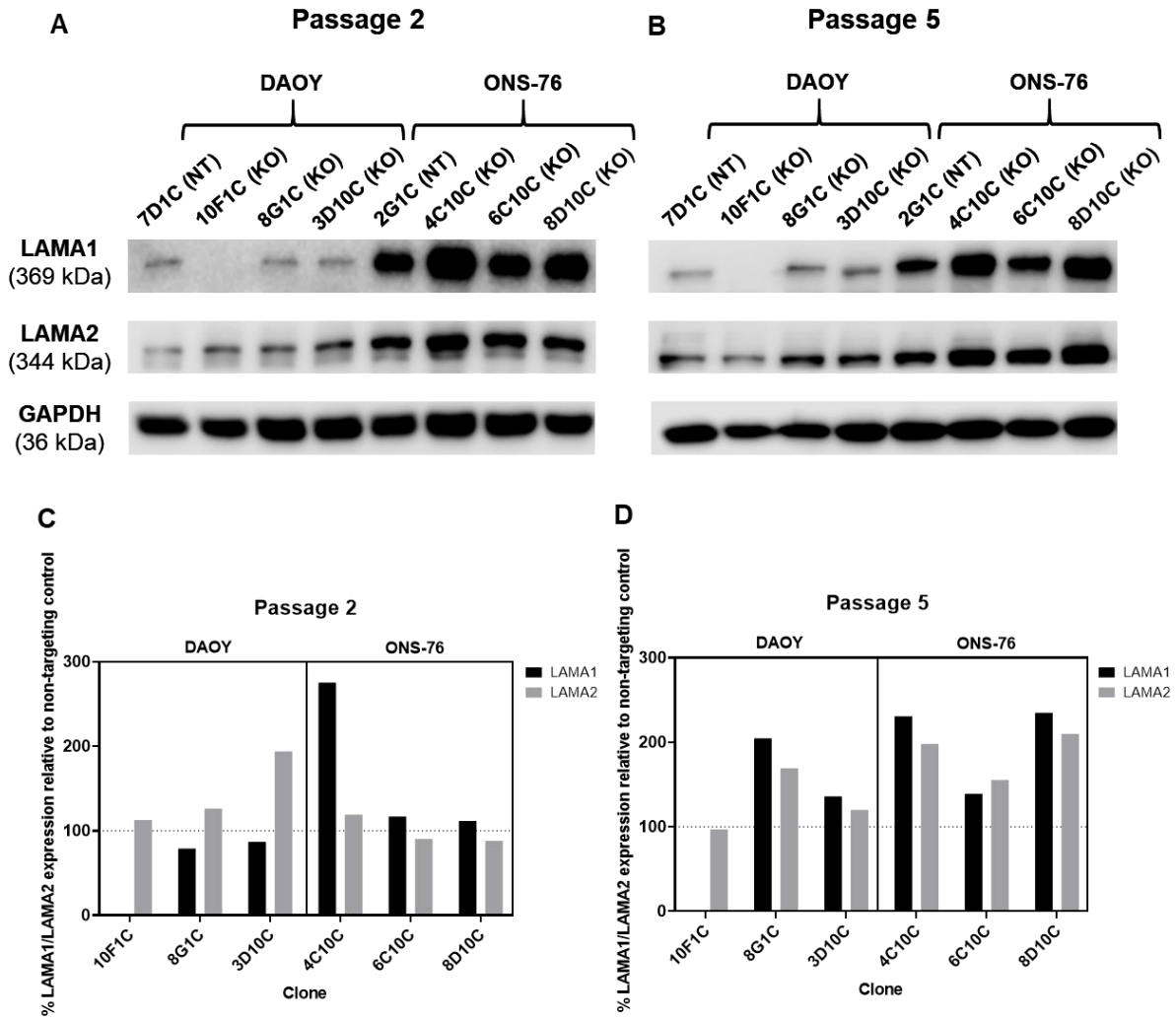


Figure 4.9 Western blotting of clonal cell lines, derived from DAOY and ONS-76 cells co-transfected with Cas9 nuclease-enhanced green fluorescent proteins (EGFP) mRNA and Laminin Subunit α1 (*LAMA1*) and Laminin Subunit α2 (*LAMA2*) single guide (sgRNAs), reveals that LAMA1 and LAMA2 expression is restored to the same level as non-targeting control cell lines after 2 and 5 passages. The relative expression of LAMA1 and LAMA2 after 2 (**A** and **C**) and 5 passages (**B** and **D**) was restored to the same level, or above, as the respective non-targeting control cell lines in all the DAOY KO and ONS-76 KO cell lines, apart from the DAOY KO cell line 10F1C. In this cell line the complete loss of LAMA1 protein expression was maintained over both 2 and 5 passages. Western blotting analyses were normalised to GAPDH as a loading control. The normalised expression of LAMA1 and LAMA2 in the KO cell lines was then calculated as a percentage relative to their respective non-targeting control cell line. The dotted line in C and D represents 100% LAMA1 and LAMA2. Full length blots can be observed in Appendix Figure 4.

4.8 Analysing the LAMA1 amino acid sequence in the DAOY KO cell line 10F1C

Once we had decided to continue with downstream experiments using the DAOY KO cell line 10F1C, we sought to determine the altered LAMA1 amino acid sequence that was now being expressed in this cell line, as a consequence of identical biallelic thymine insertions in *LAMA1* (Table 4.1). This was achieved by translating the 10F1C *LAMA1* nucleotide sequence (obtained from Sanger Sequencing) into an amino acid sequence, using the Expasy online DNA/RNA translation tool (https://web.expasy.org/translate/). This amino acid sequence was then aligned to the wild-type LAMA1 amino acid sequence, using the online multiple sequence alignment tool, Clustal Omega (https://www.ebi.ac.uk/Tools/msa/clustalo/). The results of this analysis are displayed in Figure 4.10.

As can be observed in Figure 4.10, the identical biallelic insertion of a thymine nucleotide (highlighted in green) in the *LAMA1* sgRNA target site (highlighted in yellow), resulted in a frameshift mutation which caused the installation of a premature stop codon (highlighted in red; TAA); truncating LAMA1 to 578 amino acids long, instead of 3075, in 10F1C (Figure 4.10 A and B). The LAMA1 antibody used throughout this study binds LAMA1 between the amino acids 590 and 689. Given that this is after where LAMA1 is truncated to in 10F1C, this explains why the truncated version of LAMA1 was not detected at all by western blotting in this cell line (Figure 4.10 B). Furthermore, it is possible that this truncated form of LAMA1 in 10F1C was now degraded by the proteasome, as a misfolded protein (Reynaud, 2010). It is also worth noting that cells are unable to synthesise laminin-111 without LAMA1, as not only is the co-expression of all three subunits required for the formation of laminin-111, but the secretion of intact LAMA1 drives the expression of the laminin-111 β and γ subunits (Yurchenco *et al.*, 1997).

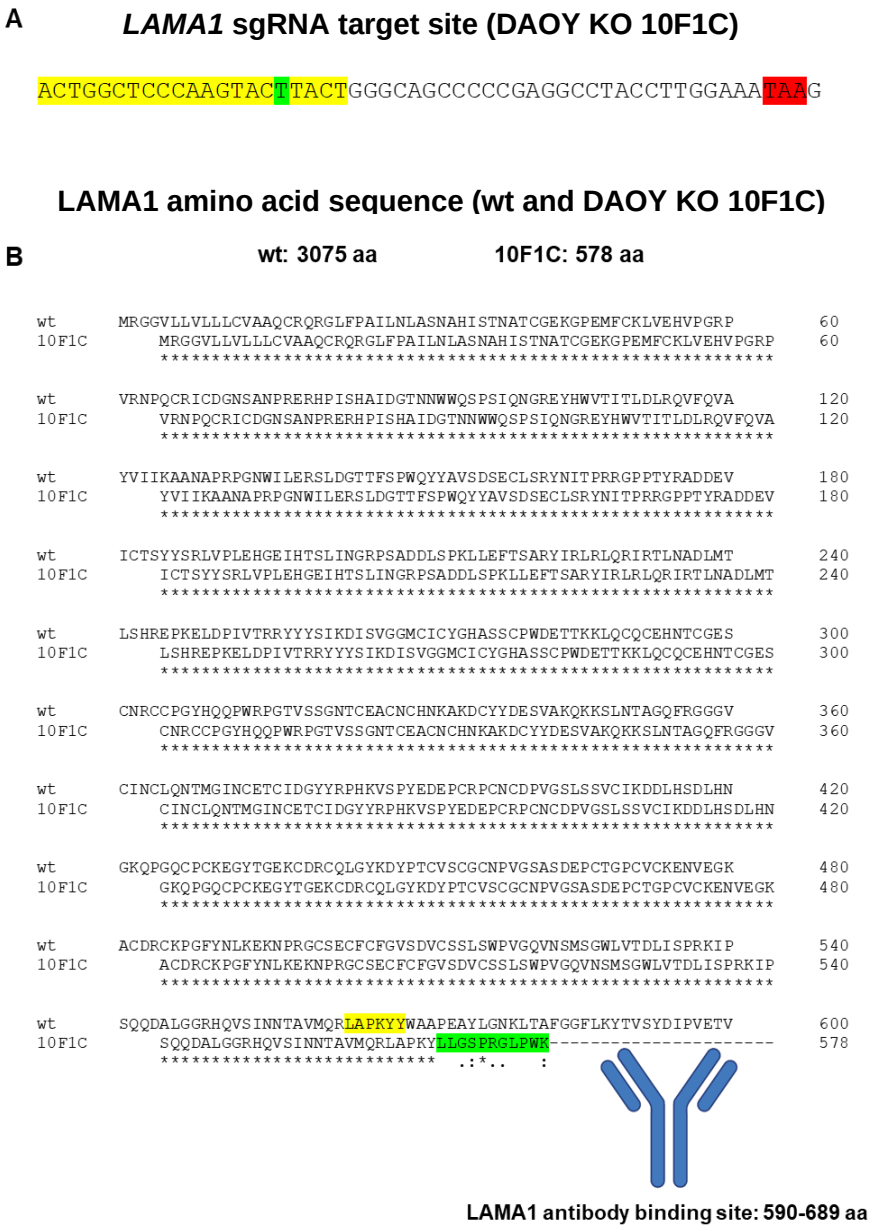


Figure 4.10 Laminin Subunit α1 (LAMA1) is truncated in the DAOY KO cell line 10F1C as a result of the identical biallelic insertion of a thymine nucleotide in the *LAMA1* single guide (sgRNA) target site. The LAMA1 nucleotide sequence obtained from the DAOY KO cell line 10F1C (by Sanger Sequencing) was translated into an amino acid (aa) sequence which was then aligned to the wild-type (wt) amino acid sequence. This identified that the insertion of a thymine nucleotide (highlighted in green), in the *LAMA1* sgRNA target site (highlighted in yellow) (**A**), resulted in a frameshift mutation in LAMA1 and the installation or a premature stop codon (highlighted in red; TAA); truncating LAMA1 to 578 amino acids long, instead of 3075 (**B**). Also highlighted in green in B, is the alternative 11 amino acid sequence caused by the frameshift mutation, before the truncation of LAMA1. Additionally, as illustrated in B, the LAMA1 antibody used in this study does not detect the truncated form of LAMA1 in 10F1C, as it binds between the amino acids 590 and 689, and LAMA1 is truncated to 578 amino acids in 10F1C.

4.9 Assessing differences in phenotype and viability between the DAOY non-targeting and LAMA1 knockout cell lines

To determine if the LAMA1 knockout in the DAOY cell line 10F1C (henceforth referred to as 'DAOY LAM$^{-/-}$ cell line') had resulted in any phenotypic changes compared to the DAOY non-targeting cell line 7D1C (henceforth referred to as 'DAOY NT cell line'), brightfield microscope images of both cell lines growing in standard 2D cell culture were captured. As displayed in Figure 4.11, the DAOY LAM$^{-/-}$ cell line generally exhibited a much more elongated cell shape than the DAOY NT cell line, suggesting that LAMA1 may have a role in the maintenance of cell shape in SHH medulloblastoma cells. Furthermore, this change in cellular morphology has often been associated with increased cellular stress, suggesting that the lack of LAMA1 protein expression may increase cellular stress in SHH medulloblastoma cells (Mori, Shibanuma and Nose, 2004).

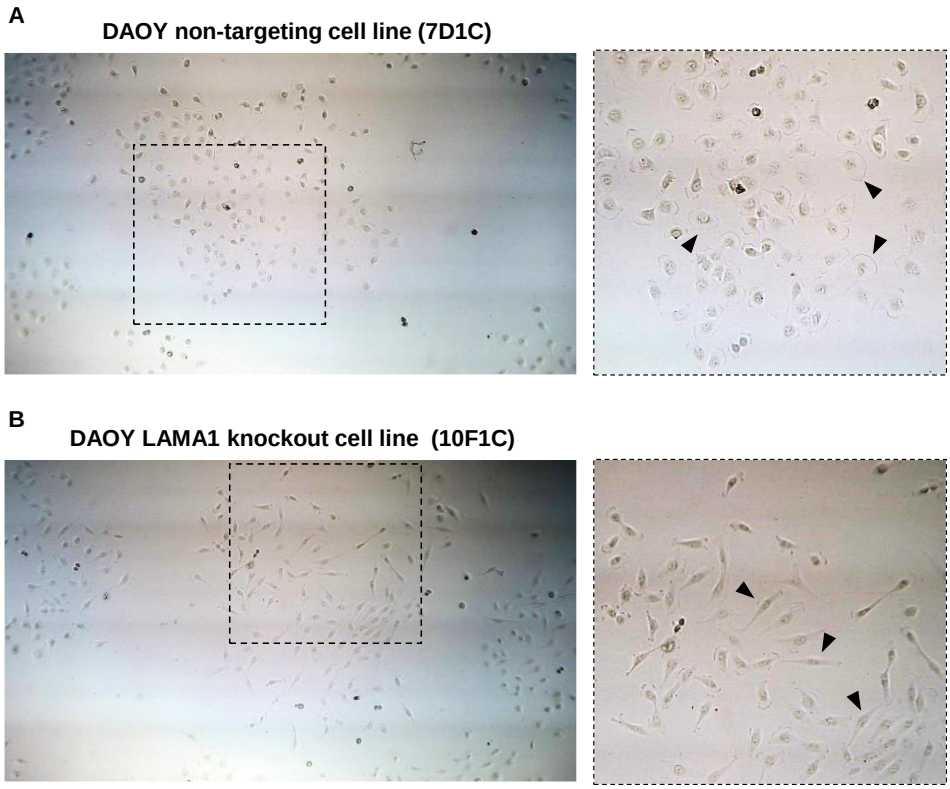


Figure 4.11 Brightfield images (4 X magnification) demonstrate that the DAOY Laminin Subunit α1 (LAMA1) knockout cell line (10F1C) exhibits a changed phenotype compared to the DAOY non-targeting cell line. DAOY LAMA1 knockout cells (**B**) exhibit a more elongated cell shape than DAOY non-targeting cells (**A**). Black arrows indicate typical cells. Representative images are shown. Scale bar: 100 µm.

Furthermore, to also assess if the LAMA1 knockout had an effect on the viability of the DAOY cell line, DAOY NT and DAOY LAM$^{-/-}$ cells were seeded into the wells of a 96 well plate and grown for 7 days. Their viability was then measured using CellTiter-Glo® on day 1, 4 and 7. As shown in Figure 4.12, there was no significant difference in viability between the cell lines at any of the time points, suggesting that LAMA1 did not affect the viability, and therefore cellular stress, of the DAOY cell line in 2D culture.

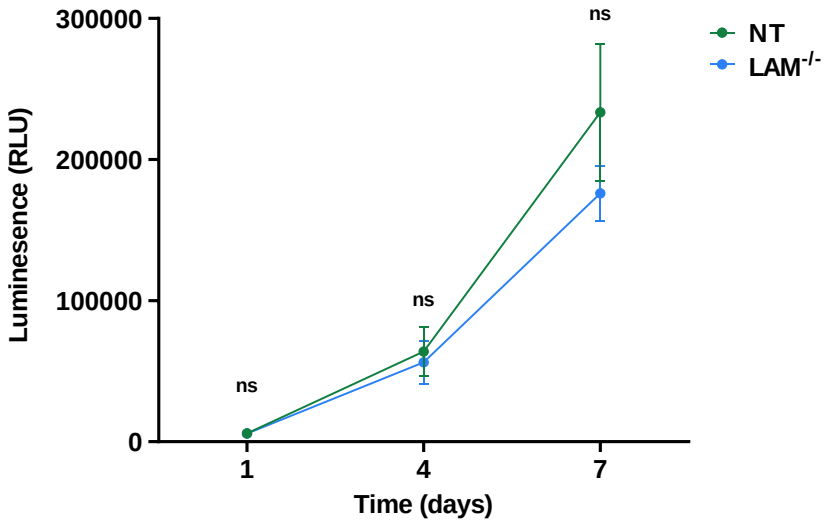


Figure 4.12 The viability of the DAOY cell line is not significantly changed by the knockout of Laminin Subunit α1 (LAMA1) in 2D culture. DAOY NT and DAOY LAM$^{-/-}$ cells were seeded into the wells of 96 well plate and grown for 7 days. Their viability was then measured using CellTiter-Glo® on day 1, 4 and 7. There was no significant different in viability between the cell lines at any of the time points. Error bars represent the mean ± SEM; n=3, with at least 3 internal replicates. Significance was calculated using Two-Way ANOVA analyses with Sidak's multiple comparisons post-hoc test.

4.10 Summary points

- DAOY and ONS-76 SHH medulloblastoma cells, successfully co-transfected with Cas9 nuclease-EGFP mRNA and either *LAMA1* and *LAMA2* sgRNAs or a non-targeting sgRNA, were identified and isolated by FACS for EGFP expression.

- From the isolated EGFP positive cells, that had been co-transfected with *LAMA1* and *LAMA2* sgRNAs, 11 DAOY KO and 14 ONS-76 KO cell lines were established from either 1 or 10 parent cells.

- DNA mismatch detection assays identified that the majority of DAOY KO and ONS-76 KO cell lines possessed INDELs in both *LAMA1* and *LAMA2.*

- Western blotting initially indicated that the relative expression of LAMA1, LAMA2 or both was reduced in the majority of DAOY KO and ONS-76 KO cell lines. LAMA1 expression was completely lost in the DAOY KO cell line 10F1C.

- Analysis of Sanger Sequencing data of the *LAMA1* and *LAMA2* sgRNA target sites, facilitated the identification of the position, sequence and mono/biallelic nature of the INDELs present in the DAOY KO and ONS-76 KO cell lines.

- Western blotting of the most successful DAOY KO and ONS-76 KO cell lines, demonstrated that after 2 and 5 passages their initial reduction in LAMA1 and LAMA2 expression was not maintained, apart from the complete loss of LAMA1 expression in the DAOY KO cell line 10F1C.

- By translating the 10F1C *LAMA1* nucleotide sequence (containing identical biallelic thymine insertions in *LAMA1*) into an amino acid sequence, and then aligning it to the wild-type LAMA1 amino acid sequence, it was identified that LAMA1 is truncated to 578 amino acids, instead of 3075, due to the installation of a premature stop codon, in this cell line.

- The DAOY knockout cell line 10F1C exhibits a more elongated cell shape in standard 2D cell culture conditions, when compared to the non-targeting DAOY cell line 7D1C.

- Due to the impact of COVID-19, we decided to continue with downstream experiments focusing on the role of LAMA1 in SHH medulloblastoma using the DAOY KO cell line 10F1C, instead of repeating the knockout process.

Chapter 5: Investigating the role of LAMA1 in SHH medulloblastoma progression

5.1 Introduction

After successfully creating a LAMA1 knockout SHH medulloblastoma cell line, we next wanted to validate the previously identified 'laminin regulated genes' (section 3.3). Furthermore, in order to decipher how LAMA1 confers better survival in *LAM*^{high} SHH medulloblastoma patients, we also set out to investigate what aspects of SHH medulloblastoma progression were affected by LAMA1, i.e., tumour growth, migration, invasion, apoptosis evasion and drug sensitivity.

We initially aimed to use the same 3D hyaluronan hydrogel model described in Chapter 3, in order to study this. However, due to persistent batch issues and significantly delayed delivery times (due to the COVID-19 pandemic), we were unable to continue growing medulloblastoma cell lines within the hyaluronan hydrogel. We therefore decided to switch to a 3D spheroid model, which are commonly used to study tumour growth, migration, invasion and drug sensitivity (Vinci *et al.*, 2012, 2013; Zanoni *et al.*, 2016; Roper *et al.*, 2021). The specific spheroid model we chose to use had been previously optimised by Dr Sophie Roper (a former PhD student in Dr Coyle's lab). In this model cells are seeded into Ultra-Low Attachment plates, causing them to form cell aggregates which can then be grown in suspension for extended periods of time. This model is much higher throughput than the hydrogel model and has a much shorter and simpler set-up (Roper and Coyle, 2022). Furthermore, the dimensions of the individual spheroids (volume and diameter) can be measured and used as an indication of viability, in addition to measuring the actual viability of the spheroids, using Cell-Titer Glo® (Roper and Coyle, 2022). Details of the methodologies of all the spheroid related models and assays used in this study can be found in section 2.10.

In the aforementioned study by our group, immunohistochemical (IHC) staining demonstrated that DAOY and ONS-76 SHH medulloblastoma cell lines deposit a sub-group specific laminin-111/211 shell-like structure around nodules, when grown in a hyaluronan hydrogel for 3 weeks. We hypothesised that this was linked to the more

favourable overall survival exhibited by *LAM*^{high} SHH medulloblastoma patients (Linke *et al.*, 2020). We therefore needed to test if this laminin-111/211 shell-like structure was also formed by SHH medulloblastoma cell lines when grown in the 3D spheroid model. Furthermore, we hypothesised that this laminin-111/211 shell-like structure may also be comprised of other ECM components. Consequently, we also sought to identify ECM protein candidates from SHH medulloblastoma patient and cell line datasets, and validate them as part of the laminin-111/211 shell-like structure deposited by SHH medulloblastoma cell lines when grown in a 3D spheroid model.

The aims of this chapter were to:

A) Validate that SHH medulloblastoma cell lines also form a laminin-111/211 shell-like structure when grown in a 3D spheroid model, as well as identify and validate additional ECM components of the shell-like structure.
B) Assess how the expression of 'laminin regulated genes' is affected by the knockout of LAMA1 in SHH medulloblastoma cells, in both 2D and 3D spheroid culture, using the DAOY LAM$^{-/-}$ cell line.
C) Assess how the knockout of LAMA1 affects the growth, migration, invasion, apoptosis evasion and drug sensitivity of SHH medulloblastoma cells in 2D and 3D spheroid culture, using the DAOY LAM$^{-/-}$ cell line.

5.2 Validating the formation of a laminin-111/211 shell-like structure by SHH medulloblastoma cell lines grown in a 3D spheroid model

To validate that the previously identified laminin-111/211 shell-like structure formed by SHH medulloblastoma cell lines grown in a hyaluronan hydrogel for 3 weeks was also formed by the same cell lines when grown in the 3D spheroid model, we stained DAOY and ONS-76 wild-type spheroids that had been grown for 1, 7, 14 and 21 days for laminin-111/211, using an antibody which detects both LAMA1 and LAMA2 (and therefore laminin-111/211). IHC was utilised to detect laminin-111/211 in day 7, day 14 and day 21 spheroids. However, too much spheroid material was lost during the processing of spheroid blocks for IHC to be conducted on spheroids younger than 7 days, thus immunofluorescence (IF) was used to stain day 1 spheroids. All spheroids stained using IHC, had previously been grown, processed and sectioned by Dr Sophie Roper.

As displayed in Figure 5.1, IF indicated that the DAOY and ONS-76 cell lines already express laminin-111/222 after 1 day of growth as a spheroid (Figure 5.1 A). Furthermore, IHC revealed that there was also an observable laminin-111/211 shell structure in day 14 and day 21 DAOY and ONS-76 spheroids (Figure 5.1 B). In the DAOY cell line, the laminin-111/211 shell structure was more localised to the periphery of the spheroid, with some staining throughout, whereas in the ONS-76 cell line this structure seemed to be more localised around the core of the spheroid; this is particularly clear in the image of the day 21 ONS-76 spheroid (Figure 5.1 B). Although some laminin-111/211 staining was present in day 7 spheroids, it was not possible to draw any conclusions regarding its organisation. Overall, these findings indicate that SHH medulloblastoma cell lines also form a laminin-111/211 shell-like structure when grown in the 3D spheroid model.

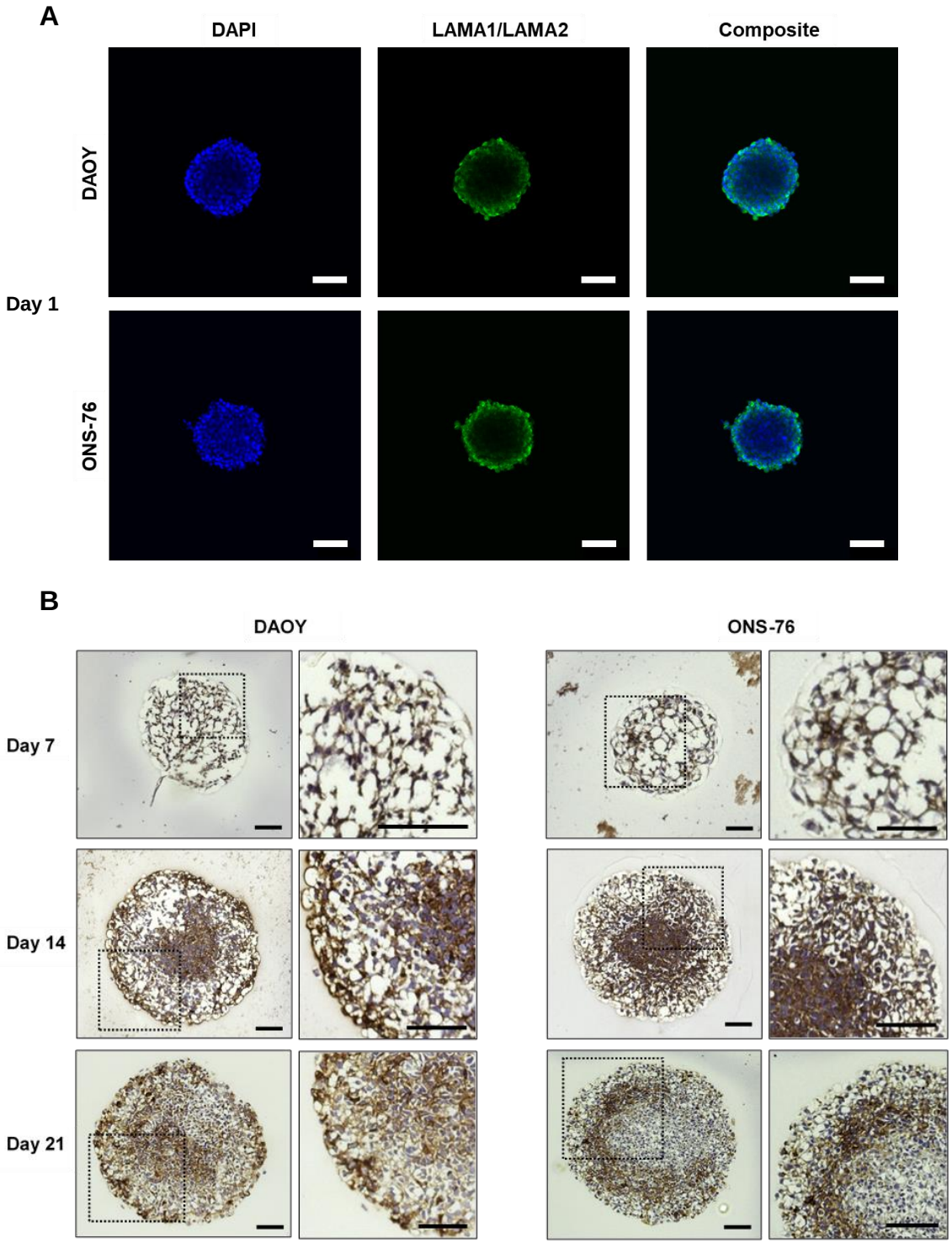


Figure 5.1 Immunofluorescent (IF) and immunohistochemical (IHC) staining of day 1, 7, 14 and 21 DAOY and ONS-76 spheroids for laminin-111/211 reveals shell-like structure. IF staining of day 1 spheroids indicated (**A**) that the DAOY and ONS-76 cell lines exhibit laminin-111/222 expression after 1 day of growth as a spheroid. IHC (**B**) revealed a laminin-111/211 shell structure in day 14 and day 21 DAOY and ONS-76 spheroids. In the DAOY cell line the laminin-111/211 shell structure was more localised to the periphery of the spheroid, with some staining throughout, whereas in the ONS-76 cell line this structure was more localised around the core of the spheroid. IF spheroid images are comprised of the middle 10 images of a 30 image Z-stack starting from the bottom of the spheroid. Representative images are shown. Scale bar: 100 µm.

5.3 Identifying additional components of the SHH medulloblastoma laminin-111/211 shell-like structure

The previous differential gene expression analysis of the SHH *LAM*^{high} medulloblastomas in the Cavalli dataset (section 3.3.2), identified that other ECM components were also upregulated in these tumours. We therefore wanted to delineate if any of these components were also part of the laminin-111/211 shell-like structure formed by SHH medulloblastoma cell lines when grown in long-term 3D spheroid and hydrogel models. Furthermore, in a recent study by Trombetta-Lima *et al*., proteomic analysis of decellularised patient tumours identified that 19 ECM proteins are differentially expressed in medulloblastomas, when compared to normal cerebellum (Trombetta-Lima *et al.*, 2021). We therefore hypothesised that the ECM components which were most likely to also comprise the laminin-111/211 shell-like structure were amongst these 19 medulloblastoma-specific ECM proteins.

In order to identify which of these ECM components were also part of the SHH medulloblastoma laminin-111/211 shell structure, we cross referenced the genes that we had previously identified to be upregulated in *LAM*^{high} SHH patient tumours in the Cavalli dataset (section 3.3.2), with the 19 ECM proteins that had been found to be differentially expressed in medulloblastoma in the Trombetta-Lima study. Eight overlapping medulloblastoma ECM proteins were identified: COL1A1 (Collagen Type-I α1 Chain), COL5A1 (Collagen Type-V α1 Chain), COL6A1 (Collagen Type-VI α1 Chain), COL6A2 (Collagen Type-VI α2 Chain), COL6A3 (Collagen Type-VI α3 Chain), LUM (Lumican), FBLN5 (Fibulin 5) and FBN1 (Fibrillin 1) (Figure 5.2). Of these 8 ECM proteins, 5 of them were isoforms of collagen α chains, including the α1, 2 and 3 chain of Type VI collagen. Interestingly, no overlapping genes were identified between the *LAM*^{low} SHH patient tumours and the 19 medulloblastoma ECM proteins, suggesting that these tumours may also express low levels of other ECM components, not just laminin-111/211.

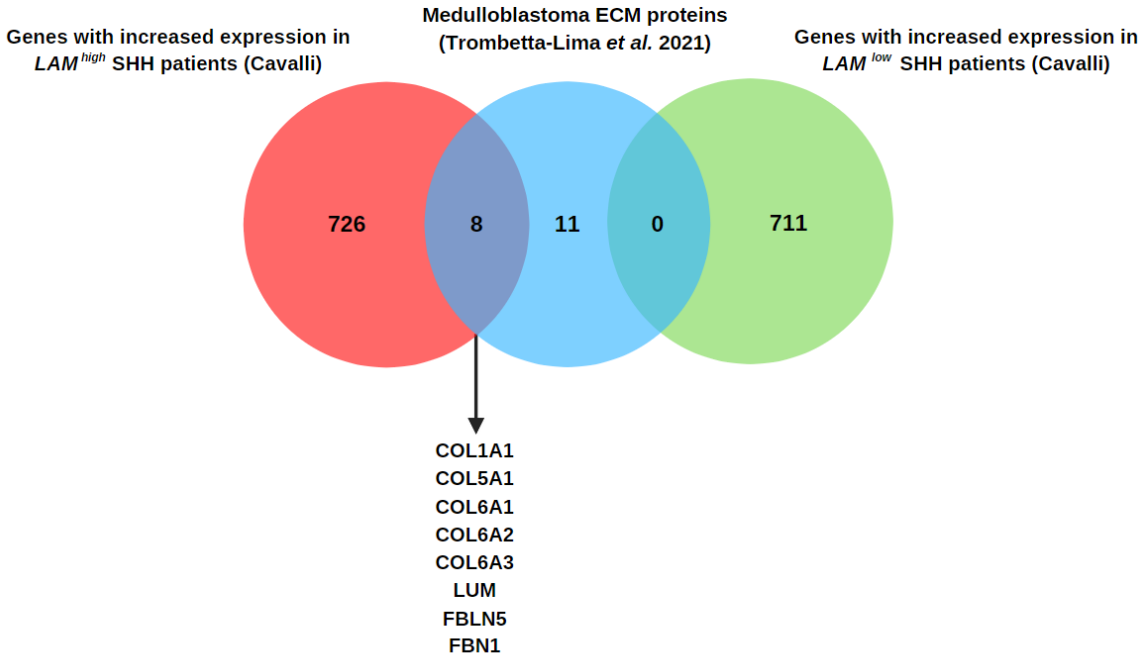


Figure 5.2 Workflow of identifying candidate extracellular matrix (ECM) proteins for validation as additional components of the SHH medulloblastoma laminin-111/211 shell-like structure previously identified by our group (Linke *et al.*). Candidate ECM proteins were identified by cross referencing the genes upregulated in *LAM*^{high} SHH patient tumours in the Cavalli dataset (section 3.3.2) with the 19 ECM proteins that were found to be differentially regulated in medulloblastoma patient tumours by Trombetta-Lima *et al.*. Eight overlapping ECM proteins were identified: : COL1A1 (Collagen Type-I α1 Chain), COL5A1 (Collagen Type-V α1 Chain), COL6A1 (Collagen Type-VI α1 Chain), COL6A2 (Collagen Type-VI α2 Chain), COL6A3 (Collagen Type-VI α3 Chain), LUM (Lumican), FBLN5 (Fibulin 5) and FBN1 (Fibrillin 1). The genes upregulated in *LAM*^{low} SHH patient tumours in the Cavalli dataset (section 3.3.2) were also cross referenced with the 19 medulloblastoma ECM proteins, of which none were found to overlap.

After identifying these 8 candidate medulloblastoma ECM proteins, we sought to ascertain which ones were the most promising for validation as additional components of the SHH laminin-111/211 shell structure. To do this, we initially conducted gene expression-based survival analysis of the 8 medulloblastoma ECM proteins on the SHH medulloblastoma patients in the Cavalli dataset, in order to identify if any of them were correlated with the same pattern of survival as *LAMA1/LAMA2*, i.e., high expression is correlated with better overall survival and low expression is correlated

with worse overall survival. The results of this survival analysis are displayed in Figure 5.3. Interestingly, all 8 medulloblastoma ECM proteins were found to be significantly correlated with the same pattern of survival as *LAMA1/LAMA2*, suggesting that they may all be part of the laminin-111/211 shell-like structure (Figure 5.3 A – H).

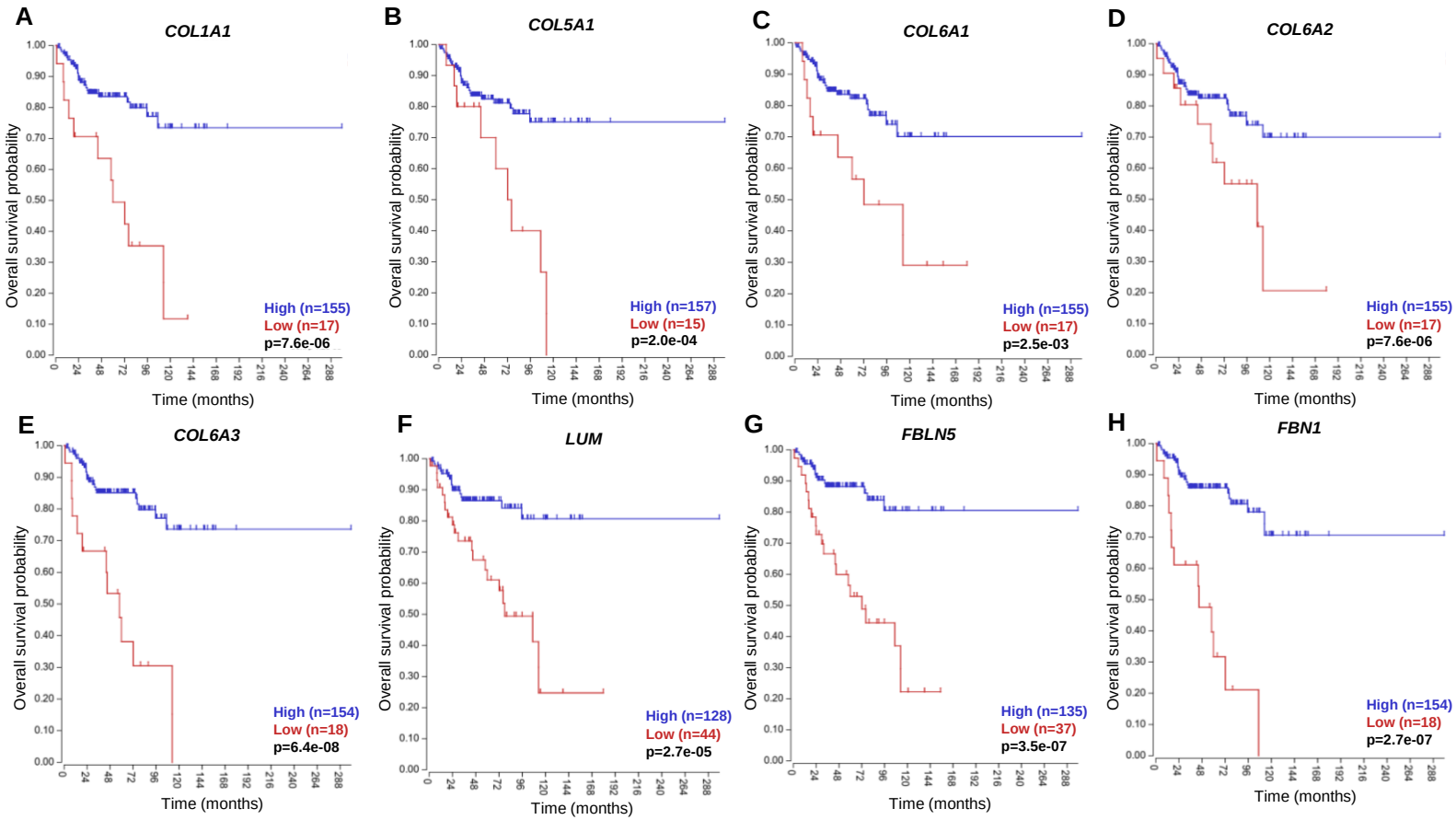


Figure 5.3 Survival analysis of 8 medulloblastoma ECM components reveals a consistent pattern of favourable overall survival correlated with high gene expression in SHH medulloblastoma patients. Gene expression-based survival analysis of *COL1A1* (Collagen Type-I α1 Chain; **A**), *COL5A1* (Collagen Type-V α1 Chain; **B**), *COL6A1* (Collagen Type-VI α1 Chain; **C**), *COL6A2* (Collagen Type-VI α2 Chain; **D**), *COL6A3* (Collagen Type-VI α3 Chain; **E**), *LUM* (Lumican; **F**), *FBLN5* (Fibulin 5; **G**) *and FBN1* (Fibrillin 1; **H**) was conducted on the SHH patients in the Cavalli dataset (SHH: n=223) (using the R2:KaplanScan tool to generate Kaplan Meier curves), to identify if any of them conferred the same pattern of survival as Laminin Subunit α1 (*LAMA1*) / Laminin Subunit α2 (*LAMA2*), i.e. high expression is correlated with better overall survival, whereas low expression is correlated with worse overall survival. All 8 ECM proteins were significantly correlated with the same pattern of survival as *LAMA1/LAMA2*. Survival curves were compared using the Log-rank (Mantel-Cox) test. Significant differences in survival were considered those where $p<0.05$.

We therefore analysed the expression of the 8 medulloblastoma ECM proteins in single cell RNA sequencing (scRNAseq) data of ONS-76 cells grown in a hyaluronan hydrogel, previously obtained by Dr Franziska Linke. This analysis was conducted to identify which of the ECM proteins exhibited the greatest level of expression by SHH medulloblastoma cells grown in a 3D cell culture model (Figure 5.4 A). Although the scRNAseq data is of cells grown in a hyaluronan hydrogel, not a spheroid, we hypothesised that because the laminin-111/211 shell was conserved across the two models, then so would any other components.

From this analysis, we identified that the medulloblastoma ECM proteins with the greatest level of expression were: *COL6A1* (expressed by 81% of cells), *COL1A1* (expressed by 75% of cells) and *COL6A3* (expressed by 74% of cells) (Figure 5.4 A). However, as two of these proteins (*COL6A1* and *COL6A3*) were both α chains of type-VI collagen, we chose to only select the most highly expressed chain, *COL6A1*, for validation. Instead of *COL6A3*, therefore, we selected the most highly expressed non-collagen component for validation, *LUM,* which was expressed by 30% of cells (Figure 5.4 A). Furthermore, 3D Orbitrap secondary ion mass spectrometry (3D OrbiSIMS) analysis was also conducted on the ONS-76 cells grown in hyaluronan hydrogels by Dr Franziska Linke. This technique facilitates the high resolution, label free and spatial chemical characterisation of biological materials, such as cells and tissues, using surface mass spectrometry of liberated secondary ion fragments that are generated by primary ion impaction from the top 1 - 2 nm of the material. From this analysis a distinct shell-like structure of sulphur ions around ONS-76 nodules was identified (Figure 5.4 B). Given that LUM contains tyrosine sulphates, we hypothesised that these sulphur ions may in fact be derived from LUM, further qualifying its selection for validation as a component of the SHH medulloblastoma laminin-111/211 shell.

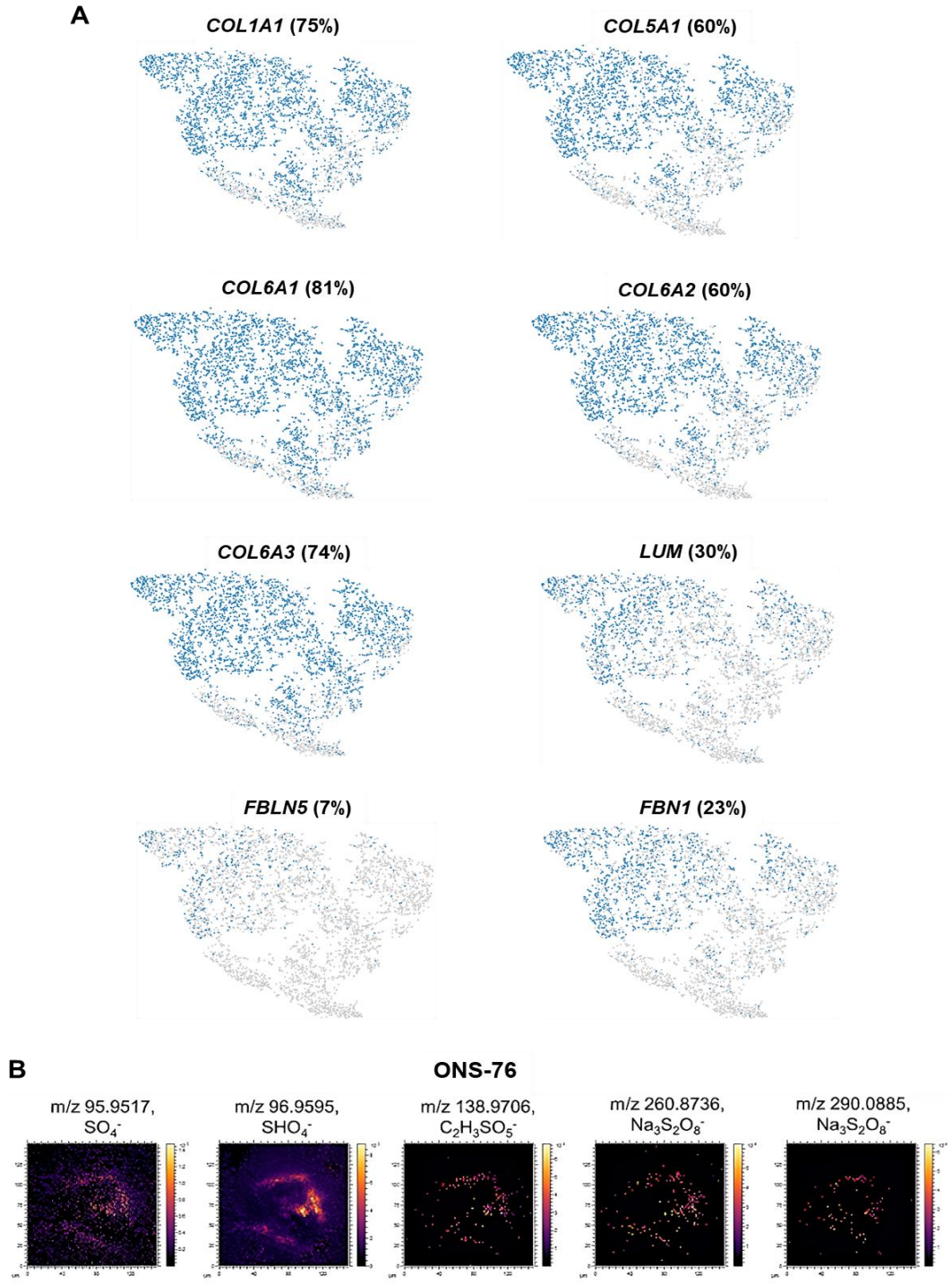


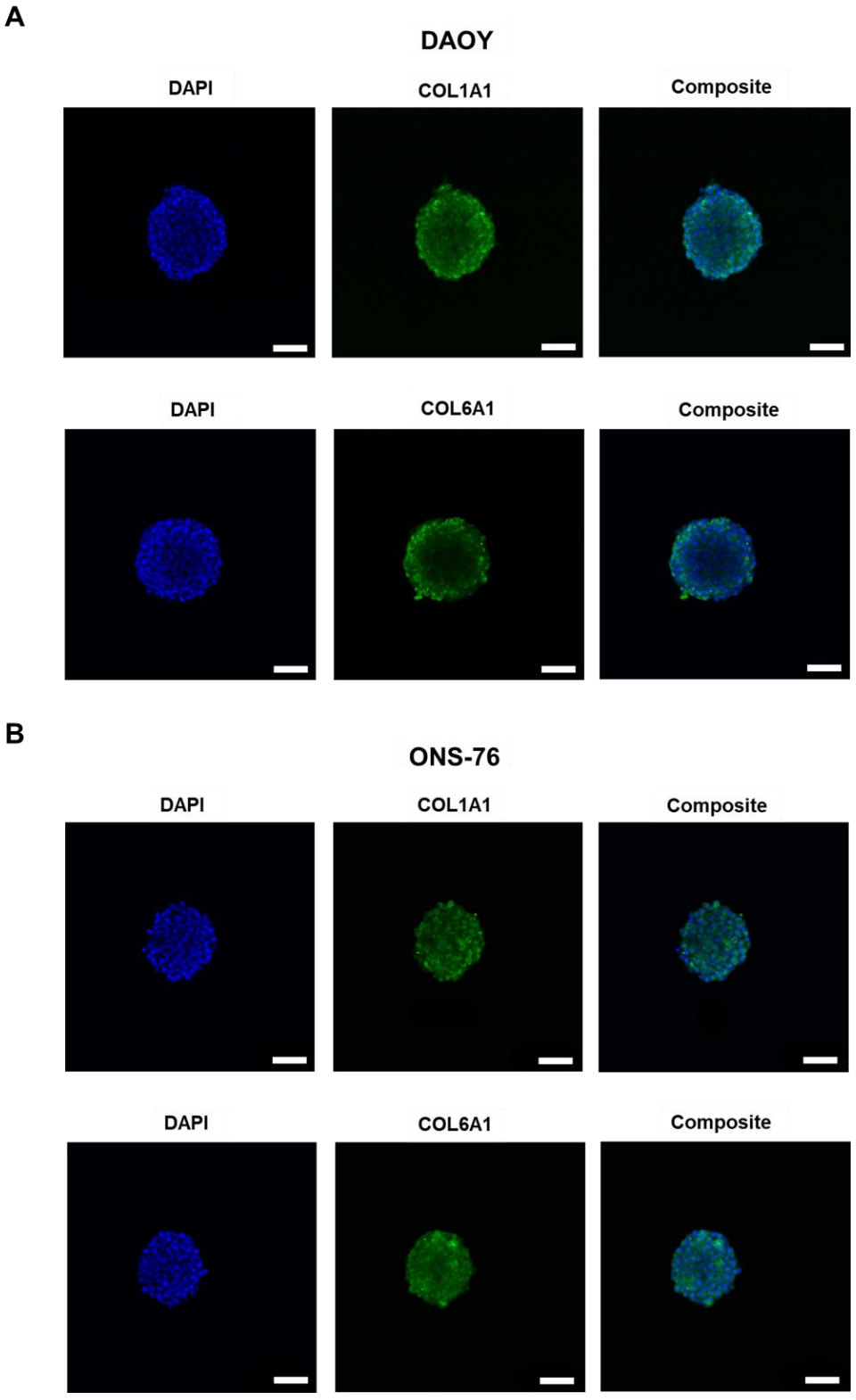
Figure 5.4 Single cell RNA sequencing (scRNAseq) and 3D Orbitrap secondary ion mass spectrometry (3D OrbiSIMS) analysis of ONS-76 cells grown in a hyaluronan hydrogel, identifies Collagen Type-I α1 Chain (COL1A1), Collagen Type-VI α1 Chain (COL6A1) and Lumican (LUM) for validation as additional components of the laminin-111/211 shell structure observed in SHH medulloblastoma cell lines when grown in 3D culture. The gene expression of the 8 medulloblastoma extracellular matrix (ECM) proteins (identified in Figure 5.2) were assessed in scRNAseq data of ONS-76 cells grown in hyaluronan hydrogels (obtained by Dr Franziska Linke), by calculating the percentage of cells in the dataset which expressed each gene (**A**). The majority of cells (>50%) expressed the collagen subunits *COL1A1, COL5A1* (Collagen Type-V α1)*, COL6A1, COL6A2* (Collagen Type-VI α2) and *COL6A3* (Collagen Type-VI α3). *LUM*, *FBLN5* (Fibulin 5) and *FBN1* (Fibrillin 1) were expressed by 30%, 7% and 23% of cells, respectively. Cells highlighted in blue indicates that they express the gene of interest. 3D OrbiSIMS analysis of the ONS-76 cells grow in a hyaluronan hydrogel by Dr Franziska Linke (**B**) identified a distinct shell-like structure of sulphur ions around ONS-76 nodules. The colour scale indicates the intensity of the named ion within the ONS-76 nodules (black: least intense, to yellow: most intense).

In summary, we selected the two most highly expressed collagens, COL1A1 and COL6A1, as well as LUM, as the medulloblastoma ECM proteins to be tested as part of the laminin-111/211 shell-like structure in SHH medulloblastoma spheroids. As mentioned above, COL1A1 and COL6A1 are α subunits of type-I and type-VI collagen, respectively. Whereas, LUM is a small leucine rich proteoglycan (SLRP), which has a major role in the coordination of collagen fibril formation and organisation (Kalamajski and Oldberg, 2010; Lopez and Bonassar, 2021). It is ubiquitously expressed throughout the ECM of the body and is especially enriched in the cornea (Baba *et al.*, 2001; Li *et al.*, 2017).

We then validated COL1A1, COL6A1 and LUM in DAOY and ONS-76 wild-type spheroids that had been grown for 1 and 21 days. This was achieved by staining the spheroids for the ECM proteins, using IF (day 1) and IHC (day 21). IF staining of day 1 spheroids for LUM was not conducted due to issues obtaining a suitable fluorescent secondary antibody (goat anti-donkey).

As displayed in Figure 5.5 A, IF indicated that both COL1A1 and COL6A1 were already expressed in day 1 DAOY and ONS-76 spheroids (Figure 5.5 A and B). Furthermore, IHC revealed that COL1A1, COL6A1 and LUM all also formed shell-like structures in day 21 DAOY and ONS-76 spheroids (Figure 5.5 C). Similar to laminin-111/211 (Figure 5.1 B), COL1A1, COL6A1 and LUM structures were detected at the periphery of the DAOY spheroids, with some staining throughout (Figure 5.5 C). In the ONS-76 spheroids COL1A1 and COL6A1 structures seemed to be more localised around the core of the spheroid (Figure 5.5 C), as was also observed by laminin-111/211 (Figure 5.1 B), whereas, LUM was mainly localised to the periphery (Figure 5.5 C). However, COL6A1 also formed an additional structure around the periphery of ONS-76 spheroids, similar to that of the DAOY spheroids (Figure 5.5 C).

In summary, these findings suggest that the laminin-111/211 shell-like structure formed by SHH medulloblastoma cell lines in the 3D spheroid model is in fact also comprised of other ECM components, including COL1A1, COL6A1 and LUM.



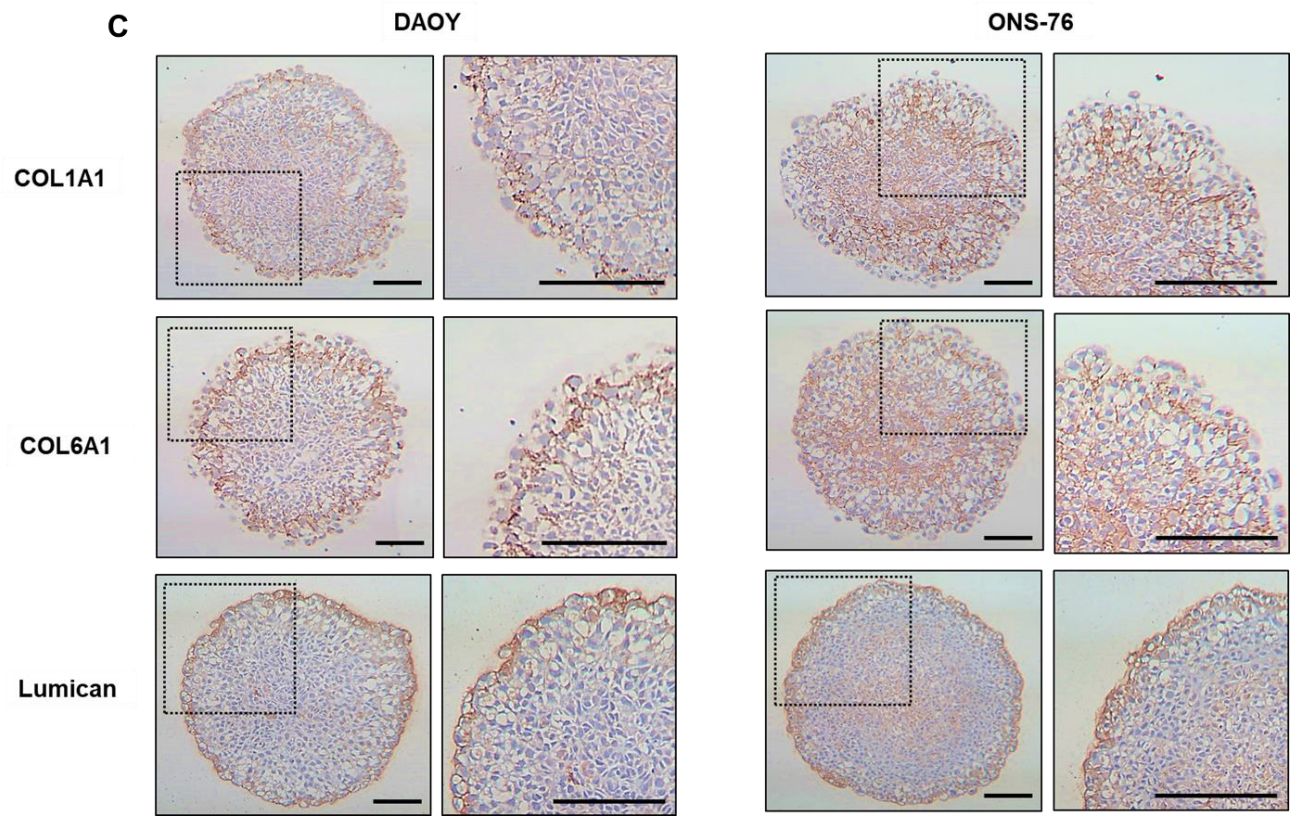


Figure 5.5 Immunofluorescent (IF) and immunohistochemical (IHC) staining of day 1 (IF) and 21 (IHC) DAOY and ONS-76 spheroids for Collagen Type-I α1 Chain (COL1A1), Collagen Type-VI α1 Chain COL6A1 and Lumican (LUM), validates that they are part of the laminin-111/211 shell-like structure previously observed in SHH medulloblastoma cell lines grown in 3D cell culture models. IF demonstrated that both COL1A1 and COL6A1 are expressed in day 1 DAOY (**A**) and ONS-76 spheroids (**B**). IHC revealed that COL1A1, COL6A1 and LUM all also formed shell-like structures in day 21 DAOY and ONS-76 spheroids (**C**). IF spheroid images are comprised of the middle 10 images of a 30 image Z-stack starting from the bottom of the spheroid. Representative images shown. Scale bar: 100 µm.

5.4 Growing the DAOY LAM$^{-/-}$ cell line in a 3D spheroid model

After validating that SHH medulloblastoma cell lines also form the ECM shell-like structure when grown as a spheroid, we sought to determine how the lack of LAMA1 would affect the growth of SHH medulloblastoma cells in this model. To do this, the DAOY NT and DAOY LAM$^{-/-}$ cell lines were grown as spheroids for 7 days and their volume and viability (assessed by imaging and CellTiter-Glo® respectively) were measured at days 1, 4 and 7, as shown in Figure 5.6 A.

As can be seen in Figure 5.6 B–D, the DAOY LAM$^{-/-}$ cell line was unable to form viable spheroids capable of sustained growth. Both the volume and viability of the DAOY NT spheroids were significantly greater than that of the DAOY LAM$^{-/-}$ spheroids after 4 and 7 days in culture ($p<0.05$ for all comparisons; Figure 5.6 C and D). In fact, this was also true after just 2 days in culture (Appendix Figure 5). Furthermore, the DAOY LAM$^{-/-}$ spheroids did not seem to increase in volume or viability over the entire time course (Figure 5.6 B–D). In addition, the DAOY NT spheroids formed a distinct spherical structure, with a defined outer edge, whereas the DAOY LAM$^{-/-}$ spheroids exhibited a much looser structure, with a less defined outer edge (Figure 5.6 B). Moreover, cells on the periphery of the DAOY LAM$^{-/-}$ spheroids seemed to be unable to adhere to the main structure, as can clearly be observed in the day 7 image of DAOY LAM$^{-/-}$ spheroids (Figure 5.6 B). These findings suggest that that LAMA1 is essential for the formation of independent 3D cell structures in SHH medulloblastoma cells, and that it may also have a role in cell-cell adhesion.

To confirm that the LAMA1 knockout was maintained when the cell line was grown as a spheroid, we conducted western blotting for LAMA1 on protein isolated from DAOY LAM$^{-/-}$ spheroids (Figure 5.6 E). As displayed in Figure 5.6 E, complete loss of LAMA1 protein expression was maintained by the DAOY LAM$^{-/-}$ cell line in the spheroid model.

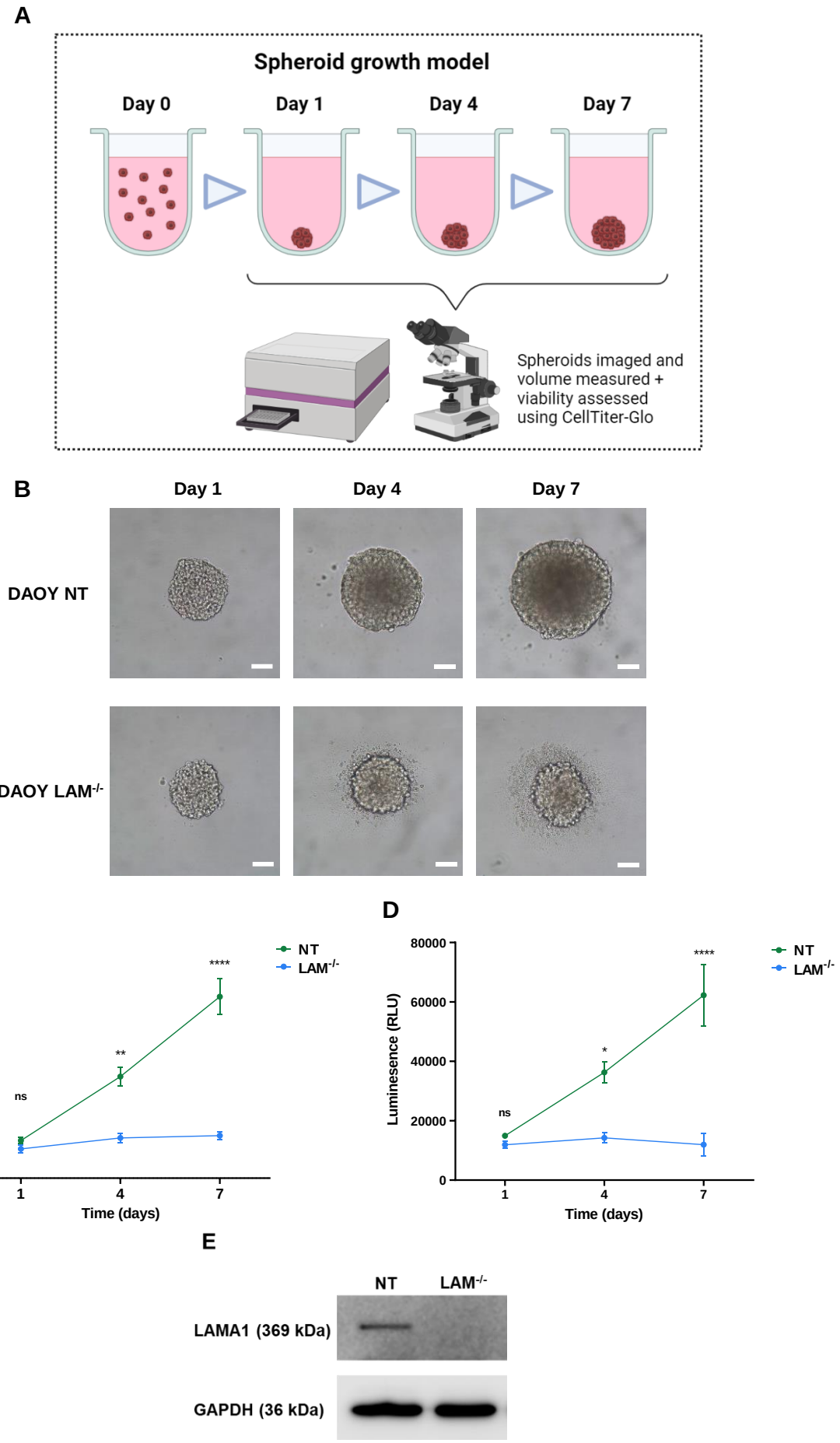

A
Spheroid growth model
Day 0
Day 1
Day 4
Day 7
Spheroids imaged and volume measured + viability assessed using CellTiter-Glo
B
Day 1
Day 4
Day 7
DAOY NT
DAOY LAM-/-
C
Spheroid volume (um3) x 10^7
Time (days)
NT
LAM-/-
ns
**
****
D
Luminescence (RLU)
Time (days)
NT
LAM-/-
ns
*
****
E
NT
LAM-/-
LAMA1 (369 kDa)
GAPDH (36 kDa)

Figure 5.6 Growth of the DAOY LAM$^{-/-}$ cell line in a 3D spheroid model indicates that Laminin Subunit α1 (LAMA1) is essential to the formation of independent 3D cell structures in SHH medulloblastoma. DAOY NT and DAOY LAM$^{-/-}$ cell lines were grown as spheroids for 7 days (**A**). Brightfield images (10 X magnification) of the spheroids demonstrated that the DAOY NT cell line formed spheroids with a distinct spherical structure and defined outer edge. Whereas, the DAOY LAM$^{-/-}$ cell line formed spheroids which exhibited a much looser structure and less defined outer edge (**B**). Both the volume and viability of the spheroids were measured after 1, 4 and 7 days in culture (**C** and **D**), which were both significantly reduced in the DAOY LAM$^{-/-}$ cell line compared to the DAOY NT cell line after 4 days in culture. Error bars represent the mean ± SEM; n=3, with at least 3 internal replicates. Significance was calculated using Two-Way ANOVA analyses with Sidak's multiple comparisons post-hoc test (*p<0.05, **p≤0.01, ****p≤0.0001). Representative images are shown. Scale bar: 100 µm. Western blotting for LAMA1 using protein isolated from DAOY LAM$^{-/-}$ spheroids grown for 1 day indicates that the LAMA1 knockout is maintained in the DAOY LAM$^{-/-}$ cell line in the spheroid model (**E**). A representative blot of 3 independent repeats is shown. Uncropped, exemplar blots of the antibody used here can be observed in Appendix Figure 1.

Since the DAOY LAM$^{-/-}$ cell line was unable to form independent spheroids capable of growth, we wanted to determine whether the DAOY LAM$^{-/-}$ spheroids were able to grow if they were embedded in hyaluronan, the backbone of the brain ECM (Necas *et al.*, 2008). To do this, we grew the DAOY LAM$^{-/-}$ spheroids in an adapted version of a hybrid spheroid-hydrogel model (thesis by Dr Sophie Roper). In this model, spheroids were grown for 1 day and then embedded within the same hyaluronan hydrogel used in Chapter 3, their volume and relative outgrowth (to day 1) were then measured by imaging, as illustrated in Figure 5.7 A. We also attempted to measure the viability of spheroids grown in this model using both Cell-Titer-Glo® and Presto Blue™, although this was unsuccessful. This was possibly due to the relatively small cell number constituting each spheroid of only ~500 cells and the potential interference of the hydrogel with the viability reagents. However, as demonstrated in a study conducted by Dr Sophie Roper, SHH spheroid volume and viability are indicative of each other (Roper and Coyle, 2022).

As displayed in Figure 5.7 B-D, both the DAOY NT and DAOY LAM$^{-/-}$ spheroids were capable of growth over a 4 day time course in this model. However, the length of time they were able to grown in this model was restricted, as after 6 days the volume of both DAOY NT and DAOY LAM$^{-/-}$ spheroids decreased (Appendix Figure 6).

After 2 days in the hydrogel, the volume of the DAOY LAM$^{-/-}$ spheroids was significantly smaller than the DAOY NT spheroids, as also demonstrated in the standard spheroid model ($p \leq 0.001$ for all comparisons; Figure 5.7 C). However, the relative outgrowth of the DAOY LAM$^{-/-}$ spheroids was not significantly different to the DAOY NT spheroids, although it was still reduced (Figure 5.7 D). This suggested that LAMA1 is not essential for the growth of SHH medulloblastoma 3D cell structures when they are supported by a hyaluronan ECM substitute.

As in the standard spheroid model, we also wanted to confirm that the LAMA1 knockout in the DAOY LAM$^{-/-}$ cell line was maintained in the spheroid-hydrogel model. However, we were unable to extract sufficient RNA or protein for analysis from the spheroids grown in this model. We attributed this to the fact that the spheroids only constitute roughly 500 cells to start with and the hydrogel could have interfered with RNA and protein extraction, reducing their yield.

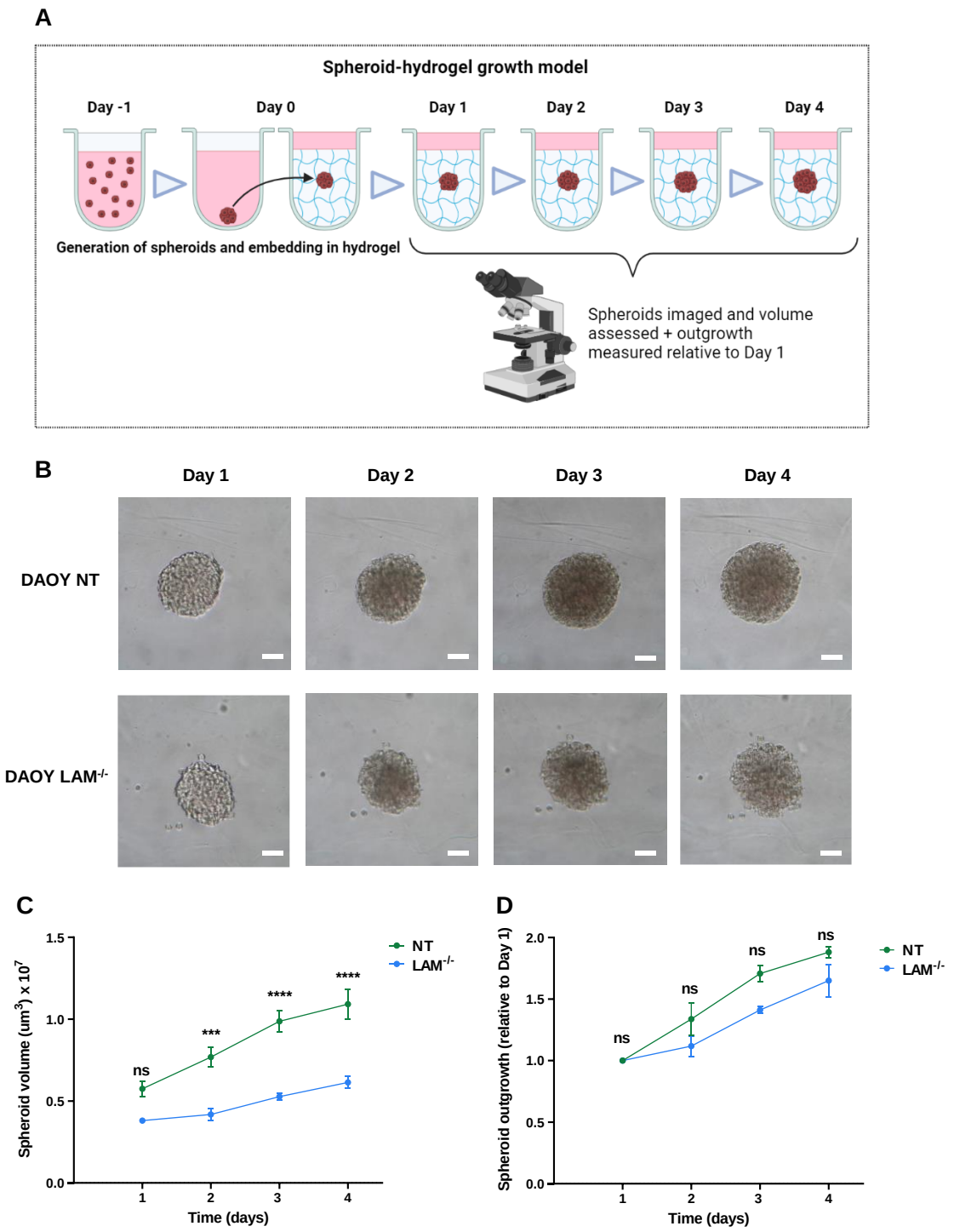


Figure 5.7 Growth of the DAOY LAM$^{-/-}$ cell line in a hybrid 3D spheroid-hydrogel model indicates that SHH medulloblastoma cells are able to grow as a 3D structure without Laminin Subunit α1 (LAMA1), when supported by an extracellular matrix (ECM) substitute. DAOY NT and DAOY LAM$^{-/-}$ cell lines were grown as spheroids for 1 day before being embedded within the same hyaluronan hydrogel used in Chapter 3, and grown for 4 days (**A**). Brightfield images (10 X magnification) of the spheroids over the time course (**B**) were used to assess the volume (**C**) and relative outgrowth to day 1 (**D**) of the spheroids. From day 2, the volume of the DAOY LAM$^{-/-}$ spheroids was significantly smaller than the DAOY NT spheroids. The outgrowth of the DAOY LAM$^{-/-}$ spheroids was not significantly different to the DAOY NT spheroids over the entire time course, although it was reduced. Error bars represent the mean ± SEM; n=3, with at least 3 internal replicates. Significance was calculated using Two-Way ANOVA analyses with Sidak's multiple comparisons post-hoc test (***p≤0.001, ***p≤0.0001). Representative images are shown. Scale bar: 100 µm.

5.5 Assessing the expression of 'laminin regulated genes' in the DAOY LAM$^{-/-}$ cell line in 2D and 3D spheroid culture

In order to assess whether the expression of the previously identified 'laminin regulated genes' were indeed affected by LAMA1, we firstly analysed their gene expression by qRT-PCR in the DAOY NT and DAOY LAM$^{-/-}$ cell lines, grown in 2D and standard spheroid culture. We chose to conduct these analyses on spheroids that had been grown for 1 day, as both the volume and viability of the DAOY LAM$^{-/-}$ spheroids were found to be significantly reduced compared to the DAOY NT spheroids after more than 1 day in culture (Appendix Figure 5) and we therefore wanted to ensure that these factors did not affect the expression of the 'laminin regulated genes'.

qRT-PCR analysis demonstrated that the gene expression of *NFKBIZ*, *MMP-2*, *ITGA5, ITGAV* and *CLU* were all significantly increased in the DAOY LAM$^{-/-}$ cell line, compared to the DAOY NT cell line, in 2D culture ($p \leq 0.01$ for all comparisons; Figure 5.8 A). Although not significant, *ITGB3* and *RPSA* also both exhibited increased gene expression in the DAOY LAM$^{-/-}$ cell line, while *TPPP3* and *TTYH1* showed a decrease in gene expression (Figure 5.8 A). The expression of *CD44* remained unchanged (Figure 5.8 A). *TWIST1* and *YBX1* gene expression was also assessed as our group has identified that these genes are overexpressed in medulloblastoma and have roles in its progression, and therefore served as controls of changes in global gene expression that could have potentially been caused by the LAMA1 knockout. The expression of both of these genes was unchanged in the DAOY LAM$^{-/-}$ cell line, suggesting that global gene expression was unchanged by the LAMA1 knockout (Figure 5.8 A).

Due to the very low RNA yield from the spheroids, qRT-PCR analysis was only conducted on the genes which exhibited a significant change in expression in 2D culture (*NFKBIZ*, *MMP-2*, *ITGA5, ITGAV* and *CLU*), as well as *CD44* as it is one of the

most essential receptors with regards to medulloblastoma ECM interaction (Figure 5.8 B). The gene expression of *NFKBIZ*, *MMP-2*, *ITGAV and CLU* were all found to also be significantly increased in the DAOY LAM$^{-/-}$ cell line compared to the DAOY NT cell line, when grown as a spheroid ($p<0.05$ for all comparisons; Figure 5.8 B). The expression of *ITGAV* and *CD44* were also increased in the DAOY LAM$^{-/-}$ cell line, although not significantly (Figure 5.8 B).

These findings suggested that the gene expression of *NFKBIZ*, *MMP-2, ITGAV* and *CLU* were downregulated by LAMA1 in SHH medulloblastoma (i.e. increased in the DAOY LAM$^{-/-}$ cell line), across both 2D and 3D spheroid culture.

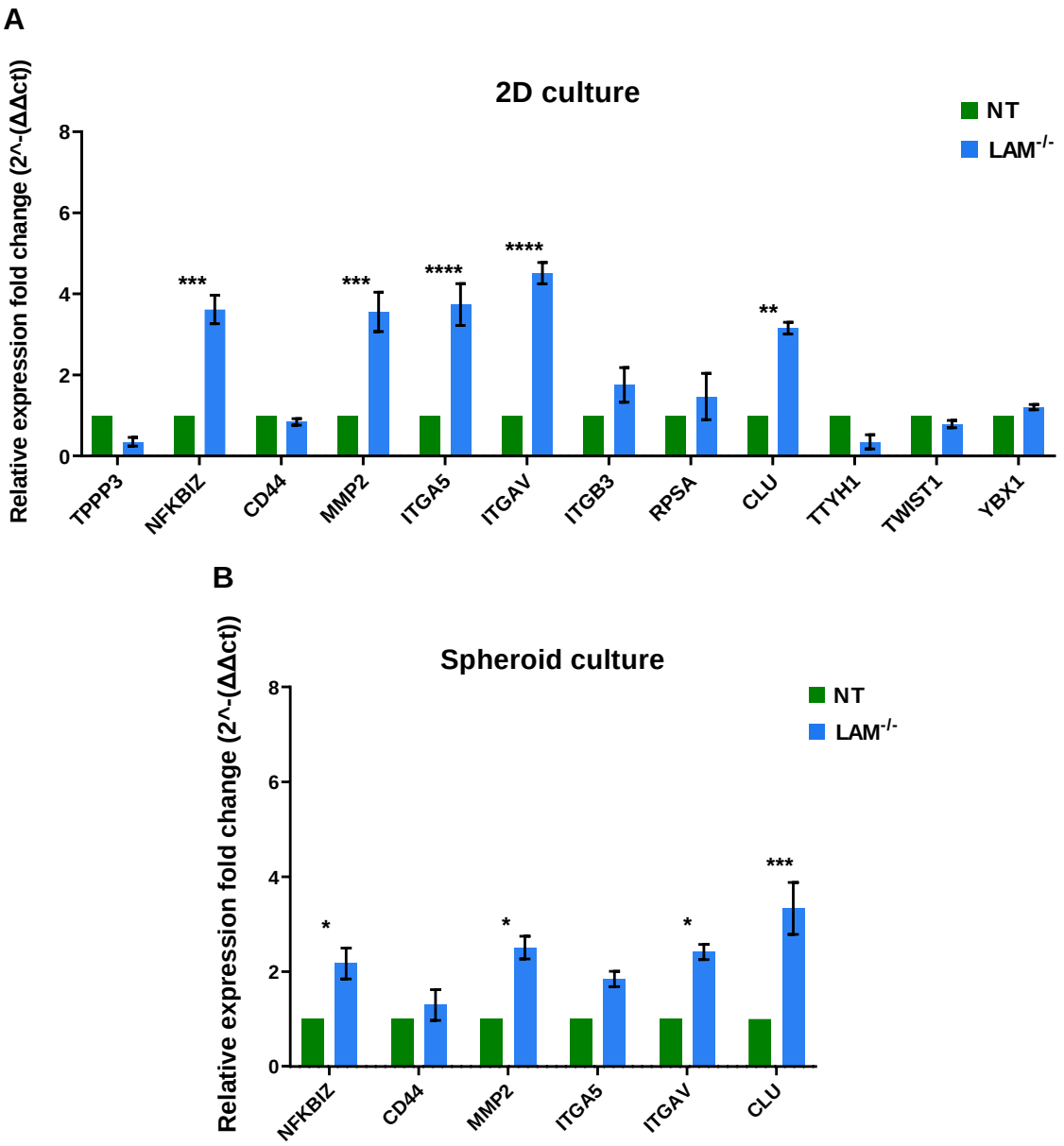


Figure 5.8 qRT-PCR gene expression analysis of the of 'laminin regulated genes' indicates that the gene expression of NF-κB Inhibitor Zeta (*NFKBIZ*), Matrix Metalloproteinase-2 (*MMP-2*), Integrin Subunit A V (*ITGAV*) and Clusterin (*CLU*) are increased in the in the DAOY LAM$^{-/-}$ cell line in 2D and 3D spheroid culture. qRT-PCR analysis demonstrated that in 2D culture, the gene expression of *NFKBIZ, MMP-2,* Integrin Subunit A 5 (*ITGA5*), *ITGAV* and *CLU* were all found to be significantly increased in the DAOY LAM$^{-/-}$ cell line, compared to the DAOY NT cell line (**A**). In 3D spheroid culture, the expression of *NFKBIZ*, *MMP-2*, *ITGAV* and *CLU* were all also found to also be significantly increased in the DAOY LAM$^{-/-}$ cell line, compared to the DAOY NT cell line (**B**). Relative fold changes in gene expression between the DAOY NT and DAOY LAM$^{-/-}$ cell lines was calculated using the ΔΔCt method (section 2.12.7). Mean ± SEM plotted; n=3. Significance was assessed using One-Way ANOVA analyses with Dunnett's multiple comparisons test; *p<0.05, **p≤0.01, ***p≤0.001, ****p≤0.0001. All significant comparisons are highlighted, otherwise comparisons are not significant.

Of the ‘laminin regulated genes’ which exhibited significantly altered gene expression in the DAOY LAM$^{-/-}$ cell line across both 2D and spheroid culture (*NFKBIZ, MMP-2, ITGAV* and *CLU*), MMP-2, and CLU were selected to be next be analysed by western blotting, as they exhibited the greatest level of change in gene expression in the DAOY LAM$^{-/-}$ cell line in spheroid culture (Figure 5.8 B). Furthermore, MMP-2 is an ECM remodelling enzyme that has been shown to promote tumour invasion and metastasis and has a previously identified role in medulloblastoma progression; therefore, it is highly relevant to the interaction of SHH medulloblastoma with the ECM (Vince *et al.*, 2001; Egeblad and Werb, 2002; Mook, Frederiks and Van Noorden, 2004; Özen *et al.*, 2004; Bauvois, 2012; Jiang and Li, 2021). Additionally, CLU plays a key role in apoptosis evasion in tumours, as well as functioning as a negative regulator of MMP-2, and MMP-9; another ECM remodelling enzyme, from the same family of MMP-2, which has also been shown to promote tumour invasion and metastasis and have a role in medulloblastoma progression (Vince *et al.*, 2001; Jones and Jomary, 2002; Özen *et al.*, 2004; Zhang *et al.*, 2005; Shapiro *et al.*, 2015; Bonacini *et al.*, 2019; Oh *et al.*, 2019). B-cell Lymphoma 2 protein (BCL-2) was also selected for western blotting analysis as it is a key regulator of apoptosis evasion (which is overexpressed in several tumour types, including medulloblastoma) and is regulated by CLU (Schüller, Schober, Kretzschmar, Herms, *et al.*, 2004; Levesley *et al.*, 2011; Othman *et al.*, 2014; Peng *et al.*, 2019; Singh, Letai and Sarosiek, 2019; Warren, Wong-Brown and Bowden, 2019). Finally, CD44 was selected for analysis because, as previously mentioned, it is the most essential cell surface receptor with regards to cellular interaction with the brain ECM and has been shown by our group to be highly expressed by SHH medulloblastoma cells grown in a hyaluronan hydrogels and as 3D spheroids (Linke *et al.*, 2020).

Western blotting analysis of the selected proteins indicated that in 2D culture the expression of MMP-2 was significantly increased in the DAOY LAM$^{-/-}$ cell line

compared to the DAOY NT cell line, whereas the expression of CD44 and BCL-2 were both significantly reduced ($p<0.05$ for all comparisons; Figure 5.10 A and B). CLU expression was also reduced in the DAOY LAM$^{-/-}$ cell line, however this reduction was not significant (Figure 5.9 A and B). Furthermore, in spheroid culture the protein expression of MMP-2 was also found to be increased in the DAOY LAM$^{-/-}$ cell line compared to the DAOY NT cell line, although, this was not significant (Figure 5.9 A and C). However, due to technical difficulties at the chemiluminescent imaging stage of MMP-2 immunoblotting of spheroid protein, the findings regarding MMP-2 expression in spheroid culture are limited. Conversely, the protein expression of CD44 and BCL-2 were both found to be significantly reduced in the DAOY LAM$^{-/-}$ spheroids, corroborating the same findings in 2D culture ($p<0.05$ for all comparisons; Figure 5.9 A and C). CLU protein expression was also reduced, however not significantly (Figure 5.9 A and C). Overall, these findings demonstrate that LAMA1 expression increases the protein expression of CD44 and BCL-2 across both 2D and 3D spheroid culture.

This analysis did not completely align with the above gene expression analysis of the 'laminin regulated genes'. Firstly, *CD44* expression was found be unchanged at a gene level in the DAOY LAM$^{-/-}$ cell line in 2D and spheroid culture, whereas protein expression was significantly reduced across both culture methods (Figure 5.8 and 5.9). Furthermore, *CLU* gene expression was found to be significantly increased in the DAOY LAM$^{-/-}$ cell line in 2D and spheroid culture, whereas CLU protein expression was not significantly altered in either culture method (Figure 5.8 and 5.9). Conversely, *MMP-2* gene expression was found to be significantly increased in the DAOY LAM$^{-/-}$ cell line in both 2D and spheroid culture, a finding which was corroborated by protein expression analysis; however, the increase in MMP-2 protein expression in spheroid culture was not significant (Figure 5.8 and 5.9).

The reason for these differences between gene and protein expression could be due to LAMA1 specific regulation of gene transcription, as well as protein turnover and post-translational modifications in SHH medulloblastoma.

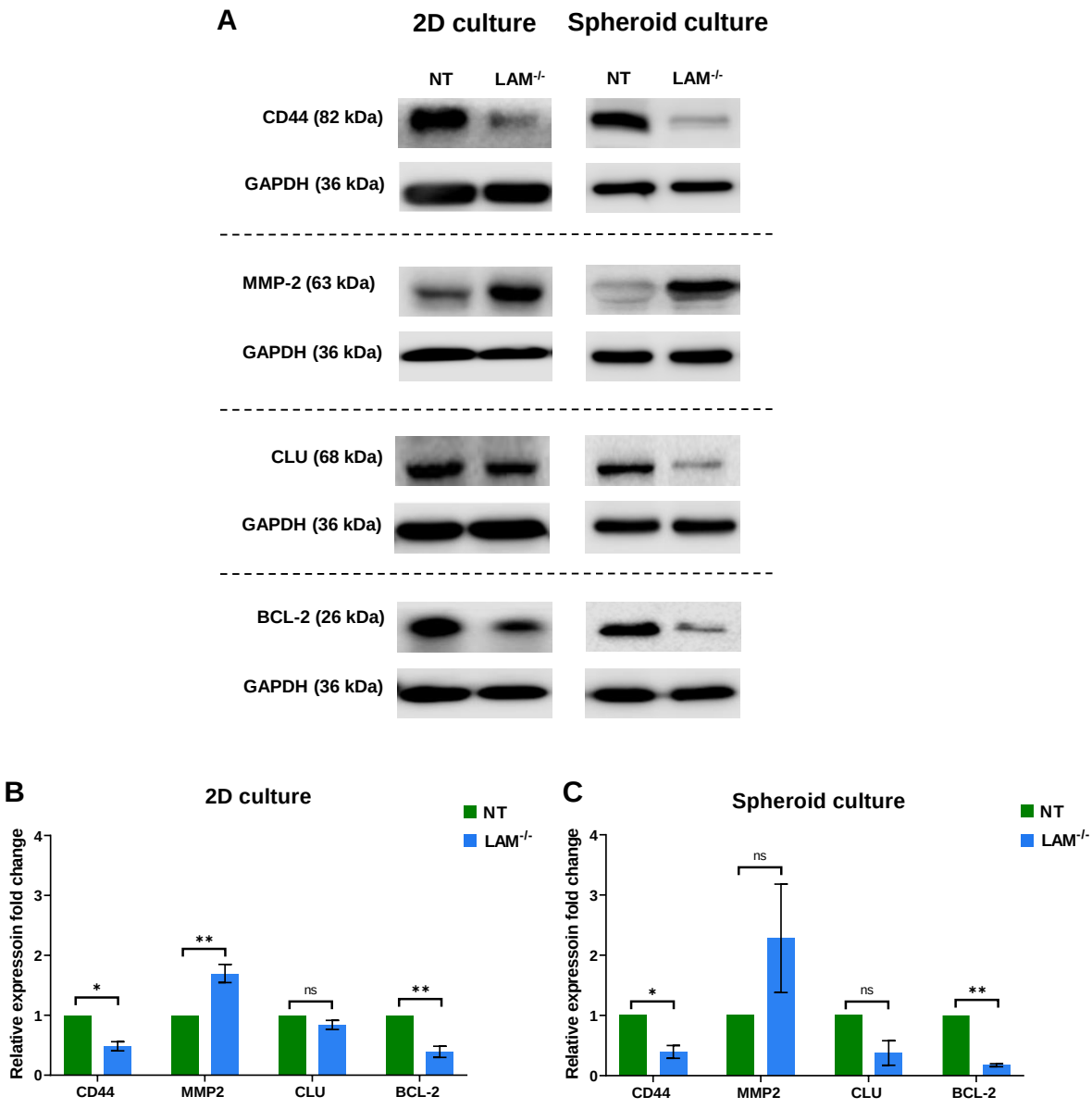


Figure 5.9 Western blotting analysis demonstrates a reduction in Cluster of Differentiation 44 (CD44) and B-cell Lymphoma 2 protein (BCL-2) expression in the DAOY LAM$^{-/-}$ cell line in 2D culture and spheroids cultured for 1 day. Western blotting of CD44, Matrix Metalloproteinase-2 (MMP-2), Clusterin (CLU) and BCL-2 (**A**) indicated that in 2D culture the expression of MMP-2 was significantly increased in the DAOY LAM$^{-/-}$ cell line compared to the DAOY NT cell line, whereas the expression of CD44 and BCL-2 were both significantly reduced (**B**). In spheroid culture, the expression of CD44 and BCL-2 were also found to be significantly reduced in the DAOY LAM$^{-/-}$ cell line (**C**). Western blotting analyses were conducted relative to GAPDH as a loading control. Protein expression in the DAOY LAM$^{-/-}$ cell line was then normalised to the DAOY NT cell line in order to calculate relative fold changes in protein expression. Representative blots are shown. Uncropped, exemplar blots of the antibodies used here can be observed in Appendix Figure 1. Mean ± SEM plotted; n=3. Significance was assessed using One-Way ANOVA analyses with Dunnett's multiple comparisons test; *$p<0.05$, **$p\leq0.01$.

5.5.1 Assessing the secretion of MMP-2 and MMP-9 in the DAOY LAM$^{-/-}$ cell line in 2D and 3D spheroid culture

As the DAOY LAM$^{-/-}$ cell line exhibited significantly increased MMP-2 gene and protein expression (although not significantly at a protein level when grown as a spheroid), we sought to determine if the level of the functional MMP-2 secreted by the DAOY LAM$^{-/-}$ cell line was also changed. This was achieved by conducting gelatin zymography on supernatants collected from the DAOY NT and DAOY LAM$^{-/-}$ cell lines grown in 2D for 48 hours and spheroid culture for 1 day (Figure 5.10). As previously mentioned, gelatin zymography also detects MMP-9 secretion, so this was also assessed.

As displayed in Figure 5.10 A-D, the secretion of both Pro-MMP-9 and active MMP-2 were found to be significantly increased in the DAOY LAM$^{-/-}$ cell line compared to the DAOY NT cell line in 2D culture, whereas the level of Pro-MMP-2 secretion was unchanged. Active MMP-9 secretion was not detected (Figure 5.10 A). As the zymography bands of the supernatants derived from spheroids were very faint (despite concentrating the supernatants with a protein concentrator spin column), it was not possible to conduct densitometry analysis (Figure 5.10 E). Nevertheless, it was possible to still to observe an increase in Pro-MMP-9 and MMP-2 secretion in the DAOY LAM$^{-/-}$ cell line when grown as a spheroid (Figure 5.10 E).

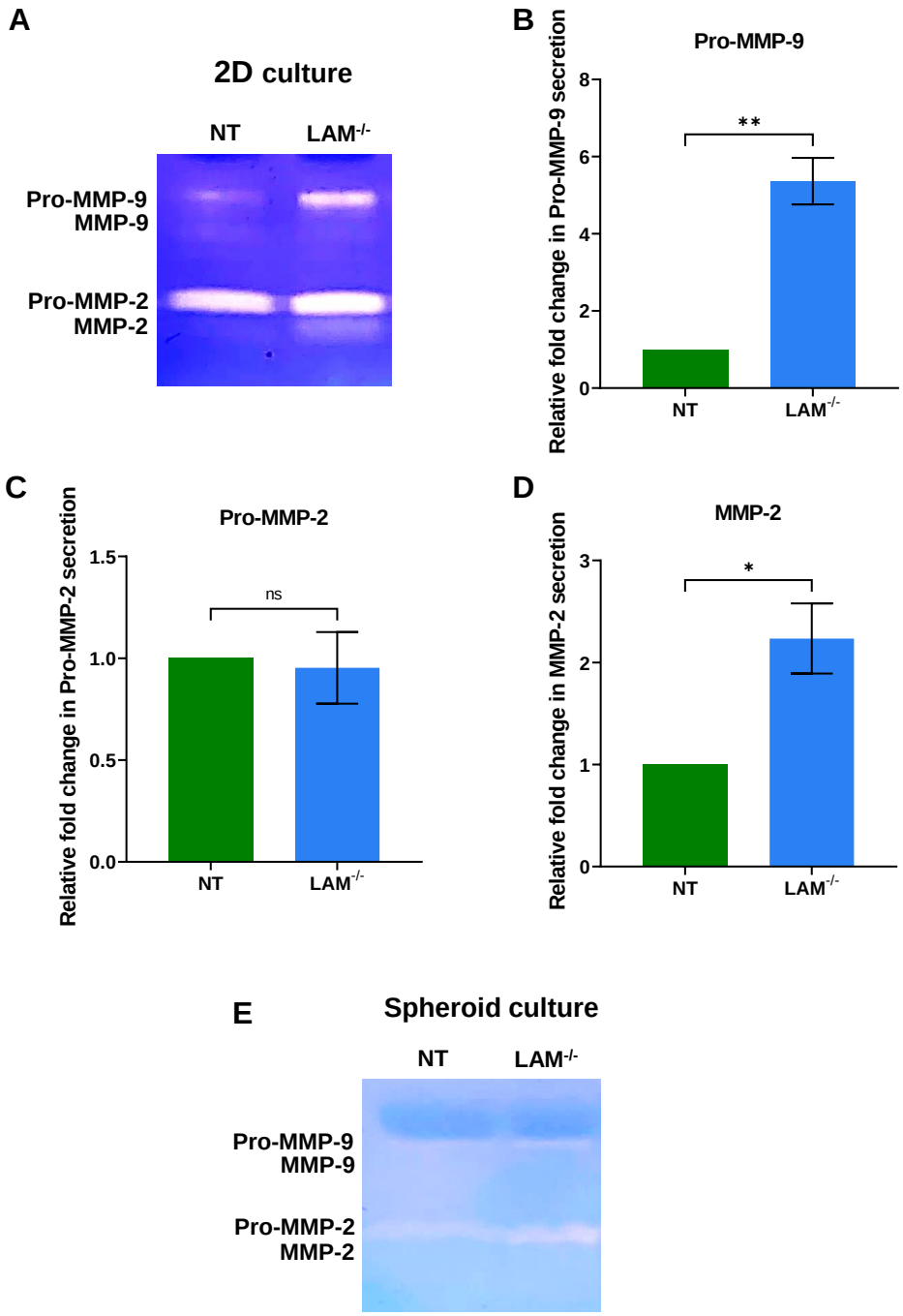


Figure 5.10 Gelatin zymography demonstrates an increase in Pro-Matrix Metalloproteinase-9 (Pro-MMP-9) and active Matrix Metalloproteinase-2 (MMP-2) secretion in DAOY LAM$^{-/-}$ cells in 2D culture. Gelatin zymography of supernatants derived from the DAOY LAM$^{-/-}$ and DAOY NT cell lines grown in 2D culture (**A**), identified that the secretion of Pro-MMP-9 (**B**) and active MMP-2 (**D**) were significantly increased in the DAOY LAM$^{-/-}$ cell line. The level of Pro-MMP-2 secretion was unchanged (**C**). Active MMP-9 secretion was not detected. It was not possible to conduct densitometry analysis on the bands of the zymography conducted on supernatants derived from spheroids (**E**) as they were too faint. All DAOY LAM$^{-/-}$ values were normalised to those of the DAOY NT to calculate relative fold changes in MMP secretion. Recombinant MMP-2 was added to the first lane of each zymogram as a positive control. Representative zymograms are shown. Mean ± SEM plotted; n=3. Significance was assessed by an unpaired t-test; *$p<0.05$, **$p\leq0.01$.

5.6 Investigating the role of LAMA1 in the migration and invasion of SHH medulloblastoma

LAMA1 has been shown to have a key role in cellular migration in tumours, as well as in non-disease conditions (Kuratomi *et al.*, 1999; Heng *et al.*, 2011; Ichikawa-Tomikawa *et al.*, 2012; Aumailley, 2013). Furthermore, CD44, a protein we have shown to exhibit reduced expression in the DAOY LAM$^{-/-}$ cell line (Figure 5.10), has also been shown to mediate tumour migration, as well as invasion (Merzak, Koocheckpour and Pilkington, 1994; Chetty *et al.*, 2012; Mooney *et al.*, 2016; Ma, Dong and Chang, 2019). In addition, we have demonstrated that the DAOY LAM$^{-/-}$ cell line exhibits a significant increase in the expression and secretion of MMP-2, as well as the secretion of Pro-MMP-9 in 2D culture (Figure 5.8, 5.9 and 5.10). These are both ECM degrading enzymes that have also been linked to increased invasion in tumours (Vince *et al.*, 2001; Egeblad and Werb, 2002; Mook, Frederiks and Van Noorden, 2004; Özen *et al.*, 2004; Bauvois, 2012; Chetty *et al.*, 2012; Jiang and Li, 2021). We therefore hypothesised that the migration and invasion of DAOY SHH medulloblastoma cells may be affected by the knockout of LAMA1. To investigate this, we employed an adapted spheroid-hyaluronan hydrogel migration assay (thesis by Dr Sophie Roper), as well as Transwell™ migration and invasion assays (previously optimised by Dr Macha Aldighieri) (Roper and Coyle, 2022).

5.6.1 Assessing migration of the DAOY LAM$^{-/-}$ cell line using a spheroid-hydrogel migration assay

In the spheroid-hydrogel migration assay, spheroids were grown for 1 day before being seeded on top of the same hyaluronan hydrogel used in the spheroid-hydrogel growth model, as illustrated in Figure 5.11 A. The relative outgrowth (to day 0) of the spheroids

across the surface of the hydrogel was then assessed from images captured over 3 days, as an indication of cellular migration.

As displayed in Figure 5.11 B and C, the migration of the DAOY LAM$^{-/-}$ spheroids was significantly reduced compared to the DAOY NT spheroids, after 2 and 3 days ($p<0.05$ for all comparisons; Figure 5.11 B and C). Furthermore, in Figure 5.11 B it can be observed that by day 3 the DAOY NT spheroids had lost all spheroid structure and had completely spread out across the surface of the hydrogel, whereas the DAOY LAM$^{-/-}$ spheroids retained some spheroid structure, indicating that they had not completely spread out across the hydrogel. These findings suggest that LAMA1 has a role in the migration of SHH medulloblastoma cells. However, since we have identified that the protein expression of CD44, the primary cellular receptor for hyaluronan, is reduced in the DAOY LAM$^{-/-}$ cell line, it also possible that its reduction in migration is a consequence of reduced CD44-mediated cellular adhesion to hyaluronan.

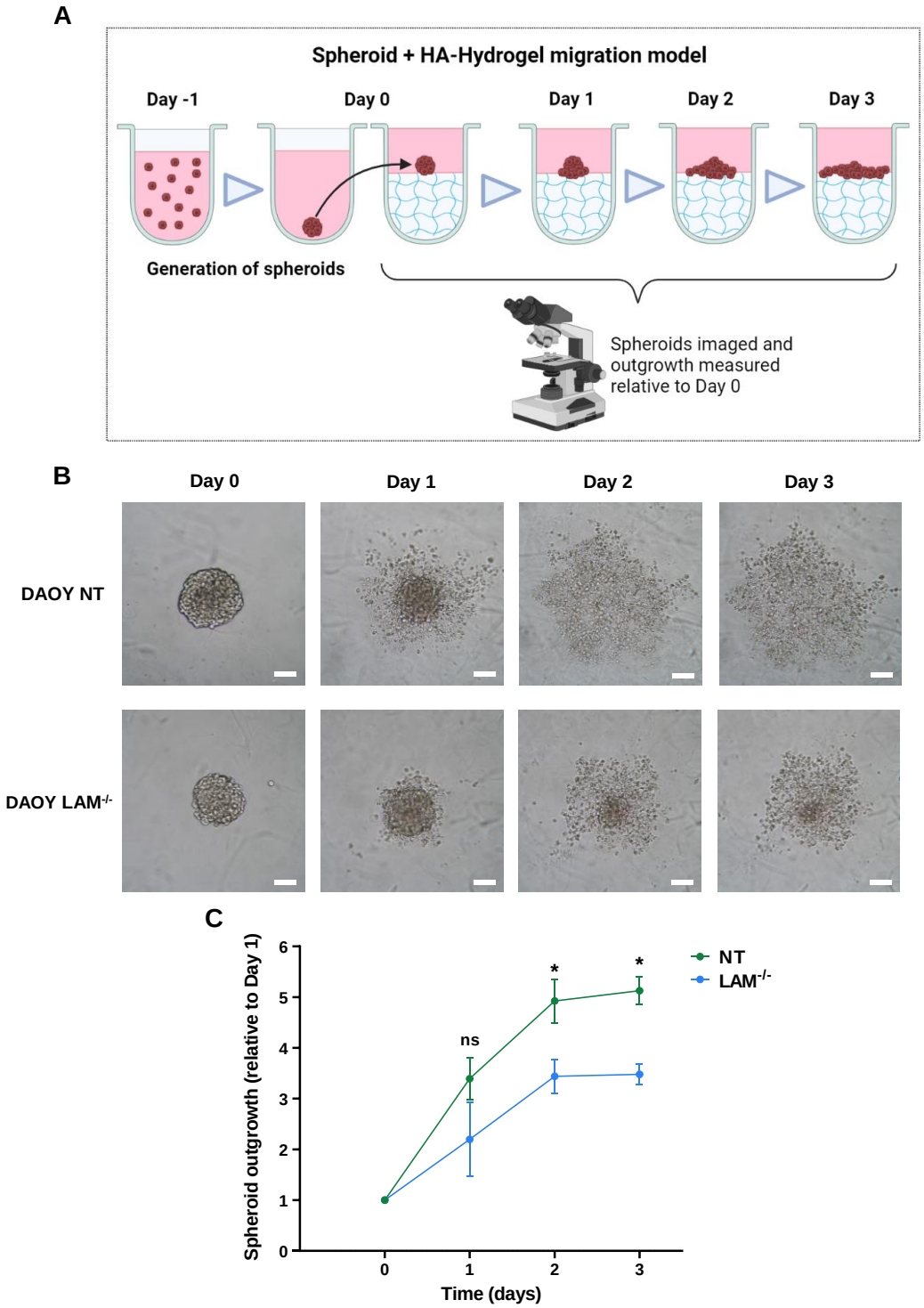


Figure 5.11 A spheroid-hydrogel migration assay suggests that Laminin Subunit α1 (LAMA1) increases the migration of SHH medulloblastoma cells. Spheroids were grown for 1 day before being seeded on top of the same hyaluronan based hydrogel used in the spheroid-hydrogel growth model (**A**). Brightfield images (10 X magnification) captured over 3 days (**B**) were then used to assess the relative outgrowth (to day 0) of the spheroids across the surface of the hydrogel (**C**), as an indication of cellular migration. The migration of the DAOY LAM$^{-/-}$ spheroids was significantly reduced compared to the DAOY NT spheroids after 2 and 3 days. Error bars represent the mean ± SEM; n=3, with 3 internal replicates. Significance was calculated using Two-Way ANOVA analyses with Sidak's multiple comparisons post-hoc test (*p<0.05). Representative images are shown. Scale bar: 100 µm.

5.6.2 Assessing migration and invasion of the DAOY LAM$^{-/-}$ cell line using Transwell™ assays

As illustrated in Figure 5.12 A, in the Transwell™ migration assay DAOY NT and DAOY LAM$^{-/-}$ cells were seeded into a Transwell™ insert in serum free media in a 24 well plate. Media containing 10% FBS was then added to the bottom of the well, creating a nutrient gradient to stimulate the cells to migrate through the pores of the insert. After 2 days the number of migrated cells was then determined by assessing the viability of the cells in the well underneath the insert and then comparing this to a viability standard curve of known cell numbers. The only difference between the migration and invasion assays, was that in the invasion assay the insert was coated with collagen-IV in order to replicate a basement membrane. Laminin-111 (another component of basement membranes) is typically also used to coat the inserts in this model; however, since we were studying the effect of LAMA1 (and therefore laminin-111), this was omitted.

The migration assay also indicated that migration was significantly reduced in the DAOY LAM$^{-/-}$ cell line compared to the DAOY NT cell line, corroborating the findings of the spheroid-hydrogel assay (Figure 5.12 B). Furthermore, the invasion assay demonstrated that invasion was not significantly altered in the DAOY LAM$^{-/-}$ cell line compared to the DAOY NT cell line (Figure 5.12 C). These findings suggest that LAMA1 increases the migration of SHH medulloblastoma cells, but not invasion.

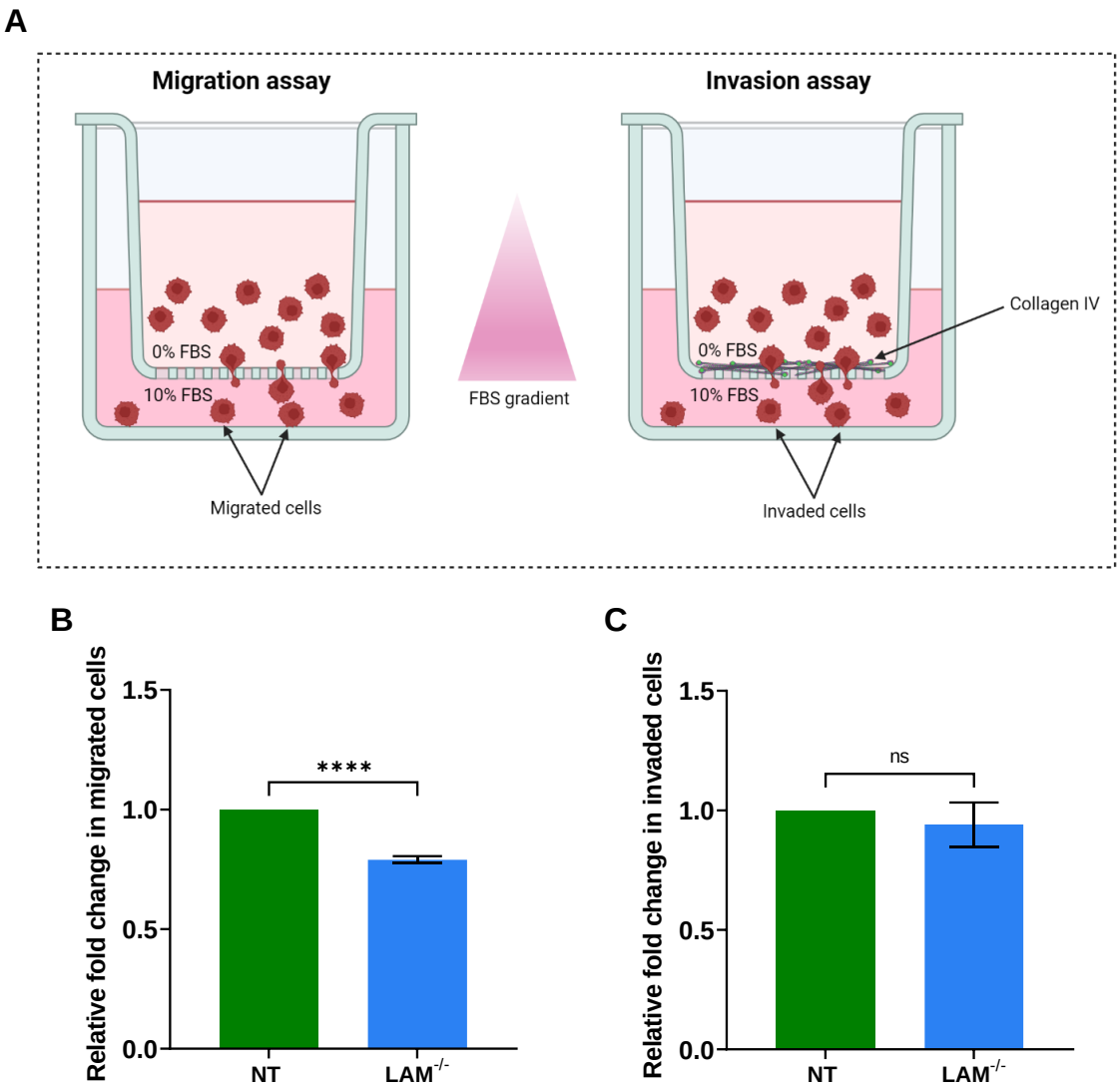


Figure 5.12 Transwell™ migration and invasion assays suggest that Laminin Subunit α1 (LAMA1) increases the migration of SHH medulloblastoma cells, but not invasion. In the Transwell™ migration assay DAOY NT and DAOY LAM$^{-/-}$ cells were seeded into a Transwell™ insert in serum free media in a 24 well plate. Media containing 10% Fetal Bovine Serum (FBS) was then added to the bottom of the well, creating a nutrient gradient to stimulating cells to migrate through the pores of the insert. After 2 days the number of migrated cells was determined by assessing the viability of the cells in the well underneath the insert and then comparing this to a viability standard curve of known cell numbers. In the invasion assay the methodology was the same, apart from the insert was coating with collagen-IV in order to replicate a basement membrane (**A**). The migration assay indicated that migration was significantly reduced in the DAOY LAM$^{-/-}$ cell line compared to the DAOY NT cell line (**B**). The invasion assay indicated that invasion was not significantly altered in the DAOY LAM$^{-/-}$ cell line compared to the DAOY NT cell line (**C**). All DAOY LAM$^{-/-}$ cell line values were normalised to those of the DAOY NT cell line to calculate the relative fold change in migration and invasion. Mean ± SEM plotted; n=3. Significance was assessed by an unpaired t-test; ****p≤0.0001.

5.7 Investigating the role of LAMA1 in apoptosis in SHH medulloblastoma

As previously discussed, BCL-2 has a significant role in apoptosis evasion and is upregulated in a number of different tumour types, including medulloblastoma (Nakasu *et al.*, 1994; Schiffer *et al.*, 1996; Schüller, Schober, Kretzschmar, Herms, *et al.*, 2004; Levesley *et al.*, 2011; Ashour *et al.*, 2016). Given that BCL-2 protein expression was reduced in the DAOY LAM$^{-/-}$ cell line, we hypothesised that LAMA1 may affect the regulation of apoptosis in SHH medulloblastoma, via the upregulation of BCL-2.

To test this hypothesis, we initially employed two caspase-3/7 apoptosis assays in order to establish the level of apoptosis in the DAOY NT and DAOY LAM$^{-/-}$ cell lines in 2D and day 1 spheroid culture (as mentioned previously, this time point was chosen as both the volume and viability of DAOY LAM$^{-/-}$ spheroids were found to be significantly reduced compared to the DAOY NT spheroids after more than 1 day in culture [Appendix Figure 5]). We then assessed the sensitivity of the DAOY NT and DAOY LAM$^{-/-}$ cell lines to a BCL-2 small-molecule inhibitor (ABT-737), in 2D and spheroid-hydrogel assays, to determine if SHH medulloblastoma cells were dependent on the LAMA1 mediated upregulation of BCL-2 to evade apoptosis.

5.7.1 Assessing apoptosis in the DAOY NT and DAOY LAM$^{-/-}$ cell lines

Apoptosis (or caspase-3/7 activity) was assessed using both a luminescence based assay and a fluorescence based assay. These two assays were used because the luminescent assay directly quantifies the level of apoptosis, whereas, the fluorescent assay allows for individual apoptotic cells to be visualised, although the number of apoptotic cells can also be used to quantify the level of apoptosis. In the luminescent assay, the Caspase-Glo® 3/7 Apoptosis Assay reagent is added to cells and a luminescent signal is produced, proportional to the level of caspase-3/7 activity, which

can be assessed in a microplate reader as an indication of the level of apoptosis in cells. In the fluorescent assay the CellEvent™ Caspase-3/7 Green Detection Apoptosis Assay reagent is incubated with cells and the number of fluorescent nuclei can then be assessed by fluorescent microscopy and used as an indication of the level of apoptosis. Further details of the methodology of these assays can be observed in section 2.10.

The luminescent caspase-3/7 assay indicated that in 2D culture the level of apoptosis was unchanged between the DAOY NT and DAOY LAM$^{-/-}$ cell lines (Figure 5.13 A). Conversely, in spheroid culture the level of apoptosis was found to be significantly increased in the DAOY LAM$^{-/-}$ cell line (Figure 5.13 B). These findings were corroborated by the fluorescent caspase-3/7 assay, which also indicated that the level of apoptosis was only significantly increased in the DAOY LAM$^{-/-}$ cell line when it was grown in spheroid culture (Figure 5.14 and 5.15). Furthermore, in Figure 5.15 A, it can be observed that in the DAOY LAM$^{-/-}$ spheroids, apoptotic cells (green nuclei) were mainly those either on the periphery of the spheroids or ones that had completely detached from the main spheroid structure. These findings suggest that LAMA1 has a role in apoptosis evasion in SHH medulloblastoma, when cells are grown as an independent spheroid.

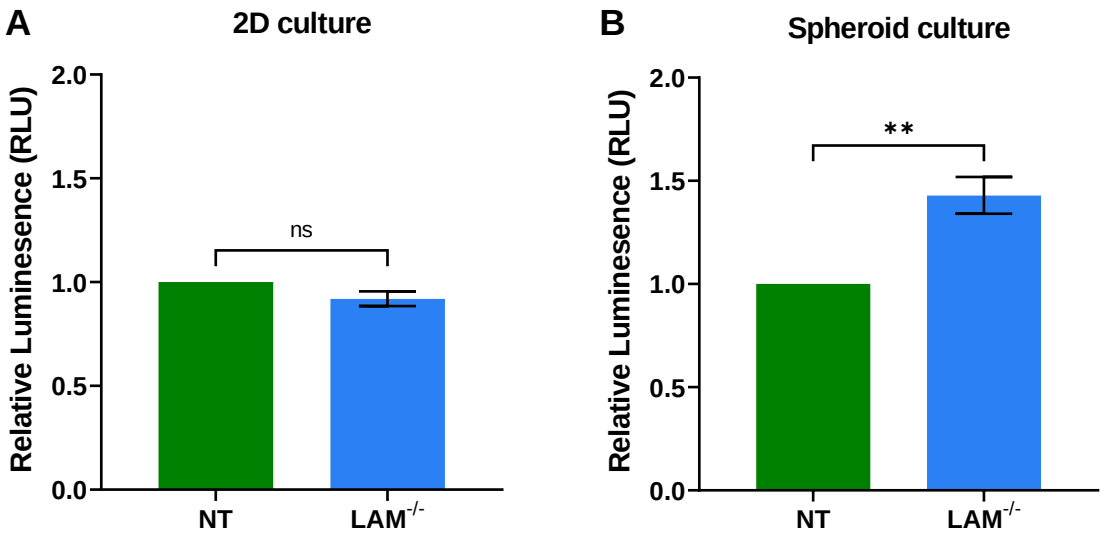


Figure 5.13 Luminescent caspase-3/7 assay indicates that apoptosis is only significantly increased in the DAOY LAM$^{-/-}$ cell line compared to the DAOY NT cell line in spheroid culture. The signal produced by the luminescent caspase-3/7 assay was used as an indication of the level of apoptosis in DAOY NT and DAOY LAM$^{-/-}$ cell lines grown in 2D (**A**) and as a spheroid for 1 day (**B**). Apoptosis was found to be significantly increased in the DAOY LAM$^{-/-}$ cell line in day 1 spheroid culture. Mean ± SEM plotted; n=3 for 2D culture, n=4 for spheroid culture, with 3 internal replicates. All DAOY LAM$^{-/-}$ cell line values were normalised to those of the DAOY NT cell line to calculate relative fold changes in luminescence. Significance was assessed by an unpaired t-test; **p≤0.01.

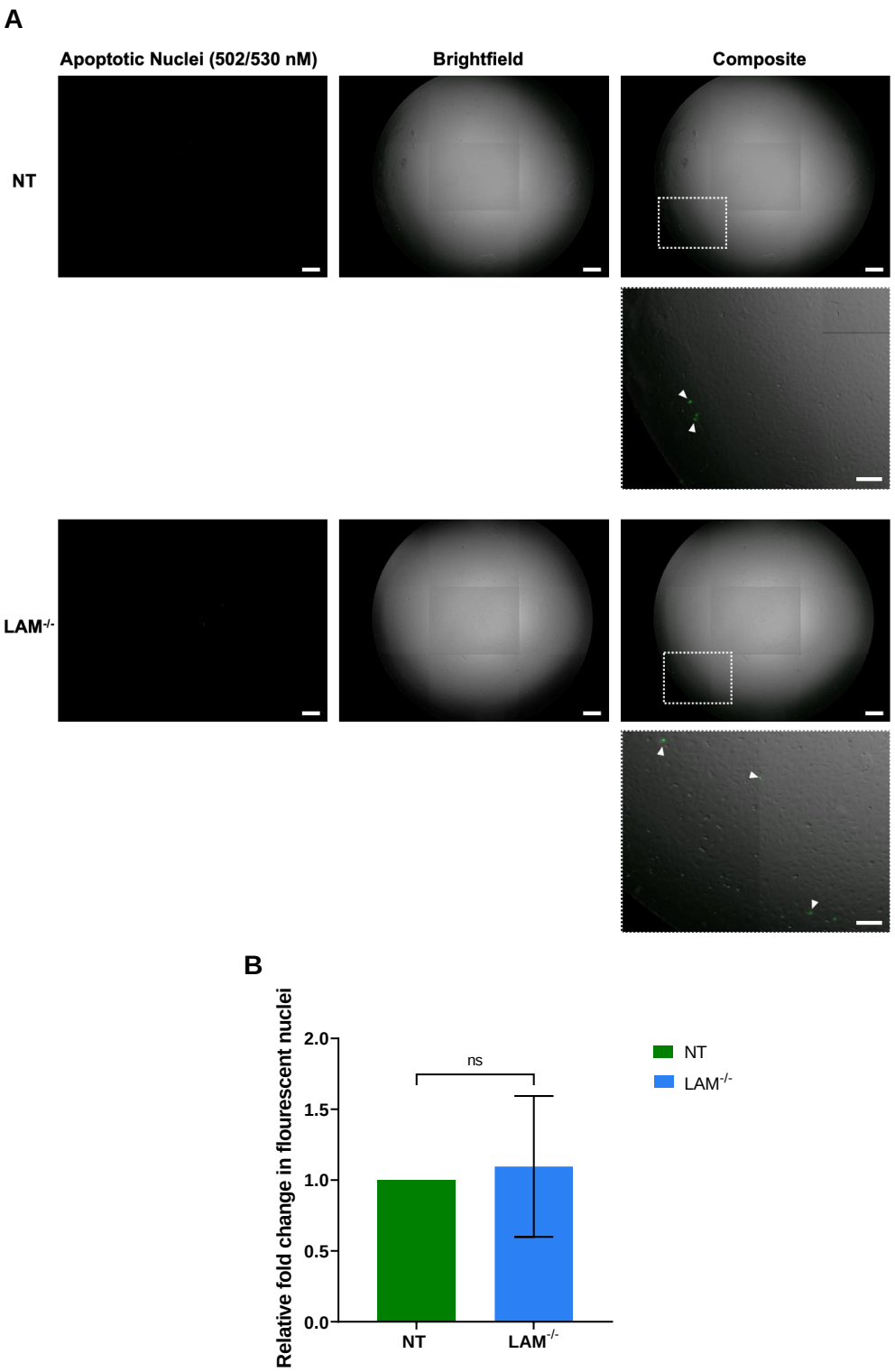


Figure 5.14 Fluorescent caspase-3/7 assay indicates that apoptosis is not significantly changed between the DAOY NT and DAOY LAM$^{-/-}$ cell lines in 2D culture. Green nuclei identified from images (4 X magnification) of the DAOY NT and DAOY LAM$^{-/-}$ cells in 2D culture (**A**) were counted and used as an indication of the level of apoptosis (**B**). All DAOY LAM$^{-/-}$ cell line values were normalised to those of the DAOY NT cell line to calculate the relative fold change in fluorescent nuclei. Mean ± SEM plotted; n=3, with 1 internal replicate. Significance was assessed by an unpaired t-test. Representative images are shown. Images are a merge of 9 individual images, spanning a single well of a 96 well plate. Images with a white boarder are enlarged from the above composite image, as denoted by a white dotted box. Scale bar: 100 µm.

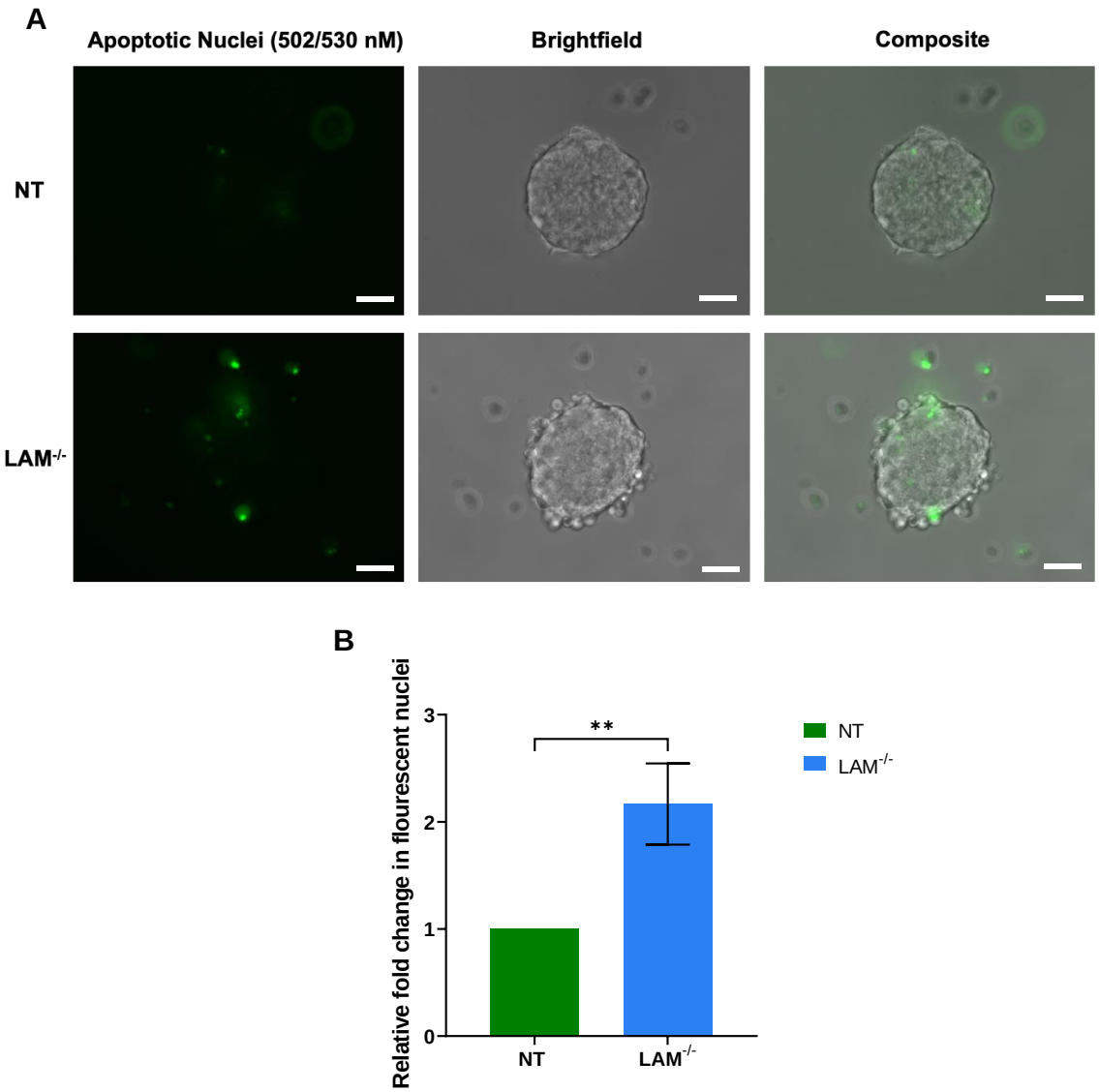


Figure 5.15 Fluorescent caspase-3/7 assay indicates that apoptosis is significantly increased in the DAOY LAM$^{-/-}$ cell line compared to the DAOY NT cell line in spheroid culture. Green nuclei identified from images (20 X magnification) of day 1 DAOY NT and DAOY LAM$^{-/-}$ spheroids (**A**) were counted and used as an indication of the level of apoptosis (**B**). Apoptosis was found to be significantly increased in the DAOY LAM$^{-/-}$ cell line in day 1 spheroid culture. All DAOY LAM$^{-/-}$ cell line values were normalised to those of the DAOY NT cell line to calculate the relative fold change in fluorescent nuclei. Mean ± SEM plotted; n=3, with at least 2 internal replicates. Significance was assessed by an unpaired t-test (**p≤0.01). Representative images are shown. Scale bar: 100 µm.

We did also attempt to measure the level of apoptosis in the spheroid-hydrogel model, using the luminescent and fluorescent caspase-3/7 assays, however this was this was unsuccessful. As with the viability assays, this may have been due to the relatively

small size and cell number of the individual spheroids and the potential interference of the hydrogel with the assay reagents.

5.7.2 Assessing the sensitivity of the DAOY NT and DAOY LAM$^{-/-}$ cell lines to the BCL-2 small-molecule inhibitor ABT-737

In order to assess if the DAOY LAM$^{-/-}$ cell line exhibited an altered sensitivity to ABT-737 compared to the DAOY NT cell line, we initially conducted a 2D drug response assay to determine the ABT-737 IC_{50} for each cell line. In the drug response assay, cells were seeded into a 96 well plate and incubated overnight, before being treated with a range of ABT-737 concentrations and a vehicle control (DMSO). After 3 days, cell viability was measured. This was then used to calculate the IC_{50} of each cell line, using a variable slope model, as an indication of their sensitivity to ABT-737. This assay is illustrated in Figure 5.16 A.

This assay demonstrated that the ABT-737 IC_{50} of the DAOY LAM$^{-/-}$ cell line (34.20 µM) was significantly lower than that of the DAOY NT cell line (50.93 µM; $p<0.0001$), indicating that the DAOY LAM$^{-/-}$ cell line is more sensitive to ABT-737 in 2D culture (Figure 5.16 B).

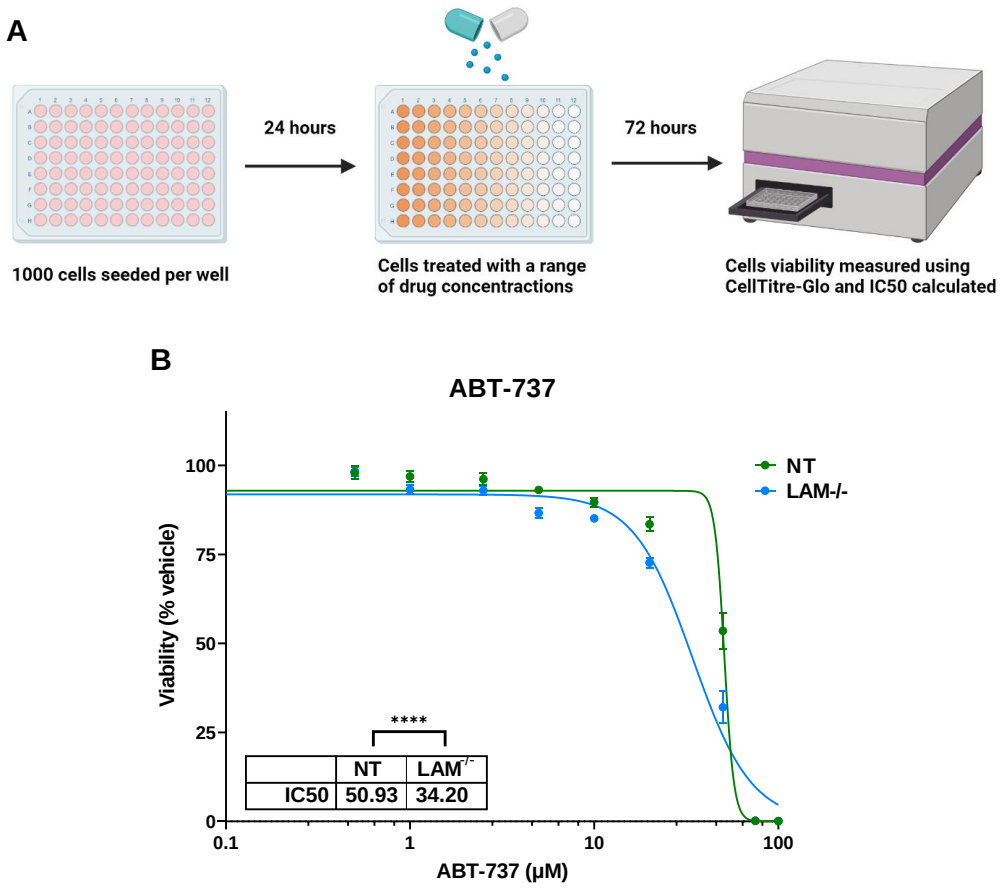


Figure 5.16 The DAOY LAM$^{-/-}$ cell line is more sensitive to ABT-737 than the DAOT NT cell line in 2D culture. In drug response assays cells were seeded into a 96 well plate and incubated overnight, before being treated with a range of concentration of ABT-737 and a vehicle control (DMSO). After being incubated for 3 days, cell viability was measured (**A**). This was then used to calculate the IC_{50} of each cell line by plotting the data using a variable slope model (**B**). The ABT-737 IC_{50} of the DAOY LAM$^{-/-}$ cell line (34.20 μM) was found to be significantly lower than that of the DAOY NT cell line (50.93 μM). The 2 highest concentrations of ABT-737 caused a similar reduction in cell viability between the two cell lines, meaning the DAOY LAM$^{-/-}$ data points for these concentrations had to be plotted behind those of the DAOY NT. Mean ± SEM plotted; n=4, with 3 internal replicates. A variable slope model with four parameters was used to calculate IC_{50} values. Significance was assessed by an unpaired t-test (****p≤0.0001).

Once we had demonstrated that the DAOY LAM$^{-/-}$ cell line was more sensitive to ABT-737 in 2D culture, we sought to determine if this was specifically a consequence of increased apoptosis in cells. To do this, we conducted the luminescent and fluorescent apoptosis assays on DAOY NT and DAOY LAM$^{-/-}$ cells that had been treated with 50 μM of ABT-737 (the IC_{50} for the DAOY NT cell line). As displayed in Figure 5.17, when treated with 50 μM of ABT-737, the level of apoptosis in the DAOY LAM$^{-/-}$ cell line was

significantly greater than in the DAOY NT cell line, as determined by both the luminescent and fluorescent apoptosis assays. Together with the results of the drug response assay, these findings suggests that SHH medulloblastoma cells are somewhat dependent on the LAMA1 mediated upregulation of BCL-2 to evade apoptosis in 2D culture.

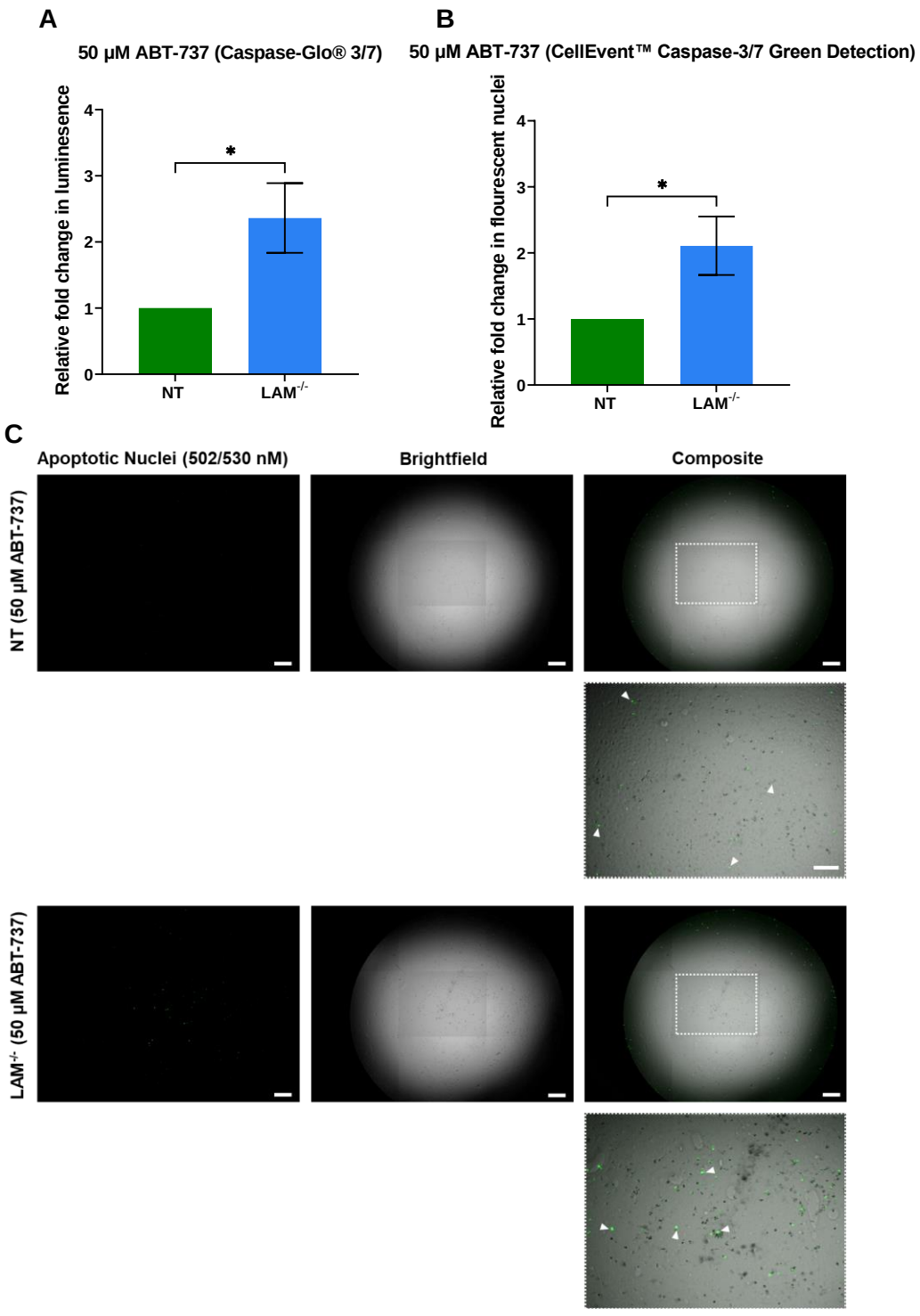


Figure 5.17 Apoptosis is increased in DAOY LAM$^{-/-}$ cells treated with ABT-737, compared to the DAOY NT cell line. Luminescent (**A**) and fluorescent (**B** and **C**) apoptosis assays conducted on DAOY NT and DAOY LAM$^{-/-}$ cells treated with 50 µM of ABT-737 (the IC_{50} for the DAOY NT cell line) demonstrate that the level of apoptosis in the DAOY LAM$^{-/-}$ cell line was significantly greater than in the DAOY NT cell line. All DAOY LAM$^{-/-}$ cell line values were normalised to those of the DAOY NT cell line to calculate the relative fold change in luminescence/fluorescent nuclei. Mean ± SEM plotted; n=3, with 1 internal replicate. Significance was assessed by an unpaired t-test (*$p<0.05$). Representative images are shown (4 X magnification). Images are a merge of 9 individual images, spanning a single well of a 96 well plate. Images with a white boarder are enlarged from the above composite image, as denoted by a white dotted box. Scale bar: 100 µm.

We next sought to determine if this increased sensitivity to ABT-737 exhibited by the DAOY LAM$^{-/-}$ cell line in 2D culture was maintained in spheroid culture. However, the DAOY LAM$^{-/-}$ cell line was not capable of maintained growth in the standard spheroid model, meaning we could not use this model to investigate this (Figure 5.6). We therefore decided to utilise an adapted version of the hybrid spheroid-hydrogel model, in which the DAOY LAM$^{-/-}$ cell line was capable of growth over a 3 day period (Figure 5.7); the same duration as the 2D drug response assay (Figure 5.16). In this assay, as illustrated in Figure 5.18, DAOY NT and DAOY LAM$^{-/-}$ spheroids were grown for 1 day before then being embedded in hyaluronan-based hydrogel. The next day spheroids were treated with 5 different concentration of ABT-737, as well as a vehicle control. The relative outgrowth of the treated spheroids was then measured by imaging over a 3 day time course and compared to the spheroids treated with the vehicle control, as an indication of drug response.

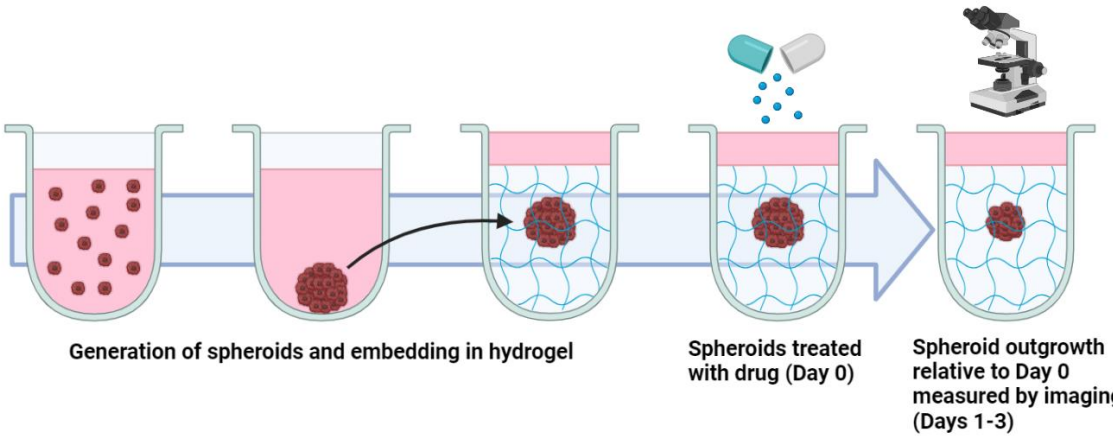


Figure 5.18 Illustration of the hybrid spheroid-hydrogel drug assay used in this study. Spheroids were grown for 1 day before then being embedded in hyaluronan-based hydrogel. The next day spheroids were treated 5 different concentration of drug, as well as a vehicle control. The outgrowth of the spheroids, relative to the vehicle control spheroids, was then measured by imaging over a 3 day time course, as an indication of spheroid response to the drug.

DAOY NT spheroids treated with 50 and 75 µM of ABT-737 exhibited significantly reduced outgrowth compared to the vehicle control spheroids 3 days post treatment ($p<0.05$ for all comparisons; Figure 5.19 B). Although not significant, the outgrowth of

DAOY NT spheroids treated with 1, 10 and 20 μM of ABT-737 also exhibited a reduction in outgrowth compared to those treated with the vehicle control (Figure 5.19 B). Conversely, despite exhibiting some level of reduction in outgrowth to all concentrations of ABT-737, none were found be significant in the DAOY $LAM^{-/-}$ spheroids (Figure 5.19 D). These findings indicate that when grown as a spheroid embedded within a brain specific hydrogel, DAOY $LAM^{-/-}$ spheroids are in fact less sensitive to ABT-737 than DAOY NT spheroids, contrary to the findings in 2D culture.

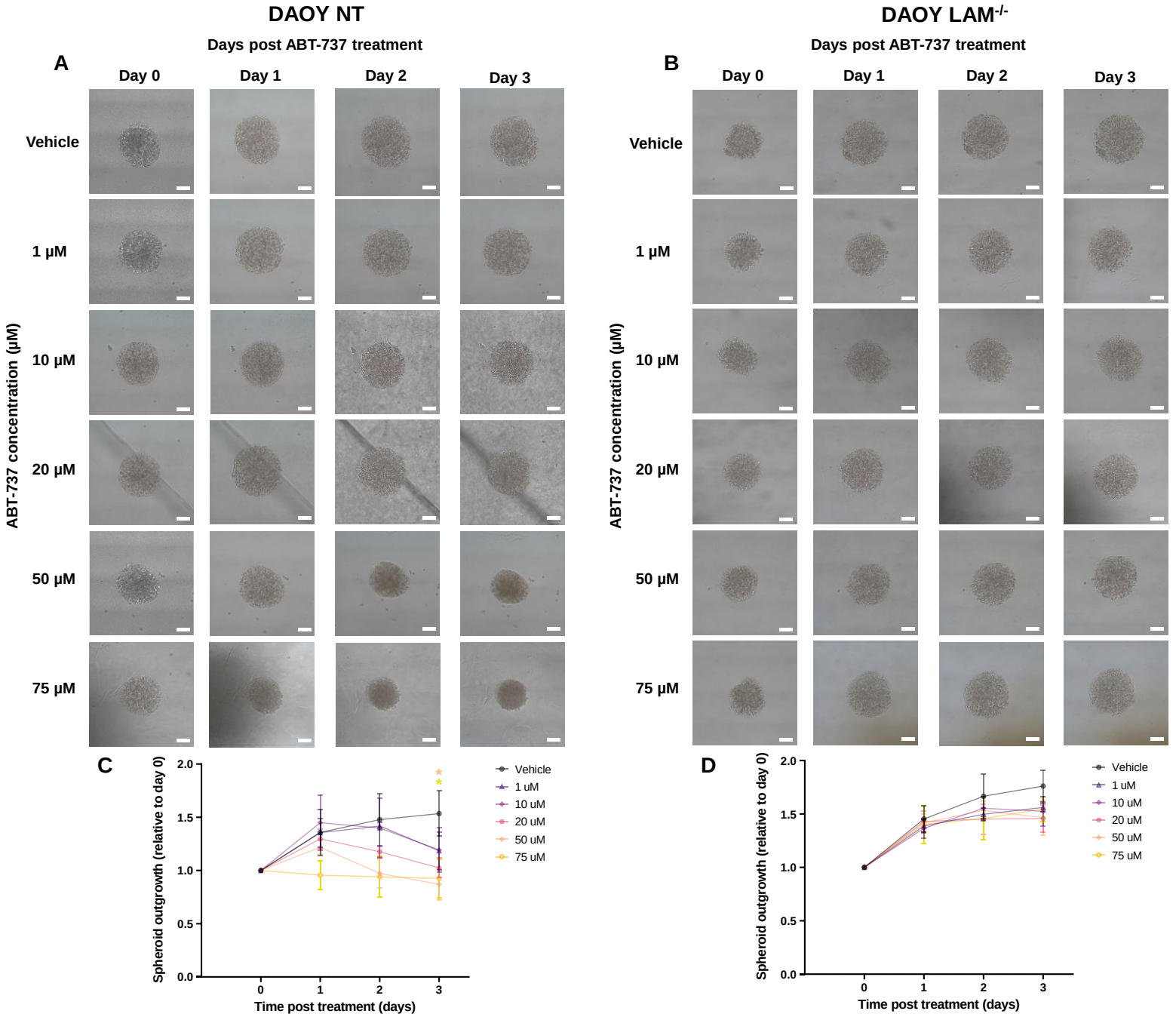


Figure 5.19 Hybrid spheroid-hydrogel drug assays demonstrate that DAOY NT spheroids are more sensitive to ABT-737 than DAOY LAM$^{-/-}$ spheroids. Brightfield images (10 X magnification) of DAOY NT (**A**) and DAOY LAM$^{-/-}$ (**B**) spheroids treated with 1, 10, 20, 50 and 75 µM of ABT-737, as well as a vehicle control (DMSO), were analysed to determine how the outgrowth of spheroids was affected by ABT-737, compared to the vehicle control over the time course of the assay (**C** and **D**). DAOY NT spheroids treated with 50 µM and 75 µM of ABT-737 exhibited significantly reduced outgrowth at day 3 post treatment. Error bars represent the mean ± SEM; n=3, with 1 or 2 internal replicates. Significance was calculated using Two-Way ANOVA analyses with Sidak's multiple comparisons post-hoc test (*p<0.05). Representative images are shown. Scale bar: 100 µm.

5.8 Assessing the sensitivity of the DAOY NT and DAOY LAM$^{-/-}$ cell lines to Vincristine and Cisplatin

As the DAOY LAM$^{-/-}$ cell line exhibited differential sensitivity to ABT-737 in the 2D viability assay and the hybrid spheroid-hydrogel drug assay, we sought to investigate how the knockout of LAMA1 affected the sensitivity of SHH medulloblastoma cells to vincristine and cisplatin (standard of care drugs used in medulloblastoma treatment), using the same assays.

As displayed in Figure 5.20, the 2D drug response assays indicated that the IC_{50} values for vincristine and cisplatin were not significantly different between the DAOY NT and DAOY LAM$^{-/-}$ cell lines. However, the DAOY NT cell line was significantly more sensitive to 10 nM and 100 nM concentrations of vincristine, compared to the DAOY LAM$^{-/-}$ cell line (Figure 5.20 A) Furthermore, the DAOY LAM$^{-/-}$ vincristine IC_{50} was also found to be greater than that of the DAOY NT cell line. Overall, these findings suggest that LAMA1 does not confer a significant difference in sensitivity to vincristine and cisplatin in SHH medulloblastoma cells in 2D culture, although it does indicate a trend of increased vincristine sensitivity mediated by LAMA1.

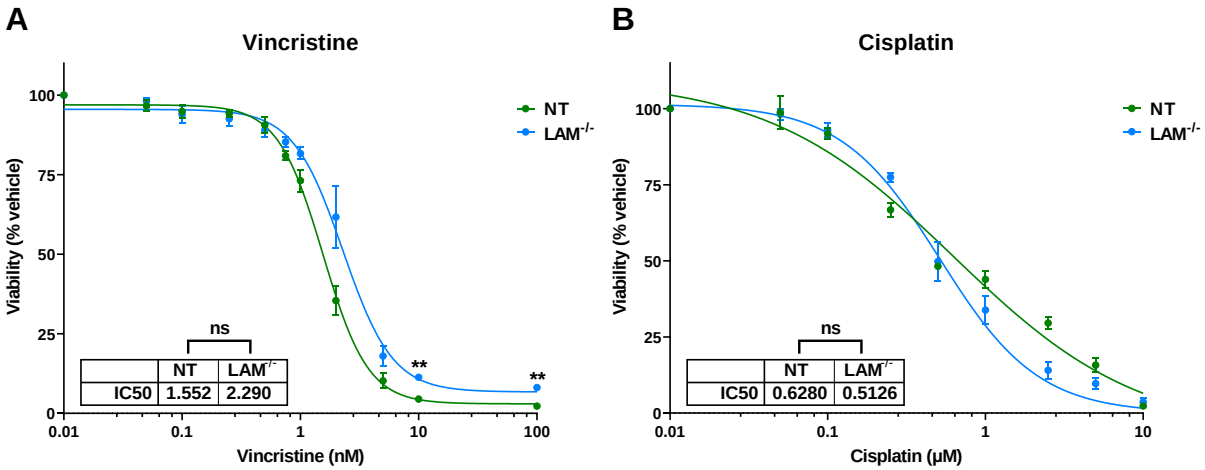


Figure 5.20 Vincristine and cisplatin drug response assays indicate that Laminin Subunit α1 (LAMA1) does not confer a significant difference in sensitivity to either drug. 2D drug response assays were used to calculate the vincristine (**A**) and cisplatin (**B**) IC_{50} values of the DAOY NT and DAOY $LAM^{-/-}$ cell lines. Neither of the IC_{50} values were found to be significantly different between the DAOY NT and DAOY $LAM^{-/-}$ cell lines, although, the DAOY NT cell line was significantly more sensitive to 10 nM and 100 nM of vincristine compared to the DAOY $LAM^{-/-}$ cell line. Mean ± SEM plotted; n=3, with 3 internal replicates. A variable slope model with four parameters was used to calculate IC_{50} values. Significance between IC_{50} values and individual concentrations of vincristine and cisplatin were assessed by an

Once we had determined the sensitivity of the DAOY NT and DAOY $LAM^{-/-}$ cell lines to vincristine and cisplatin in the 2D viability assay, we then assessed their sensitivity in the spheroid-hydrogel drug assay (as illustrated in Figure 5.18).

DAOY NT spheroids treated with 10 nM and 100 nM of vincristine exhibited significantly reduced outgrowth compared to the vehicle control spheroids at 2 days post treatment ($p<0.05$ for all comparisons; Figure 5.21 A and C). Furthermore, DAOY NT spheroids treated with all concentrations of vincristine, apart from 1 nM, exhibited significantly reduced outgrowth 3 days post treatment ($p<0.01$ for all comparisons; Figure 5.21 A and C). In contrast, DAOY $LAM^{-/-}$ spheroids treated with 100 nM of vincristine only exhibited significantly reduced outgrowth compared to the vehicle control spheroids at 2 days post treatment ($p<0.01$; Figure 5.21 B and D). In addition, DAOY $LAM^{-/-}$ spheroids treated with 5 nM, 10 nM and 100 nM of vincristine exhibited significantly reduced outgrowth at 3 days post treatment ($p<0.05$ for all comparisons; Figure 5.21 C and D). These findings indicate that the DAOY NT spheroids are more

sensitive to vincristine in the spheroid-hydrogel assay, which is corroborated by the trend identified in the 2D drug response assay (Figure 5.20 A).

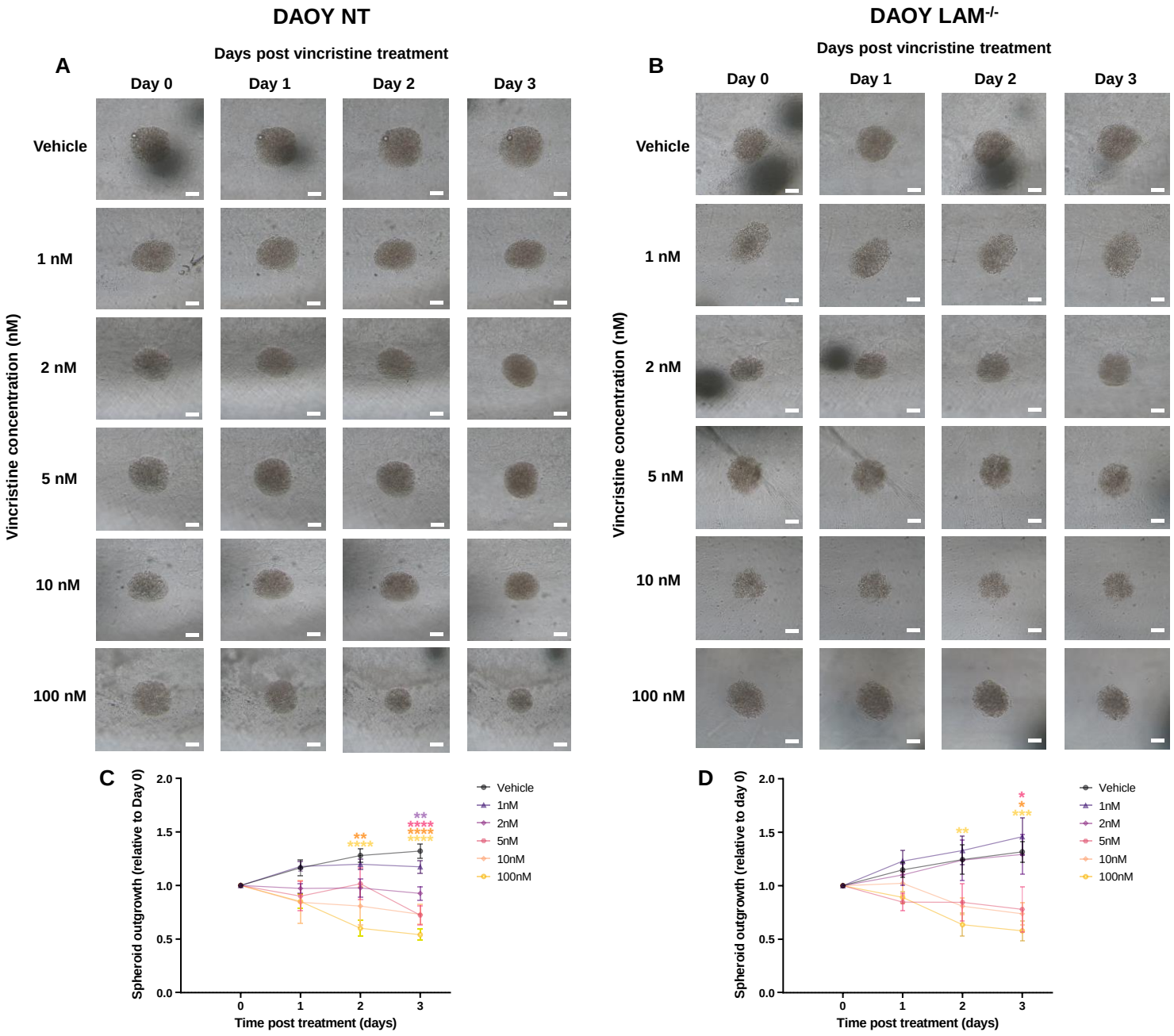


Figure 5.21 Hybrid spheroid-hydrogel drug assays demonstrate that DAOY NT spheroids are more sensitive to vincristine than DAOY LAM$^{-/-}$ spheroids. Brightfield images (10 X magnification) of DAOY NT (**A**) and DAOY LAM$^{-/-}$ (**B**) spheroids treated with 1 nM, 2 nM, 5 nM, 10 nM and 100 nM of vincristine, as well as a vehicle control (DMSO), were analysed to determine how the outgrowth of spheroids was affected by vincristine, compared to the vehicle control over the time course of the assay (**C** and **D**). DAOY NT spheroids treated with 10 nM and 100 nM of vincristine exhibited significantly reduced outgrowth at 2 days post treatment. At 3 days post treatment all concentrations of vincristine, bar 1 nM, significantly reduced the outgrowth of DAOY NT spheroids. DAOY LAM$^{-/-}$ spheroids treated with 100 nM of vincristine exhibited significantly reduced outgrowth at 2 days post treatment. At 3 days post treatment 5 nM, 10 nM and 100 nM of vincristine significantly reduced the outgrowth of DAOY LAM$^{-/-}$ spheroids. Error bars represent the mean ± SEM; n=3, with 1 or 2 internal replicates. Significance was calculated using Two-Way ANOVA analyses with Sidak's multiple comparisons post-hoc test (*p<0.05, **p≤0.01, p≤***0.001, p≤****0.0001). Representative images are shown. Scale bar: 100 µm.

Furthermore, DAOY NT spheroids treated with 10 µM of cisplatin exhibited significantly reduced outgrowth compared to the vehicle control spheroids at 2 and 3 days post treatment ($p<0.01$ for all comparisons; Figure 5.22 A and C). The outgrowth of DAOY NT spheroids, treated with 0.5 µM, 1 µM and 5 µM of cisplatin were all also reduced at 3 days post treatment, but not significantly (Figure 5.22 A and C). Similarly, only the DAOY $LAM^{-/-}$ spheroids treated with the highest concentration of cisplatin (10 µM) exhibited significantly reduced outgrowth compared to the vehicle control spheroids, which was observed at 1, 2 and 3 days post treatment ($p<0.05$ for all comparisons; Figure 5.22). However, the outgrowth of the DAOY $LAM^{-/-}$ spheroids treated with the remaining concentrations of cisplatin did not exhibit any reduction in outgrowth over the time course of the assay. These findings indicate that there is no difference in cisplatin sensitivity between the DAOY NT and $LAM^{-/-}$ spheroids in the spheroid-hydrogel assay, corroborating the findings of the 2D drug response assay.

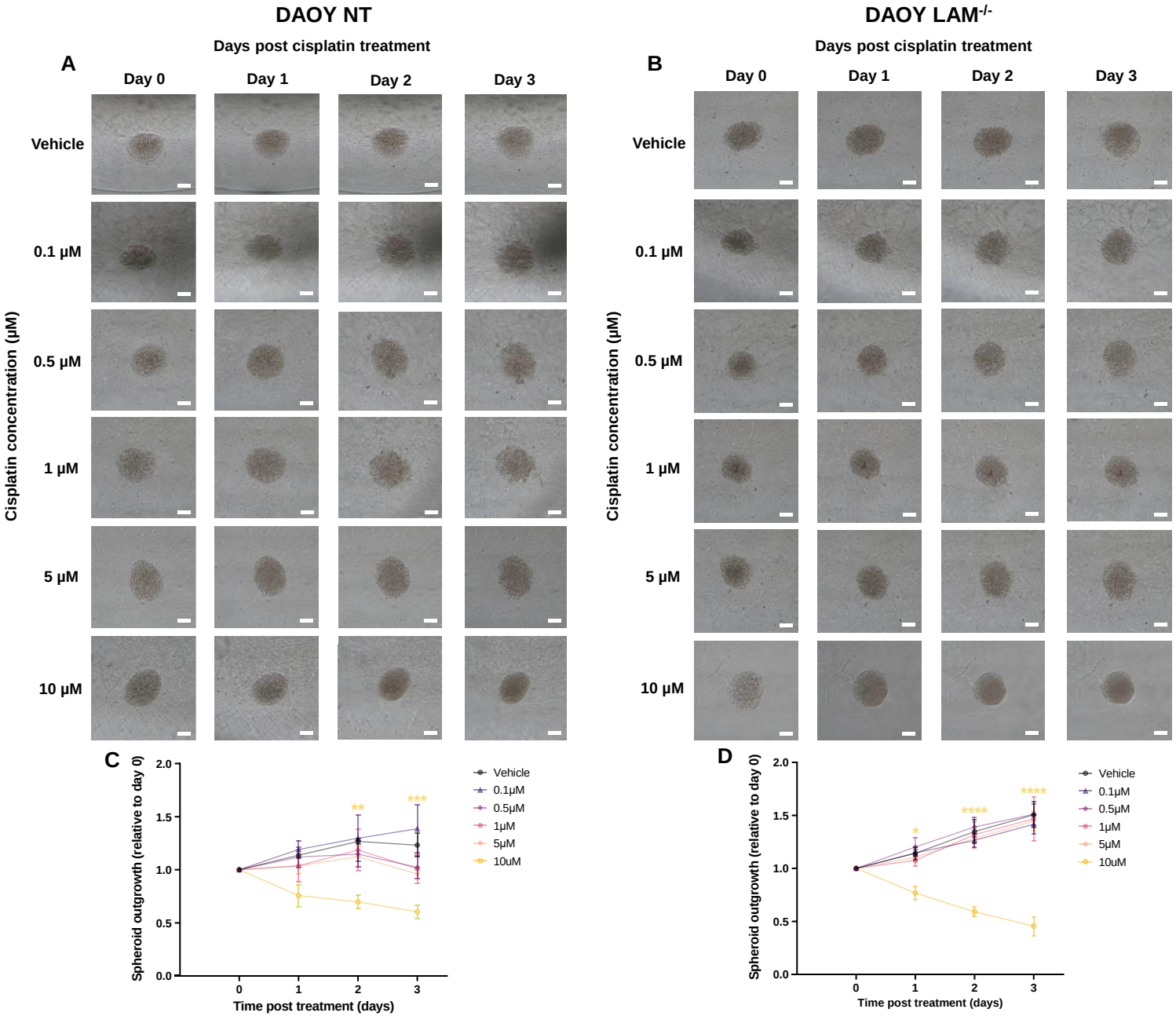


Figure 5.22 Hybrid spheroid-hydrogel drug assays demonstrate that there is no difference in cisplatin sensitivity between the DAOY NT and DAOY LAM$^{-/-}$ spheroids. Brightfield images (10 X magnification) of DAOY NT (**A**) and DAOY LAM$^{-/-}$ (**B**) spheroids treated with 0.1 µM, 0.5 µM, 1 µM, 5 µM and 10 µM of cisplatin, as well as a vehicle control (DMF), were analysed to determine how the outgrowth of spheroids was affected by cisplatin, compared to the vehicle control over the time course of the assay (**C** and **D**). DAOY NT spheroids treated with 10 µM of cisplatin exhibited significantly reduced outgrowth at 2 and 3 days post treatment. DAOY LAM$^{-/-}$ spheroids treated with 10 µM of cisplatin exhibited significantly reduced outgrowth at 1, 2 and 3 days post treatment. Error bars represent the mean ± SEM; n=3, with 1 or 2 internal replicates. Significance was calculated using Two-Way ANOVA analyses with Sidak's multiple comparisons post-hoc test (*p<0.05, **p≤0.01, p≤***0.001, p≤****0.0001). Representative images are shown. Scale bar: 100 µm.

5.9 Summary points

- Immunofluorescent and immunohistochemical staining of DAOY and ONS-76 spheroids demonstrated that SHH medulloblastoma cell lines also form a laminin-111/211 shell-like structure when grown as a spheroid, validating spheroids as an appropriate model to use to study LAMA1 in SHH medulloblastoma.

- Combinational analysis of genomic and proteomic SHH medulloblastoma patient datasets, in addition to scRNAseq and 3D OrbiSIMs SHH medulloblastoma cell line datasets, identified COL1A1, COL6A1 and lumican as candidates to comprise additional components of the SHH medulloblastoma laminin-111/211 shell-like structure.

- Immunofluorescent and immunohistochemical staining of DAOY and ONS-76 spheroids validated COL1A1, COL6A1 and lumican as components of the SHH medulloblastoma laminin-111/211 shell-like structure.

- DAOY LAM$^{-/-}$ cells were unable to form standard spheroids capable of sustained growth but were able to grow as a spheroid when supported by a hyaluronan hydrogel in a hybrid spheroid-hydrogel model.

- Western blotting demonstrated that the protein expression of CD44 and BCL-2 were significantly reduced in the DAOY LAM$^{-/-}$ cell line in 2D and spheroid culture.

- Zymography analysis of cell line supernatants indicated that the secretion of pro-MMP-9 and MMP-2 was significantly increased in the DAOY LAM$^{-/-}$ cell line in 2D culture.

- Spheroid-hydrogel and Transwell® migration models demonstrated that migration was significantly reduced in DAOY LAM$^{-/-}$ cells. Although, in the spheroid-hydrogel model, this reduction in migration could also be a consequence of reduced CD44-mediated cellular adhesion to hyaluronan.

- A Transwell® and invasion model indicated that invasion was not reduced in DAOY LAM$^{-/-}$ cells.

- Luminescent and fluorescent caspase-3/7 assays demonstrated that apoptosis is only significantly increased in the DAOY LAM$^{-/-}$ cell line when grown as a spheroid.

- A 2D drug response assay revealed that the DAOY LAM$^{-/-}$ cell line is significantly more sensitive to ABT-737 (BCL-2 small-molecule inhibitor) in 2D culture.

- Luminescent and fluorescent caspase-3/7 assays confirmed that there was an increase in apoptosis in DAOY LAM$^{-/-}$ cells treated with ABT-737 in 2D culture.

- A spheroid-hydrogel drug assay demonstrated that DAOY LAM$^{-/-}$ spheroids are in fact more resistant to ABT-737, as well as vincristine, when grown as a spheroid embedded in hyaluronan hydrogel.

Chapter 6: Proteomic analysis of DAOY NT and DAOY LAM$^{-/-}$ cell lines grown in 2D and spheroid culture

6.1 Introduction

In the previous chapter we identified that LAMA1 affected migration, apoptosis and drug sensitivity in SHH medulloblastoma, using the DAOY LAM$^{-/-}$ cell line. Although we had established some initial protein candidates, the expression of which were altered by LAMA1 (CD44, MMP-2 and BCL-2), we next wanted to more comprehensively assess unbiased global changes in protein expression, which underpinned these phenotypes. Furthermore, we also wanted to identify additional LAMA1-regulated pathways that could also contribute to the differential survival of *LAM*^{high} and *LAM*^{low} SHH medulloblastoma patients.

To achieve this, we decided to conduct proteomic analysis of the DAOY NT and DAOY LAM$^{-/-}$ cell lines grown in 2D and day 1 spheroid culture using liquid chromatography-tandem mass spectrometry (LC-MS/MS), in order to identify differentially expressed proteins in the DAOY LAM$^{-/-}$ cell line that were therefore up or down regulated by LAMA1, as illustrated in Figure 6.1. LC-MS/MS is one of the most commonly used techniques in MS-based proteomic analysis of biological samples, and can identify over 1000 proteins in one sample (Hawkridge, 2014).

Once the LAMA1 regulated proteins had been identified by LC-MS/MS, we aimed to assess their interaction by the generation of Protein-Protein interaction networks (as determined by curated databases, experimentation, gene neighbourhoods, gene fusions, gene co-occurrences, textmining, co-expression and protein homology) using STRING analysis. Furthermore, we also aimed to map these proteins onto known molecular pathways using KEGG pathway mapping analysis (Figure 6.1). We hypothesised that the combination of these analyses would allow for the specific molecular pathways that were regulated by LAMA1 in SHH medulloblastoma to be identified.

The aims of this chapter were to:

A) Identify proteins with altered expression in the DAOY LAM$^{-/-}$ cell line relative to the DAOY NT control cell line (that were therefore up or down regulated by LAMA1) in 2D and day 1 spheroid culture, using LC-MS/MS proteomic analysis.
B) Assess the interaction of LAMA1 regulated proteins, as well any molecular pathways they are part of, using a combination of STRING Protein-Protein interaction analysis and KEGG pathway mapping analysis.

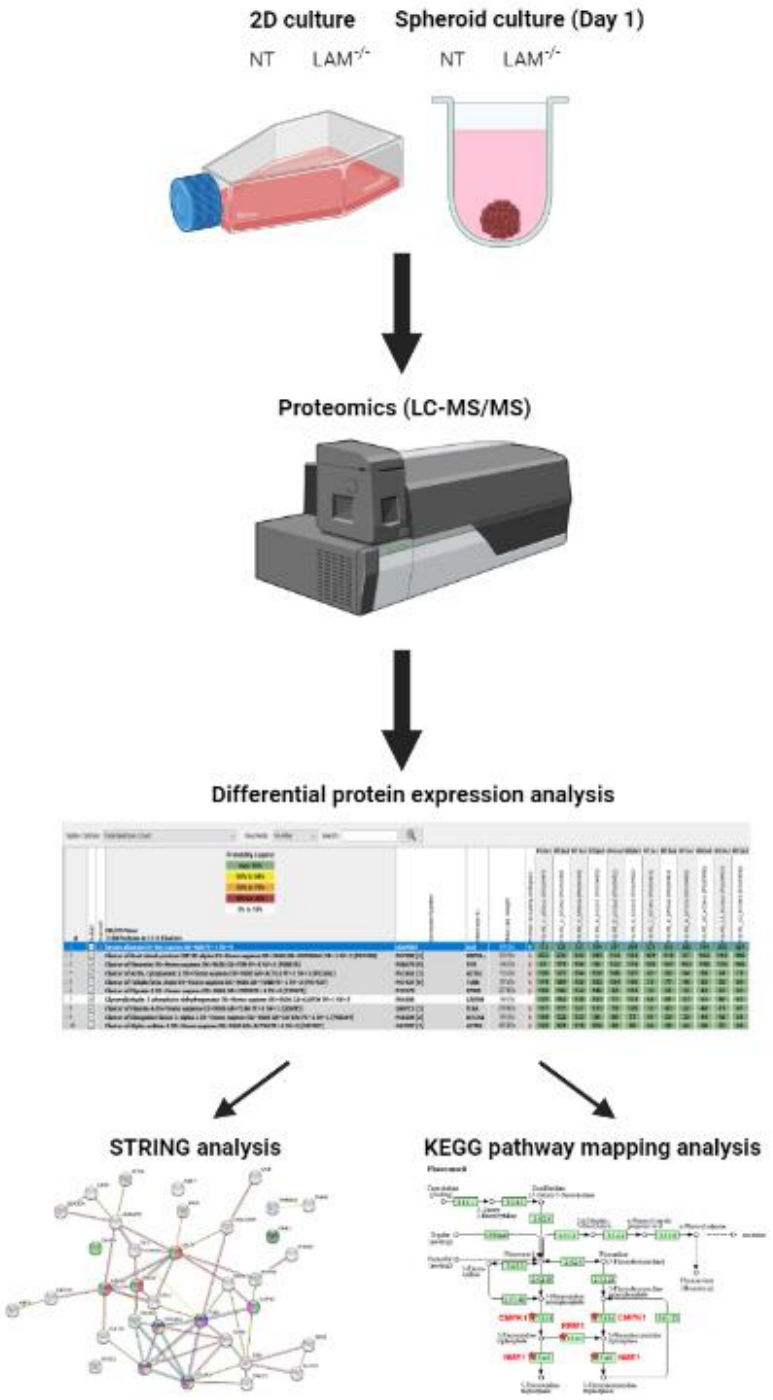


Figure 6.1 Illustration of the liquid chromatography-tandem mass spectrometry (LC-MS/MS) proteomics workflow used in this study. DAOY NT and DAOY LAM$^{-/-}$ cell lines grown in 2D culture or as a spheroid for 1 day, were analysed by LC-MS/MS proteomic analysis in order to identify proteins differentially regulated by Laminin Subunit α1 (LAMA1) in SHH medulloblastoma. STRING and Kyoto Encyclopaedia of Genes and Genomes (KEGG) pathway mapping analyses were then conducted on the identified LAMA1 regulated proteins.

6.2 Identifying LAMA1 regulated proteins in SHH medulloblastoma

In LC-MS/MS, the quantity of proteins within a sample can also be assessed by the Total Spectrum Counts (TSC) of each protein, which represents the sum of the total numbers of peptide reads for a given protein (Hawkridge, 2014). Here, proteomics data, containing 3 biological replicates for each cell line and cell culture method, were filtered and differential protein expression analysis was conducted, in order to identify proteins which exhibited altered expression in the DAOY LAM$^{-/-}$ cell line, and were therefore up or down regulated by LAMA1 in SHH medulloblastoma.

Four different methods of differential protein expression analysis, based on the number of biological replicates (in both cell lines) which contained TSC values ≥2 for each protein, were used to identify LAMA1 regulated proteins in either 2D or spheroid culture (Figure 6.2). This allowed us to include proteins with missing TSC values in biological replicates, which is a common occurrence in this technique due to its detection limit (Aguilan, Kulej and Sidoli, 2020). As displayed in Figure 6.2, Method 1 and Method 2 used cut-offs to identify target proteins when there were 3 TSC values in one cell line and 0 (Method 1) or 1 (Method 2) TSC values in the other. Whereas, Method 3 and Method 4 used a statistical analysis workflow outlined by Aguilan *et al.* to identify target proteins when there were 3 TSC values in one cell line and 2 (Method 3) or 3 (Method 4) TSC values in the other. The number of differentially expressed proteins identified using each method, in the analysis of the cell lines in both 2D and spheroid culture, is also shown in Figure 6.2. Further details of how each of the methods was conducted can be found in section 2.14.2.

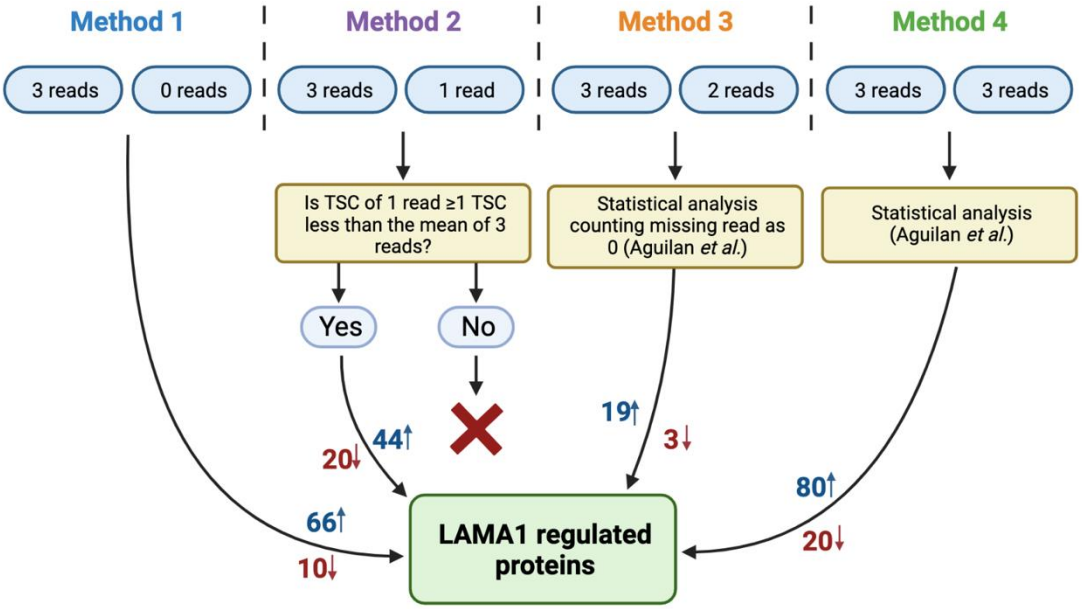


Figure 6.2 Illustration of the methods used to identify differentially expressed proteins in the DAOY LAM$^{-/-}$ cell line grown in 2D and spheroid culture. The number of 'reads' refers to the number of biological replicates which contained Total Spectrum Count (TSC) values ≥2. Blue numbers refer to proteins with decreased expression in the DAOY LAM$^{-/-}$ cell line (and therefore upregulated by Laminin Subunit α1 [LAMA1]) and red numbers refer to the number of proteins with increased expression in the DAOY LAM$^{-/-}$ cell line (and therefore downregulated by LAMA1), in both 2D and spheroid culture.

The proteins identified using all 4 methods were then combined into lists of proteins up and downregulated by LAMA1 for each cell line in 2D and spheroid culture, to be used in downstream analysis. These protein lists are displayed in Table 6.1 (2D culture) and Table 6.2 (spheroid culture). In 2D culture, 183 proteins were found to be upregulated by LAMA1, whereas only 18 proteins were found to be downregulated (Table 6.1). In spheroid culture, 26 proteins were found to be upregulated by LAMA1, while 35 proteins were found to be downregulated (Table 6.2).

Table 6.1 Proteins identified to exhibit differential protein expression in the DAOY LAM$^{-/-}$ cell line in 2D culture. The colour of each section to indicates the differential expression analysis method used to identify them (Figure 6.2).

Method 1

Decreased expression in LAM$^{-/-}$ (2D)			Increased expression in LAM$^{-/-}$ (2D)		
Protein	Mean TSC NT	Mean TSC LAM$^{-/-}$	Protein	Mean TSC NT	Mean TSC LAM$^{-/-}$
CDK1	7.667	0.000	SNRPA	0.000	2.000
PLAA	7.000	0.000			
EPHB2	6.333	0.000			
FHL1	6.000	0.000			
EIF5A	5.667	0.000			
NME1	5.333	0.000			
NUDT5	5.333	0.000			
ATP6V1B2	5.333	0.000			
ABCF1	5.000	0.000			
RRM1	5.000	0.000			
TTLL12	4.667	0.000			
OTUB1	4.667	0.000			
ACO2	4.333	0.000			
AIMP1	4.333	0.000			
PEBP1	4.333	0.000			
DCTN2	4.000	0.000			
DDX6	4.000	0.000			
BASP1	4.000	0.000			
RCC1	4.000	0.000			
MYL6	4.000	0.000			
HSD17B10	4.000	0.000			
ANP32E	4.000	0.000			
TOMM34	4.000	0.000			
VTA1	4.000	0.000			
NAA15	3.667	0.000			
PDAP1	3.667	0.000			
DFFA	3.333	0.000			
CMPK1	3.333	0.000			
DYNC1LI1	3.333	0.000			
AIMP2	3.333	0.000			
TRIP13	3.333	0.000			
TCEA1	3.333	0.000			
NCAPH	3.333	0.000			
DNM2	3.000	0.000			
RIC8A	3.000	0.000			
BAG6	3.000	0.000			
PCNP	3.000	0.000			
BAG3	3.000	0.000			
FAM49B	3.000	0.000			
ATXN10	2.667	0.000			
GSTM3	2.667	0.000			
MAPK1	2.667	0.000			
TMOD3	2.667	0.000			
TXLNA	2.667	0.000			
TGM2	2.667	0.000			
CLUH	2.667	0.000			
FLII	2.333	0.000			
ADRM1	2.333	0.000			
HAT1	2.333	0.000			
IGF2BP3	2.333	0.000			
SEC24C	2.333	0.000			
ARHGEF1	2.333	0.000			
DPP3	2.333	0.000			
CRIP2	2.333	0.000			
ATP6V1H	2.333	0.000			
BTF3	2.333	0.000			
UBLCP1	2.000	0.000			
FERMT2	2.000	0.000			
MYL12A	2.000	0.000			

Method 2

Decreased expression in LAM$^{-/-}$ (2D)			Increased expression in LAM$^{-/-}$ (2D)		
Protein	Mean TSC NT	TSC LAM$^{-/-}$	Protein	TSC NT	Mean TSC LAM$^{-/-}$
GANAB	22.667	13.000	HNRNPL	4.000	5.333
ENO2	15.667	5.000	GLS	4.000	5.000
CKB	12.333	2.000	FHL2	3.000	4.000
EEF1D	9.333	8.000	PZP	2.000	3.667
CTPS1	7.000	2.000	RPN2	2.000	3.000
STMN1	5.667	2.000	HNRNPUL1	2.000	3.000
DDAH1	5.667	2.000	SRSF2	2.000	3.000
ERO1A	5.333	4.000			
TRIP6	5.333	3.000			
HK1	5.000	4.000			
CCAR2	4.667	2.000			
APMAP	4.333	2.000			
DDB1	4.333	2.000			
PYGB	4.333	2.000			
RANGAP1	4.333	2.000			
AK2	4.333	2.000			
GNAI3	4.000	3.000			
RPL17-C18orf32	4.000	2.000			
VAT1	4.000	2.000			
PGM1	4.000	3.000			
CORO1B	4.000	2.000			
EWSR1	4.000	3.000			
LUC7L2	3.667	2.000			
GPS1	3.667	2.000			
CSRP1	3.667	2.000			
ECH1	3.333	2.000			
CNDP2	3.333	2.000			
ADSS	3.333	2.000			
DYNC1LI2	3.333	2.000			
TJP1	3.000	2.000			
ENAH	3.000	2.000			
TP53	3.000	2.000			

Method 3

Decreased expression in LAM$^{-/-}$ (2D)			Increased expression in LAM$^{-/-}$ (2D)		
Protein	p-value	Log2 Fold Change	Protein	p-value	Log2 Fold Change
TPT1	0.007	-2.421	COL1A1	0.018	2.537
UBA2	0.007	-2.091			
ACOT7	0.010	-2.330			
ECPAS	0.010	-2.005			
LIMA1	0.010	-2.179			
MARCKS	0.012	-2.347			
FEN1	0.012	-1.526			
CTSD	0.015	-2.273			
GNPDA1	0.018	-1.981			
GLUD1	0.019	-1.774			
RPA1	0.019	-2.027			
CKAP5	0.028	-1.489			
LTA4H	0.033	-1.978			
TARS	0.036	-2.137			
RPS13	0.040	-1.688			
RANBP1	0.042	-1.582			
VPS35	0.044	-1.515			
CTTN	0.049	-2.264			

Method 4

Decreased expression in LAM$^{-/-}$ (2D)			Increased expression in LAM$^{-/-}$ (2D)		
Protein	p-value	Log2 Fold Change	Protein	p-value	Log2 Fold Change
PRMT1	2.67434E-05	-1.986	SYNCRIP	0.006	0.580
NASP	0.002	-1.266	ATP5F1B	0.016	1.127
ADSL	0.002	-1.419	GSN	0.032	1.578
YWHAG	0.003	-0.545	RPN1	0.032	1.433
SRM	0.004	-1.376	TMX1	0.035	0.760
SF3B2	0.005	-1.787	DDX5	0.035	0.679
FSCN1	0.005	-0.722	TPM4	0.037	0.402
PRKAR1A	0.005	-0.751	A2M	0.039	1.464
ACTN4	0.005	-0.516	ITGB1	0.048	1.036
SCRN1	0.006	-0.770			
EIF3B	0.006	-1.270			
PSMA4	0.006	-0.747			
PSMD11	0.007	-0.385			
CD44	0.007	-0.986			
FKBP4	0.007	-0.939			
ENO1	0.008	-0.835			
NAP1L1	0.008	-0.675			
PARK7	0.008	-1.658			
PAICS	0.008	-0.809			
DNAJC7	0.009	-1.096			
PA2G4	0.009	-1.017			
PSMD7	0.009	-1.216			
DBNL	0.009	-1.402			
ETFB	0.010	-0.958			
SMC2	0.010	-1.258			
DPYSL3	0.011	-1.698			
MAPRE1	0.011	-1.294			
TAGLN2	0.011	-1.132			
TKT	0.012	-0.495			
PSMB7	0.014	-0.772			
PSMA6	0.014	-0.957			
STIP1	0.014	-1.700			
EEF1A1	0.014	-0.885			
EIF4H	0.015	-0.833			
TNPO1	0.015	-1.596			
CAPZB	0.015	-1.213			
SQSTM1	0.016	-1.334			
MYBBP1A	0.016	-1.679			
ETF1	0.016	-0.536			
GCN1	0.017	-2.282			
CCT6A	0.017	-0.827			
PPA1	0.018	-1.243			
KPNB1	0.019	-0.542			
PSMB3	0.020	-1.249			
CCT4	0.020	-0.894			
GOT2	0.021	-1.287			
CSE1L	0.021	-2.206			
GANAB	0.021	-1.494			
ST13	0.021	-1.019			
ERP29	0.023	-0.867			
EIF3A	0.024	-1.529			
RUVBL2	0.024	-0.631			
RPS8	0.025	-0.330			
RPL5	0.028	-0.496			
HSPA4	0.028	-0.990			
EIF3F	0.029	-1.167			
39326	0.029	-0.909			
EIF3I	0.030	-0.711			
YWHAB	0.030	-0.562			
STRAP	0.031	-0.781			
KRT18	0.031	-2.346			
SAE1	0.033	-0.889			
IARS	0.033	-0.848			
TUFM	0.036	-0.881			
ANXA1	0.036	-0.319			
SUGT1	0.036	-1.026			
TPD52L2	0.036	-0.993			
PDIA3	0.037	-0.324			
IPO7	0.038	-1.271			
EIF3G	0.039	-1.420			
KRT8	0.041	-0.914			
MTHFD1	0.044	-1.060			
PFN1	0.046	-1.049			
PGLS	0.046	-0.448			
PSMD13	0.048	-0.904			
HSP90AB1	0.049	-0.742			
EEF1D	0.050	-0.550			

Table 6.2 Proteins identified to exhibit differential protein expression in the DAOY LAM$^{-/-}$ cell line in spheroid (Sph) culture. The colour of each section to indicates the differential expression analysis method used to identify them (Figure 6.2).

Method 1

Decreased expression in LAM$^{-/-}$ (Sph)

Protein	Mean TSC NT	Mean TSC LAM$^{-/-}$
GANAB	11.667	0.000
PSMA7	3.667	0.000
ECH1	2.667	0.000
HIST1H4A	2.667	0.000
CKB	2.667	0.000
BASP1	2.333	0.000
ERP44	2.333	0.000

Increased expression in LAM$^{-/-}$ (Sph)

Protein	Mean TSC NT	Mean TSC LAM$^{-/-}$
LGALS3BP	0.000	6.333
DBN1	0.000	5.667
CAPN2	0.000	3.000
GNB1	0.000	2.667
RTCB	0.000	2.667
COL1A1	0.000	2.667
EIF2S2	0.000	2.667
PGM3	0.000	2.333
TMPO	0.000	2.000

Method 2

Decreased expression in LAM$^{-/-}$ (Sph)

Protein	Mean TSC NT	TSC LAM$^{-/-}$
TPI1	8.333	5.000
RPS8	7.333	6.000
RPL13	7.000	4.000
UCHL1	5.333	3.000
CAPZB	5.333	2.000
YWHAG	5.333	4.000
PDLIM1	4.000	2.000
RAN	4.000	3.000
RPA1	4.000	2.000
HIST1H2BK	4.000	3.000
PRPF19	3.333	2.000
SRSF6	3.000	2.000

Increased expression in LAM$^{-/-}$ (Sph)

Protein	TSC NT	Mean TSC LAM$^{-/-}$
GSN	3.000	12.667
PDIA3	4.000	5.667
COL6A1	3.000	4.667
HNRNPR	3.000	4.333
CALD1	3.000	4.333
MVP	2.000	4.333
TGFBI	2.000	4.000
CALU	2.000	3.667
ITGB1	2.000	3.667
P4HA2	2.000	3.667
IDH1	2.000	3.333
SRRT	2.000	3.000
ACSL3	2.000	3.000

Method 3

Decreased expression in LAM$^{-/-}$ (2D)

Protein	p-value	Log2 Fold Change
FUBP1	0.044	-1.835

Increased expression in LAM$^{-/-}$ (2D)

Protein	p-value	Log2 Fold Change
IMMT	0.033	1.569
HDLBP	0.043	1.600

Method 4

Decreased expression in LAM$^{-/-}$ (2D)

Protein	p-value	Log2 Fold Change
HIST1H1D	0.013	-1.420
SEC61A1	0.013	-1.330
RPL8	0.026	-0.845
MDH2	0.027	-1.068
ATP2A2	0.036	-1.052
PLOD3	0.045	-0.177

Increased expression in LAM$^{-/-}$ (2D)

Protein	p-value	Log2 Fold Change
AHNAK	0.002	1.429
COL6A3	0.006	2.292
AHCY	0.015	0.696
CALR	0.015	1.638
HSPA5	0.015	0.599
MSN	0.015	1.160
ACTR3	0.021	1.417
NCL	0.026	0.626
DDX39A	0.028	0.771
ANXA6	0.044	0.690
CKAP4	0.046	0.987

To visualise the spread of the proteins identified by Method 3 and 4, the data was plotted using a volcano plot (since Log2 fold change and p-values were generated using these methods), as displayed in Figure 6.3. The number of proteins identified to be upregulated by LAMA1 in 2D was greater than those identified to be downregulated (Figure 6.3 A), whereas in spheroid culture the number of proteins identified to be up and down regulated by LAMA1 was more evenly distributed (Figure 6.3 B).

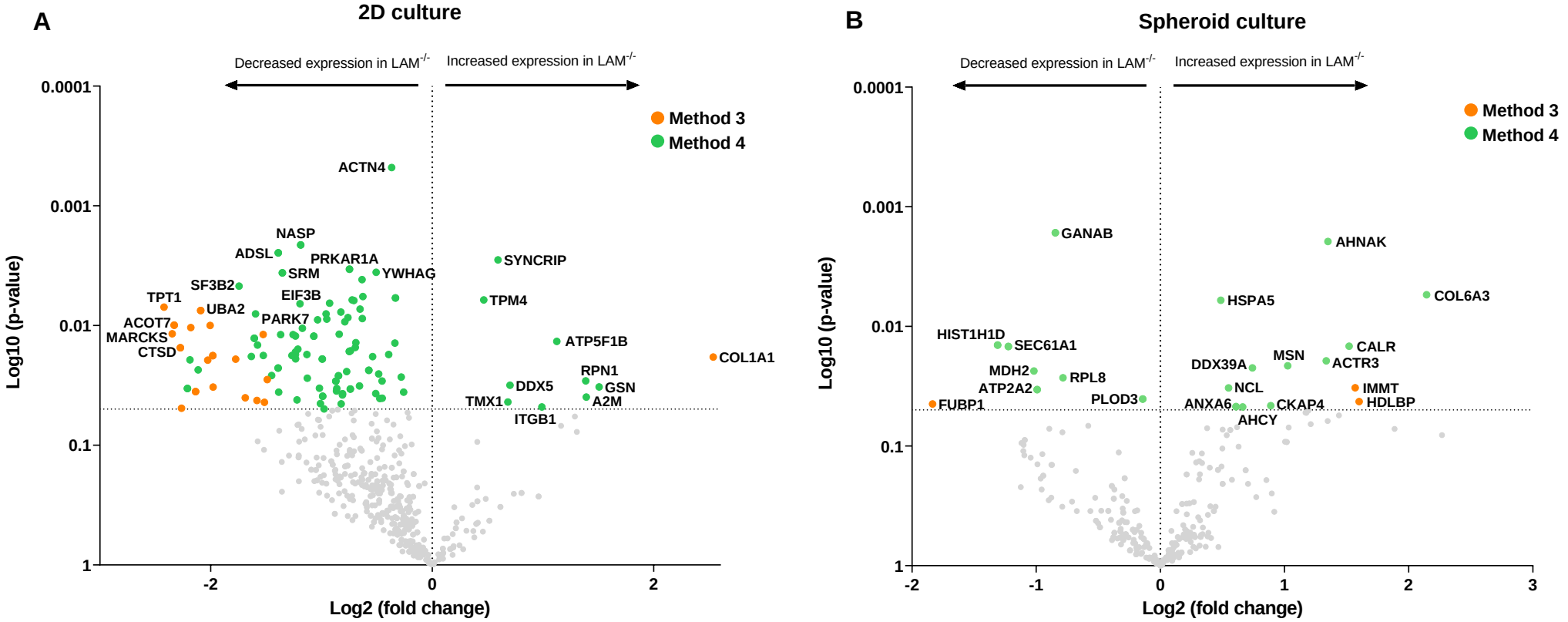


Figure 6.3 Differential protein expression analysis between the DAOY NT and DAOY LAM$^{-/-}$ cell lines grow in 2D and 3D spheroid culture. This analysis was used to identify proteins that were differentially expressed in the DAOY LAM$^{-/-}$ cell line relative to the DAOY NT cell line (and therefore up or downregulated by Laminin Subunit α1 [LAMA1]) in 2D (**A**) and spheroid (**B**) culture. Each dot represents one protein. The colour of each dot indicates which differential protein expression analysis method was used to identify them (Figure 6.2). Significance was calculated, after the data had undergone a Log2 transformation and two step normalisation, using a heteroscedastic t-test or a homoscedastic t-test, depending on if the variances between the two sets of biological replicates were significantly different (as determined by an F-test). The Log2 fold change indicates the mean expression level for each protein.

6.3 STRING Protein-Protein interaction and KEGG pathway mapping analysis of LAMA1 regulated proteins

In order to decipher how the LAMA1 up or down regulated proteins interacted with each other, as well as which molecular pathways they were significantly associated with, we utilised STRING Protein-Protein Interaction and KEGG pathway mapping (via the DAVID bioinformatics tool) analyses, respectively. In some cases, we were also able to conduct additional KEGG pathway mapping analysis within the STRING software, which allowed us to colour coordinate nodes within the Protein-Protein interaction networks within their KEGG pathway.

6.3.1 Analysis of proteins upregulated by LAMA1 in SHH medulloblastoma cells in 2D culture

The results of the STRING and KEGG pathway analyses of the 183 proteins identified to be upregulated by LAMA1 in 2D culture are displayed in Figure 6.4. STRING analysis identified that 75% of these proteins were part of one large Protein-Protein interaction network (Figure 6.4 A). Furthermore, KEGG pathway mapping analysis identified 28 different pathways significantly associated with the proteins. The top pathway identified by this analysis was metabolic pathways, which 29 of the input proteins were involved in. In addition, combined STRING and KEGG pathway mapping analysis identified that 6 highly interactive proteins (Proteasome 20S Subunit Beta 7 (PSMB7), Proteasome 26S Subunit, Non-ATPase 11 (PSMD11), Proteasome 26S Subunit, Non-ATPase 7 (PSMD7), Proteasome 20S Subunit Beta 3 (PSMB3), Proteasome 20S Subunit Alpha 4 (PSMA4) and ADRM1 26S Proteasome Ubiquitin Receptor (ADRM1)) were all part of pathways relating to amyotrophic lateral sclerosis, Parkinson's disease, prion disease, Huntington's disease, spinocerebellar ataxia and the proteasome, as indicated by the red box in Figure 6.4 A. Furthermore, another 5

proteins (Enolase 1 (ENO1), Enolase 2 (ENO2), Transketolase (TKT), Aconitase 2 ACO2, Hexokinase 1 (HK1) and 6-Phosphogluconolactonase (PGLS)) were also identified to be highly interactive and all relate to metabolic pathways and carbon metabolism, as indicated by the blue box in Figure 6.4 A.

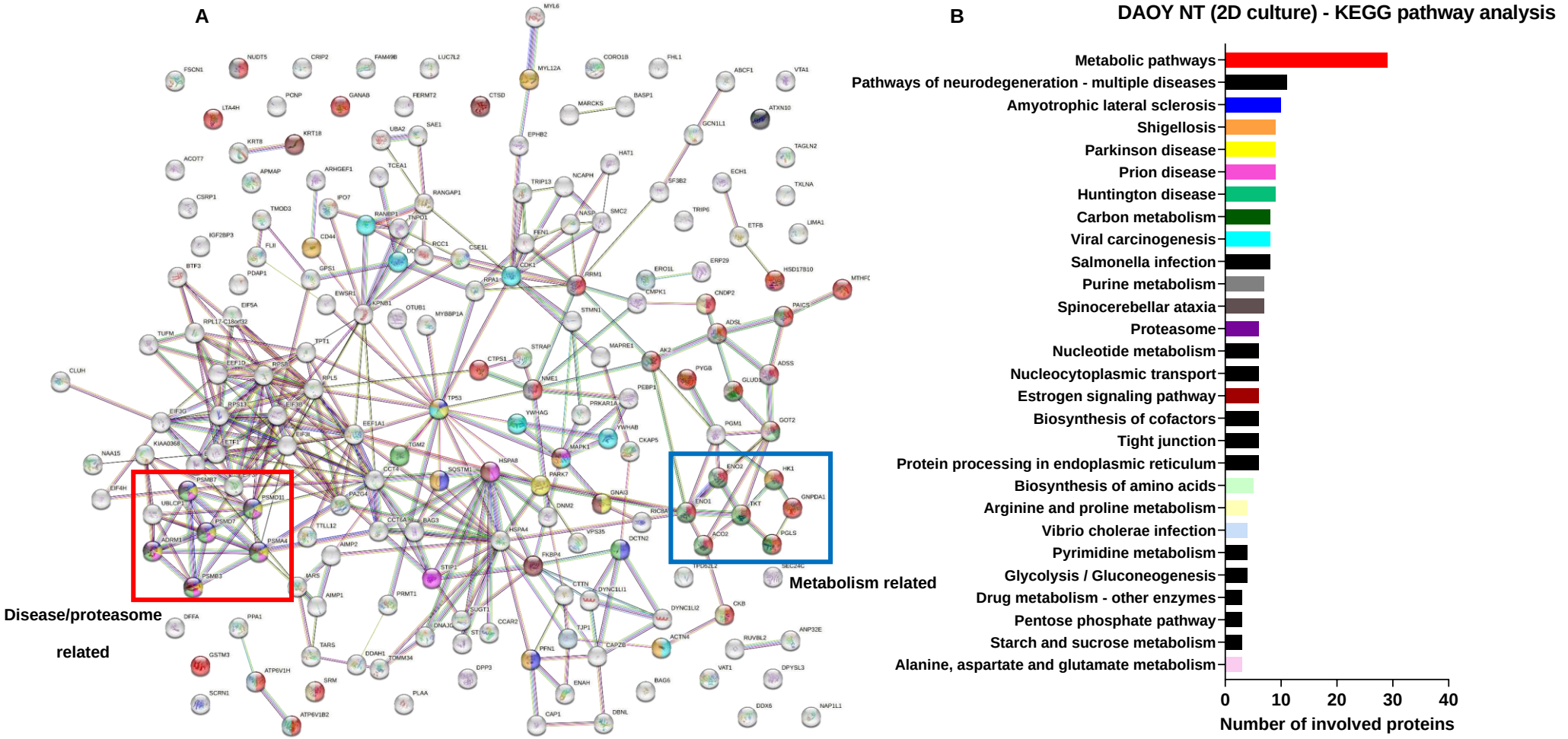


Figure 6.4 STRING Protein-Protein Interaction and Kyoto Encyclopaedia of Genes and Genomes (KEGG) pathway mapping analysis of proteins identified to be upregulated by Laminin Subunit α1 (LAMA1) in 2D culture, identify a large network of protein interaction, as well as 28 associated KEGG pathways, respectively. STRING Protein-Protein interaction analysis (**A**) was conducted with a high confidence score of 0.7. The number and colour of lines connecting nodes illustrates the 'active interaction sources' (curated databases: light blue, experimentally determined: pink, dark gene neighbourhood: green, gene fusions: red, gene co-occurrence: dark blue, textmining: light green, co-expression: black, protein homology: lilac) that were used to determine the interaction. KEGG pathway mapping analysis (**B**) was conducted using the online bioinformatics tool DAVID. Significantly associated pathways were considered those where $p<0.05$. KEGG pathway mapping analysis was also conducted as part of the STRING analysis, allowing the colour of the protein nodes in the Protein-Protein interaction networks to be coordinated with the colour of the bars of each pathway in the KEGG pathway mapping analysis, indicating which proteins were used to identify the pathways. Bars that have been coloured black indicate where the KEGG pathway mapping analysis conducted by the STRING software did not overlap with that conducted using DAVID. Nodes within coloured boxes indicate groups of highly interactive proteins that are associated with the same KEGG pathways.

Assessment of the metabolic pathways KEGG pathway diagram, which highlighted the metabolic pathways associated with the input proteins (Appendix Figure 7), identified that metabolic pathways relating to amino acid metabolism, nucleotide metabolism and carbohydrate metabolism were upregulated by LAMA1. This was corroborated by the fact that the KEGG pathway mapping analysis also identified several pathways that are part of these types of metabolism, including: carbon metabolism, purine metabolism, nucleotide metabolism, biosynthesis of amino acids, arginine and proline metabolism, pyrimidine metabolism, glycolysis/gluconeogenesis, starch and sucrose metabolism and alanine, aspartate and glutamate metabolism (Figure 6.4).

Several of the other top identified pathways related to diseases of the nervous system: pathways of neurodegeneration – multiple diseases, amyotrophic lateral sclerosis, prion disease, Parkinson's disease, Huntington's disease and spinocerebellar ataxia (Figure 6.4). By assessing the input proteins that were associated with these pathways, we identified that 6 components of the proteasome, which was also an identified KEGG pathway, were shared between all of them (PSMB7, PSMD7, PSMA4, PSMD11, PSMB3, ADRM1). This is also illustrated by the red box in Figure 6.4 A, although the KEGG pathway neurodegeneration – multiple diseases was not identified by the KEGG pathway mapping analysis conducted by the STRING software.

The proteasome is the key component of the ubiquitin-proteasome system (UPS), which is responsible for the degradation of short-lived, regulatory, damaged or misfolded proteins in cells, which have been tagged with ubiquitin on exposed lysine residues. The eukaryotic 26S proteasome consists of two sub-complexes: the 20S core particle (CP), where protein degradation occurs, and the 19S regulatory particle (RP), which controls substrate recognition, unfolding and translocation to the 20S core particle (Figure 6.5) (Lander *et al.*, 2012; Budenholzer *et al.*, 2017; Rousseau and Bertolotti, 2018).

The 6 components of the proteasome identified to be upregulated by LAMA1 in SHH medulloblastoma in 2D culture, are displayed in the labelled proteasome KEGG pathway diagram in Figure 6.5. PSMD11 and PSMD7 are lid components of proteasome RP, whereas ADRM1 is a base component (Figure 6.5). In addition, PSMA4 is a component of the α rings within the CP, whereas PSMB7 and PSMB3 are components of the CP's β rings (Figure 6.5).

It is worth mentioning that the upregulation of the proteasome by LAMA1 could be one mechanism underpinning some of the discrepancies observed between the gene and protein expression of the 'laminin regulated genes' in section 5.5.

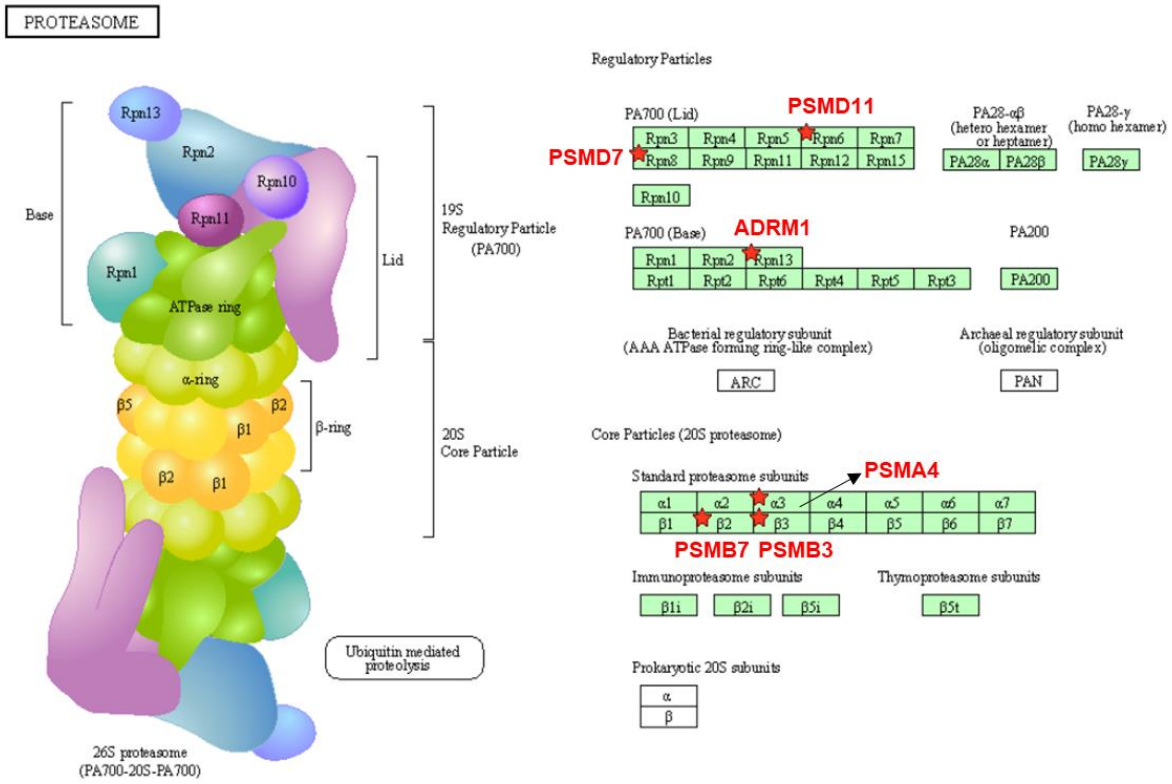


Figure 6.5 Kyoto Encyclopaedia of Genes and Genomes (KEGG) pathway mapping analysis of proteins upregulated by Laminin Subunit α1 (LAMA1) in 2D culture identifies the proteasome as an associated pathway. Proteasome components Proteasome 20S Subunit Beta 7 (PSMB7), Proteasome 26S Subunit, Non-ATPase 11 (PSMD11), Proteasome 26S Subunit, Non-ATPase 7 (PSMD7), Proteasome 20S Subunit Beta 3 (PSMB3), Proteasome 20S Subunit Alpha 4 (PSMA4) and ADRM1 26S Proteasome Ubiquitin Receptor (ADRM1) were all identified to be upregulated by LAMA1 in SHH medulloblastoma in 2D culture. Red stars indicate where these proteins fall within the KEGG pathway. The gene names, aliases or alternative proteins within the pathway, which were used in the input of the analysis, are displayed next to their corresponding pathway protein in red text. The KEGG pathway diagram was generated as part of the KEGG pathway mapping analysis using the online

Finally, although estrogen signalling was not one of the top pathways identified, it is of specific interest as estrogen signalling upregulates the expression of CD44 and BCL-2, both of which we have previously shown to be upregulated by LAMA1 (section 5.4) (Choi *et al.*, 2001; Durst *et al.*, 2001; C. Yang *et al.*, 2020; Medrano-González *et al.*, 2021; Pereira Maurício de Barros *et al.*, 2021; Kawiak and Kostecka, 2022). Estrogen is a steroid-hormone which regulates many aspects of cellular growth and differentiation throughout the life of both males and females, by altering gene expression in target tissues (Belcher, 2008). Estrogen predominately influences gene

expression via the direct genomic pathway (nuclear-initiated signalling) by binding to the estrogen receptors (ER) α or β in the cytoplasm, which then translocate to the nucleus where they activate the transcription of estrogen sensitive genes (Chen, Zeng and Tse, 2008; Fuentes and Silveyra, 2019). Estrogen can also alter gene expression via the indirect genomic pathway by binding to membrane bound ERs (membrane-initiated signalling) which activate second-messenger cascades and transcription factors, as well as modulate membrane-based ion channels (Belcher, 2008; Chen, Zeng and Tse, 2008; Fuentes and Silveyra, 2019).

The 6 components of the estrogen signalling KEGG pathway identified to be upregulated by LAMA1 in SHH medulloblastoma in 2D culture were FKBP Prolyl Isomerase 4 (FKBP4), Heat Shock Protein Family A Member 8 (HSPA8), Keratin 18 (KRT18), Cathepsin D (CTSD), Mitogen-Activated Protein Kinase 1 (MAPK1) and G Protein Subunit Alpha I3 (GNAI3), as shown in the labelled estrogen signalling KEGG pathway in Figure 6.6. FKPB4 and HSPA8 are part of the multi-protein inhibitory complex which is bound to estrogen receptors in the absence of the estrogen. Furthermore, KRT18 and CTSD are proteins that are specifically upregulated by genomic estrogen signalling. In addition, MAPK1 is activated by non-genomic estrogen signalling and can enhance genomic estrogen signalling (Atanaskova *et al.*, 2002; Chen, Zeng and Tse, 2008; Fuentes and Silveyra, 2019). Finally, GNAI3 is also involved in pathways activated by non-genomic estrogen signalling.

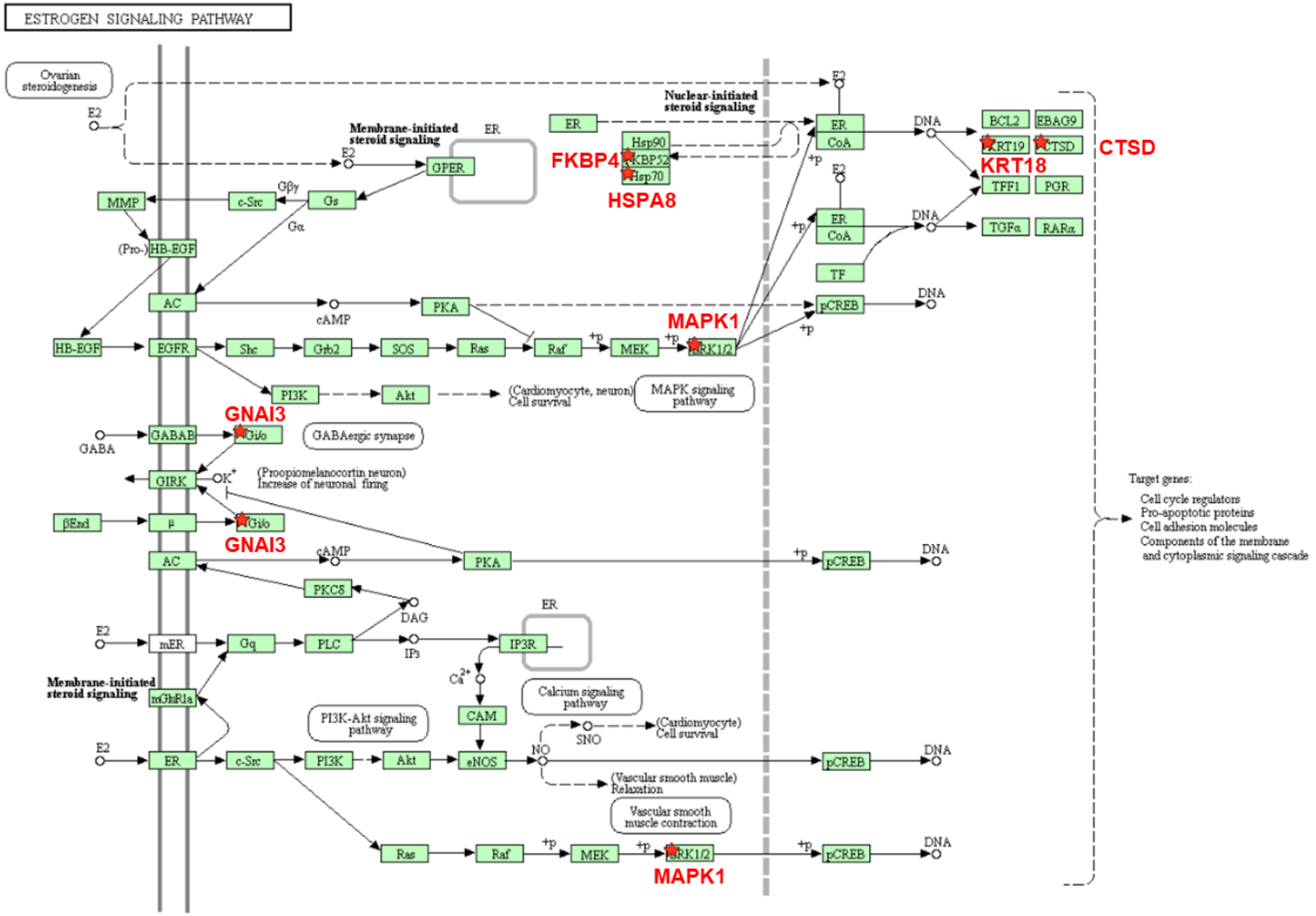


Figure 6.6 Kyoto Encyclopaedia of Genes and Genomes (KEGG) pathway mapping analysis of proteins upregulated by Laminin Subunit α1 (LAMA1) in 2D culture, identifies estrogen signalling as an associated pathway. Estrogen signalling components FKBP Prolyl Isomerase 4 (FKBP4), Heat Shock Protein Family A Member 8 (HSPA8), Keratin 18 (KRT18), Cathepsin D (CTSD), Mitogen-Activated Protein Kinase 1 (MAPK1) and G Protein Subunit Alpha I3 (GNAI3) were all identified to be upregulated by LAMA1 in SHH medulloblastoma in 2D culture. Red stars indicate where these proteins fall within the KEGG pathway. The gene names, aliases or alternative proteins within the pathway, which were used in the input of the analysis, are displayed next to their corresponding pathway protein in red text. The KEGG pathway diagram was generated as part of the KEGG pathway mapping analysis using the online bioinformatics tool DAVID.

In summary, this analysis revealed that pathways relating to amino acid metabolism, nucleotide metabolism, carbohydrate metabolism, the proteasome and estrogen signalling were upregulated by LAMA1 in SHH medulloblastoma in 2D culture. This range of essential metabolic processes upregulated by LAMA1 illustrates its importance in SHH medulloblastoma progression. Furthermore, upregulation of the proteasome and estrogen signalling have both been previously shown to have a role in medulloblastoma pathogenesis (Belcher, 2008; Belcher, Ma and Le, 2009; Cookman and Belcher, 2015; Vriend and Marzban, 2017; Hoerig *et al.*, 2021).

6.3.2 Analysis of proteins downregulated by LAMA1 in SHH medulloblastoma cells in 2D culture

The results of the STRING and KEGG pathway analyses of the 18 proteins identified to be downregulated by LAMA1 in 2D culture are displayed in Figure 6.10. STRING analysis identified that 78% of these proteins were part of 2 separate Protein-Protein interaction networks (Figure 6.7 A). In addition, aside from these networks, Ribophorin I (RPN1) and Ribophorin II (RPN2) were also found to be highly interactive (Figure 6.7 A). Furthermore, KEGG pathway mapping analysis identified 4 pathways significantly associated with these proteins: proteoglycans in cancer, the spliceosome, various types N-glycan biosynthesis and N-glycan biosynthesis (Figure 6.9 B). STRING analysis was unable to conduct KEGG pathways from the input proteins, therefore, colour coordinating the protein nodes with the KEGG pathway they are part of (as in Figure 6.4) was not possible.

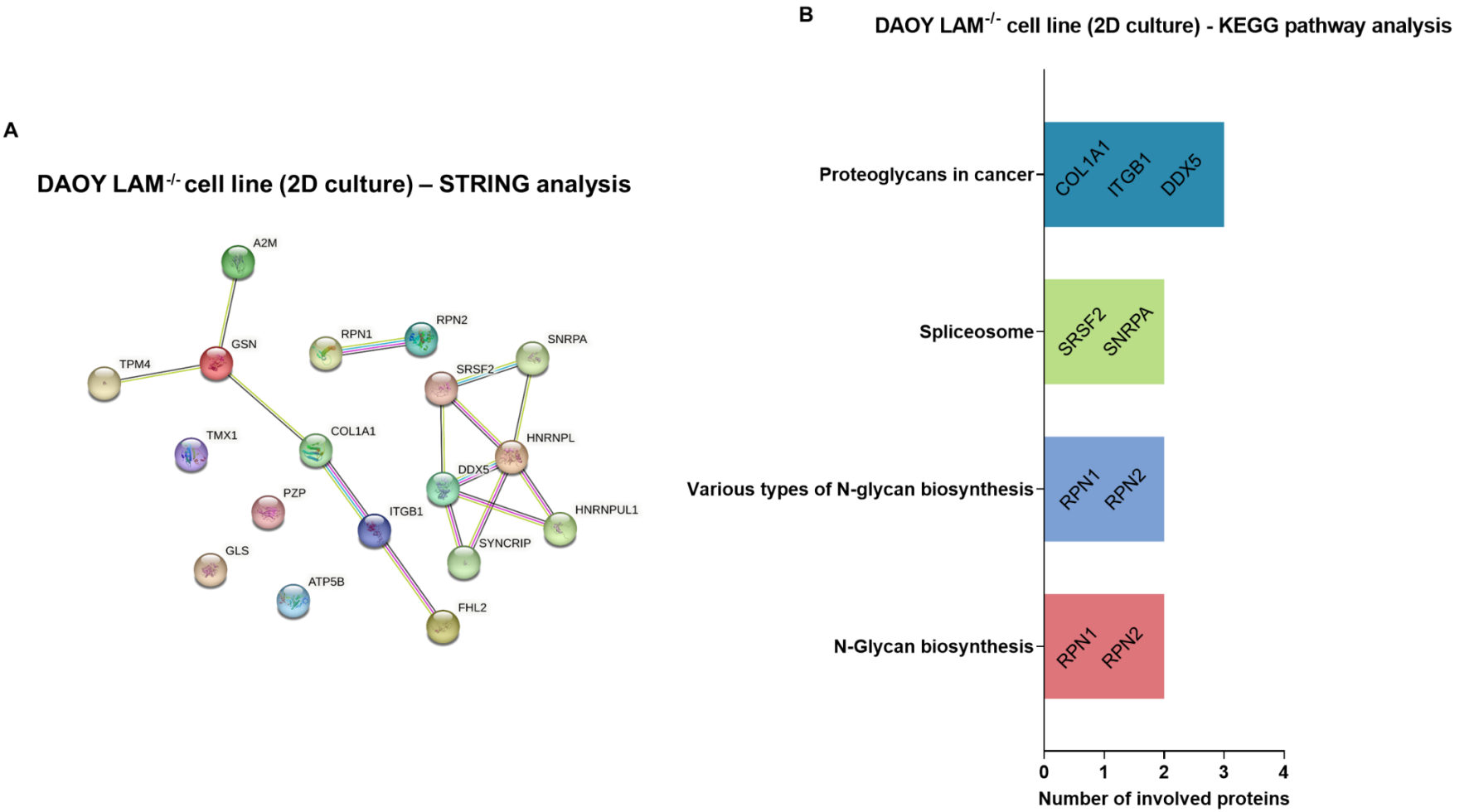


Figure 6.7 STRING Protein-Protein Interaction and Kyoto Encyclopaedia of Genes and Genomes (KEGG) pathway mapping analysis of proteins identified to be downregulated by Laminin Subunit α1 (LAMA1) in 2D culture, identify two interaction network of proteins, as well as 4 associated KEGG pathways, respectively. STRING Protein-Protein interaction analysis (**A**) was conducted with a medium confidence score of 0.4. The number and colour of lines connecting nodes illustrates the 'active interaction sources' (curated databases: light blue, experimentally determined: pink, dark gene neighbourhood: green, gene fusions: red, gene co-occurrence: dark blue, textmining: light green, co-expression: black, protein homology: lilac) that were used to determine the interaction. KEGG pathway mapping analysis (**B**) was conducted using the online bioinformatics tool DAVID. Significantly associated pathways were considered those where $p<0.05$. The names of the input proteins used to identify the KEGG pathways are labelled within the bars of the chart. STRING analysis did not identify any KEGG pathways from the input proteins, therefore colour coordinating the protein nodes with the KEGG pathway they are part of (as in Figure 6.4) was not possible.

Next, we also wanted to determine the specific parts of the major pathways identified by the KEGG pathway mapping analysis that were being downregulated by LAMA1 in SHH medulloblastoma in 2D culture. The top pathway identified was proteoglycans in cancer, which refers to the modulation of many intracellular pathways by different proteoglycans via their interaction with cell surface receptors. We chose to focus on this pathway as the emphasis of this study is on SHH medulloblastoma's interaction with the ECM, of which proteoglycans are a major constituent (Wade *et al.*, 2013). The input proteins that identified this KEGG pathway were specifically related to collagen-integrin signalling and decorin-TLR signalling pathways. However, as only one protein was identified in the latter pathway, we decided not to examine it further.

As previously mentioned in section 5.3, collagens form large networks and are a crucial part of the ECM (Shoulders and Raines, 2009; Neel *et al.*, 2013). Whereas, integrins are a family of heterodimeric cell surface receptors, which allow cells to attach to and interact with a range of different ECM components, as well as other cells (Barczyk, Carracedo and Gullberg, 2010; Su *et al.*, 2020). The integrin family consists of 18 α subunits, which recognise the binding substrate and 8 β subunits, which mediate the activation of intracellular kinase signalling upon the binding of the substrate. These subunits dimerise to form 24 types of integrin receptors, which can each bind to different ECM components and modulate the activity of a host of different downstream signalling pathways, including Ras-ERK, PI3K-AKT, MAPK and FAK (Humphries, Byron and Humphries, 2006; Su *et al.*, 2020).

The components of collagen-integrin signalling (within the proteoglycans in cancer KEGG pathway) identified to be downregulated by LAMA1 in SHH medulloblastoma in 2D culture, were Collagen Type-I α1 Chain (COL1A1) and Integrin Subunit Beta 1 (ITGB1), as shown in the labelled KEGG pathway diagram in Figure 6.8. COL1A1 is an α subunit of type-I collagen and ITGB1 is an integrin β subunit, which can form integrin receptors with many types of α subunits (Su *et al.*, 2020). As displayed in

Figure 6.8, these two proteins directly interact in the KEGG pathway when ITGB1 forms a heterodimer with the integrin α2 subunit, resulting in cell adhesion and spreading.

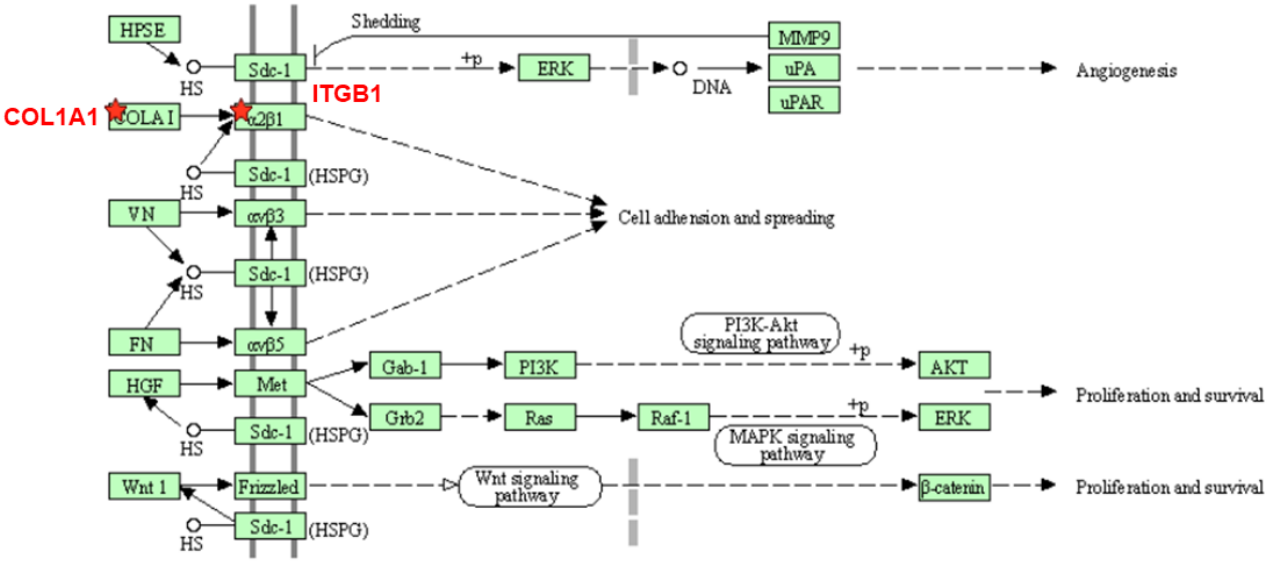


Figure 6.8 Kyoto Encyclopaedia of Genes and Genomes (KEGG) pathway mapping analysis of proteins downregulated by Laminin Subunit α1 (LAMA1) in SHH medulloblastoma cells in 2D culture, identified proteoglycans in cancer (specifically collagen-integrin interaction) as an associated pathway. The components of collagen-integrin interaction (within the KEGG pathway of proteoglycans in cancer) Collagen Type-I α1 Chain (COL1A1) and Integrin Subunit Beta 1 (ITGB1) were identified to be downregulated by LAMA1 in SHH medulloblastoma in 2D culture. Red stars indicate where these proteins fall within the KEGG pathway. The gene names, aliases, components of a protein complex or alternative proteins within the pathway, which were used in the input of the analysis, are displayed next to their corresponding pathway protein in red text. The KEGG pathway diagram was generated as part of the KEGG pathway mapping analysis using the online bioinformatics tool DAVID.

In summary, the smaller number of proteins downregulated by LAMA1 in 2D culture were associated with ECM-receptor interaction, as opposed to the proteins that were upregulated by LAMA1, which were mainly associated with metabolic pathways. This corroborates the finding that LAMA1 distinctly alters cellular activity in SHH medulloblastoma in 2D culture.

6.3.3 Analysis of proteins upregulated by LAMA1 in SHH medulloblastoma cells in spheroid culture

The results of the STRING and KEGG pathway analyses for the 26 proteins identified to be upregulated by LAMA1 in spheroid culture are displayed in Figure 6.9. STRING analysis identified that 81% of these proteins were part of one Protein-Protein interaction network (Figure 6.9 A). Furthermore, a group of 5 highly interactive proteins (Proteasome 20S Subunit Alpha 7 (PSMA7), Ribosomal Protein S8 (RPS8), Ribosomal Protein L8 (RPL8), Ribosomal Protein L13 (RPL13) and SEC61 Translocon Subunit Alpha 1 (SEC61A1)) were identified, as indicated by the red box in Figure 6.9 A. Additionally, another group of 4 highly interactive proteins (Replication Protein A1 [RPA1], Histone H2B type 1-K [HIST1H2BK], Histone H4 [HIST1H4A] and H1.3 Linker Histone [HIST1H1D]) were identified, as indicated by the blue box. However, KEGG pathway mapping analysis did not identify any pathways that were significantly associated with the input proteins.

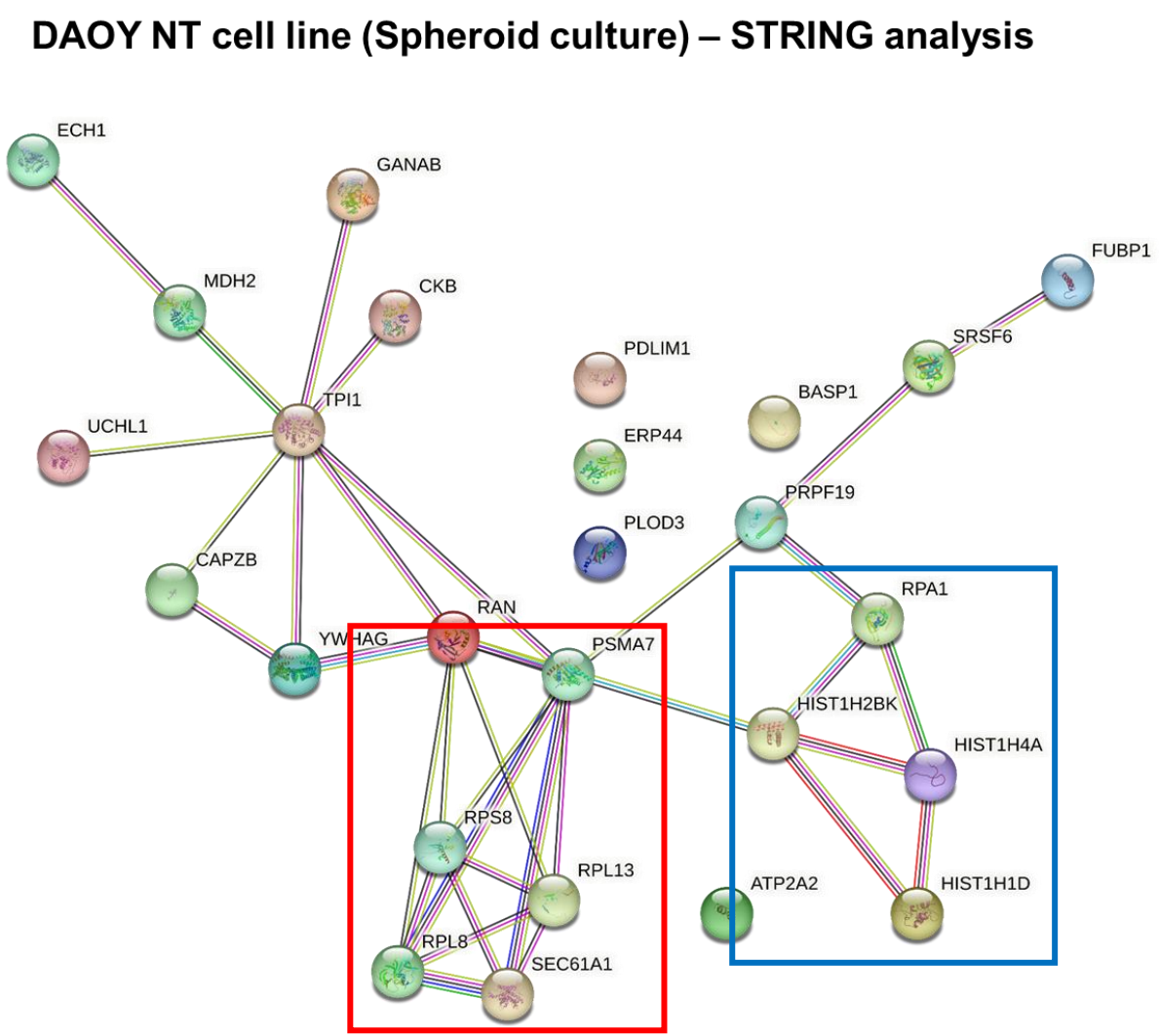


Figure 6.9 STRING Protein-Protein Interaction analysis of proteins identified to be upregulated by Laminin Subunit α1 (LAMA1) in day 1 spheroid culture, identifies one large interaction network of proteins. STRING Protein-Protein interaction analysis was conducted with a medium confidence score of 0.4. The number and colour of lines connecting nodes illustrates the 'active interaction sources' (curated databases: light blue, experimentally determined: pink, dark gene neighbourhood: green, gene fusions: red, gene co-occurrence: dark blue, textmining: light green, co-expression: black, protein homology: lilac) that were used to determine the interaction. Nodes within coloured boxes indicate groups of highly interactive proteins.

6.3.4 Analysis of proteins downregulated by LAMA1 in SHH medulloblastoma cells in spheroid culture

The results of the STRING and KEGG pathway mapping analyses of the 35 proteins identified to be downregulated by LAMA1 in spheroid culture are displayed in Figure 6.10. STRING analysis showed that 83% of these proteins were part of one large Protein-Protein interaction network (Figure 6.10 A). Furthermore, KEGG pathway mapping analysis demonstrated that the proteins were significantly associated with 13 different KEGG pathways (Figure 6.10 B). In addition, combined STRING and KEGG pathway mapping analysis identified that 4 highly interactive proteins (COL1A1, COL6A1, COL6A3 and ITGB1) were all part of the focal adhesion, PI3K-AKT signalling and ECM-receptor interaction KEGG pathways, as indicated by the red box in Figure 6.10 A. Moreover, another 3 proteins (Heat Shock Protein Family A Member 5 (HSPA5), Protein Disulfide Isomerase Family A Member 3 (PDIA3) and Calreticulin (CALR)) were also identified to be highly interactive and relate to the KEGG pathways protein processing in the endoplasmic reticulum and antigen processing and presentation, as indicated by the red box in Figure 6.10 A.

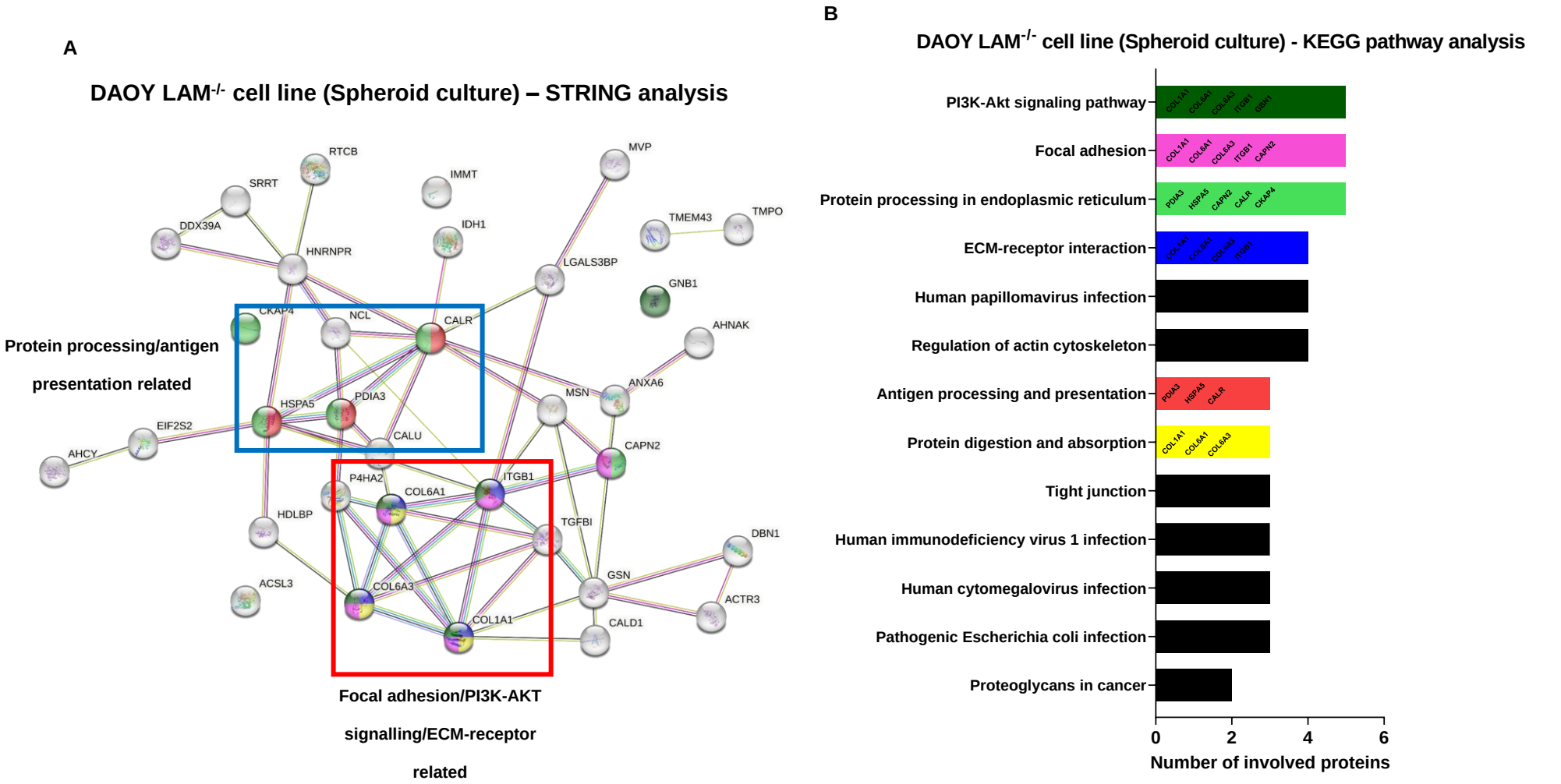


Figure 6.10 STRING Protein-Protein Interaction and Kyoto Encyclopaedia of Genes and Genomes (KEGG) pathway mapping analysis of proteins identified to be downregulated by Laminin Subunit α1 (LAMA1) in day 1 spheroid culture, identify 1 large interaction network of proteins, as well as 13 associated KEGG pathways, respectively. STRING Protein-Protein interaction analysis (**A**) was conducted with a medium confidence score of 0.4. The number and colour of lines connecting nodes illustrates the 'active interaction sources' (curated databases: light blue, experimentally determined: pink, dark gene neighbourhood: green, gene fusions: red, gene co-occurrence: dark blue, textmining: light green, co-expression: black, protein homology: lilac) that were used to determine the interaction. KEGG pathway mapping analysis (**B**) was conducted using the online bioinformatics tool DAVID. Significantly associated pathways were considered those where $p<0.05$. KEGG pathway mapping analysis was also conducted as part of the STRING analysis, allowing the colour of the protein nodes in the Protein-Protein interaction networks to be coordinated with the colour of the bars of each pathway in the KEGG pathway mapping analysis, indicating which proteins were used to identify the pathway. Bars that have been coloured black indicate where the KEGG pathway mapping analysis conducted by the STRING software did not overlap with that conducted using DAVID. Nodes within coloured boxes indicate groups of highly interactive proteins that are associated with the same KEGG pathways.

As in sections 6.3.1 and 6.3.2, we next wanted to elucidate the specific parts of the top pathways, identified by the KEGG pathway mapping analysis, that were being downregulated by LAMA1 in SHH medulloblastoma in spheroid culture. PI3K-AKT signalling and focal adhesion were two of the top pathways (Figure 6.10). By assessing the input proteins that were associated with both of these pathways we identified that 4 out of 5 of them were shared. These shared proteins were ITGB1, COL1A1, COL6A1 and COL6A3. This is also highlighted by the red box in Figure 6.10 A. Although the ECM-receptor interaction KEGG pathway was also identified by these proteins, we did not assess this pathway further, as it simply highlights the interaction between collagens and integrins, which has been previously illustrated (Figure 6.8). Interestingly, ITGB1 and COL1A1 were also identified as differentially regulated proteins in the DAOY LAM$^{-/-}$ cell line in 2D culture, whereas the collagen type-VI alpha subunits, COL6A1 and COL6A3, were only found to be differentially regulated in spheroid culture (Table 6.1 and 6.2).

The PI3K-AKT pathway is a highly conserved pathway which regulates a wide range of biological processes, including cell cycle progression, cell survival and proliferation, as well as apoptosis (Jiang *et al.*, 2020). In the PI3K-AKT pathway, PI3Ks are activated by ligand-cell surface receptor interactions, including ECM components binding to integrins, and chemokines, hormones and neurotransmitters binding to G-protein coupled receptors (GPCR). Active PI3Ks then primarily activate AKT, which is then able to modulate a diverse range of downstream pathways (Hemmings and Restuccia, 2012; Jiang *et al.*, 2020).

The components of the PI3K-AKT signalling KEGG pathway identified to be downregulated by LAMA1 in SHH medulloblastoma in spheroid culture were COL1A1, COL6A1, COL6A3, ITGB1 and G Protein Subunit Beta 1 (GNB1) (Figure 6.11). As displayed in Figure 6.11, the collagens COL1A1, COL6A1 and COL6A3 all bind to ITGB1 in order to activate PI3K, via FAK. Furthermore, GNB1 is a β subunit of a GPCR,

which activates PI3K, upon stimulation by either chemokines, hormones or neurotransmitters.

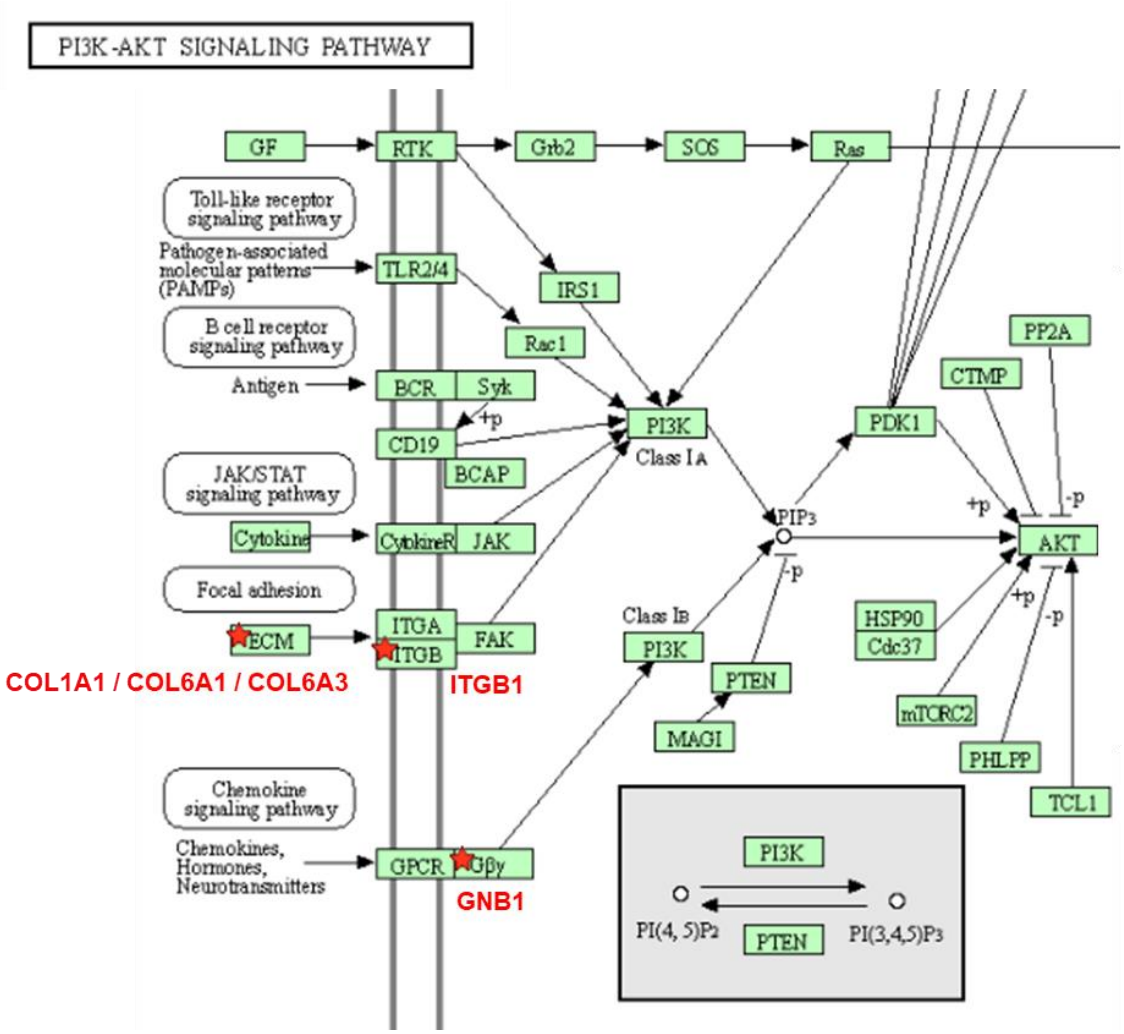


Figure 6.11 Kyoto Encyclopaedia of Genes and Genomes (KEGG) pathway mapping analysis of proteins downregulated by Laminin Subunit α1 (LAMA1) in spheroid culture, identifies phosphatidylinositol-3 kinase-AKT serine/threonine kinase 1 (PI3K-AKT) signalling as an associated KEGG pathway. The components of the PI3K-AKT signalling KEGG pathway, Collagen Type-I α1 Chain (COL1A1), Collagen Type-VI α1 Chain (COL6A1), Collagen Type-VI α3 Chain (COL6A3), Integrin Subunit Beta 1 (ITGB1) and G Protein Subunit Beta 1 (GNB1) were identified to be downregulated by LAMA1 in SHH medulloblastoma in spheroid culture. Red stars indicate where these proteins fall within the KEGG pathway. The gene names, aliases, components of a protein complex or alternative proteins within the pathway, which were used in the input of the analysis, are displayed next to their corresponding pathway protein in red text. The KEGG pathway diagram was generated as part of the KEGG pathway mapping analysis using the online bioinformatics tool DAVID.

Furthermore, focal adhesions (FA) are large protein assemblies formed in the plasma membrane upon the activation of integrins by a range of ECM components, including collagens and laminins (Zhu, Plow and Qin, 2021). FA facilitate the mechanical linkage of the cellular cytoskeleton to the surrounding ECM and transmit regulatory signals between the cell and the ECM in a bidirectional manner; furthermore, FA and FA signalling have been shown to have critical roles in cellular spreading, migration, proliferation and survival (Murphy *et al.*, 2020; Zhu, Plow and Qin, 2021; Schumacher *et al.*, 2022) Upon formation, FA can modulate a host of different downstream signalling pathways, a large proportion of which are mediated by the activation of FAK, through integrin signalling (Mishra and Manavathi, 2021). Interestingly, one the pathways that can be activated by FA formation is the PI3K-AKT signalling pathway.

The components of the FA KEGG pathway identified to be downregulated by LAMA1 in SHH medulloblastoma in spheroid culture were COL1A1, COL6A1, COL6A3, ITGB1 and CAPN2 (Figure 6.12). As displayed in Figure 6.12, the collagens COL1A1, COL6A1 and COL6A3 all bind to ITGB1 in order to activate FAK, which directly activates Calpain 2 (CAPN2) (Figure 6.12).

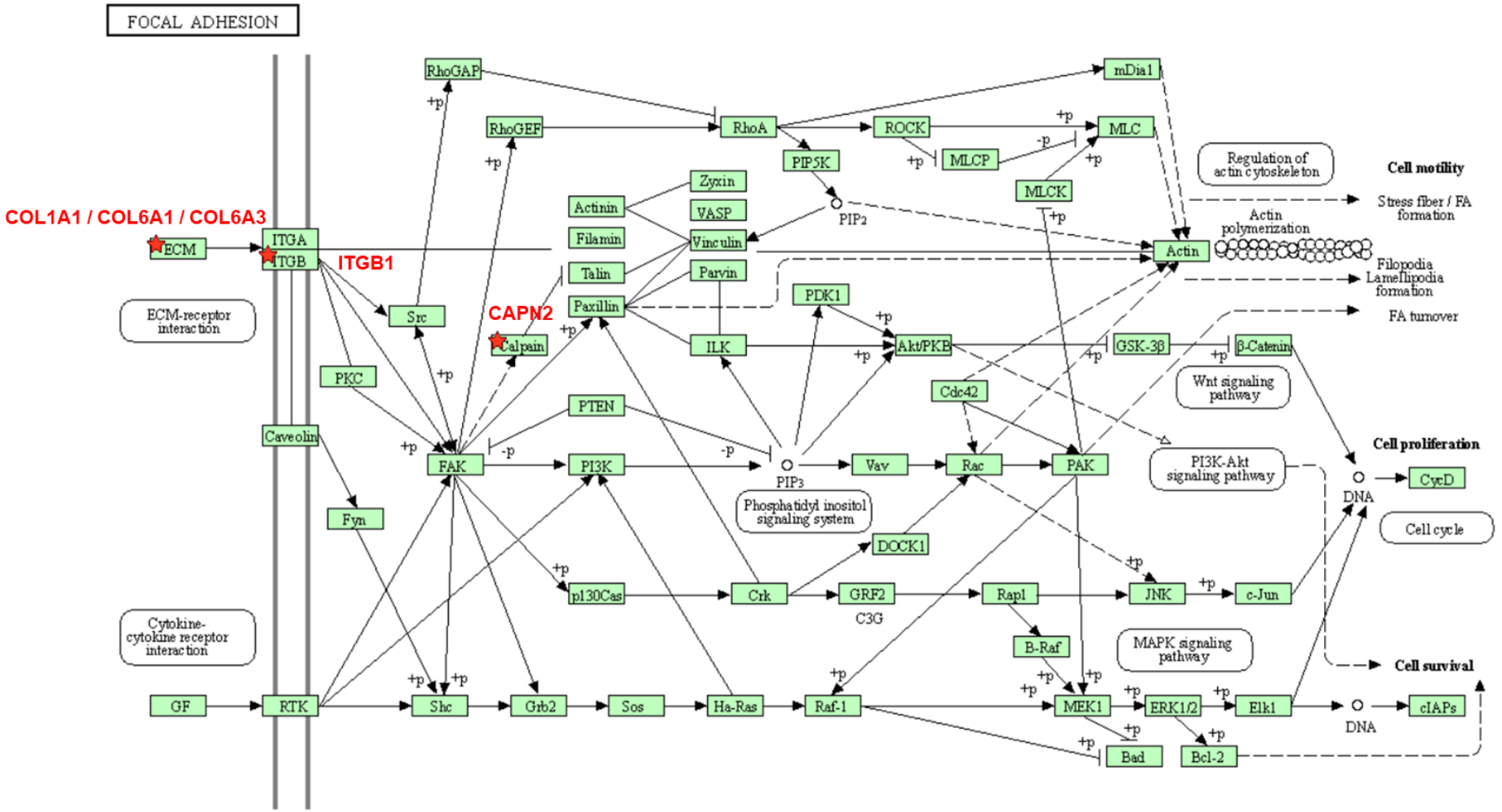


Figure 6.12 Kyoto Encyclopaedia of Genes and Genomes (KEGG) pathway mapping analysis of proteins downregulated by Laminin Subunit α1 (LAMA1) in spheroid culture, identifies focal adhesion signalling as an associated KEGG pathway. The components of the focal adhesion KEGG pathway, Collagen Type-I α1 Chain (COL1A1), Collagen Type-VI α1 Chain (COL6A1), Collagen Type-VI α3 Chain (COL6A3), Integrin Subunit Beta 1 (ITGB1) and Calpain 2 (CAPN2) were identified to be downregulated by LAMA1 in SHH medulloblastoma in spheroid culture. Red stars indicate where these proteins fall within the KEGG pathway. The gene names, aliases, components of a protein complex or alternative proteins within the pathway, which were used in the input of the analysis, are displayed next to their corresponding pathway protein in red text. The KEGG pathway diagram was generated as part of the KEGG pathway mapping analysis using the online bioinformatics tool DAVID.

Finally, protein processing in the endoplasmic reticulum (ER) was the other top KEGG pathway associated with the input proteins. The endoplasmic reticulum is a highly structured and complex organelle and contains many different proteins that are associated with its diverse range of functions. The ER primarily serves as a site for the synthesis of secreted and integral membrane proteins, the folding and post-translation modification of proteins, protein turnover, carbohydrate metabolism, lipid and steroid synthesis, calcium storage and apoptosis regulation (Schwarz and Blower, 2016).

The components of the endoplasmic reticulum KEGG pathway identified to be downregulated by LAMA1 in SHH medulloblastoma in spheroid culture were Cytoskeleton Associated Protein 4 (CKAP4), Heat Shock Protein Family A Member 5 (HSPA5), Protein Disulfide Isomerase Family A Member 3 (PDIA3), Calreticulin (CALR) and Calpain 2 (CAPN2) (Figure 6.13). As shown in Figure 6.13, CKAP4 plays a role in the anchoring of ribosomes. Furthermore, HSPA5 functions as a molecular chaperone which assists in the folding of proteins in the lumen of the ER. In addition, PDIA3 and CALR directly interact within the ER to regulate the folding of glycoproteins. Finally, CAPN2 is a calcium activated protease which is involved in the regulation of apoptosis. Interestingly, BCL-2, which we have shown to be upregulated by LAMA1 in spheroid culture, is an upstream regulator of CAPN2.

Similarly to the upregulation of the proteasome by LAMA1, the downregulation of protein processing in the endoplasmic reticulum by LAMA1 could also be a mechanism underpinning some the discrepancies observed between the gene and protein expression of the ‘laminin regulated genes’ in section 5.5. This is because protein modification (specifically glycosylation) by the endoplasmic reticulum can determine the stability and therefore the half-life of proteins in cells (Shental-Bechor and Levy, 2009). Thus, downregulation of this process could alter the rate at which proteins are degraded.

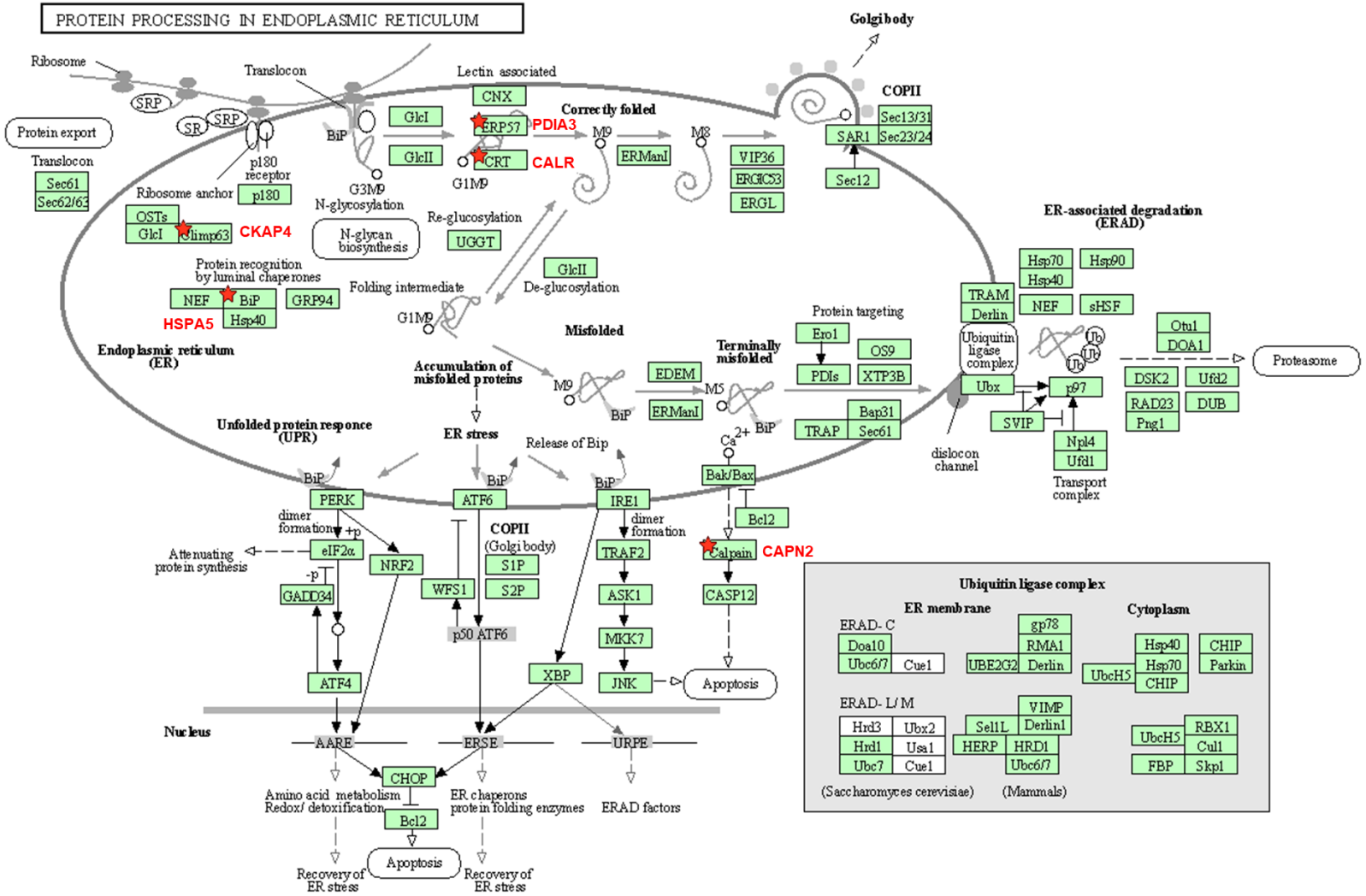


Figure 6.13 Kyoto Encyclopaedia of Genes and Genomes (KEGG) pathway mapping analysis of proteins downregulated by Laminin Subunit α1 (LAMA1) in spheroid culture, identifies protein processing in the endoplasmic reticulum as an associated KEGG pathway. The components of the protein processing in the endoplasmic reticulum KEGG pathway, Cytoskeleton Associated Protein 4 (CKAP4), Heat Shock Protein Family A Member 5 (HSPA5), Protein Disulfide Isomerase Family A Member 3 (PDIA3), Calreticulin (CALR) and Calpain 2 (CAPN2) were identified to be downregulated by LAMA1 in SHH medulloblastoma in spheroid culture. Red stars indicate where these proteins fall within the KEGG pathway. The gene names, aliases, components of a protein complex or alternative proteins within the pathway, which were used in the input of the analysis, are displayed next to their corresponding pathway protein in red text. The KEGG pathway diagram was generated as part of the KEGG pathway mapping analysis using the online bioinformatics tool DAVID.

In summary, this analysis revealed that pathways relating PI3K-AKT signalling/focal adhesion and protein processing in the endoplasmic reticulum were downregulated by LAMA1 in SHH medulloblastoma spheroid culture.

6.4 Identifying overlapping LAMA1 regulated proteins between 2D and spheroid culture

We next wanted to establish which of the LAMA1 regulated proteins were conserved across 2D and spheroid culture, as well as what molecular pathways they were part of, in order to delineate the differences in cellular behaviour that were observed between the cell lines in both culture methods. For example, the LAMA1-mediated upregulation of CD44 and BCL-2 protein expression was observed in both 2D culture and spheroid culture (section 5.4). This was achieved by overlapping the proteins identified to either be upregulated or downregulated by LAMA1 in 2D culture with those identified in spheroid culture (Figure 6.14 A and B). However, as shown in Figure 6.14 A, too few overlapping proteins were identified to conduct KEGG pathway analysis. Therefore, only STRING Protein-Protein interaction analysis was used, in order to assess how interactive the conserved, LAMA1 regulated proteins were (Figure 6.14 C and D).

As displayed in Figure 6.14 A, 8 proteins were found to be upregulated by LAMA1 in SHH medulloblastoma in both 2D and spheroid culture: Brain Abundant Membrane Attached Signal Protein 1 (BASP1), Glucosidase II Alpha Subunit (GANAB), Creatine Kinase B (CKB), Enoyl-CoA Hydratase 1 (ECH1), Ribosomal Protein S8 (RPS8), Tyrosine 3-Monooxygenase/Tryptophan 5-Monooxygenase Activation Protein Gamma (YWHAG), Capping Actin Protein Of Muscle Z-Line Subunit Beta (CAPZB) and Replication Protein A1 (RPA1). STRING Protein-Protein interaction analysis

demonstrated that only 2 of these proteins were interactive with each other: CAPZB and YWHAG (Figure 6.14 C).

Three proteins were found to be downregulated by LAMA1 in SHH medulloblastoma in both 2D and spheroid culture: Gelsolin (GSN), ITGB1 and COL1A1 (Figure 6.14 B). Furthermore, ITGB1 and GSN were both shown to interact with COL1A1 by STRING Protein-Protein interaction analysis (Figure 6.14 D). In addition, COL1A1 and ITGB1 interaction was also identified in the KEGG pathways found be associated with the proteins downregulated by LAMA1 in both 2D (proteoglycans in cancer) and spheroid (PI3K-AKT and focal adhesion) culture. These findings suggest that it may be the conserved LAMA1-mediated downregulation of COL1A1 and ITGB1, and the subsequent reduction in their interaction, that maintains some of the differences in cellular behaviour observed between the DAOY NT and DAOY $LAM^{-/-}$ cell lines.

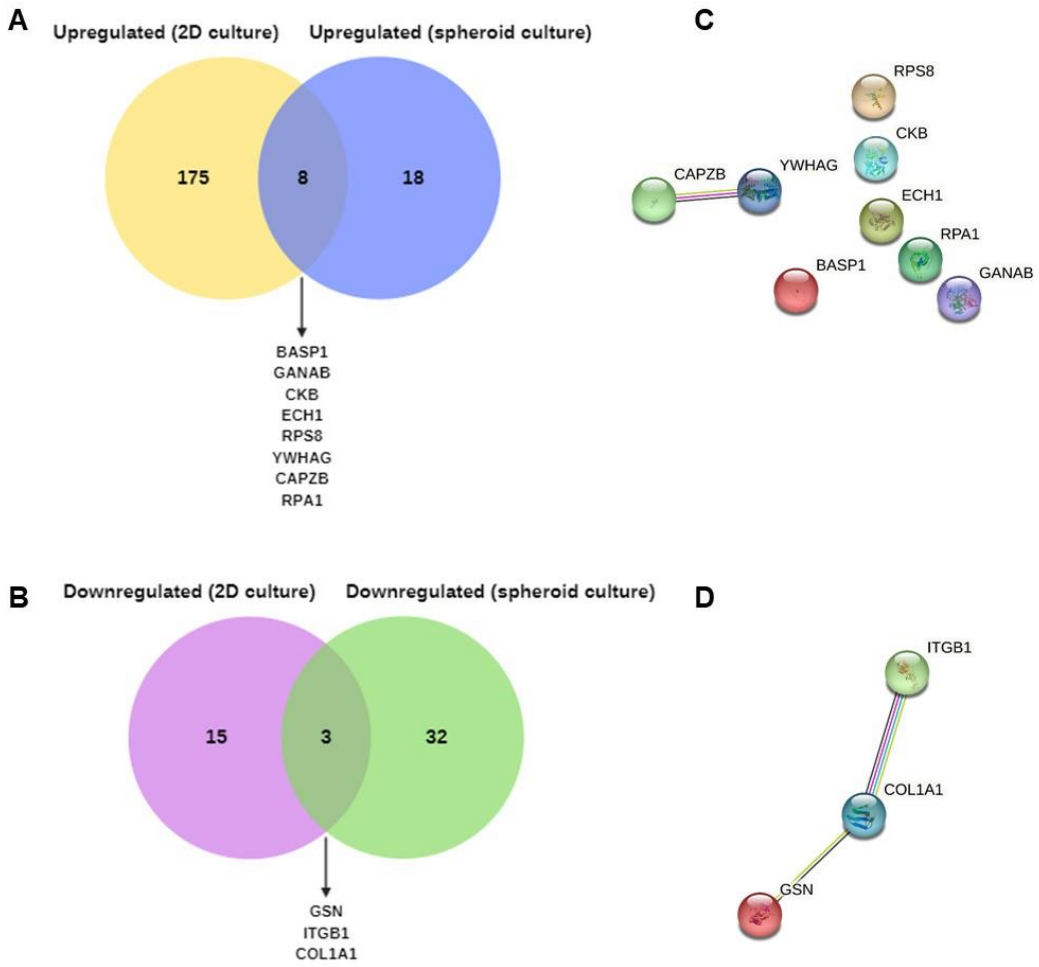


Figure 6.14 Laminin Subunit α1 (LAMA1) upregulates 8 proteins and downregulates 3 in SHH medulloblastoma cells in both 2D and spheroid culture. Proteins identified to be either upregulated (**A**) or downregulated (**B**) by LAMA1 in 2D culture, were overlapped those identified in spheroid culture. STRING Protein-Protein Interaction analysis was then conducted on the identified proteins in order to assess how interactive they were (**C** and **D**). STRING Protein-Protein interaction analysis was conducted with a medium confidence score of 0.4. The number and colour of lines connecting nodes illustrates the 'active interaction sources' (curated databases: light blue, experimentally determined: pink, dark gene neighbourhood: green, gene fusions: red, gene co-occurrence: dark blue, textmining: light green, co-expression: black, protein homology: lilac) that were used to determine the interaction.

Intriguingly, COL1A1 was also identified as a component of the ECM shell-like structure, which we previously demonstrated to form around SHH medulloblastoma cell lines when grown in spheroid culture (section 6.2). In addition, another component of the ECM shell, COL6A1, was also identified to exhibit increased expression in the

DAOY LAM$^{-/-}$ cell line (and therefore be downregulated by LAMA1), however, just in spheroid culture (Table 6.2). Since, we had already established that these ECM proteins were of importance with regards to the SHH medulloblastoma ECM, we decided to validate these findings by western blotting (Figure 6.15). As displayed in Figure 6.15, western blotting demonstrated that in 2D culture, COL1A1 protein expression was significantly greater in the DAOY LAM$^{-/-}$ cell line than the DAOY NT cell line, whereas COL6A1 expression remained unchanged. However, in spheroid culture the expression of both proteins was significantly greater in the DAOY LAM$^{-/-}$ cell line (Figure 6.20; $p<0.05$ for all comparisons). These findings corroborated those of the proteomics analysis and suggest that LAMA1 influences the expression of the other components of the SHH medulloblastoma ECM shell, COL1A1 and COL6A1, further illustrating their importance as components of the SHH medulloblastoma ECM.

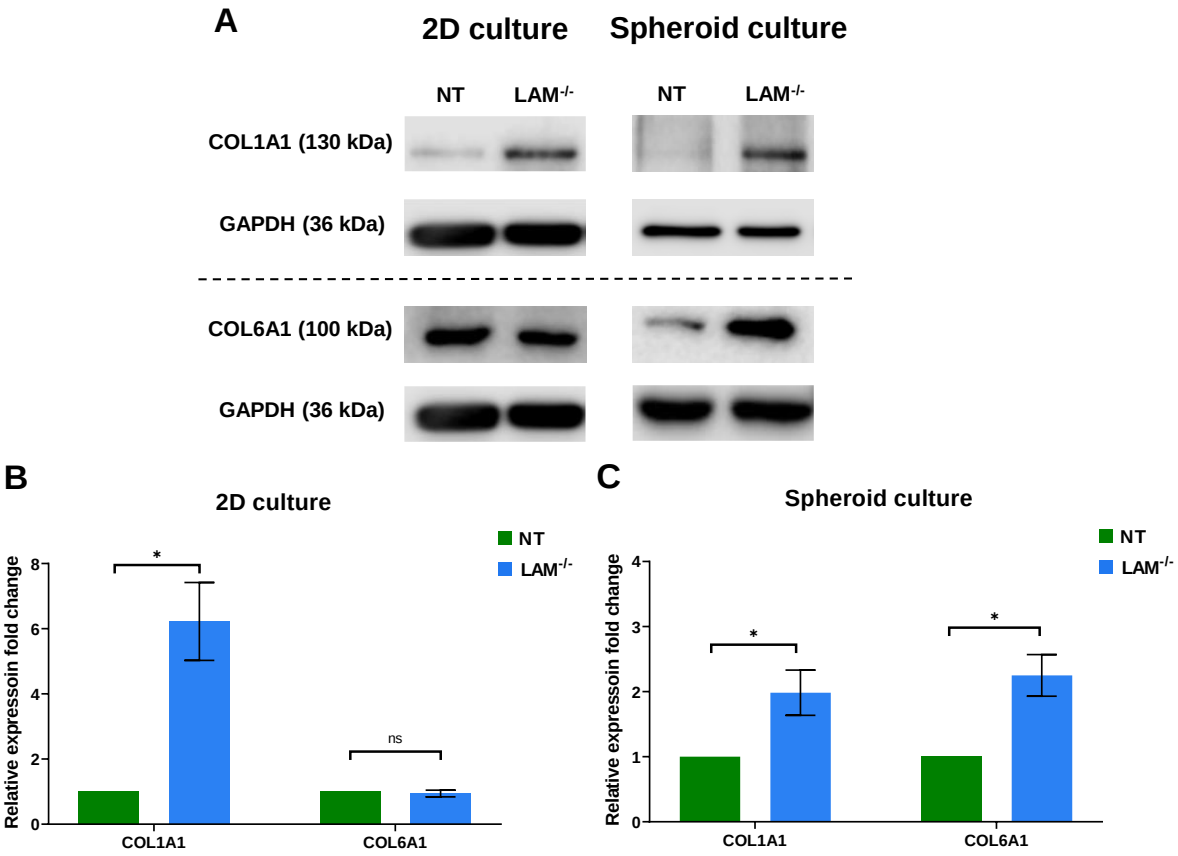


Figure 6.15 Western blotting analysis of Collagen Type-I α1 Chain (COL1A1) and Collagen Type-VI α1 Chain (COL6A1) protein expression in the DAOY NT and DAOY LAM$^{-/-}$ cell lines, suggests that they are regulated by Laminin Subunit α1 (LAMA1) in SHH medulloblastoma. Western blotting of COL1A1 and COL6A1 (**A**) indicated a significant increase in COL1A1 (2D and spheroid culture) and COL6A1 (spheroid culture) expression in in the DAOY LAM$^{-/-}$ cell line compared to the DAOY NT (**B** and **C**). Western blotting analyses were conducted relative to GAPDH as a loading control. Protein expression in the DAOY LAM$^{-/-}$ cell line was then normalised to the DAOY NT cell line, in order to calculate relative fold changes in protein expression. Representative blots are shown. Full length, exemplar blots of the antibodies used here can be observed in Appendix Figure 1. Mean ± SEM plotted; n=3. Significance was assessed by an unpaired t-test; *p<0.05, **p≤0.01.

6.5 Summary points

- LAMA1 regulated proteins were identified in 2D and spheroid culture using 4 differential expression analysis methods, 2 of which utilised a LC-MS/MS statistical analysis methodology described by Aguilan *et al*.

- In 2D culture, 183 proteins were identified to be upregulated by LAMA1 in SHH medulloblastoma cells, whereas 18 proteins were identified to be downregulated.

- In spheroid culture, 26 proteins were identified to be upregulated by LAMA1 in SHH medulloblastoma cells, whereas 35 proteins were identified to be downregulated.

- The KEGG pathways relating to metabolic pathways, the proteasome and estrogen signalling, were associated with the proteins upregulated by LAMA1 in 2D culture.

- The KEGG pathway relating to proteoglycans in cancer was associated with the proteins downregulated by LAMA1 in 2D culture.

- The KEGG pathways related to PI3K-AKT signalling, focal adhesion and protein processing in the endoplasmic reticulum, were associated with the proteins downregulated by LAMA1 in spheroid culture.

- Eight proteins were found to be upregulated by LAMA1 in both 2D and spheroid culture: BASP1, GANAB, CKB, ECH1, RPS8, YWHAG, CAPZB and RPA1. However, STRING analysis demonstrated that they exhibit little interaction.

- Three proteins were found to be downregulated by LAMA1 in both 2D and spheroid culture: GSN, ITGB1 and COL1A1. STRING analysis demonstrated that both GSN and ITGB1 interact with COL1A1.

- Western blotting validated that COL1A1 and COL6A1, members of the previously identified SHH medulloblastoma ECM shell structure, are downregulated by LAMA1 in 2D (just COL1A1) and spheroid culture, suggesting that LAMA1 influences the expression of COL1A1 and COL6A1 in SHH medulloblastoma.

Chapter 7: Discussion

7.1 Introduction

The ECM is a highly dynamic web of macromolecules including proteoglycans, glycoproteins and fibrous proteins such collagens and laminins. It provides structural support to tissues and also regulates cellular differentiation, motility, survival and development, by interacting with specific cellular receptors, as well as controlling concentration gradients of cytokines and growth factors (Pickup, Mouw and Weaver, 2014). More recently, it has been shown that tumours often form an aberrant ECM which influences tumour progression and can have significant, pro- or anti-tumorigenic effects (Ayoub *et al.*, 2020; Henke, Nandigama and Ergün, 2020). Hence, it has been hypothesised that the characterisation of tumour ECM composition and organisation, could become an important aspect of predicting patient outcome in clinical settings and an avenue for therapeutic targeting (Ayoub *et al.*, 2020).

Our understanding of the medulloblastoma ECM is currently in its infancy, with it being the focus of only a few studies to date, one of which was recently conducted in our group. In this study ECM sub-types, that could predict patient outcome, were identified within the medulloblastoma sub-groups, through the analysis of the largest publicly available medulloblastoma dataset (Cavalli dataset) and the immunohistochemical staining of patient TMAs (Linke *et al.*, 2020). Two of these ECM sub-types were defined by either high or low *LAMA1/LAMA2* gene expression in SHH patients (LAM^{high} and LAM^{low} ECM sub-types respectively). LAM^{high} SHH medulloblastoma patients were found to be associated with a more favourable overall survival, whereas LAM^{low} patients were associated with worse survival (Linke *et al.*, 2020). In this thesis we aimed to build on these findings and study the role of *LAMA1/LAMA2* in the progression of SHH medulloblastoma and therefore delineate how their expression influences SHH medulloblastoma patient survival.

7.2 The composition and prognostic significance of the SHH medulloblastoma ECM shell

In the above mentioned study by our group (Linke *et al*., 2020), the DAOY and ONS-76 SHH medulloblastoma cell lines were shown to form a sub-group specific laminin-111/211 (LAMA1/LAMA2) shell-like structure when grown in 3D hydrogel culture for 3 weeks, which we have shown here to also be formed by the same cell lines in spheroid culture. We hypothesised that this sub-group specific shell-like structure may have a role in the differential survival exhibited by *LAM*^{high} and *LAM*^{low} SHH medulloblastoma patients. We therefore wanted to fully characterise the laminin-111/211 shell-like structure by determining if it comprised any other ECM components and establish their effect on patient survival.

7.2.1 SHH medulloblastoma cell lines form a multicomponent ECM shell-like structure in long-term 3D culture

During the course of this PhD, a study by Trombetta-Lima *et al.* identified a 19 ECM protein signature in medulloblastoma tumours, through proteomic analysis of decellularised patient tumours and the immunohistochemical staining of patient TMAs (Trombetta-Lima *et al.*, 2021). By cross referencing the genes upregulated in *LAM*^{high} SHH medulloblastoma patient tumours in the Cavalli dataset, with these 19 medulloblastoma ECM signature proteins, we identified 8 additional *LAM*^{high} SHH medulloblastoma ECM components. Of these 8, we validated that type-I (COL1A1) and type-VI (COL6A1) collagen, as well as the small leucine rich proteoglycan LUM, were also additional components of the SHH medulloblastoma laminin-111/211 shell-like structure, by immunohistochemical staining of long-term DAOY and ONS-76 spheroids. Furthermore, in a study by our group (Linke, Johnson *et al.*, 2023), the cell lines were also shown to form COL1A1, COL6A1 and LUM shell-like structures when

they were grown in long-term hyaluronan hydrogel culture. In line with these findings, a study by Conklin *et al* demonstrated that collagen fibres are enriched and aligned at the periphery of breast carcinoma (Conklin *et al.*, 2011). Moreover, a study by Jeanne *et al* demonstrated that LUM is also almost exclusively expressed at the periphery of melanoma allografts in mice (Jeanne *et al.*, 2017).

We hypothesise that each of these ECM components plays a specific function within the SHH medulloblastoma ECM shell. Firstly, the collagens (COL1A1 and COL6A1) may hold the shell together, since they are large proteins which form macromolecular networks, whose chief function is to provide mechanical support in tissues (Shoulders and Raines, 2009). In addition, since the primary function of LUM is to direct collagen fibrillogenesis, and it was found to be expressed on the outermost periphery of SHH medulloblastoma spheroids, this suggest that LUM may direct the deposition and organisation of the collagenous parts of the ECM shell, as they are deposited by the cells (Kalamajski and Oldberg, 2010; Lopez and Bonassar, 2021). In line with this, in the aforementioned study by Jeanne *et al* it was also demonstrated that the knockout of LUM significantly decreases tumoural collagen deposition (Jeanne *et al.*, 2017). Furthermore, we have demonstrated that without the expression of LAMA1, DAOY $LAM^{-/-}$ SHH medulloblastoma cells are unable to form a viable spheroid capable of growth, with cells on the periphery seemingly unable to adhere to the main spheroid structure. Therefore, since one the primary functions of LAMA1 is to bind collagens together in basement membranes, it is reasonable to propose that LAMA1 interlinks the collagenous components of the ECM shell-like structure (Aumailley, 2013). We propose that LAM^{high} SHH medulloblastomas form an ECM shell as depicted in Figure 7.1.

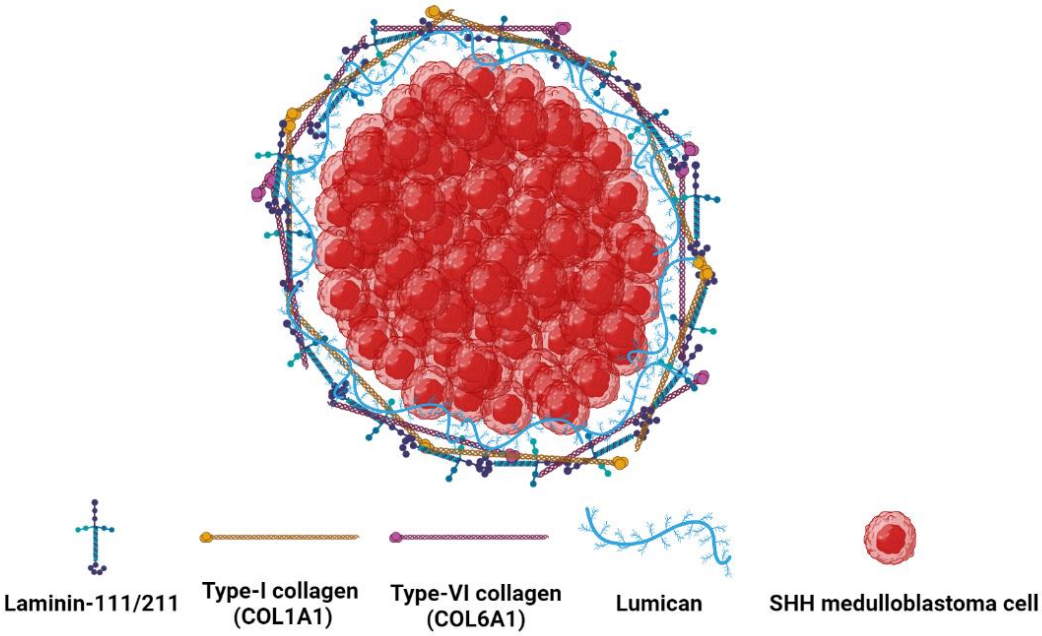


Figure 7.1 Hypothesised extracellular matrix (ECM) shell-like structure comprised of laminin-111/211, collagens and lumican, formed by *LAM*^{high} SHH medulloblastoma tumours based on the findings of this study.

However, we have also shown that when the DAOY LAM$^{-/-}$ spheroids are embedded in a hyaluronan (the backbone of the brain ECM) hydrogel they are capable of growth, therefore indicating that LAMA1 is not essential for the growth of SHH medulloblastoma cells in a brain-specific ECM. Conversely, it has been demonstrated that a biallelic knockout of LAMA1 was lethal in mouse embryos (Heng *et al.*, 2011; Ichikawa-Tomikawa *et al.*, 2012). However, as we were able to generate a biallelic LAMA1 knockout in SHH medulloblastoma cells, this suggests that LAMA1 expression is not essential to the survival of SHH medulloblastoma. This finding is line with the fact the *LAM*^{low} tumours exhibit a low level of LAMA1 gene expression but are still highly aggressive tumours.

7.2.2 Expression of the SHH medulloblastoma ECM shell components is associated with a more favourable patient survival

In this study we also demonstrated that high expression of the other components of the ECM shell, COL1A1, COL6A1 and LUM, were all also associated with more favourable overall survival in SHH medulloblastoma patients in the Cavalli dataset, further corroborating the finding that they are part of the same ECM shell-like structure as laminin-111/211. In support of this, several studies have also demonstrated that tumoural expression of collagens and LUM is associated with better patient outcome (Troup *et al.*, 2003; Coulson-Thomas *et al.*, 2013; De Wit *et al.*, 2013; Li *et al.*, 2014, 2019; Jeanne *et al.*, 2017).

In the process of identifying of COL1A1, COL6A1 and LUM, we also identified COL6A3, COL5A1, FBLN5 and FBN1 as LAM^{high} SHH medulloblastoma ECM shell component candidates. Expression of these other ECM proteins was also correlated with significantly more favourable overall survival in SHH medulloblastoma patients in the Cavalli dataset, suggesting that they may also comprise the ECM shell-like structure. However, further immunohistochemical staining of SHH medulloblastoma cell lines grow in long-term spheroid and hydrogel culture would be needed to confirm this.

Taken together, these findings suggest that the previously identified LAM^{high} SHH medulloblastoma tumours may in fact be ECM^{high} tumours. Furthermore, as we found that none of the 19 medulloblastoma ECM signature proteins were also expressed by LAM^{low} SHH medulloblastomas, this indicates that they may in fact be ECM^{low}. Future work should therefore aim to further validate these findings by staining SHH medulloblastoma patient TMAs for a combination of the ECM components, to assess if they can be used predict a more favourable patient outcome. The expression of these ECM proteins could then be used to identify low-risk SHH medulloblastoma patients, who may benefit from deescalated treatment regimens to avoid the long-term

sequela often associated with medulloblastoma treatment. In addition, the same process of identifying and validating medulloblastoma-specific ECM components should be repeated on the *LAM*^{high} and *LAM*^{low} Group 4 patients in the Cavalli dataset, since the inverse trend in survival was associated with these medulloblastoma ECM sub-types (Linke *et al.*, 2020). The expression of these Group 4 *LAM*^{high} ECM proteins could then also be assessed in patient TMAs to determine if they can be used to predict patient outcome in Group 4 medulloblastoma, and therefore inform treatment regimens.

One limitation of these findings is that the ECM components we have identified and validated in this study are only the ones deposited by SHH medulloblastoma cells *in vitro*. Other resident cell types in the brain TME, such as astrocytes, are also able to deposit ECM components (Wiese, Karus and Faissner, 2012; Wade *et al.*, 2013). In fact, one recent study demonstrated that the ability of primary SHH medulloblastoma cells to form tumouroids was dependant on astrocyte derived ECM (Cheng *et al.*, 2020). Furthermore, since the Cavalli dataset is comprised of genomic analysis of bulk tumours, other cell types of the medulloblastoma TME only represent a small proportion of the total cells from which mRNA was extracted. Therefore, if any of the medulloblastoma ECM signature proteins were deposited by cells within the TME, they may have been missed in the analysis of this dataset.

7.3 The role of LAMA1 in the migration and invasion of SHH medulloblastoma

The ability of tumour cells to migrate and invade into surrounding tissues is key to tumour progression and is mediated by a host of different cell surface receptors, ECM components and ECM digesting enzymes (Winkler *et al.*, 2020). The migration and invasion of medulloblastoma cells facilitates the formation of leptomeningeal

metastases, a key clinical feature of medulloblastoma progression, which is one of the predominant causes of morbidity and mortality in patients (Van Ommeren *et al.*, 2020). Thus, understanding how LAMA1 affects the migration and invasion of SHH medulloblastoma may be crucial to delineating the differential survival exhibited by *LAM*^{high} and *LAM*^{low} medulloblastoma patients. We therefore investigated the role that LAMA1 has on the migration and invasion of SHH medulloblastoma using the LAMA1 knockout DAOY cell line (DAOY LAM$^{-/-}$) in Transwell® migration and invasion assays, as well as a spheroid-hydrogel migration assay.

7.3.1 LAMA1 has a role in cellular migration in SHH medulloblastoma

LAMA1 has been shown to support the migration of several different tumour types (Kikkawa *et al.*, 2013). Furthermore, a study by Heng *et al* demonstrated that LAMA1 has an essential role in the migration of granule cell precursors (GCP; the cell of origin for SHH medulloblastomas) during the development of the cerebellum. Using a conditional LAMA1 knockout mouse model, it was demonstrated that without LAMA1, GCPs were unable to properly migrate into the internal granule layer (IGL) of the cerebellum and thus accumulated in the external granule layer (EGL) in a pre-migratory proliferative state. This excessive proliferation of GCPs in the EGL was counteracted by massive cell death between postnatal day 7 and 20, resulting in a smaller cerebellum in LAMA1 knockout mice (Heng *et al.*, 2011).

Considering these findings, it was therefore unsurprising that we observed a reduction in migration in the DAOY LAM$^{-/-}$ cell line in both the Transwell® and spheroid-hydrogel migration assays, thus suggesting that LAMA1 has a role in the migration of SHH medulloblastoma cells. However, in the spheroid-hydrogel model, cells are required to migrate across the top of a brain representative hyaluronan hydrogel, for which CD44 is the primary receptor. Furthermore, CD44 has been shown to be upregulated in many

tumour types, including medulloblastoma, and has a key role in promoting tumour migration through its direct interaction with hyaluronan, which facilitates cellular adhesion, as well as stimulating downstream signalling pathways (Senbanjo and Chellaiah, 2017; Qi *et al.*, 2019). Therefore, given that the DAOY LAM$^{-/-}$ cell line also exhibited reduced CD44 protein expression, this could mean that the reduction in migration observed in this assay could be in part due to a reduction in CD44-hyaluronan adhesion and signalling, not just the lack of LAMA1. To further validate the effect of just LAMA1 on cellular migration the spheroid-hydrogel model should therefore be repeated using a different hyaluronan-free hydrogel. The results of this could then be compared with the spheroid-hyaluronan hydrogel model to determine the combined effect of the LAMA1 knockout and reduction in CD44 protein expression on migration in SHH medulloblastoma.

In summary, our findings indicate that LAMA1 may have a direct role in the migration of SHH medulloblastoma cells, as well as an indirect role in cellular adhesion to the backbone of the brain ECM, hyaluronan, through the upregulation of CD44 expression. This suggests that *LAM*^{low} SHH medulloblastoma tumours may in fact be less migratory than *LAM*^{high}, meaning that this aspect of tumour progression is unlikely to underpin the worse overall survival exhibited by *LAM*^{low} tumours, since cellular migration is required for metastasis which is associated with worse patient survival. There may however be many other aspects of tumour biology underlying the aggressive nature of these tumours e.g., therapy resistance.

7.3.2 The influence of LAMA1 in the invasion of SHH medulloblastoma is unclear

LAMA1 has been shown to both promote and hinder the invasion of tumour cells, leaving its function in tumour invasion unclear (Kikkawa *et al.*, 2013). In this study, we

have shown that in a Transwell® invasion assay, where inserts are coated with type-IV collagen to represent a basement membrane, LAMA1 does not have a significant effect on invasion in SHH medulloblastoma cells. However, this result was unexpected due to the significant increase in the secretion of the ECM remodelling enzymes MMP-2 and Pro-MMP-9 exhibited by the DAOY LAM$^{-/-}$ cell line. These enzymes have been shown to be upregulated by many tumours types, including medulloblastoma, and are vital for the degradation of the ECM and subsequent cellular invasion in cancer (Popova and Jücker, 2022). Furthermore, they are both able to degrade type-IV collagen, the coating of the insert in the invasion assay used in this study, which led us to predict that the DAOY LAM$^{-/-}$ cell line would have been found to be more invasive in this model (Jezierska and Motyl, 2009; Jabłońska-Trypuć *et al.*, 2016).

There are 2 potential reasons that could explain why our prediction was wrong. Firstly, in order for MMP-9 to degrade type-IV collagen in tumours, it forms a complex with CD44 on the surface of cells, a protein which we have shown to exhibit significantly reduced expression in the DAOY LAM$^{-/-}$ cell line (Yu and Stamenkovic, 1999; Senbanjo and Chellaiah, 2017). This could have meant that although the DAOY LAM$^{-/-}$ cell line secreted more MMP-9, it was unable to degrade collagen-IV at an increased rate compared to the DAOY NT cell line, as is possessed fewer CD44 receptors for MMP-9 to complex with and was thus not found to be more invasive in this model. Although, it is worth mentioning that there is no evidence to indicate that MMP-2, the secretion of which we have also shown to be increased in the DAOY LAM$^{-/-}$ cell line, requires CD44 complexation to degrade type-IV collagen. Secondly, this finding could also be attributed to the fact that the DAOY LAM$^{-/-}$ cells are less migratory, as discussed above. Therefore, even though they may have been able to digest the type-IV collagen coating more easily, through increased MMP-2 secretion, the cells would have still been unable to subsequently migrate through the pores of the insert as quickly as the DAOY NT cells. This could explain why the 'invasion' of the DAOY LAM$^{-/-}$ cell line in the

Transwell® model was found to be more similar to the DAOY NT cell line, and the significant difference between them observed in the Transwell® migration assay was lost.

In order to overcome these limitations, as part of future work, the Transwell® invasion model should be repeated but with a coating of a different type of collagen that can be digested by MMP-9 independently of CD44 complexation, and is found in the brain, such as type-V collagen. This would allow the effect of the increased secretion of MMPs exhibited by the DAOY LAM$^{-/-}$ on invasion to be assessed more accurately. Furthermore, to assess the effect of LAMA1 on the invasive capacity of cells in a 3D-hydrogel context, a spheroid-hydrogel invasion assay, which allows for the formation of invadopodia (cell structures which allow cancer cells to penetrate basement membranes) should also be conducted as part of future work. However, the majority of spheroid-hydrogel invasion models utilise hydrogels such as basement membrane extract (BME) from Engelbreth-Holm-Swarm (EHS) mouse sarcoma (e.g. Matrigel), which contains a heterogeneous mix of different ECM proteins, including laminin-111 (Vinci, Box and Eccles, 2015; Tevis *et al.*, 2017; Aisenbrey and Murphy, 2020; Nazari, 2020). Using BME would therefore mask the effect of the LAMA1 knockout in the DAOY LAM$^{-/-}$ cell line. Thus, a customisable ECM-free hydrogel (as proposed in section 7.2.2) should be used in this model and specific ECM factors such as collagens could then be added in to represent basement membranes and replicate the invasion of tumours.

To summarise, although the increased MMP-2 and Pro-MMP-9 secretion exhibited by the DAOY LAM$^{-/-}$ cell line suggests a more invasive phenotype, these findings leave the role of LAMA1 in the invasion of SHH medulloblastoma unclear and further work, using an adapted Transwell® and alternative hydrogel invasion models, are required to delineate its effect.

7.4 LAMA1 has conflicting roles in apoptosis between 2D and 3D spheroid-hydrogel models

Apoptosis is a highly conserved cell death pathway that has a key role in cancer prevention (Letai, 2017; Singh, Letai and Sarosiek, 2019). Thus, an essential part of tumour progression is evading apoptosis (Letai, 2017). Moreover, this process is considered as one of the hallmarks of cancer (Hanahan and Weinberg, 2011; Hanahan, 2022). One of the most prominent mechanisms by which tumours evade apoptosis is through the upregulation of the anti-apoptotic BCL-2 family proteins, BCL-2, B-cell Lymphoma-Extra Large (BCL-X_L) and Myeloid Leukaemia Cell Differentiation Protein (MCL-1), which bind and sequester pro-apoptotic signals, as well as the pro-apoptotic BCL-2 family effector proteins BCL-2 Associated X-protein (BAX) and BCL-2 Antagonist/Killer (BAK), resulting in the inhibition of the intrinsic apoptosis pathway (Singh, Letai and Sarosiek, 2019). The anti-apoptotic BCL-2 family protein, BCL-2, is highly expressed in medulloblastoma, where it has been shown by several studies to have a role in apoptosis evasion (Nakasu *et al.*, 1994; Schiffer *et al.*, 1996; Schüller, Schober, Kretzschmar and Herms, 2004; Bar *et al.*, 2007; Levesley *et al.*, 2011; Wen *et al.*, 2011; Othman *et al.*, 2014; Lin *et al.*, 2016). Furthermore, it has been demonstrated that laminin-111 upregulates BCL-2 expression in ovarian cancer (Yoshida *et al.*, 2001). In line with this we have shown here that BCL-2 is downregulated in the DAOY LAM$^{-/-}$ SHH medulloblastoma cell line in both 2D culture and day 1 spheroids. These results suggested that LAMA1 may have a role in the regulation of apoptosis in SHH medulloblastoma and that DAOY LAM$^{-/-}$ cells may therefore be more prone to apoptosis. We investigated this by assessing the sensitivity of the DAOY NT and DAOY LAM$^{-/-}$ cells lines to the BCL-2 small-molecule inhibitor ABT-737 in a 2D drug response assay and a spheroid-hydrogel drug assay.

In the 2D drug response assay, DAOY LAM$^{-/-}$ cells were more sensitive to ABT-737 than the DAOY NT cell line. In addition, apoptosis assays indicated that DAOY LAM$^{-/-}$

cells also exhibited a greater increase in apoptosis in response to ABT-737 treatment. These results initially indicated that the upregulation of BCL-2 by LAMA1 may be a mechanism of apoptosis evasion in SHH medulloblastomas. However, the 3D spheroid-hydrogel drug assay suggested that the inverse trend was true and that DAOY LAM$^{-/-}$ spheroids were in fact less sensitive to ABT-737, indicating that when embedded in a hyaluronan hydrogel an anti-apoptotic mechanism is activated in DAOY LAM$^{-/-}$ spheroids, allowing them to evade ABT-737 induced apoptosis.

However, there are several limitations to these findings. Firstly, because it was not possible to extract sufficient protein for analysis from the spheroids embedded in hydrogels, we were unable to assess if the reduced expression of BCL-2 in the DAOY LAM$^{-/-}$ cell line was maintained in this model. Furthermore, in the spheroid-hydrogel drug assays we were unable to measure the level of apoptosis or the viability of the spheroids in response to ABT-737, as we did in 2D culture, and were only able to use spheroid volume as an indication of spheroid viability. This meant that we cannot draw definitive conclusions regarding the effect ABT-737 on the spheroids in this assay. Finally, ABT-737 is also a BCL-X_L inhibitor which means that to more conclusively demonstrate that the difference in ABT-737 sensitivity exhibited by the DAOY NT and DAOY LAM$^{-/-}$ cell lines in the 2D and spheroid-hydrogel assays was a consequence of altered BCL-2 expression, the protein expression of BCL-X_L should also be assessed in the cell lines. However, as mentioned above this would not be possible for spheroids embedded in hydrogel due to the low protein yield. To mitigate these limitations, the sensitivity of the DAOY NT and DAOY LAM$^{-/-}$ cell lines to ABT-737 and their expression of BCL-2 and BCL-X_L should be assessed in a different hydrogel model which supports the growth of the cell lines long-term as either a spheroid or as single cells. The growth of the cell lines in such a model would mean that there would be a much greater cell number than the ~500 cells/spheroid in the spheroid-hydrogel model shown here, and

would likely mean that it would be possible to measure cell viability, the level of cellular apoptosis and extract sufficient protein for analysis.

In summary, the finding that the knockout of LAMA1 decreases the sensitivity of SHH medulloblastoma cells to ABT-737 induced apoptosis in a spheroid-hydrogel culture model, suggests that an anti-apoptotic/drug resistance mechanism is activated in DAOY LAM$^{-/-}$ spheroids embedded in hyaluronan hydrogel. This could mean that this mechanism is activated in *LAM*^{low} SHH medulloblastoma patients, enabling the tumours to become more resistant to apoptosis than *LAM*^{high} tumours, and may be part of the reason that *LAM*^{low} tumours are correlated with a worse overall survival. However, a considerable amount of further investigation would be required to demonstrate this.

7.5 LAMA1 increases vincristine sensitivity in SHH medulloblastoma in a 3D spheroid-hydrogel model

Chemotherapy remains one of the primary tools used in medulloblastoma treatment regimens (Northcott *et al.*, 2019). Furthermore, resistance to chemotherapy, after gross total surgical resection of the tumour, has been hypothesised to facilitate medulloblastoma relapse, which is almost universally fatal (Pizer and Clifford, 2009). In addition, it has been previously reported that laminins (including laminin-111) are specifically involved in drug resistance pathways in several tumour types (Fridman *et al.*, 1990; Sethi *et al.*, 1999; Cordes *et al.*, 2009; Işeri *et al.*, 2010). Therefore, an understanding of how LAMA1 affects the sensitivity of SHH medulloblastoma cells to relevant chemotherapies is vital to delineating how it confers differential survival in the *LAM*^{high} and *LAM*^{low} SHH medulloblastoma ECM sub-types.

We investigated this by assessing the sensitivity of DAOY NT and DAOY LAM$^{-/-}$ cells lines to the medulloblastoma standard of care chemotherapeutics vincristine and cisplatin, in a 2D drug response assay and a spheroid-hydrogel drug assay. In the 2D drug response assay we found no significant difference in the vincristine and cisplatin IC_{50} values between the cell lines, although, the DAOY LAM$^{-/-}$ cell line did exhibit decreased sensitivity to the highest concentrations of vincristine. These results initially suggested that the knockout of LAMA1 did not significantly alter the sensitivity of SHH medulloblastoma cells to these chemotherapeutics, although it did confer some level of decreased vincristine sensitivity. The 3D spheroid-hydrogel drug assay also indicated that the DAOY LAM$^{-/-}$ spheroids were less sensitive to vincristine, as did the results of the ABT-737 3D spheroid-hydrogel drug assay. These findings suggest that a LAMA1-independent drug resistance mechanism is activated in DAOY LAM$^{-/-}$ spheroids when embedded in hyaluronan hydrogel, allowing them to evade vincristine induced apoptosis. Furthermore, since the DAOY LAM$^{-/-}$ spheroids were specifically less sensitive to vincristine and not cisplatin, this suggests that this hypothesised LAMA1-independent drug resistance mechanism may render cells less sensitive to the inhibition of microtubule polymerisation (the mechanism of action of vincristine), but not the alkylation of DNA (the mechanism of action of cisplatin) (Below and Das, 2022; Gold and Raja, 2022).

The limitations of these findings are similar to those discussed in the previous section and mainly pertain to the lack of viability data in the spheroid-hydrogel model. Without it, we cannot draw definitive conclusions regarding the effect vincristine and cisplatin on the spheroids in this assay. In addition, only the highest concentrations of ABT-737 and cisplatin caused a significant reduction in the outgrowth of spheroids in this assay, suggesting that there may be limited drug penetration into the hydrogel. This also suggests that findings derived from this assay may be limited. Therefore, the sensitivity of the DAOY NT and DAOY LAM$^{-/-}$ cell lines to vincristine and cisplatin should be

assessed in a different long-term hydrogel drug assay which would allow for the viability of the cell lines to measured, as proposed in section 7.3. Furthermore, this assay should also be extensively optimised, using a large range of drug concentrations, to ensure sufficient drug penetration into the hydrogel.

In summary, the findings in this study suggest that the knockout of LAMA1 decreases the sensitivity of SHH medulloblastoma cells to vincristine in a spheroid-hydrogel culture. As discussed in section 7.4, this suggests that an anti-apoptotic/drug resistance pathway is activated in DAOY LAM$^{-/-}$ spheroids embedded in a hyaluronan hydrogel.

7.6 Proteomics analysis of DAOY NT and DAOY LAM$^{-/-}$ cell lines identifies pathways that may underpin LAMA1-mediated phenotypes in SHH medulloblastoma

In this study LC-MS/MS proteomics analysis was conducted on the DAOY NT and DAOY LAM$^{-/-}$ cell lines grown in 2D and 3D spheroid culture. This was conducted in order to assess unbiased changes in global protein expression caused by the knockout of LAMA1 and therefore identify further protein candidates and associated molecular pathways (using KEGG pathway mapping analysis) which underpinned the differences in cellular migration, apoptosis and drug sensitivity caused by the knockout of LAMA1 in SHH medulloblastoma cells.

In 2D culture, this analysis identified 183 proteins that were upregulated by LAMA1, which were associated with amino acid metabolism, nucleotide metabolism and carbohydrate metabolism, as well as direct genomic estrogen signalling and the proteasome. Furthermore, 18 proteins were found to be downregulated by LAMA1 in 2D culture, which were associated with ECM-cell interactions. In spheroid culture, 26

proteins were identified to be upregulated by LAMA1, however, they were not found be significantly associated with any KEGG pathway. Finally, 35 proteins were found to be downregulated by LAMA1 in spheroid culture. These were associated with pathways relating to ECM-interaction, as well as PI3K-AKT and focal adhesion signalling pathways.

Here we have discussed how the proteins and pathways identified by this analysis may relate to the differences in migration, apoptosis and drug sensitivity between that DAOY NT and DAOY LAM$^{-/-}$ cell lines identified in this study.

7.6.1 Estrogen signalling as a mechanism of LAMA1-mediated BCL-2 and CD44 upregulation in SHH medulloblastoma

KEGG pathway mapping analysis identified that proteins associated with direct genomic estrogen signalling were upregulated by LAMA1 in SHH medulloblastoma cells in 2D culture. Direct genomic estrogen signalling has been shown to play a crucial role in cerebellar development (independently of sex), as well in proliferation, migration and apoptosis evasion in medulloblastoma (Chen, Zeng and Tse, 2008; Belcher, Ma and Le, 2009; Liang and Shang, 2013; Cookman and Belcher, 2015; Hernández-Rojas *et al.*, 2022). In fact, medulloblastomas have been shown to arise from estrogen receptor β positive (ERβ^{+}) GCPs and exclusively express ERβ themselves (Belcher, 2008; Mancuso *et al.*, 2010). Furthermore, in one study, estrogen signalling was shown facilitate the evasion of apoptosis in SHH medulloblastoma through the upregulation of BCL-2 expression (Cookman and Belcher, 2015). This could suggest that the LAMA1-mediated upregulation of BCL-2 that we have observed in this study, could in fact be a consequence of LAMA1-mediated estrogen signalling in SHH medulloblastoma. In addition, CD44 expression has also been demonstrated to be upregulated by estrogen signalling in breast cancer, ovarian cancer and cervical

adenocarcinoma; also suggesting that CD44 may be upregulated by LAMA1-mediated estrogen signalling in SHH medulloblastoma (Durst *et al.*, 2001; Bourguignon *et al.*, 2005; C. Yang *et al.*, 2020; Pereira Maurício de Barros *et al.*, 2021).

Two of the proteins (FKPB4 and HSPA8) within the estrogen signalling KEGG pathway that were identified to be upregulated by LAMA1 in SHH medulloblastoma cells, are part of a multi-protein inhibitory complex which binds to estrogen receptors in the absence of the estrogen, initially suggesting that the direct genomic estrogen signalling pathway may not be active in these cells (Fuentes and Silveyra, 2019). However, contradictory to this, two further proteins, the expression of which are activated by estrogen signalling (KRT18 and CTSD), were also identified to be upregulated by LAMA1 in SHH medulloblastoma cells, in addition to CD44 and BCL-2. This can possibly be explained by the fact that estrogen receptors can be activated via phosphorylation in the absence of estrogen, by pathways such as MAPK signalling cascades; this is known as ligand-independent genomic estrogen signalling (Cui, Shen and Li, 2013; Fuentes and Silveyra, 2019). Furthermore, MAPK1, a MAPK family member which directly phosphorylates ERs, was also found to be upregulated by LAMA1 in SHH medulloblastoma and associated with the KEGG estrogen signalling pathway. It has previously been shown that laminins (including laminin-111) are able to activate MAPK1 in several tumour types via laminin-binding integrins, suggesting that this may be a mechanism by which LAMA1 could upregulate ligand-independent genomic estrogen signalling in *LAM*^{high} SHH medulloblastomas (Khan and Falcone, 2000; Kariya and Miyazaki, 2004; Degen *et al.*, 2012; Siqueira *et al.*, 2016; Berardi *et al.*, 2017; Ramovs, te Molder and Sonnenberg, 2017; Meireles Da Costa *et al.*, 2021). However, as previously mentioned, direct genomic estrogen signalling is crucial to cerebellar development and has a role in the progression of medulloblastoma, therefore, this suggests that LAMA1 may activate estrogen signalling in parallel with

estrogen itself in *LAM*^{high} SHH medulloblastomas. This proposed pathway is illustrated in Figure 7.2.

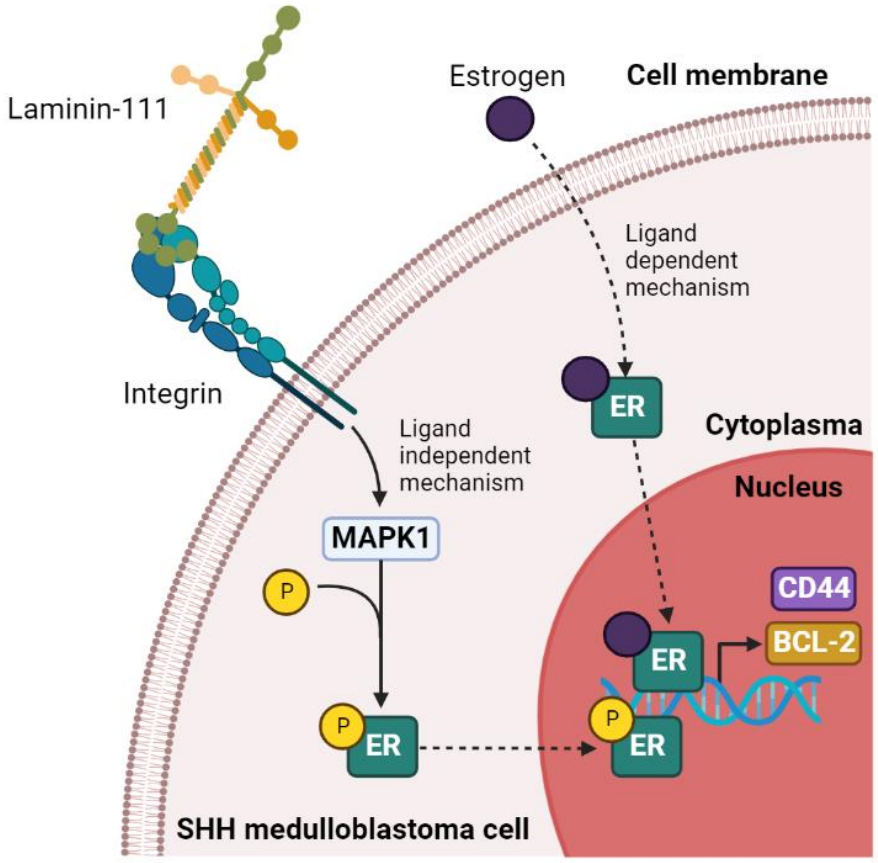


Figure 7.2 Hypothesised pathways of CD44 and BCL-2 upregulation via laminin-111 mediated ligand-independent direct genomic estrogen signalling and classical direct genomic estrogen signalling in *LAM*^{high} SHH medulloblastoma. Laminin-111 binds to integrin receptors which in turn activates MAPK1. MAPK1 then phosphorylates and activates estrogen receptors, which translocate to the nucleus and activate the transcription of CD44 and BCL-2. Estrogen also binds to estrogen receptors, allowing them to translocate to the nucleus and activate CD44 and BCL-2 transcription.

To fully validate these findings western blotting for MAPK1 as well as phosphorylated-ERβ should be carried out in the DAOY NT and DAOY LAM$^{-/-}$ cell lines in both 2D and spheroid culture. Furthermore, DAOY LAM$^{-/-}$ cells could also be stimulated with estrogen to assess whether this specifically restores BCL-2 and CD44 expression and thus demonstrate if they are indeed regulated by estrogen signalling in SHH medulloblastoma cells.

One limitation of this finding is that the proteins identified to be associated with the direct genomic estrogen signalling pathway were only identified to be upregulated by LAMA1 in SHH medulloblastoma in 2D culture. However, the LAMA1-mediated upregulation of CD44 and BCL-2 protein expression, was also identified in spheroid culture, suggesting that the activation of direct genomic estrogen signalling may be maintained across the two culture methods.

In summary, these findings suggest that ligand-independent direct genomic estrogen signalling in SHH medulloblastoma cells may be upregulated by a LAMA1-integrin-MAPK1 activation axis, which in turn upregulates the expression of BCL-2, CD44, KRT18 and CTSD. Furthermore, we have shown that two of these proteins may underpin the LAMA1-mediated effects on apoptosis (BCL-2) and cellular migration (CD44) in SHH medulloblastoma cells that we have observed in this study. This highlights that ligand-independent/dependant direct genomic estrogen signalling may be an important pathway in the progression of *LAM*^{high} SHH medulloblastomas and thus represent a therapeutic target for the treatment of these less aggressive tumours. In support of this, the use of ER inhibitors to treat medulloblastoma has already been proposed and a phase II clinical trial of the MAPK inhibitor ulixertinib is currently in progress (Belcher, 2009; trial number: NCT03698994).

7.6.2 LAMA1-mediated decrease in COL1A1, COL6A1, COL6A3 and ITGB1 expression as a mechanism for increased apoptosis and drug sensitivity in SHH medulloblastoma

In this study proteomic analysis identified that the collagen α subunits COL1A1, COL6A1 and COL6A3, as well as the collagen binding integrin receptor, ITGB1, were all downregulated by LAMA1 in SHH medulloblastoma spheroids (and therefore upregulated in the DAOY LAM$^{-/-}$ spheroids). A combination of consultation of the

literature and KEGG pathway mapping analysis, identified that these proteins may underpin the decrease in sensitivity to ABT-737 and vincristine exhibited by the DAOY LAM$^{-/-}$ cell line in the spheroid-hydrogel drug assay, by modulating molecular pathways and the mechanical properties of the ECM.

The interaction between tumour cells and certain ECM components, such as collagens, has long been shown to increase chemoresistance in many cancer types through a process known as cell-adhesion-mediated drug resistance (CAM-DR), although, the exact mechanisms which define this are yet to fully be delineated (Y. Huang *et al.*, 2021). However, the interaction of collagens, including type-I (COL1A1) and type-VI (COL6A1 and COL6A3), with ITGB1 has been shown to be one of the main activators of CAM-DR in several cancer types (Damiano *et al.*, 1999; Y. Huang *et al.*, 2021). Furthermore, type-I collagen and ITGB1 have been shown to co-localise in medulloblastoma patients (Liang *et al.*, 2008). Moreover, 3 recent studies have identified several molecular mechanisms activated by type-I collagen-ITGB1 interaction that may mediate CAM-DR and that have also been shown to have a role in the progression of medulloblastoma. We hypothesised that these mechanisms may also be activated in the DAOY LAM$^{-/-}$ spheroids (which exhibited increased COL1A1 and ITGB1 expression) in the spheroid-hydrogel model and may therefore underpin their decreased sensitivity to ABT-737 and vincristine.

Firstly, Baltes *et al*. identified that breast cancer cells exhibited enhanced chemoresistance in response to ITGB1 activation by type-I collagen, via the upregulation of the ABC drug transporters ABCB1, ABCC1 and ABCG2 (Baltes *et al.*, 2020). A growing pool of literature, including ongoing research in our group, has shown that ABC drug transporters (including ABCB1 and ABCG2) are pathogenic drivers of medulloblastoma which are more highly expressed in high-risk patients, where they could have roles in chemo and radioresistance and thus represent promising therapeutic targets (Ingram *et al.*, 2013; Othman *et al.*, 2014; Morfouace *et al.*, 2015;

Wijaya *et al.*, 2020; Nasir *et al.*, 2021; Zhu, Miller and Schuetz, 2022). Furthermore, Deng *et al*. demonstrated that ITGB1 activation by type-I collagen also conveyed chemoresistance in gastric cancer cells, however, this was attributed to the activation of the *YBX1* (YB-1) transcription factor (Deng *et al.*, 2021). Research within our group has demonstrated that YB-1 is a mediator of multi-drug resistance, which activates ABCB1 transcription, in medulloblastoma (Taylor, Kerr and Coyle, 2021; Taylor *et al.* in submission). Finally, Lv *et al*. showed that type-I collagen could upregulate BCL-2 via the activation of ITGB1 in gastric cancer (Lv *et al.*, 2021). As previously mentioned BCL-2 is highly expressed in medulloblastomas, and has a role in apoptosis evasion and drug resistance.

To summarise, these studies suggest that increased type-I collagen-ITGB1 interaction may contribute to the decreased sensitivity to ABT-737 and vincristine exhibited by the DAOY LAM$^{-/-}$ spheroids, through the upregulation of all or some of the pre-existing medulloblastoma targets, YBX1, the ABC transporters ABCB1 and ABCG2, as well as BCL-2. However, it is worth reiterating that although these studies only focussed on the interaction of ITGB1 with type-I collagen, type-VI collagen is also able to activate ITGB1 and so the other collagens identified to be upregulated in the DAOY LAM$^{-/-}$ spheroids (COL6A1 and COL6A3) may have also been able to activate these pathways in the spheroid-hydrogel drug assay.

To delineate if any of these pathways or targets are indeed down regulated by LAMA1 in SHH medulloblastoma, future work should investigate the expression YB-1, ABC-transporters and BCL-2 in the DAOY LAM$^{-/-}$ spheroids embedded in hydrogel.

KEGG pathway mapping analysis identified that COL1A1, COL6A1, COL6A3 and ITGB1 were associated with both the PI3K-AKT and focal adhesion signalling pathways, as the interaction between the collagens and ITGB1 activates FAK, the primary molecule in ECM-integrin signalling, which can activate both pathways (Yan

et al., 2015). Furthermore, the upregulation of the PI3K-AKT and focal adhesion signalling pathways have also been shown to have a crucial role in decreasing drug sensitivity in many tumour types, including medulloblastoma in the case of PI3K-AKT, and are crucial to CAM-DR (Guerreiro *et al.*, 2008; Buonamici *et al.*, 2010; Martini *et al.*, 2014; Dimitrova and Arcaro, 2015; Eke and Cordes, 2015; Ma, Cao and Ding, 2020; Rascio *et al.*, 2021). This could suggest that increased collagen-ITGB1 interaction may also contribute to the decreased drug sensitivity exhibited by the DAOY LAM$^{-/-}$ spheroids through the activation of the PI3K-AKT and focal adhesion signalling pathways. However, of the proteins downregulated by LAMA1 in spheroid culture (and therefore upregulated in the DAOY LAM$^{-/-}$ spheroids), only 1 additional protein was identified to be to be part of each pathway, aside from the collagens and ITGB1: GNB1, another activator of the PI3K-AKT signalling, and CAPN2, a downstream target of the focal adhesion signalling. It is therefore unclear from this analysis if these pathways are upregulated in the DAOY LAM$^{-/-}$ spheroids. Therefore, future work should investigate the expression of key proteins, e.g. phosphorylated AKT/FAK, within these pathways in the DAOY LAM$^{-/-}$ spheroids to more conclusively determine if they are affected by LAMA1 expression in SHH medulloblastoma.

The above pathways identified from the literature and KEGG pathway mapping analysis of proteomics data, which we have hypothesised could contribute to the decreased sensitivity of the DAOY LAM$^{-/-}$ spheroids to ABT-737 and vincristine, are shown in Figure 7.3.

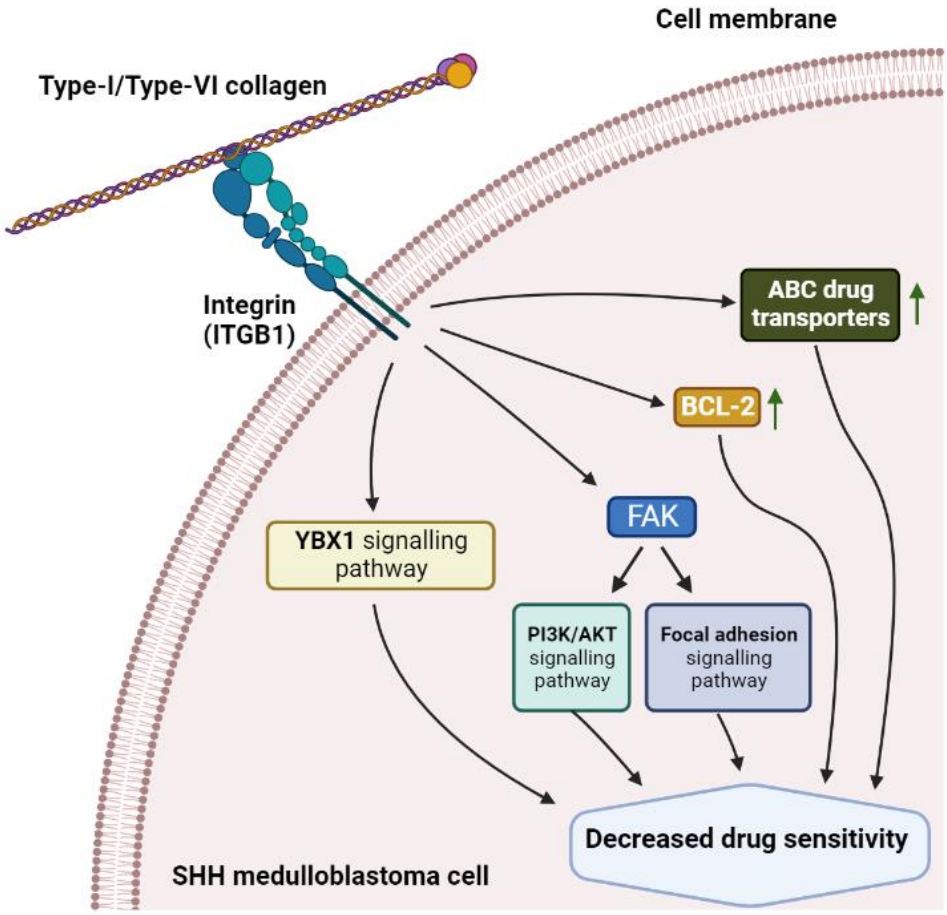


Figure 7.3 Hypothesised mechanisms of how type-I/type-VI collagen-ITGB1 interaction could mediate decreased drug sensitivity in DAOY LAM$^{-/-}$ spheroids. Type-I and type-VI collagens bind to ITGB1 receptors which could upregulate YB-1, BCL-2, ABC transporters, as well as PI3K-AKT and focal adhesion signalling pathways, which have all been shown to contribute to decreased drug sensitivity in tumours.

Another mechanism by which the drug sensitivity of the DAOY LAM$^{-/-}$ spheroids could have been lowered is through the alteration of the stiffness of their ECM. The increased stiffness of the ECM has been reported to be greatly increased in many tumour types and is caused by the aberrant expression of ECM components, of which collagens are the most common (Najafi, Farhood and Mortezaee, 2019). Furthermore, ECM stiffness has been shown to enhance drug resistance in tumours. It is hypothesised that the stiffer ECM acts as a diffusion barrier that prevents therapeutics from penetrating the tumour, in addition to activating pro-tumorigenic intracellular pathways (Sounni and Noel, 2013; Grasset *et al.*, 2018; Najafi, Farhood and Mortezaee, 2019; Henke,

Nandigama and Ergün, 2020). In addition, the average stiffness of medulloblastoma has been reported to 27 kPa, over 11 times stiffer than that of normal cerebellum, suggesting that ECM stiffness may have a role in medulloblastoma progression (Abramczyk and Imiela, 2018). This indicates that in the spheroid-hydrogel drug assays the increased expression of collagens (COL1A1, COL6A1 and COL6A3) exhibited by the DAOY LAM$^{-/-}$ spheroids could have increased the stiffness of their surrounding hydrogel, therefore decreasing their sensitivity to the ABT-737 and vincristine.

This could also explain why the decrease in drug sensitivity in the DAOY LAM$^{-/-}$ cell line was primarily detected in the spheroid-hydrogel model, as in the 2D drug response assay the cells were grown on cell culture plastic, the high stiffness (~10,000 kPa) of which may have masked any difference in stiffness caused by increased expression of collagens in the DAOY LAM$^{-/-}$ cell line. Furthermore, another reason for this could be that, as shown in this study, the spheroids retain type-I and type-VI collagens within their structure; it is therefore possible that in spheroid-hydrogel culture the collagens deposited by the cell lines were able to more readily activate ITGB1, and the drug resistance pathways previously discussed.

To validate this, in future work the DAOY NT and DAOY LAM$^{-/-}$ cell lines should be grown in a different long-term 3D hydrogel model, as previously suggested, and the stiffness of the hydrogel should then be measured to assess if the increased collagen expression in the DAOY LAM$^{-/-}$ cell line affects the stiffness of the hydrogel. Although this could be conducted on the spheroids embedded in the hyaluronan hydrogel, as used in this study, it is unlikely that that the global stiffness of the hydrogel would be altered by the spheroids after only 4 days.

Finally, as previously discussed, we identified that COL1A1 and COL6A1 are part of the ECM shell formed by SHH medulloblastoma cell lines grown in 3D hydrogels and

spheroids. The upregulation of these collagens in the absence of LAMA1 in the DAOY LAM$^{-/-}$ cell line suggests that SHH medulloblastoma cells may require high amounts of ECM, and the upregulation of the collagens may have been as a consequence of an ECM compensatory mechanism. Furthermore, this could mean that all SHH medulloblastomas (including *LAM^{low}* tumours) may exhibit some level of ECM component protein expression and it may in fact be the specific combination of ECM proteins which influences survival in SHH medulloblastoma patients. This could also be elucidated by the staining of SHH medulloblastoma patient TMAs for a panel of the candidate medulloblastoma ECM proteins, as proposed in section 7.1.2.

Taken together these findings suggest that COL1A1, COL6A1, COL6A3 and ITGB1 may mediate the decreased drug sensitivity exhibited by the DAOY LAM$^{-/-}$ spheroids through a combination of the stimulation of intracellular pathways and increased ECM stiffness. In addition, this could also suggest that the worse overall survival exhibited by *LAM^{low}* SHH medulloblastoma patients could be as a consequence of decreased drug sensitivity. However, a limitation of these findings is that the proteomics analysis which identified the upregulation of the collagens and ITGB1 in the DAOY LAM$^{-/-}$ cell line was conducted on cells grown in the standard spheroid model, instead of the spheroid-hydrogel model (due to insufficient protein yield), which was used to identify the decrease in drug sensitivity in DAOY LAM$^{-/-}$ spheroids. We therefore do not know for certain that these collagens and ITGB1 were also upregulated in DAOY LAM$^{-/-}$ spheroids when embedded in the hyaluronan hydrogel, although it is likely since they were upregulated in standard spheroids, and ITGB1 and COL1A1 were also upregulated in 2D culture. Therefore, to validate this, proteomics analysis of the DAOY NT and DAOY LAM$^{-/-}$ cell lines grown in the same long-term hydrogel previously proposed in sections 7.3 and 7.4 should be a part of future work.

7.7 Concluding statement

This thesis has begun to demonstrate the importance and influence of the tumour-deposited ECM protein LAMA1 in SHH medulloblastoma progression. By creating a knockout of LAMA1 in a SHH medulloblastoma cell line, we have shown that LAMA1 enhances the migration and drug sensitivity of SHH medulloblastoma cells using 3D cell culture models. In addition, proteomic analysis identified molecular pathways that could underpin these effects, including ligand-independent direct genomic estrogen signalling and collagen-ITGB1 signalling. Furthermore, we have identified that SHH medulloblastoma cells form a multicomponent ECM shell-like structure in long-term 3D culture, in addition to laminin-111/211, which is significantly associated with more favourable patient survival.

7.8 Future work

Future work should include a LAMA1 knockout in the ONS-76 SHH medulloblastoma cell line, as attempted in this study, in order to further validate the role of LAMA1 in SHH medulloblastoma cellular migration and drug sensitivity. However, the alternative migration, invasion and long-term hydrogel drug assays proposed here should also be used to validate these findings more robustly in both cell lines. In addition, the knockout of LAMA2 should also be conducted in both the DAOY and ONS-76 cell lines, to investigate its role in SHH medulloblastoma progression, since it was the expression of *LAMA1* and *LAMA2* which defined the LAM^{high} and LAM^{low} SHH medulloblastoma ECM sub-types, on which this study is based. Furthermore, the staining of patient TMAs for the panel of the SHH medulloblastoma ECM proteins identified here should be conducted in order to further delineate the role of the SHH medulloblastoma ECM shell-like structure on patient survival. Finally, since this thesis has mainly focused on

the effect of the ECM on medulloblastoma, future work should also investigate the role of the cellular part of the brain TME in tumour progression.

References

Abramczyk, H. and Imiela, A. (2018) 'The biochemical, nanomechanical and chemometric signatures of brain cancer', *Spectrochimica Acta - Part A: Molecular and Biomolecular Spectroscopy*. The Authors, 188, pp. 8–19. doi: 10.1016/j.saa.2017.06.037.

Aguilan, J. T., Kulej, K. and Sidoli, S. (2020) 'Guide for protein fold change and p-value calculation for non-experts in proteomics', *Molecular Omics*. The Royal Society of Chemistry, 16(6), pp. 573–582. doi: 10.1039/D0MO00087F.

Aisenbrey, E. A. and Murphy, W. L. (2020) 'Synthetic alternatives to Matrigel', *Nature reviews. Materials*. NIH Public Access, 5(7), p. 539. doi: 10.1038/S41578-020-0199-8.

Allnoch, L. *et al.* (2022) 'Astrocyte depletion alters extracellular matrix composition in the demyelinating phase of Theiler's murine encephalomyelitis', *PLoS ONE*. PLOS, 17(6). doi: 10.1371/JOURNAL.PONE.0270239.

Annabi, B. *et al.* (2010) 'Pharmacological targeting of β-adrenergic receptor functions abrogates NF-κB signaling and MMP-9 secretion in medulloblastoma cells', *OncoTargets and Therapy*. doi: 10.2147/OTT.S14503.

Aruffo, A. *et al.* (1990) 'CD44 is the principal cell surface receptor for hyaluronate', *Cell*, 61(7), pp. 1303–1313. doi: 10.1016/0092-8674(90)90694-A.

Ashour, A. E. *et al.* (2016) 'Thymoquinone inhibits growth of human medulloblastoma cells by inducing oxidative stress and caspase-dependent apoptosis while suppressing NF-κB signaling and IL-8 expression', *Molecular and Cellular Biochemistry*. Springer New York LLC, 416(1–2), pp. 141–155. doi: 10.1007/s11010-016-2703-4.

Atanaskova, N. *et al.* (2002) 'MAP kinase/estrogen receptor cross-talk enhances estrogen-mediated signaling and tumor growth but does not confer tamoxifen resistance', *Oncogene 2002 21:25*. Nature Publishing Group, 21(25), pp. 4000–4008.

doi: 10.1038/sj.onc.1205506.

ATCC (2023) *Daoy - HTB-186 | ATCC*. Available at: https://www.atcc.org/products/htb-186#product-references (Accessed: 16 March 2023).

Attieh, Y. *et al.* (2017) 'Cancer-associated fibroblasts lead tumor invasion through integrin-β3-dependent fibronectin assembly', *The Journal of cell biology*. J Cell Biol, 216(11), pp. 3509–3520. doi: 10.1083/JCB.201702033.

Aumailley, M. *et al.* (2005) 'A simplified laminin nomenclature', *Matrix Biology*. Elsevier, 24(5), pp. 326–332. doi: 10.1016/J.MATBIO.2005.05.006.

Aumailley, M. (2013) 'The laminin family', *Cell Adhesion & Migration*. Monique Aumailley, 7(1), pp. 48–55. doi: 10.4161/cam.22826.

Ayoub, R. *et al.* (2020) 'Assessment of cognitive and neural recovery in survivors of pediatric brain tumors in a pilot clinical trial using metformin', *Nature medicine*. NIH Public Access, 26(8), p. 1285. doi: 10.1038/S41591-020-0985-2.

Baba, H. *et al.* (2001) 'Expression and Localization of Lumican in the Ischemic and Reperfused Rat Heart', *JAPANESE CIRCULATION JOURNAL*. The Japanese Circulation Society, 65(5), pp. 445–450. doi: 10.1253/JCJ.65.445.

Baltes, F. *et al.* (2020) 'β1-Integrin binding to collagen type 1 transmits breast cancer cells into chemoresistance by activating ABC efflux transporters', *Biochimica et Biophysica Acta (BBA) - Molecular Cell Research*. Elsevier, 1867(5), p. 118663. doi: 10.1016/J.BBAMCR.2020.118663.

Bandopadhayay, P. *et al.* (2014) 'BET-bromodomain inhibition of MYC-amplified medulloblastoma', *Clin Cancer Res*, 20(4), pp. 912–925. doi: 10.1158/1078-0432.CCR-13-2281.

Bandtlow, C. E. and Zimmermann, D. R. (2000) ‘Proteoglycans in the developing brain: new conceptual insights for old proteins.’, *Physiological reviews*. doi: 10.1152/physrev.2000.80.4.1267.

Bar, E. E. *et al.* (2007) ‘Hedgehog signaling promotes medulloblastoma survival via BclII’, *American Journal of Pathology*, 170(1), pp. 347–355. doi: 10.2353/ajpath.2007.060066.

Barczyk, M., Carracedo, S. and Gullberg, D. (2010) ‘Integrins’, *Cell and Tissue Research*. Springer, 339(1), p. 269. doi: 10.1007/S00441-009-0834-6.

Basiouni, S., Fuhrmann, H. and Schumann, J. (2012) ‘High-efficiency transfection of suspension cell lines’, *BioTechniques*. Future Science Ltd London, UK , 53(2), pp. 1–4. doi: 10.2144/000113914/ASSET/IMAGES/LARGE/FIGURE3.JPEG.

Bauvois, B. (2012) ‘New facets of matrix metalloproteinases MMP-2 and MMP-9 as cell surface transducers: Outside-in signaling and relationship to tumor progression’, *Biochimica et Biophysica Acta - Reviews on Cancer*, pp. 29–36. doi: 10.1016/j.bbcan.2011.10.001.

Beck, K., Hunter, I. and Engel, J. (1990) ‘Structure and function of laminin: anatomy of a multidomain glycoprotein.’, *The FASEB Journal*. FASEB, 4(2), pp. 148–160. doi: 10.1096/fasebj.4.2.2404817.

Belcher, S. M. (2008) ‘Rapid signaling mechanisms of estrogens in the developing cerebellum’, *Brain Research Reviews*. Elsevier, 57(2), pp. 481–492. doi: 10.1016/J.BRAINRESREV.2007.07.020.

Belcher, S. M. (2009) ‘Blockade of estrogen receptor signaling to improve outlook for medulloblastoma sufferers’, *Future Oncology*, 5(6), pp. 751–754. doi: 10.2217/fon.09.69.

Belcher, S. M., Ma, X. and Le, H. H. (2009) ‘Blockade of Estrogen Receptor Signaling Inhibits Growth and Migration of Medulloblastoma’, *Endocrinology*. The Endocrine Society, 150(3), p. 1112. doi: 10.1210/EN.2008-1363.

Below, J. and Das, J. M. (2022) ‘Vincristine’, *xPharm: The Comprehensive Pharmacology Reference*. StatPearls Publishing, pp. 1–4. doi: 10.1016/B978-008055232-3.62853-3.

Berardi, D. E. *et al.* (2017) ‘Laminin modulates the stem cell population in LM05-E murine breast cancer cells through the activation of the MAPK/ERK pathway’, *Cancer Research and Treatment*, 49(4), pp. 869–879. doi: 10.4143/crt.2016.378.

Bhoopathi, P. *et al.* (2011) ‘MMP-2 mediates mesenchymal stem cell tropism towards medulloblastoma tumors’, *Gene Therapy*, 18, pp. 692–701. doi: 10.1038/gt.2011.14.

Bolin, S. *et al.* (2018) ‘Combined BET bromodomain and CDK2 inhibition in MYC-driven medulloblastoma’, *Oncogene*, 37, pp. 2850–2862. doi: 10.1038/s41388-018-0135-1.

Bonacini, M. *et al.* (2019) ‘Clusterin Silencing in Prostate Cancer Induces Matrix Metalloproteinases by an NF- B-Dependent Mechanism’, *Journal of Oncology*. Hindawi Limited, 2019. doi: 10.1155/2019/4081624.

Bonnans, C., Chou, J. and Werb, Z. (2014) ‘Remodelling the extracellular matrix in development and disease’, *Nature reviews. Molecular cell biology*. Nat Rev Mol Cell Biol, 15(12), pp. 786–801. doi: 10.1038/NRM3904.

Bourguignon, L. Y. W. *et al.* (2005) ‘Hyaluronan-CD44 interaction with IQGAP1 promotes Cdc42 and ERK signaling, leading to actin binding, Elk-1/estrogen receptor transcriptional activation, and ovarian cancer progression’, *Journal of Biological Chemistry*. Elsevier, 280(12), pp. 11961–11972. doi: 10.1074/jbc.M411985200.

van Bree, N. F. H. N. and Wilhelm, M. (2022) ‘The Tumor Microenvironment of Medulloblastoma: An Intricate Multicellular Network with Therapeutic Potential’, *Cancers*, 14(20). doi: 10.3390/cancers14205009.

Budenholzer, L. *et al.* (2017) ‘Proteasome Structure and Assembly’, *Journal of Molecular Biology*, 429(22), pp. 3500–3524. doi: 10.1016/j.jmb.2017.05.027.

Buonamici, S. *et al.* (2010) ‘Interfering with resistance to smoothened antagonists by inhibition of the PI3K pathway in medulloblastoma’, *Science Translational Medicine*. American Association for the Advancement of Science, 2(51). doi: 10.1126/SCITRANSLMED.3001599/SUPPL_FILE/2-51RA70_SM.PDF.

Carbone, A. *et al.* (1995) ‘Expression of the monomeric 67-kd laminin-binding protein in human lymphomas as defined by MLuC5 monoclonal antibody and paraffin section immunohistochemistry’, *Human pathology*. Hum Pathol, 26(5), pp. 541–546. doi: 10.1016/0046-8177(95)90251-1.

Casey, T. *et al.* (2009) ‘Molecular signatures suggest a major role for stromal cells in development of invasive breast cancer’, *Breast cancer research and treatment*. Breast Cancer Res Treat, 114(1), pp. 47–62. doi: 10.1007/S10549-008-9982-8.

Cavalli, F. M. G. *et al.* (2017) ‘Intertumoral Heterogeneity within Medulloblastoma Subgroups’, *Cancer Cell*, 31(6), pp. 737-754.e6. doi: 10.1016/j.ccell.2017.05.005.

Chang, C. H., Housepian, E. M. and Herbert, C. (1969) ‘An operative staging system and a megavoltage radiotherapeutic technic for cerebellar medulloblastomas.’, *Radiology*. doi: 10.1148/93.6.1351.

Chen, G. G., Zeng, Q. and Tse, G. M. K. (2008) ‘Estrogen and its receptors in cancer’, *Medicinal Research Reviews*, 28(6), pp. 954–974. doi: 10.1002/MED.20131.

Cheng, Y. *et al.* (2020) ‘Sustained hedgehog signaling in medulloblastoma tumoroids

is attributed to stromal astrocytes and astrocyte-derived extracellular matrix', *Laboratory Investigation 2020 100:9*. Nature Publishing Group, 100(9), pp. 1208–1222. doi: 10.1038/s41374-020-0443-2.

Chetty, C. *et al.* (2012) 'MMP-9 induces CD44 cleavage and CD44 mediated cell migration in glioblastoma xenograft cells', *Cellular Signalling*. NIH Public Access, 24(2), pp. 549–559. doi: 10.1016/j.cellsig.2011.10.008.

Choi, K. C. *et al.* (2001) 'Estradiol Up-Regulates Antiapoptotic Bcl-2 Messenger Ribonucleic Acid and Protein in Tumorigenic Ovarian Surface Epithelium Cells', *Endocrinology*. Oxford Academic, 142(6), pp. 2351–2360. doi: 10.1210/ENDO.142.6.8144.

Clifford, S. C. *et al.* (2006) 'Wnt/Wingless pathway activation and chromosome 6 loss characterize a distinct molecular sub-group of medulloblastomas associated with a favorable prognosis.', *Cell cycle (Georgetown, Tex.)*. doi: 10.4161/cc.5.22.3446.

Cohen, K. *et al.* (2019) 'MEDU-34. PILOT STUDY OF A SURGERY AND CHEMOTHERAPY-ONLY APPROACH IN THE UPFRONT THERAPY OF CHILDREN WITH WNT-POSITIVE STANDARD RISK MEDULLOBLASTOMA', *Neuro-Oncology*. Oxford University Press, 21(Suppl 2), p. ii110. doi: 10.1093/NEUONC/NOZ036.192.

Coluccia, D. *et al.* (2016) *Medulloblastoma: Tumor biology and relevance to treatment and prognosis paradigm*, *Current Neurology and Neuroscience Reports*. Springer US. doi: 10.1007/s11910-016-0644-7.

Conklin, M. W. *et al.* (2011) 'Aligned collagen is a prognostic signature for survival in human breast carcinoma', *American Journal of Pathology*. Elsevier Inc., 178(3), pp. 1221–1232. doi: 10.1016/j.ajpath.2010.11.076.

Cook Sangar, M. L. *et al.* (2017) 'Inhibition of CDK4/6 by palbociclib significantly extends survival in medulloblastoma patient-derived xenograft mouse models', *Clinical*

Cancer Research. American Association for Cancer Research Inc., 23(19), pp. 5802–5813. doi: 10.1158/1078-0432.CCR-16-2943/274486/AM/INHIBITION-OF-CDK4-6-BY-PALBOCICLIB-SIGNIFICANTLY.

Cookman, C. J. and Belcher, S. M. (2015) 'Estrogen Receptor-β Up-Regulates IGF1R Expression and Activity to Inhibit Apoptosis and Increase Growth of Medulloblastoma', *Endocrinology*. Oxford Academic, 156(7), pp. 2395–2408. doi: 10.1210/EN.2015-1141.

Cordes, N. *et al.* (2009) 'Fibronectin and laminin increase resistance to ionizing radiation and the cytotoxic drug Ukrain® in human tumour and normal cells in vitro', *Int J Radiat Biol*. Taylor & Francis, 79(9), pp. 709–720. doi: 10.1080/09553000310001610240.

Coulson-Thomas, V. J. *et al.* (2013) 'Lumican expression, localization and antitumor activity in prostate cancer', *Experimental Cell Research*. Academic Press, 319(7), pp. 967–981. doi: 10.1016/J.YEXCR.2013.01.023.

Cox, T. R. (2021) 'The matrix in cancer', *Nature Reviews Cancer*, 21, pp. 217–238. doi: 10.1038/s41568-020-00329-7.

Cui, J., Shen, Y. and Li, R. (2013) 'Estrogen synthesis and signaling pathways during aging: from periphery to brain', *Trends in Molecular Medicine*, 13(3), pp. 197–209. doi: 10.1016/j.molmed.2012.12.007.

Damiano, J. S. *et al.* (1999) 'Cell Adhesion Mediated Drug Resistance (CAM-DR): Role of Integrins and Resistance to Apoptosis in Human Myeloma Cell Lines', *Blood*. American Society of Hematology, 93(5), pp. 1658–1667. doi: 10.1182/BLOOD.V93.5.1658.

Degen, M. *et al.* (2012) 'MAPK/ERK-dependent translation factor hyperactivation and dysregulated laminin γ2 expression in oral dysplasia and squamous cell carcinoma',

The American journal of pathology. Am J Pathol, 180(6), pp. 2462–2478. doi: 10.1016/J.AJPATH.2012.02.028.

Deng, S. *et al.* (2021) 'Promotion of gastric tumor initiating cells in a 3D collagen gel culture model via YBX1/ SPP1/NF-κB signaling', *Cancer Cell Int*, 21, p. 599. doi: 10.1186/s12935-021-02307-x.

Digiacomo, V. and Meruelo, D. (2016) 'Looking into laminin receptor: Critical discussion regarding the non-integrin 37/67-kDa laminin receptor/RPSA protein', *Biological Reviews*. Blackwell Publishing Ltd, 91(2), pp. 288–310. doi: 10.1111/BRV.12170.

Dimitrova, V. and Arcaro, A. (2015) 'Targeting the PI3K/AKT/mTOR Signaling Pathway in Medulloblastoma', *Current Molecular Medicine*. Bentham Science Publishers, 15(1), pp. 82–93. doi: 10.2174/1566524015666150114115427.

Durst, B. *et al.* (2001) 'The influence of hormones on CD44 expression in endometrial and breast carcinomas', *Oncology Reports*. Spandidos Publications, 8(5), pp. 987–993. Available at: http://www.spandidos-publications.com/10.3892/or.8.5.987/abstract (Accessed: 10 November 2022).

Eberhart, C. G. *et al.* (2003) 'Medulloblastomas with systemic metastases: Evaluation of tumor histopathology and clinical behavior in 23 patients', *Journal of Pediatric Hematology/Oncology*. doi: 10.1097/00043426-200303000-00004.

Eberhart, C. G., Tihan, T. and Burger, P. C. (2000) 'Nuclear localization and mutation of β-catenin in medulloblastomas', *Journal of Neuropathology and Experimental Neurology*. doi: 10.1093/jnen/59.4.333.

Egeblad, M. and Werb, Z. (2002) 'Regulation of MMP activity NEW FUNCTIONS FOR THE MATRIX METALLOPROTEINASES IN CANCER PROGRESSION', 2, pp. 161–174. doi: 10.1038/nrc745.

Eke, I. and Cordes, N. (2015) ‘Focal adhesion signaling and therapy resistance in cancer’, *Seminars in Cancer Biology*. Elsevier Ltd, 31, pp. 65–75. doi: 10.1016/j.semcancer.2014.07.009.

Ellison, D. W. (2010) ‘Childhood medulloblastoma: Novel approaches to the classification of a heterogeneous disease’, *Acta Neuropathologica*. doi: 10.1007/s00401-010-0726-6.

Erdogan, B. *et al.* (2017) ‘Cancer-associated fibroblasts promote directional cancer cell migration by aligning fibronectin’, *Journal of Cell Biology*. Rockefeller University Press, 216(11), pp. 3799–3816. doi: 10.1083/JCB.201704053.

Filippakopoulos, P. and Knapp, S. (2012) ‘The bromodomain interaction module’, *FEBS Letters*. doi: 10.1016/j.febslet.2012.04.045.

Frantz, C., Stewart, K. M. and Weaver, V. M. (2010) ‘The extracellular matrix at a glance’, *Journal of Cell Science*, 123(123), pp. 4195–4200. doi: 10.1242/jcs.023820.

Fridman, R. *et al.* (1990) ‘Reconstituted basement membrane (matrigel) and laminin can enhance the tumorigenicity and the drug resistance of small cell lung cancer cell lines’, *Proceedings of the National Academy of Sciences of the United States of America*, 87(17), pp. 6698–6702. doi: 10.1073/pnas.87.17.6698.

Fuentes, N. and Silveyra, P. (2019) ‘Estrogen receptor signaling mechanisms’, *Adv Protein Chem Struct Biol*, (116), pp. 135–170. doi: 10.1016/bs.apcsb.2019.01.001.

Fujii, K. and Miyashita, T. (2014) ‘Gorlin syndrome (nevoid basal cell carcinoma syndrome): Update and literature review’, *Pediatrics International*, 56(5), pp. 667–674. doi: 10.1111/ped.12461.

Gajjar, A. J. and Robinson, G. W. (2014) ‘Medulloblastoma - Translating discoveries from the bench to the bedside’, *Nature Reviews Clinical Oncology*. doi:

10.1038/nrclinonc.2014.181.

Gao, Q. *et al.* (2019) ‘Erratum: Heterotypic CAF-tumor spheroids promote early peritoneal metastatis of ovarian cancer (Journal of Experiments Medicine DOI: 10.1084/jem.20181850)’, *Journal of Experimental Medicine*. Rockefeller University Press, 216(10), p. 2448. doi: 10.1084/JEM.20180765.

Garzia, L. *et al.* (2018) ‘A Hematogenous Route for Medulloblastoma Leptomeningeal Metastases’, *Cell*. doi: 10.1016/j.cell.2018.01.038.

Gerber, N. U. *et al.* (2014) ‘Recent developments and current concepts in Medulloblastoma’, *Cancer Treatment Reviews*. doi: 10.1016/j.ctrv.2013.11.010.

Gibson, P. *et al.* (2010) ‘Subtypes of medulloblastoma have distinct developmental origins’, *Nature*. Nature Publishing Group, 468(7327), pp. 1095–1099. doi: 10.1038/nature09587.

Gilbertson, R. J. and Ellison, D. W. (2008) ‘The Origins of Medulloblastoma Subtypes’, *Annual Review of Pathology: Mechanisms of Disease*. doi: 10.1146/annurev.pathmechdis.3.121806.151518.

Giussani, M. *et al.* (2015) ‘Tumor-extracellular matrix interactions: Identification of tools associated with breast cancer progression’, *Seminars in cancer biology*. Semin Cancer Biol, 35, pp. 3–10. doi: 10.1016/J.SEMCANCER.2015.09.012.

Gkretsi, V. and Stylianopoulos, T. (2018) ‘Cell adhesion and matrix stiffness: Coordinating cancer cell invasion and metastasis’, *Frontiers in Oncology*, 8(MAY). doi: 10.3389/fonc.2018.00145.

Gold, J. M. and Raja, A. (2022) ‘Cisplatin’, *StatPearls*. StatPearls Publishing. Available at: https://www.ncbi.nlm.nih.gov/books/NBK547695/ (Accessed: 13 April 2023).

Goodison, S., Urquidi, V. and Tarin, D. (1999) ‘CD44 cell adhesion molecules’, *Journal*

of Clinical Pathology - Molecular Pathology. BMJ Publishing Group, pp. 189–196. doi: 10.1136/mp.52.4.189.

Grammel, D. *et al.* (2012) 'Sonic hedgehog-associated medulloblastoma arising from the cochlear nuclei of the brainstem', *Acta Neuropathologica*. Springer-Verlag, 123(4), pp. 601–614. doi: 10.1007/s00401-012-0961-0.

Grasset, E. M. *et al.* (2018) 'Matrix Stiffening and EGFR Cooperate to Promote the Collective Invasion of Cancer Cells', *Cancer research*. Cancer Res, 78(18), pp. 5229–5242. doi: 10.1158/0008-5472.CAN-18-0601.

Guerreiro, A. S. *et al.* (2008) 'Targeting the PI3K p110α isoform inhibits medulloblastoma proliferation, chemoresistance, and migration', *Clinical Cancer Research*, 14(21), pp. 6761–6769. doi: 10.1158/1078-0432.CCR-08-0385.

Gupta, T. *et al.* (2022) 'Omission of Upfront Craniospinal Irradiation in Patients with Low-Risk WNT-Pathway Medulloblastoma Is Associated with Unacceptably High Risk of Neuraxial Failure', *Clinical cancer research : an official journal of the American Association for Cancer Research*. Clin Cancer Res, 28(19), pp. 4180–4185. doi: 10.1158/1078-0432.CCR-22-0758.

Hanahan, D. (2022) 'Hallmarks of Cancer: New Dimensions', *Cancer Discovery*. American Association for Cancer Research, 12(1), pp. 31–46. doi: 10.1158/2159-8290.CD-21-1059.

Hanahan, D. and Weinberg, R. A. (2011) 'Hallmarks of cancer: the next generation', *Cell*. Cell, 144(5), pp. 646–674. doi: 10.1016/J.CELL.2011.02.013.

Hawkridge, A. M. (2014) 'CHAPTER 1 Practical Considerations and Current Limitations in Quantitative Mass Spectrometry-based Proteomics', in. Royal Society of Chemistry, pp. 1–25. doi: 10.1039/9781782626985-00001.

Hemmings, B. A. and Restuccia, D. F. (2012) 'PI3K-PKB / Akt Pathway', *Cold Spring Harbor Perspectives in Medicine*, 4(9), pp. 1–4.

Heng, C. *et al.* (2011) 'Functional role of laminin α1 chain during cerebellum development', *Cell Adhesion & Migration*, 5(6), pp. 480–489. doi: 10.4161/cam.5.6.19191.

Henke, E., Nandigama, R. and Ergün, S. (2020) 'Extracellular Matrix in the Tumor Microenvironment and Its Impact on Cancer Therapy', *Frontiers in Molecular Biosciences*. Frontiers Media S.A., 6, p. 160. doi: 10.3389/FMOLB.2019.00160/BIBTEX.

Hernández-Rojas, R. *et al.* (2022) 'The interplay between estrogen receptor beta and protein kinase C, a crucial collaboration for medulloblastoma cell proliferation and invasion', *Cellular Signalling*, 92(September 2021). doi: 10.1016/j.cellsig.2022.110246.

Heussen, C. and Dowdle, E. B. (1980) 'Electrophoretic analysis of plasminogen activators in polyacrylamide gels containing sodium dodecyl sulfate and copolymerized substrates', *Analytical biochemistry*. Anal Biochem, 102(1), pp. 196–202. doi: 10.1016/0003-2697(80)90338-3.

Hoerig, C. M. *et al.* (2021) 'Exploring the role and clinical implications of proteasome inhibition in medulloblastoma', *Pediatric Blood and Cancer*, 68(10), pp. 1–9. doi: 10.1002/pbc.29168.

Holgado, B. L. *et al.* (2017) 'Tailoring Medulloblastoma Treatment Through Genomics: Making a Change, One Subgroup at a Time', *Annual Review of Genomics and Human Genetics*, 18(1), pp. 143–166. doi: 10.1146/annurev-genom-091416-035434.

Hoshino, A. *et al.* (2015) 'Tumour exosome integrins determine organotropic metastasis', *Nature 2015 527:7578*. Nature Publishing Group, 527(7578), pp. 329–

335. doi: 10.1038/nature15756.

Huang, G. H. *et al.* (2016) 'Medulloblastoma stem cells: Promising targets in medulloblastoma therapy', *Cancer Science*. John Wiley & Sons, Ltd, 107(5), pp. 583–589. doi: 10.1111/CAS.12925.

Huang, J. *et al.* (2021) 'Extracellular matrix and its therapeutic potential for cancer treatment', *Signal Transduction and Targeted Therapy*. Springer US, 6(1). doi: 10.1038/s41392-021-00544-0.

Huang, Y. *et al.* (2021) 'CAM-DR: Mechanisms, Roles and Clinical Application in Tumors', *Frontiers in Cell and Developmental Biology*, 9(July), pp. 1–17. doi: 10.3389/fcell.2021.698047.

Humphries, J. D., Byron, A. and Humphries, M. J. (2006) 'Integrin ligands at a glance', *Journal of Cell Science*, 119(19), pp. 3901–3903. doi: 10.1242/jcs.03098.

Ichikawa-Tomikawa, N. *et al.* (2012) 'Laminin α1 is essential for mouse cerebellar development', *Matrix Biology*, 31(1), pp. 17–28. doi: 10.1016/J.MATBIO.2011.09.002.

Ingram, W. J. *et al.* (2013) 'ABC transporter activity linked to radiation resistance and molecular subtype in pediatric medulloblastoma', *Experimental Hematology and Oncology*. BioMed Central Ltd., 2(1), pp. 1–17. doi: 10.1186/2162-3619-2-26/TABLES/1.

Insua-Rodríguez, J. and Oskarsson, T. (2016) 'The extracellular matrix in breast cancer', *Advanced drug delivery reviews*. Adv Drug Deliv Rev, 97, pp. 41–55. doi: 10.1016/J.ADDR.2015.12.017.

Isaacson, K. J. *et al.* (2017) 'Matrix-metalloproteinases as targets for controlled delivery in cancer: an analysis of upregulation and expression', *Journal of controlled release : official journal of the Controlled Release Society*. NIH Public Access, 259, p.

62. doi: 10.1016/J.JCONREL.2017.01.034.

Işeri, Ö. D. *et al.* (2010) 'Gene expression analysis of drug-resistant MCF-7 cells: Implications for relation to extracellular matrix proteins', *Cancer Chemotherapy and Pharmacology*, 65(3), pp. 447–455. doi: 10.1007/s00280-009-1048-z.

Jabłońska-Trypuć, A. *et al.* (2016) 'Matrix metalloproteinases (MMPs), the main extracellular matrix (ECM) enzymes in collagen degradation, as a target for anticancer drugs', *https://doi.org/10.3109/14756366.2016.1161620*. Taylor & Francis, 31(S1), pp. 177–183. doi: 10.3109/14756366.2016.1161620.

Jeanne, A. *et al.* (2017) 'Lumican delays melanoma growth in mice and drives tumor molecular assembly as well as response to matrix-targeted TAX2 therapeutic peptide', *Scientific Reports*, 7(1), pp. 1–16. doi: 10.1038/s41598-017-07043-9.

Jezierska, A. and Motyl, T. (2009) 'Matrix metalloproteinase-2 involvement in breast cancer progression: A mini-review', *Medical Science Monitor*.

Jiang, H. and Li, H. (2021) 'Prognostic values of tumoral MMP2 and MMP9 overexpression in breast cancer: a systematic review and meta-analysis', *BMC Cancer*. BioMed Central Ltd, 21(1), pp. 1–13. doi: 10.1186/S12885-021-07860-2/FIGURES/5.

Jiang, K. *et al.* (2019) 'Differentially expressed genes ASPN, COL1A1, FN1, VCAN and MUC5AC are potential prognostic biomarkers for gastric cancer', *Oncology Letters*. Spandidos Publications, 17(3), pp. 3191–3202. doi: 10.3892/OL.2019.9952/DOWNLOAD.

Jiang, N. *et al.* (2020) *Role of PI3K/AKT pathway in cancer: the framework of malignant behavior*, *Molecular Biology Reports*. Springer Netherlands. doi: 10.1007/s11033-020-05435-1.

Jones, D. T. W. *et al.* (2012) 'Dissecting the genomic complexity underlying medulloblastoma', *Nature*. doi: 10.1038/nature11284.

Jones, S. E. and Jomary, C. (2002) 'Clusterin', *The International Journal of Biochemistry & Cell Biology*. Pergamon, 34(5), pp. 427–431. doi: 10.1016/S1357-2725(01)00155-8.

Kalamajski, S. and Oldberg, Å. (2010) 'The role of small leucine-rich proteoglycans in collagen fibrillogenesis', *Matrix Biology*, 29, pp. 248–253. doi: 10.1016/j.matbio.2010.01.001.

Kalluri, R. (2003) 'Basement membranes: structure, assembly and role in tumour angiogenesis', *Nature reviews. Cancer*. Nat Rev Cancer, 3(6), pp. 422–433. doi: 10.1038/NRC1094.

Kanehisa, M. and Goto, S. (2000) 'KEGG: Kyoto Encyclopedia of Genes and Genomes', *Nucleic Acids Research*. Oxford Academic, 28(1), pp. 27–30. doi: 10.1093/NAR/28.1.27.

Karamanos, N. K. *et al.* (2021) 'Extracellular matrix-based cancer targeting', *Trends in Molecular Medicine*. Elsevier Ltd, 27(10), pp. 1000–1013. doi: 10.1016/j.molmed.2021.07.009.

Kariya, Y. and Miyazaki, K. (2004) 'The basement membrane protein laminin-5 acts as a soluble cell motility factor', *Experimental Cell Research*, 297(2), pp. 508–520. doi: 10.1016/j.yexcr.2004.03.044.

Kawiak, A. and Kostecka, A. (2022) 'Regulation of Bcl-2 Family Proteins in Estrogen Receptor-Positive Breast Cancer and Their Implications in Endocrine Therapy', *Cancers 2022, Vol. 14, Page 279*. Multidisciplinary Digital Publishing Institute, 14(2), p. 279. doi: 10.3390/CANCERS14020279.

Khan, K. M. F. and Falcone, D. J. (2000) ‘Selective activation of MAPK(erk1/2) by laminin-1 peptide alpha1:Ser(2091)-Arg(2108) regulates macrophage degradative phenotype’, *The Journal of biological chemistry*. J Biol Chem, 275(6), pp. 4492–4498. doi: 10.1074/JBC.275.6.4492.

Kikkawa, Y. *et al.* (2013) ‘Laminin-111-derived peptides and cancer’, *Cell Adhesion and Migration*. Taylor and Francis Inc., pp. 150–159. doi: 10.4161/cam.22827.

Kool, M. *et al.* (2012) ‘Molecular subgroups of medulloblastoma: An international meta-analysis of transcriptome, genetic aberrations, and clinical data of WNT, SHH, Group 3, and Group 4 medulloblastomas’, *Acta Neuropathologica*. doi: 10.1007/s00401-012-0958-8.

Kool, M. *et al.* (2014) ‘Genome Sequencing of SHH Medulloblastoma Predicts Genotype-Related Response to Smoothened Inhibition’, *Cancer Cell*. Cell Press, 25(3), pp. 393–405. Available at: https://www.sciencedirect.com/science/article/pii/S1535610814000737?via%3Dihub (Accessed: 29 May 2019).

Kuratomi, Y. *et al.* (1999) ‘Identification of metastasis-promoting sequences in the mouse laminin alpha 1 chain’, *Experimental cell research*. Exp Cell Res, 249(2), pp. 386–395. doi: 10.1006/EXCR.1999.4497.

Lander, G. C. *et al.* (2012) ‘Complete subunit architecture of the proteasome regulatory particle’, *Nature*. Nature Publishing Group, 482(7384), pp. 186–191. doi: 10.1038/nature10774.

Laurent, T. C. and Fraser, J. R. (1992) ‘Hyaluronan.’, *FASEB journal : official publication of the Federation of American Societies for Experimental Biology*, 6(7), pp. 2397–404. Available at: http://www.ncbi.nlm.nih.gov/pubmed/1563592 (Accessed: 26 June 2019).

Letai, A. (2017) ‘Apoptosis and cancer’, *Annual Review of Cancer Biology*, 1, pp. 275–294. doi: 10.1146/annurev-cancerbio-050216-121933.

Levental, K. R. *et al.* (2009) ‘Matrix crosslinking forces tumor progression by enhancing integrin signaling’, *Cell*. Cell, 139(5), pp. 891–906. doi: 10.1016/J.CELL.2009.10.027.

Levesley, J. *et al.* (2011) ‘RASSF1A and the BH3-only mimetic ABT-737 promote apoptosis in pediatric medulloblastoma cell lines’, *Neuro-Oncology*. Oxford Academic, 13(12), pp. 1265–1276. doi: 10.1093/NEUONC/NOR129.

Li, Jieling *et al.* (2019) ‘The clinical significance of collagen family gene expression in esophageal squamous cell carcinoma’, *PeerJ*. PeerJ Inc., 2019(10), p. e7705. doi: 10.7717/PEERJ.7705/SUPP-14.

Li, X. *et al.* (2014) ‘Biology of Human Tumors Extracellular Lumican Inhibits Pancreatic Cancer Cell Growth and Is Associated with Prolonged Survival after Surgery’, *Clin Cancer Res*, 20(24). doi: 10.1158/1078-0432.CCR-14-0970.

Li, X. *et al.* (2017) ‘Prolonged exposure to extracellular lumican restrains pancreatic adenocarcinoma growth’, *Oncogene 2017 36:38*. Nature Publishing Group, 36(38), pp. 5432–5438. doi: 10.1038/onc.2017.125.

Li, Y. *et al.* (2018) ‘TPPP3 Promotes Cell Proliferation, Invasion and Tumor Metastasis via STAT3/ Twist1 Pathway in Non-Small-Cell Lung Carcinoma’. Cell Physiol Biochem, 50(5), pp. 2004–2016. doi: 10.1159/000494892.

Li, Y. and Yu, J. (2017) ‘Knockdown of TPPP3 to inhibit cell proliferation and invasion in human colorectal cancer.’, *https://doi.org/10.1200/JCO.2017.35.15_suppl.e23006*. American Society of Clinical Oncology, 35(15_suppl), pp. e23006–e23006. doi: 10.1200/JCO.2017.35.15_SUPPL.E23006.

Liang, J. and Shang, Y. (2013) ‘Estrogen and Cancer’. doi: 10.1146/annurev-physiol-

030212-183708.

Liang, Y. *et al.* (2008) ‘Type I collagen is overexpressed in medulloblastoma as a component of tumor microenvironment’, *Journal of Neuro-Oncology*, 86, pp. 133–141. doi: 10.1007/s11060-007-9457-5.

Lin, T. and Matsui, W. (2012) ‘Hedgehog pathway as a drug target: Smoothened inhibitors in development’, *OncoTargets and Therapy*, 5, p. 47. doi: 10.2147/OTT.S21957.

Lin, Z. *et al.* (2016) ‘Suppression of GLI sensitizes medulloblastoma cells to mitochondria-mediated apoptosis’, *Journal of Cancer Research and Clinical Oncology*. Springer Berlin Heidelberg, 142(12), pp. 2469–2478. doi: 10.1007/s00432-016-2241-1.

Linke, F. *et al.* (2020) ‘3D hydrogels reveal medulloblastoma subgroup differences and identify extracellular matrix subtypes that predict patient outcome’. doi: 10.1002/path.5591.

Linke, F. *et al.* (2023) ‘Identifying new biomarkers of aggressive Group 3 and SHH medulloblastoma using 3D hydrogel models, single cell RNA sequencing and 3D OrbiSIMS imaging’, *Acta Neuropathologica Communications*. BioMed Central, 11(1), pp. 1–18. doi: 10.1186/s40478-022-01496-4.

Lopez, S. G. and Bonassar, L. J. (2021) ‘The role of SLRPs and large aggregating proteoglycans in collagen fibrillogenesis, extracellular matrix assembly, and mechanical function of fibrocartilage’, *Connective Tissue Research*. Taylor and Francis Ltd. doi: 10.1080/03008207.2021.1903887.

Louis, D. N. *et al.* (2007) ‘The 2007 WHO classification of tumours of the central nervous system.’, *Acta neuropathologica*. doi: 10.1007/s00401-007-0243-4.

Louis, D. N. *et al.* (2016) ‘The 2016 World Health Organization Classification of Tumors of the Central Nervous System: a summary.’, *Acta neuropathologica*, 131(6), pp. 803–20. doi: 10.1007/s00401-016-1545-1.

Lu, P., Weaver, V. M. and Werb, Z. (2012) ‘The extracellular matrix: A dynamic niche in cancer progression’, *Journal of Cell Biology*. The Rockefeller University Press, pp. 395–406. doi: 10.1083/jcb.201102147.

Lv, Y. *et al.* (2021) ‘Type I collagen promotes tumor progression of integrin β1 positive gastric cancer through a BCL9L/β-catenin signaling pathway’, *Aging*, 13(14), pp. 19064–19076. doi: 10.18632/aging.203355.

Ma, H., Cao, W. and Ding, M. (2020) ‘MicroRNA-31 weakens cisplatin resistance of medulloblastoma cells via NF-κB and PI3K/AKT pathways’, *BioFactors*, 46(5), pp. 831–838. doi: 10.1002/biof.1616.

Ma, L., Dong, L. and Chang, P. (2019) ‘CD44v6 engages in colorectal cancer progression’, *Cell Death & Disease 2018 10:1*. Nature Publishing Group, 10(1), pp. 1–13. doi: 10.1038/s41419-018-1265-7.

Mammoto, T. and Ingber, D. E. (2010) ‘Mechanical control of tissue and organ development’, *Development*. doi: 10.1242/dev.024166.

Mancuso, M. *et al.* (2010) ‘Protective role of 17 β-estradiol on medulloblastoma development in Patched 1 heterozygous mice’, *International journal of cancer*. Int J Cancer, 127(12), pp. 2749–2757. doi: 10.1002/IJC.25293.

Martignone, S. *et al.* (1993) ‘Prognostic significance of the 67-kilodalton laminin receptor expression in human breast carcinomas’, *Journal of the National Cancer Institute*. J Natl Cancer Inst, 85(5), pp. 398–402. doi: 10.1093/JNCI/85.5.398.

Martini, M. *et al.* (2014) ‘PI3K/AKT signaling pathway and cancer: An updated review’,

Annals of Medicine, 46(6), pp. 372–383. doi: 10.3109/07853890.2014.912836.

Martino, M. M. *et al.* (2009) ‘Controlling integrin specificity and stem cell differentiation in 2D and 3D environments through regulation of fibronectin domain stability’, *Biomaterials*. Elsevier, 30(6), pp. 1089–1097. doi: 10.1016/J.BIOMATERIALS.2008.10.047.

Martins Cavaco, A. C. *et al.* (2020) ‘Collagen biology making inroads into prognosis and treatment of cancer progression and metastasis’, *Cancer and Metastasis Reviews*. Cancer and Metastasis Reviews, 39(3), pp. 603–623. doi: 10.1007/s10555-020-09888-5.

Massimino, M. *et al.* (2016) ‘Childhood medulloblastoma’, *Critical Reviews in Oncology/Hematology*. doi: 10.1016/j.critrevonc.2016.05.012.

McManamy, C. S. *et al.* (2007) ‘Nodule formation and desmoplasia in medulloblastomas - Defining the nodular/desmoplastic variant and its biological behavior’, *Brain Pathology*. doi: 10.1111/j.1750-3639.2007.00058.x.

Medrano-González, P. A. *et al.* (2021) ‘Proteolytic Processing of CD44 and Its Implications in Cancer’, *Stem Cells International*. Hindawi Limited, 2021. doi: 10.1155/2021/6667735.

Meireles Da Costa, N. *et al.* (2021) ‘Potential therapeutic significance of laminin in head and neck squamous carcinomas’, *Cancers*, 13(8), pp. 1–17. doi: 10.3390/cancers13081890.

Menyhárt, O. and Győrffy, B. (2020) ‘Molecular stratifications, biomarker candidates and new therapeutic options in current medulloblastoma treatment approaches’, *Cancer and Metastasis Reviews*. Springer, pp. 211–233. doi: 10.1007/s10555-020-09854-1.

Merzak, A., Koocheckpour, S. and Pilkington, G. J. (1994) 'CD44 Mediates Human Glioma Cell Adhesion and Invasion in Vitro', *Cancer Research*. American Association for Cancer Research, 54(15), pp. 3988–3992.

Millard, N. E. and De Braganca, K. C. (2016) 'Medulloblastoma', *Journal of Child Neurology*. SAGE PublicationsSage CA: Los Angeles, CA, 31(12), pp. 1341–1353. doi: 10.1177/0883073815600866.

Mishra, Y. G. and Manavathi, B. (2021) 'Focal adhesion dynamics in cellular function and disease', *Cellular Signalling*. Elsevier Inc., 85(May), p. 110046. doi: 10.1016/j.cellsig.2021.110046.

Mook, O. R. F., Frederiks, W. M. and Van Noorden, C. J. F. (2004) 'The role of gelatinases in colorectal cancer progression and metastasis', *Biochimica et Biophysica Acta (BBA) - Reviews on Cancer*. Elsevier, 1705(2), pp. 69–89. doi: 10.1016/J.BBCAN.2004.09.006.

Mooney, K. L. *et al.* (2016) 'The role of CD44 in glioblastoma multiforme', *Journal of Clinical Neuroscience*. Churchill Livingstone, pp. 1–5. doi: 10.1016/j.jocn.2016.05.012.

Morfouace, M. *et al.* (2015) 'ABCG2 transporter expression impacts group 3 medulloblastoma response to chemotherapy', *Cancer Research*, 75(18), pp. 3879–3889. doi: 10.1158/0008-5472.CAN-15-0030.

Mörgelin, M. *et al.* (1994) 'The cartilage proteoglycan aggregate: assembly through combined protein-carbohydrate and protein-protein interactions', *Biophysical Chemistry*. doi: 10.1016/0301-4622(94)85024-0.

Mori, K., Shibanuma, M. and Nose, K. (2004) 'Invasive Potential Induced under Long-Term Oxidative Stress in Mammary Epithelial Cells', *Cancer Research*. American Association for Cancer Research, 64(20), pp. 7464–7472. doi: 10.1158/0008-5472.CAN-04-1725.

Mosimann, C., Hausmann, G. and Basler, K. (2009) ‘β-Catenin hits chromatin: regulation of Wnt target gene activation’, *Nature Reviews Molecular Cell Biology*. Nature Publishing Group, 10(4), pp. 276–286. doi: 10.1038/nrm2654.

Motoyama, M. *et al.* (2005) ‘Positive and negative regulation of nuclear factor-kappaB-mediated transcription by IkappaB-zeta, an inducible nuclear protein’, *The Journal of biological chemistry*. J Biol Chem, 280(9), pp. 7444–7451. doi: 10.1074/JBC.M412738200.

Murphy, J. M. *et al.* (2020) ‘Targeting focal adhesion kinase in cancer cells and the tumor microenvironment’, *Experimental and Molecular Medicine*. Springer US, 52(6), pp. 877–886. doi: 10.1038/s12276-020-0447-4.

Najafi, M., Farhood, B. and Mortezaee, K. (2019) ‘Extracellular matrix (ECM) stiffness and degradation as cancer drivers’, *Journal of Cellular Biochemistry*, 120(3), pp. 2782–2790. doi: 10.1002/jcb.27681.

Nakasu, S. *et al.* (1994) ‘bcl-2 protein expression in tumors of the central nervous system’, *Acta Neuropathologica 1994 88:6*. Springer, 88(6), pp. 520–526. doi: 10.1007/BF00296488.

Nasir, A. *et al.* (2021) ‘ABCB1 inhibition provides a novel therapeutic target to block TWIST1-induced migration in medulloblastoma’, *Neuro-Oncology Advances*, 3(1), pp. 1–12. doi: 10.1093/noajnl/vdab030.

Nazari, S. S. (2020) ‘Generation of 3D Tumor Spheroids with Encapsulating Basement Membranes for Invasion Studies’, *Current Protocols in Cell Biology*. John Wiley & Sons, Ltd, 87(1), p. e105. doi: 10.1002/CPCB.105.

Necas, J. *et al.* (2008) *Hyaluronic acid (hyaluronan): a review*, *Veterinarni Medicina*. Available at: http://www.kalipura.it/download/Hyaluronic_acid.pdf (Accessed: 11 June 2019).

Neel, E. A. A. *et al.* (2013) ‘Collagen-Emerging collagen based therapies hit the patient ☆’, *Advanced Drug Delivery Reviews*, 65, pp. 429–456. doi: 10.1016/j.addr.2012.08.010.

Nicholson, C. and Hrabětová, S. (2017) ‘Brain Extracellular Space: The Final Frontier of Neuroscience’, *Biophysical Journal*, 113(10), pp. 2133–2142. doi: 10.1016/j.bpj.2017.06.052.

Northcott, P. A. *et al.* (2011) ‘Medulloblastoma comprises four distinct molecular variants’, *Journal of Clinical Oncology*. doi: 10.1200/JCO.2009.27.4324.

Northcott, P. A., Jones, D. T. W., *et al.* (2012) ‘Medulloblastomics: The end of the beginning’, *Nature Reviews Cancer*. doi: 10.1038/nrc3410.

Northcott, P. A., Korshunov, A., *et al.* (2012) ‘The clinical implications of medulloblastoma subgroups’, *Nature Reviews Neurology*, 8, pp. 340–351. doi: 10.1038/nrneurol.2012.78.

Northcott, P. A. *et al.* (2014) ‘Enhancer hijacking activates GFI1 family oncogenes in medulloblastoma’, *Nature*. doi: 10.1038/nature13379.

Northcott, P. A. *et al.* (2017) ‘The whole-genome landscape of medulloblastoma subtypes.’, *Nature*. Nature Publishing Group, 547(7663), pp. 311–317. doi: 10.1038/nature22973.

Northcott, P. A. *et al.* (2019) ‘Medulloblastoma’, *Nature Reviews Disease Primers*. Nature Publishing Group, 5(1), pp. 1–20. doi: 10.1038/s41572-019-0063-6.

Novak, U. and Kaye, A. H. (2000) ‘Extracellular matrix and the brain: Components and function’, *Journal of Clinical Neuroscience*. doi: 10.1054/jocn.1999.0212.

Oh, S. B. *et al.* (2019) ‘Clusterin contributes to early stage of Alzheimer’s disease pathogenesis’, *Brain Pathology*. Blackwell Publishing Ltd, 29(2), pp. 217–231. doi:

10.1111/BPA.12660.

Okamoto, I. *et al.* (2002) ‘Proteolytic cleavage of the CD44 adhesion molecule in multiple human tumors’, *American Journal of Pathology*. American Society for Investigative Pathology Inc., 160(2), pp. 441–447. doi: 10.1016/S0002-9440(10)64863-8.

Olin, A. I. *et al.* (2001) ‘The proteoglycans aggrecan and versican form networks with fibulin-2 through their lectin domain binding’, *Journal of Biological Chemistry*. doi: 10.1074/jbc.M006783200.

Van Ommeren, R. *et al.* (2020) ‘The molecular biology of medulloblastoma metastasis’, *Brain Pathology*, 30(3), pp. 691–702. doi: 10.1111/bpa.12811.

Orr, B. A. (2020) ‘Pathology, diagnostics, and classification of medulloblastoma’, *Brain Pathology ISSN*, 30(45), pp. 664–678. doi: 10.1111/bpa.12837.

Ostrom, Q. T. *et al.* (2017) ‘CBTRUS Statistical Report: Primary brain and other central nervous system tumors diagnosed in the United States in 2010–2014’, *Neuro-Oncology*. doi: 10.1093/neuonc/nox158.

Othman, R. T. *et al.* (2014) ‘Overcoming multiple drug resistance mechanisms in medulloblastoma’, *Acta Neuropathologica Communications*, 2(1), pp. 18–22. doi: 10.1186/2051-5960-2-57.

Özen, Ö. *et al.* (2004) ‘Expression of Matrix Metalloproteinases and Their Inhibitors in Medulloblastomas and Their Prognostic Relevance’, *Clinical Cancer Research*. American Association for Cancer Research, 10(14), pp. 4746–4753. doi: 10.1158/1078-0432.CCR-0625-03.

Packer, R. J. and Vezina, G. (2008) ‘Management of and prognosis with medulloblastoma: Therapy at a crossroads’, *Archives of Neurology*. doi:

10.1001/archneur.65.11.1419.

Paolillo, M. and Schinelli, S. (2019) ‘Extracellular Matrix Alterations in Metastatic Processes’, *International Journal of Molecular Sciences*, 20(4947–4964). doi: 10.3390/ijms20194947.

Peng, M. *et al.* (2019) ‘The role of Clusterin in cancer metastasis’, *Cancer Management and Research*. Cancer Manag Res, 11, pp. 2405–2414. doi: 10.2147/CMAR.S196273.

Pereira Maurício de Barros, D. *et al.* (2021) ‘17β-Estradiol Modulates the Expression of CD44 and CD326 in Estrogen-Sensitive Breast Cancer Cells’, pp. 1–13. doi: 10.21203/RS.3.RS-270944/V1.

Pickup, M. W., Mouw, J. K. and Weaver, V. M. (2014) ‘The extracellular matrix modulates the hallmarks of cancer’, *EMBO Rep*, 15(12), pp. 1243–1253. doi: 10.15252/embr.201439246.

Pizer, B. L. and Clifford, S. C. (2009) ‘The potential impact of tumour biology on improved clinical practice for medulloblastoma: progress towards biologically driven clinical trials’, *British Journal of Neurosurgery*. Taylor & Francis, 23(4), pp. 364–375. doi: 10.1080/02688690903121807.

Ponta, H., Sherman, L. and Herrlich, P. A. (2003) *CD44: From adhesion molecules to signalling regulators*. Nature Publishing Group. doi: 10.1038/nrm1004.

Popova, N. V. and Jücker, M. (2022) ‘The Functional Role of Extracellular Matrix Proteins in Cancer’, *Cancers 2022, Vol. 14, Page 238*. Multidisciplinary Digital Publishing Institute, 14(1), p. 238. doi: 10.3390/CANCERS14010238.

Pugh, T. J. *et al.* (2012) ‘Medulloblastoma exome sequencing uncovers subtype-specific somatic mutations’, *Nature*, 488(7409), pp. 106–110. doi:

10.1038/nature11329.

Qi, D. *et al.* (2019) ‘Abstract 1122: CD44 as potential therapeutic target for medulloblastoma metastasis’, in *Cancer Research*. American Association for Cancer Research (AACR), pp. 1122–1122. doi: 10.1158/1538-7445.am2019-1122.

Quail, D. F. and Joyce, J. A. (2017) ‘The Microenvironmental Landscape of Brain Tumors’, *Cancer Cell*, 31(3), pp. 326–341. doi: 10.1016/j.ccell.2017.02.009.

Radotra, B. and McCormick, D. (1997) ‘Glioma Invasion in vitro is mediated by CD44–HYALURONAN interactions’, *The Journal of Pathology*. John Wiley & Sons, Ltd, 181(4), pp. 434–438. doi: 10.1002/(SICI)1096-9896(199704)181:4<434::AID-PATH797>3.0.CO;2-S.

Ramaswamy, V. *et al.* (2016) ‘Risk stratification of childhood medulloblastoma in the molecular era: the current consensus’, *Acta Neuropathologica*. doi: 10.1007/s00401-016-1569-6.

Ramaswamy, V. and Taylor, M. D. (2017) ‘JOURNAL OF CLINICAL ONCOLOGY Medulloblastoma: From Myth to Molecular’, *J Clin Oncol*, 35. doi: 10.1200/JCO.2017.

Ramovs, V., te Molder, L. and Sonnenberg, A. (2017) ‘The opposing roles of laminin-binding integrins in cancer’, *Matrix Biology*. Elsevier B.V., 57–58, pp. 213–243. doi: 10.1016/j.matbio.2016.08.007.

Rascio, F. *et al.* (2021) ‘The pathogenic role of PI3K/AKT pathway in cancer onset and drug resistance: an updated review’, *Cancers*, 13(16). doi: 10.3390/cancers13163949.

Rauch, U. (2004) ‘Extracellular matrix components associated with remodeling processes in brain’, *CMLS, Cell. Mol. Life Sci*, 61, pp. 2031–2045. doi: 10.1007/s00018-004-4043-x.

Raybaud, C. *et al.* (2015) ‘Posterior fossa tumors in children: developmental anatomy

and diagnostic imaging', *Child's Nervous System*, pp. 1661–1676. doi: 10.1007/s00381-015-2834-z.

Remke, M. and Ramaswamy, V. (2022) 'WNT Medulloblastoma Limbo: How Low Can We Go?', *Clinical cancer research : an official journal of the American Association for Cancer Research*, 28(19), pp. 4161–4163. doi: 10.1158/1078-0432.CCR-22-1780.

Reynaud, E. (2010) 'Protein Misfolding and Degenerative Diseases', *Nature Education*, 3(9), p. 28.

Rochkind, S. *et al.* (1991) 'Extracranial metastases of medulloblastoma in adults: Literature review', *Journal of Neurology Neurosurgery and Psychiatry*, 54(1), pp. 80–86. doi: 10.1136/jnnp.54.1.80.

Roper, S. J. *et al.* (2021) '3D spheroid models of paediatric SHH medulloblastoma mimic tumour biology, drug response and metastatic dissemination', *Scientific Reports |*, 11, p. 4259. doi: 10.1038/s41598-021-83809-6.

Roper, S. J. and Coyle, B. (2022) 'Establishing an In Vitro 3D Spheroid Model to Study Medulloblastoma Drug Response and Tumor Dissemination', *Current Protocols*, 2(1). doi: 10.1002/CPZ1.357.

Roth, R. B. *et al.* (2006) 'Gene expression analyses reveal molecular relationships among 20 regions of the human CNS.', *Neurogenetics*, 7(2), pp. 67–80. doi: 10.1007/s10048-006-0032-6.

Rousseau, A. and Bertolotti, A. (2018) 'Regulation of proteasome assembly and activity in health and disease', *Nature Reviews Molecular Cell Biology*. Springer US, 19(11), pp. 697–712. doi: 10.1038/s41580-018-0040-z.

Rousselle, P. and Scoazec, J. Y. (2020) 'Laminin 332 in cancer: When the extracellular matrix turns signals from cell anchorage to cell movement', *Seminars in cancer*

biology. Semin Cancer Biol, 62, pp. 149–165. doi: 10.1016/J.SEMCANCER.2019.09.026.

Ruoslahti, E. (1996) *Brain extracellular matrix*, *Glycobiology*. Narnia. doi: 10.1093/glycob/6.5.489.

Sasaki, T., Fässler, R. and Hohenester, E. (2004) 'Laminin: The crux of basement membrane assembly', *Journal of Cell Biology*. The Rockefeller University Press, pp. 959–963. doi: 10.1083/jcb.200401058.

Schiffer, D. *et al.* (1996) 'Bcl-2 distribution in neuroepithelial tumors: an immunohistochemical study', *Journal of Neuro-Oncology 1996 27:2*. Springer, 27(2), pp. 101–109. doi: 10.1007/BF00177472.

Schüller, U., Schober, F., Kretzschmar, H. A., Herms, J., *et al.* (2004) 'Bcl-2 expression inversely correlates with tumour cell differentiation in medulloblastoma', *Neuropathology and Applied Neurobiology*. John Wiley & Sons, Ltd, 30(5), pp. 513–521. doi: 10.1111/J.1365-2990.2004.00553.X.

Schüller, U., Schober, F., Kretzschmar, H. A. and Herms, J. (2004) 'Bcl-2 expression inversely correlates with tumour cell differentiation in medulloblastoma', *Neuropathology and Applied Neurobiology*. John Wiley & Sons, Ltd, 30(5), pp. 513–521. doi: 10.1111/J.1365-2990.2004.00553.X.

Schumacher, S. *et al.* (2022) 'Bottom-up reconstitution of focal adhesion complexes', *FEBS Journal*, 289(12), pp. 3360–3373. doi: 10.1111/febs.16023.

Schwartz, M. A. (2010) 'Integrins and Extracellular Matrix in Mechanotransduction', *Cold Spring Harbor Perspectives in Biology*. Cold Spring Harbor Laboratory Press, 2(12), p. a005066. doi: 10.1101/CSHPERSPECT.A005066.

Schwarz, D. S. and Blower, M. D. (2016) 'The endoplasmic reticulum: Structure,

function and response to cellular signaling', *Cellular and Molecular Life Sciences*. Springer Basel, 73(1), pp. 79–94. doi: 10.1007/s00018-015-2052-6.

Senbanjo, L. T. and Chellaiah, M. A. (2017) 'CD44: A Multifunctional Cell Surface Adhesion Receptor Is a Regulator of Progression and Metastasis of Cancer Cells', *Frontiers in Cell and Developmental Biology*. Frontiers Media S.A., 5(MAR), p. 18. doi: 10.3389/fcell.2017.00018.

Sethi, T. *et al.* (1999) 'Extracellular matrix proteins protect small cell lung cancer cells against apoptosis: A mechanism for small cell lung cancer growth and drug resistance in vivo', *Nature Medicine*, 5(6), pp. 662–668. doi: 10.1038/9511.

Shapiro, B. *et al.* (2015) 'Clusterin, a gene enriched in intestinal stem cells, is required for L1-mediated colon cancer metastasis', *Oncotarget*. Impact Journals, LLC, 6(33), p. 34389. doi: 10.18632/ONCOTARGET.5360.

Sharma, T. *et al.* (2019) 'Second-generation molecular subgrouping of medulloblastoma: an international meta-analysis of Group 3 and Group 4 subtypes', *Acta Neuropathologica*. Springer Verlag, 138(2), pp. 309–326. doi: 10.1007/s00401-019-02020-0.

Shental-Bechor, D. and Levy, Y. (2009) 'Folding of glycoproteins: toward understanding the biophysics of the glycosylation code', *Current Opinion in Structural Biology*. Elsevier Current Trends, 19(5), pp. 524–533. doi: 10.1016/J.SBI.2009.07.002.

Shih, D. J. H. *et al.* (2014) 'Cytogenetic Prognostication Within Medulloblastoma Subgroups', *Journal of Clinical Oncology*, 32(9), pp. 886–896. doi: 10.1200/JCO.2013.50.9539.

Shoulders, M. D. and Raines, R. T. (2009) 'COLLAGEN STRUCTURE AND STABILITY', *Annual review of biochemistry*. NIH Public Access, 78, p. 929. doi:

10.1146/ANNUREV.BIOCHEM.77.032207.120833.

Singh, R., Letai, A. and Sarosiek, K. (2019) ‘Regulation of apoptosis in health and disease: the balancing act of BCL-2 family proteins’, *Nature Reviews Molecular Cell Biology*. Springer US, 20(3), pp. 175–193. doi: 10.1038/s41580-018-0089-8.

Siqueira, A. S. *et al.* (2016) ‘Laminin-111 peptide C16 regulates invadopodia activity of malignant cells through β1 integrin, Src and ERK 1/2’, *Oncotarget*. Impact Journals, LLC, 7(30), p. 47904. doi: 10.18632/ONCOTARGET.10062.

Sounni, N. E. and Noel, A. (2013) ‘Targeting the Tumor Microenvironment for Cancer Therapy’, *Clinical Chemistry*. Clinical Chemistry, 59(1), pp. 85–93. doi: 10.1373/CLINCHEM.2012.185363.

Stylianopoulos, T. *et al.* (2012) ‘Causes, consequences, and remedies for growth-induced solid stress in murine and human tumors’, *Proceedings of the National Academy of Sciences of the United States of America*. National Academy of Sciences, 109(38), pp. 15101–15108. doi: 10.1073/pnas.1213353109.

Stylianopoulos, T. *et al.* (2013) ‘Coevolution of solid stress and interstitial fluid pressure in tumors during progression: Implications for vascular collapse’, *Cancer Research*, 73(13), pp. 3833–3841. doi: 10.1158/0008-5472.CAN-12-4521.

Su, C. Y. *et al.* (2020) ‘The Biological Functions and Clinical Applications of Integrins in Cancers’, *Frontiers in Pharmacology*. Frontiers Media S.A., 11, p. 1435. doi: 10.3389/FPHAR.2020.579068/BIBTEX.

Taylor, L., Kerr, I. D. and Coyle, B. (2021) ‘Y-box binding protein-1: A neglected target in pediatric brain tumors?’, *Molecular Cancer Research*, 19(3), pp. 375–387. doi: 10.1158/1541-7786.MCR-20-0655.

Taylor, M. D. *et al.* (2012) ‘Molecular subgroups of medulloblastoma: The current

consensus', *Acta Neuropathologica*. doi: 10.1007/s00401-011-0922-z.

Tevis, Kristie M *et al.* (2017) 'Embedded Spheroids as Models of the Cancer Microenvironment', *Advanced Biosystems*. John Wiley & Sons, Ltd, 1(10), p. 1700083. doi: 10.1002/ADBI.201700083.

Thompson, M. C. *et al.* (2006) 'Genomics identifies medulloblastoma subgroups that are enriched for specific genetic alterations', *Journal of Clinical Oncology*. doi: 10.1200/JCO.2005.04.4974.

Thorne, R. F. *et al.* (2020) 'Evaluating nuclear translocation of surface receptors: recommendations arising from analysis of CD44'. Histochem Cell Biol, 153(2), pp. 77–87. Available at: https://doi.org/10.1007/s00418-019-01835-y (Accessed: 31 March 2022).

Tohgo, A. *et al.* (1994) 'Structural determination and characterization of a 40 kDa protein isolated from rat 40 S ribosomal subunit', *FEBS letters*. FEBS Lett, 340(1–2), pp. 133–138. doi: 10.1016/0014-5793(94)80188-6.

Totzke, G. *et al.* (2006) 'A novel member of the IκB family, human IκB-ζ, inhibits transactivation of p65 and its DNA binding', *Journal of Biological Chemistry*, 281(18), pp. 12645–12654. doi: 10.1074/jbc.M511956200.

Trinh, D. V. *et al.* (2008) 'The nuclear I kappaB protein I kappaB zeta specifically binds NF-kappaB p50 homodimers and forms a ternary complex on kappaB DNA', *Journal of molecular biology*. J Mol Biol, 379(1), pp. 122–135. doi: 10.1016/J.JMB.2008.03.060.

Trombetta-Lima, M. *et al.* (2021) 'Extracellular Matrix Proteome Remodeling in Human Glioblastoma and Medulloblastoma', *J. Proteome Res*, 20, p. 4707. doi: 10.1021/acs.jproteome.1c00251.

Troup, S. *et al.* (2003) ‘Reduced Expression of the Small Leucine-rich Proteoglycans, Lumican, and Decorin Is Associated with Poor Outcome in Node-negative Invasive Breast Cancer 1’.

Underhill, C. (1992) ‘CD44: The hyaluronan receptor’, *Journal of Cell Science*, pp. 293–298.

Vince, G. H. *et al.* (2001) ‘Medulloblastoma displays distinct regional matrix metalloprotease expression’, *Journal of Neuro-Oncology*. Springer, 53(2), pp. 99–106. doi: 10.1023/A:1012241031138.

Vinci, M. *et al.* (2012) ‘Advances in establishment and analysis of three-dimensional tumor spheroid-based functional assays for target validation and drug evaluation’, *BMC Biology*. BioMed Central, 10(1), pp. 1–21. doi: 10.1186/1741-7007-10-29/FIGURES/8.

Vinci, M. *et al.* (2013) ‘Tumor spheroid-based migration assays for evaluation of therapeutic agents’, *Methods in molecular biology (Clifton, N.J.)*. Methods Mol Biol, 986, pp. 253–266. doi: 10.1007/978-1-62703-311-4_16.

Vinci, M., Box, C. and Eccles, S. A. (2015) ‘Three-Dimensional (3D) Tumor Spheroid Invasion Assay’, *Journal of Visualized Experiments : JoVE*. MyJoVE Corporation, 2015(99), p. 52686. doi: 10.3791/52686.

Vriend, J. and Marzban, H. (2017) ‘The ubiquitin-proteasome system and chromosome 17 in cerebellar granule cells and medulloblastoma subgroups’, *Cellular and Molecular Life Sciences*. Springer International Publishing, 74(3), pp. 449–467. doi: 10.1007/s00018-016-2354-3.

Wade, A. *et al.* (2013) ‘Proteoglycans and their roles in brain cancer’, *FEBS Journal*. doi: 10.1111/febs.12109.

Wang, C., Tong, X. and Yang, F. (2014) 'Bioengineered 3D brain tumor model to elucidate the effects of matrix stiffness on glioblastoma cell behavior using peg-based hydrogels', *Molecular Pharmaceutics*, 11(7), pp. 2115–2125. doi: 10.1021/mp5000828.

Wang, J. *et al.* (2018) 'Medulloblastoma: From Molecular Subgroups to Molecular Targeted Therapies', *Annual Review of Neuroscience*. doi: 10.1146/annurev-neuro-070815-013838.

Wang, L. *et al.* (2014) 'Smoothened activates breast cancer stem-like cell and promotes tumorigenesis and metastasis of breast cancer', *Biomedicine and Pharmacotherapy*. Elsevier Masson SAS, 68(8), pp. 1099–1104. doi: 10.1016/j.biopha.2014.09.012.

Warren, C. F. A., Wong-Brown, M. W. and Bowden, N. A. (2019) 'BCL-2 family isoforms in apoptosis and cancer', *Cell Death and Disease*. Springer US, 10(3), pp. 112–124. doi: 10.1038/s41419-019-1407-6.

Wen, S. *et al.* (2011) 'Inhibition of NF-κB signaling commits resveratrol-treated medulloblastoma cells to apoptosis without neuronal differentiation', *Journal of Neuro-Oncology*. Springer, 104(1), pp. 169–177. doi: 10.1007/S11060-010-0496-Y/TABLES/2.

Wen, S. *et al.* (2019) 'Cancer-associated fibroblast (CAF)-derived IL32 promotes breast cancer cell invasion and metastasis via integrin β3-p38 MAPK signalling', *Cancer letters*. Cancer Lett, 442, pp. 320–332. doi: 10.1016/J.CANLET.2018.10.015.

Wiese, S., Karus, M. and Faissner, A. (2012) 'Astrocytes as a source for extracellular matrix molecules and cytokines', *Frontiers in Pharmacology*, 3 JUN(June), pp. 1–13. doi: 10.3389/fphar.2012.00120.

Wijaya, J. *et al.* (2020) 'An ABC transporter drives the Sonic Hedgehog pathway

contributing to medulloblastoma pathogenesis', *Cancer Research*. NIH Public Access, 80(7), pp. 1524–1537. doi: 10.1158/0008-5472.CAN-19-2054.An.

Williamson, D. *et al.* (2022) 'Medulloblastoma group 3 and 4 tumors comprise a clinically and biologically significant expression continuum reflecting human cerebellar development', *Cell reports*. Cell Rep, 40(5). doi: 10.1016/J.CELREP.2022.111162.

Winkler, J. *et al.* (2020) 'Concepts of extracellular matrix remodelling in tumour progression and metastasis', *Nature Communications 2020 11:1*. Nature Publishing Group, 11(1), pp. 1–19. doi: 10.1038/s41467-020-18794-x.

De Wit, M. *et al.* (2013) 'Lumican and versican are associated with good outcome in stage ii and iii colon cancer', *Annals of Surgical Oncology*. Springer, 20(3 SUPPL.), pp. 348–359. doi: 10.1245/S10434-012-2441-0/FIGURES/5.

Wong, J. C. Y. *et al.* (2010) 'Definitive endoderm derived from human embryonic stem cells highly express the integrin receptors alphaV and beta5', *Cell adhesion & migration*. Cell Adh Migr, 4(1), pp. 39–45. doi: 10.4161/CAM.4.1.10627.

Worthington, P., Pochan, D. J. and Langhans, S. A. (2015) 'Peptide Hydrogels - Versatile Matrices for 3D Cell Culture in Cancer Medicine.', *Frontiers in oncology*, 5(April), p. 92. doi: 10.3389/fonc.2015.00092.

Wu, X. *et al.* (2012) 'Clonal selection drives genetic divergence of metastatic medulloblastoma', *Nature*. doi: 10.1038/nature10825.

Xie, X., Ma, X. and Liu, Y.-G. (2019) 'Decoding Sanger Sequencing Chromatograms from CRISPR-Induced Mutations BT - Plant Genome Editing with CRISPR Systems: Methods and Protocols', 1917, pp. 33–43. doi: 10.1007/978-1-4939-8991-1.

Xu, H. *et al.* (2020) 'CD44 as a tumor biomarker and therapeutic target', *Experimental Hematology & Oncology 2020 9:1*. BioMed Central, 9(1), pp. 1–14. doi:

10.1186/S40164-020-00192-0.

Yamaguchi, Y. (2000) ‘Lecticans: Organizers of the brain extracellular matrix’, *Cellular and Molecular Life Sciences*. doi: 10.1007/PL00000690.

Yamakawa, Y. *et al.* (2017) ‘CD44 variant 9 expression as a predictor for gastric cancer recurrence: immunohistochemical and metabolomic analysis of surgically resected tissues’, *Biomedical research (Tokyo, Japan)*. Biomed Res, 38(1), pp. 41–52. doi: 10.2220/BIOMEDRES.38.41.

Yan, L. *et al.* (2015) ‘Lewis y enhances CAM-DR in ovarian cancer cells by activating the FAK signaling pathway and upregulating Bcl-2/Bcl-XL expression’, *Biochimie*. Elsevier Ltd, 113, pp. 17–25. doi: 10.1016/j.biochi.2015.01.013.

Yang, C. *et al.* (2020) ‘CD44/HA signaling mediates acquired resistance to a PI3Kα inhibitor’, *Cell Death and Disease*, 11(10), pp. 1–11. doi: 10.1038/s41419-020-03037-0.

Yang, Z. *et al.* (2020) ‘TPPP3 Associated with Prognosis and Immune Infiltrates in Head and Neck Squamous Carcinoma’, *BioMed Research International*. Hindawi Limited, 2020. doi: 10.1155/2020/3962146.

Yauch, R. L. *et al.* (2009) ‘Smoothened Mutation Confers Resistance to a Hedgehog Pathway Inhibitor in Medulloblastoma’, *Science*, 326(5952), pp. 572–574. doi: 10.1126/science.1179386.

Yoshida, Y. *et al.* (2001) ‘Role of laminin in ovarian cancer tumor growth and metastasis via regulation of Mdm2 and Bcl-2 expression’, *International journal of oncology*. Int J Oncol, 18(5), pp. 913–921. doi: 10.3892/IJO.18.5.913.

Yu, Q. and Stamenkovic, I. (1999) ‘Localization of matrix metalloproteinase 9 to the cell surface provides a mechanism for CD44-mediated tumor invasion’, *Genes &*

Development. Cold Spring Harbor Laboratory Press, 13(1), p. 35. doi: 10.1101/GAD.13.1.35.

Yurchenco, P. D. *et al.* (1997) 'The α chain of laminin-1 is independently secreted and drives seretion of its β- and γ-chain partners', *Proceedings of the National Academy of Sciences of the United States of America*, 94(19), pp. 10189–10194. doi: 10.1073/pnas.94.19.10189.

Zanoni, M. *et al.* (2016) '3D tumor spheroid models for in vitro therapeutic screening: a systematic approach to enhance the biological relevance of data obtained', *Scientific Reports 2016 6:1*. Nature Publishing Group, 6(1), pp. 1–11. doi: 10.1038/srep19103.

Zapotocky, M. *et al.* (2017) 'Differential patterns of metastatic dissemination across medulloblastoma subgroups.', *Journal of Neurosurgery Pediatrics*, 21(February), pp. 1–8. doi: 10.3171/2017.8.PEDS17264.

Zhang, H. *et al.* (2005) 'Clusterin inhibits apoptosis by interacting with activated Bax', *Nature Cell Biology 2005 7:9*. Nature Publishing Group, 7(9), pp. 909–915. doi: 10.1038/ncb1291.

Zhou, W. *et al.* (2009) 'Depletion of tubulin polymerization promoting protein family member 3 suppresses HeLa cell proliferation', *Molecular and Cellular Biochemistry*, 333, pp. 91–98. doi: 10.1007/s11010-009-0208-0.

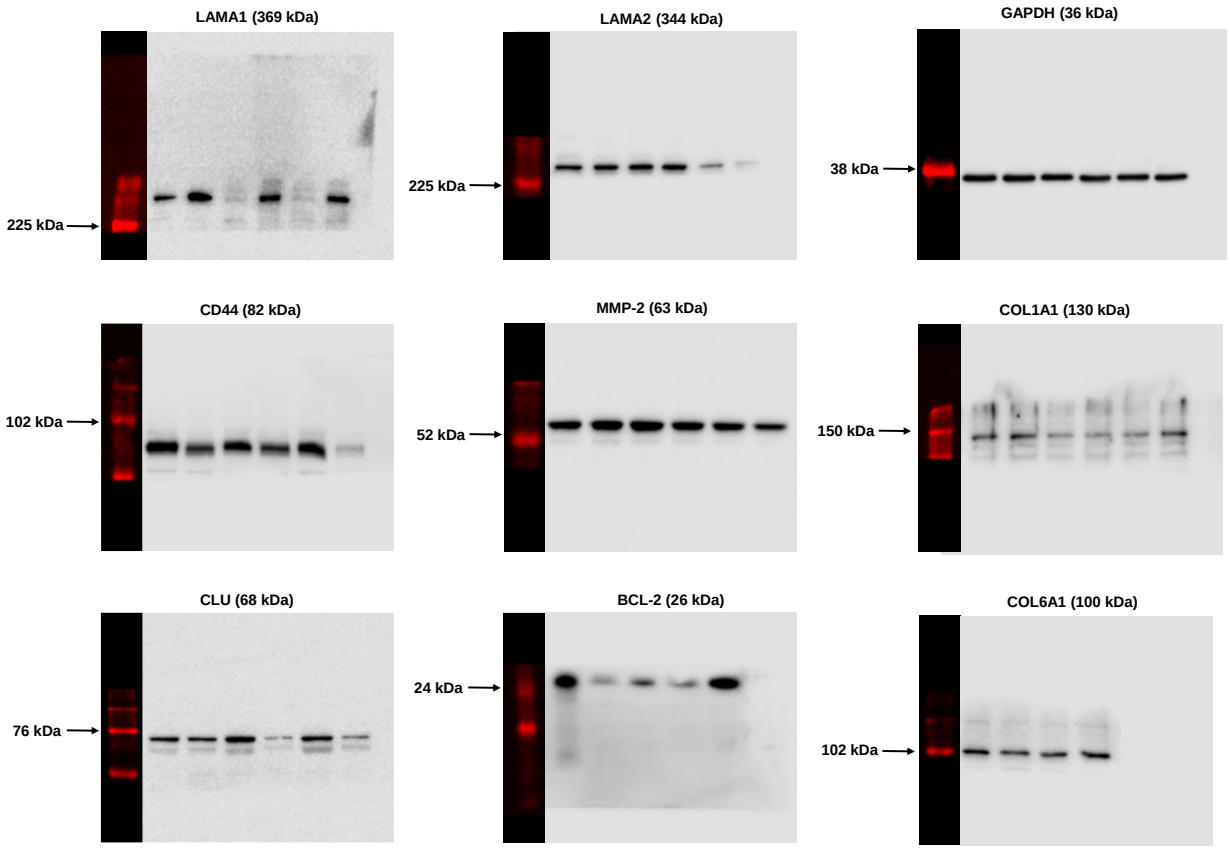
Zhu, J., Miller, J. N. and Schuetz, J. D. (2022) 'An ABC transporter as a potential target against SHH-Medulloblastoma: From Benchtop to Bedside', *Oncotarget*. Impact Journals, LLC, 13(1), p. 1017. doi: 10.18632/ONCOTARGET.28272.

Zhu, L., Plow, E. F. and Qin, J. (2021) 'Initiation of focal adhesion assembly by talin and kindlin: A dynamic view', *Protein Science*, 30(3), pp. 531–542. doi: 10.1002/pro.4014.

Zhukova, N. *et al.* (2013) ‘Subgroup-specific prognostic implications of TP53 mutation in medulloblastoma.’, *Journal of clinical oncology : official journal of the American Society of Clinical Oncology*. American Society of Clinical Oncology, 31(23), pp. 2927–35. doi: 10.1200/JCO.2012.48.5052.

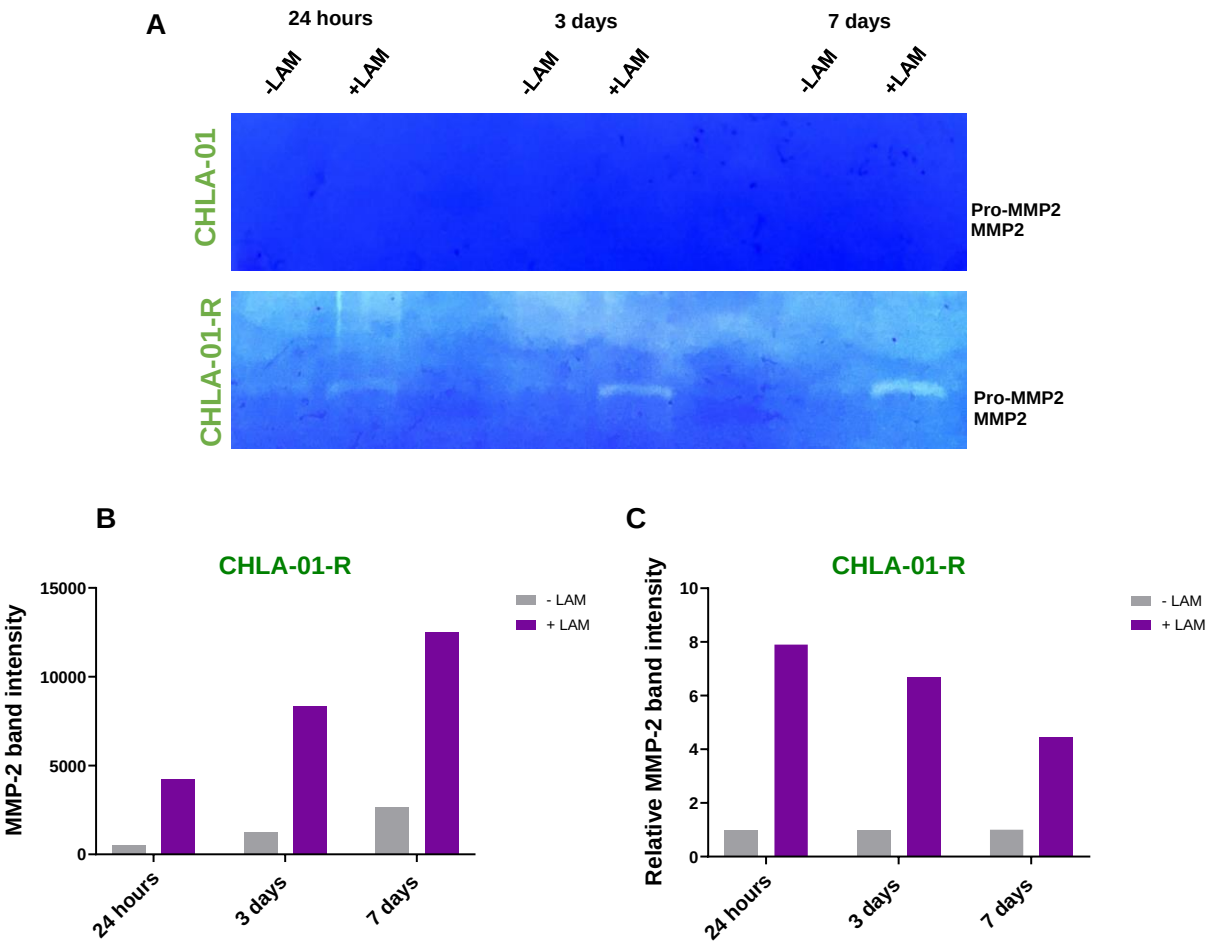
Appendix

9.1 Appendix Figure 1



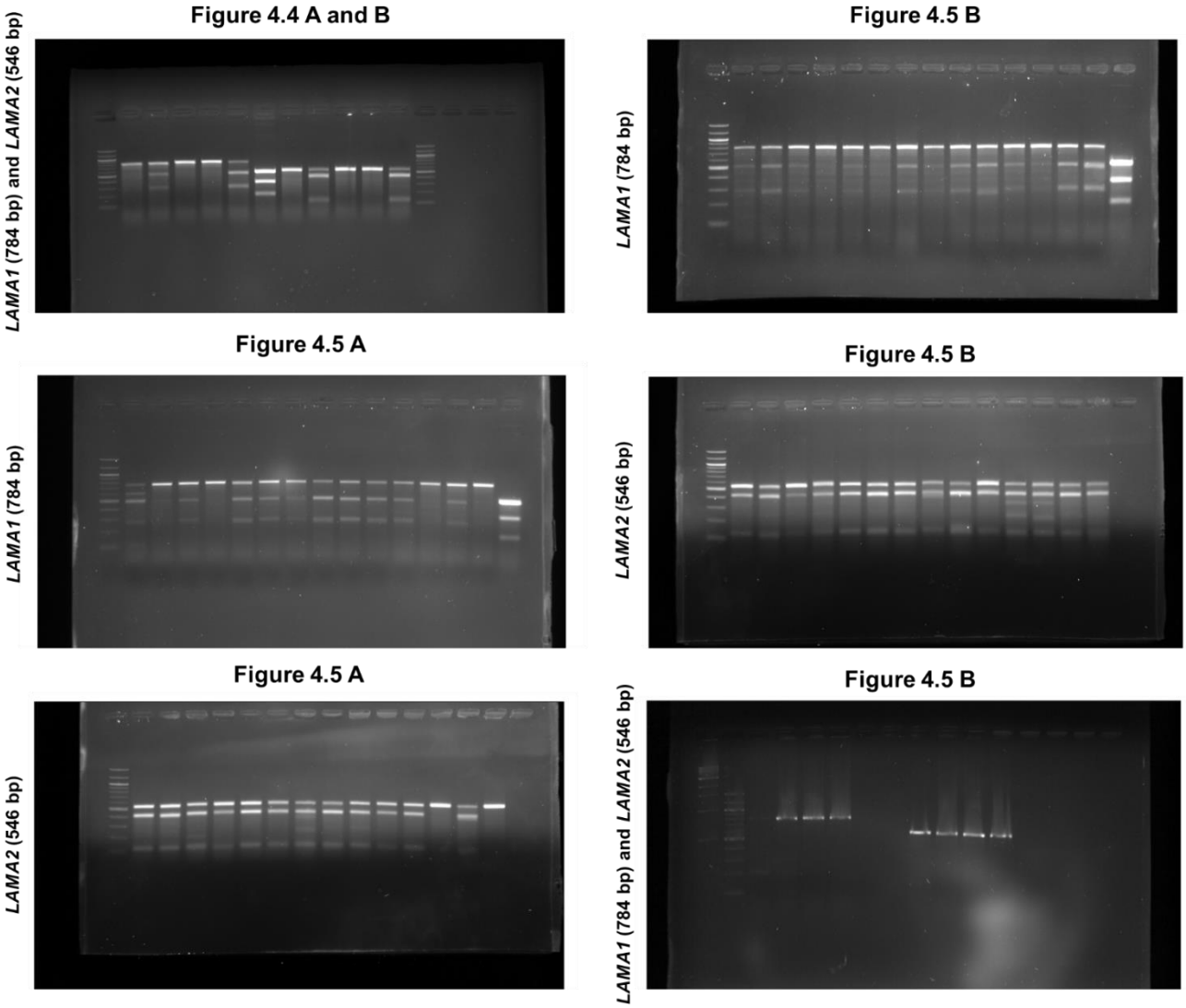
Appendix Figure 9.1. Full length exemplar immunoblots of the antibodies used in this study. Fluorescent molecular weight ladder is shown in red next to each blot.

9.2 Appendix Figure 2



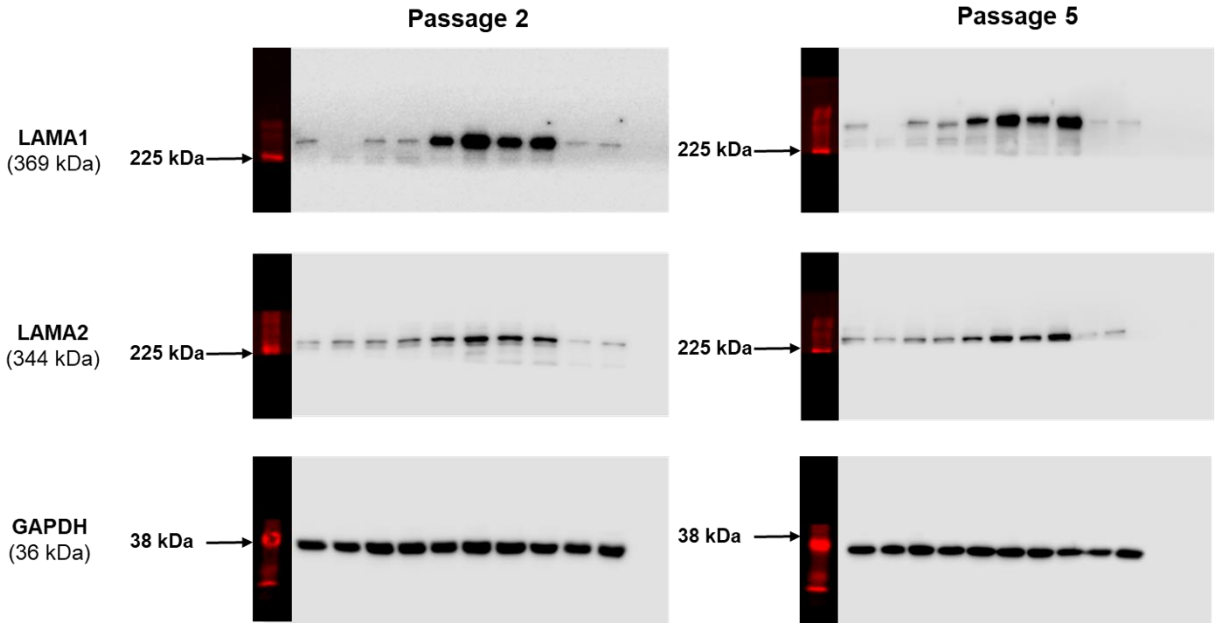
Appendix Figure 2. Laminin-111 increases MMP-2 secretion in the CHLA-01-R Group 4 medulloblastoma cell line in a 3D cell culture assay. Gelatin zymography was used to detect MMP-2 in the supernatant of Group 4 medulloblastoma cell lines (CHLA-01 and CHLA-01-R) that had been grown in a 3D cell culture assay, whereby cells were seeded into hyaluronan hydrogels with and without laminin-111 and grown for 7 days (**A**). Supernatants from the time points 24 hours, 3 days and 7 days were analysed in the zymograms. MMP-2 mediated proteolysis of the zymogram was detected as a white band, which was then analysed by densitometry analysis in order to determine the quantity of MMP-2 secretion the CHLA-01-R cell line, since this was the only cell line in which MMP-2 was detected. The results of this analysis are displayed as raw values (**B**) as well values that have been normalised to the no-laminin-111 condition (**C**). Zymography and analysis are representative of a single replicate.

9.3 Appendix Figure 3



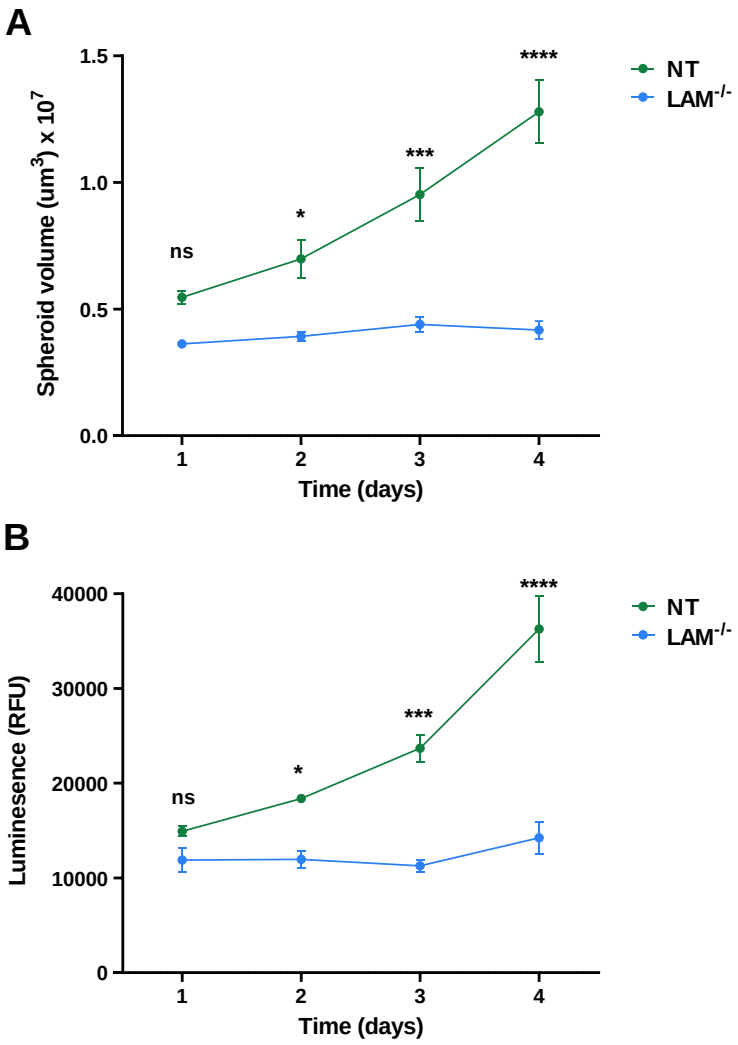
Appendix Figure 3. Uncropped agarose gel images of DNA mismatch detection assays shown in this study. Images are labelled with the figure number within the current thesis which the images are used in, as well as which PCR product is present on the gel (Laminin Subunit α1 [*LAMA1*], Laminin Subunit α2 [*LAMA2*] or both).

9.4 Appendix Figure 4



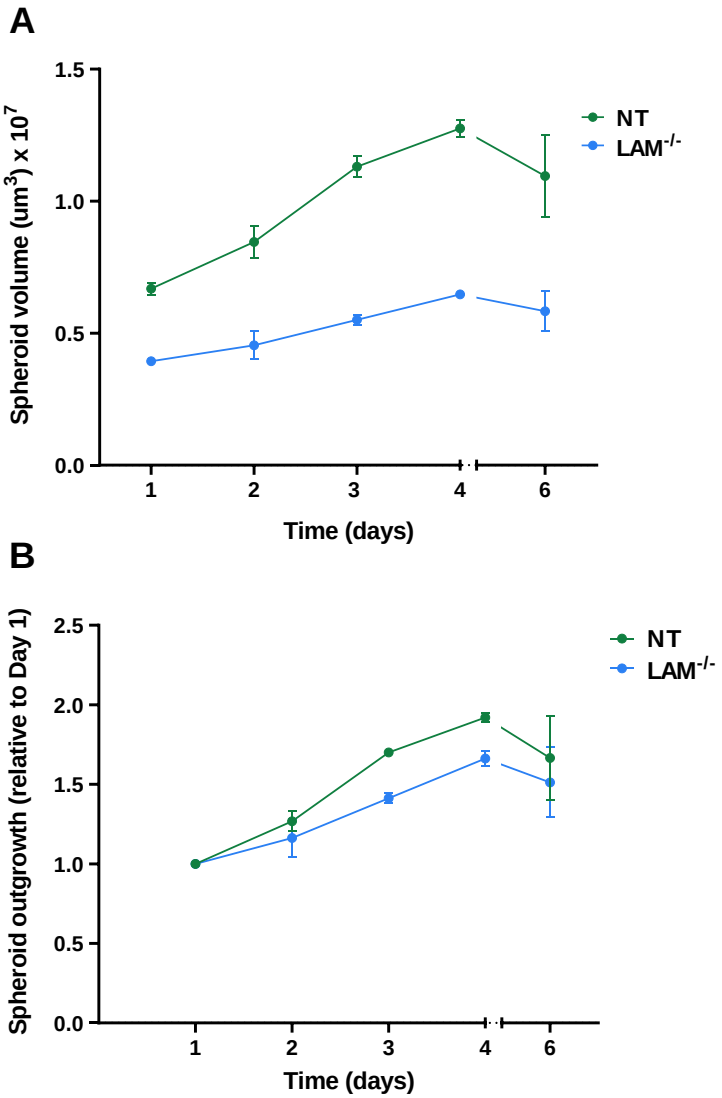
Appendix Figure 4. Full length western blots of Laminin Subunit α1 (LAMA1), Laminin Subunit α2 (LAMA2) and GAPDH in the chosen DAOY KO and ONS-76 KO cell lines after 2 and 5 passages (used in Figure 4.9). The molecular weight of the protein ladder on each blot is labelled.

9.5 Appendix Figure 5



Appendix Figure 5. The volume (A) and viability (B) of DAOY NT spheroids are significantly greater than DAOY LAM$^{-/-}$ spheroids after 2, 3 and 4 days in culture Error bars represent the mean ± SEM; n=3 with at least 3 internal replicates. Significance was calculated using Two-Way ANOVA analyses with Sidak's multiple comparisons post-hoc test (*p<0.05, **p≤0.01, ***p≤0.001, ****p≤0.0001).

9.6 Appendix Figure 6



Appendix Figure 5. The volume (A) and outgrowth (B) of DAOY NT and DAOY LAM$^{-/-}$ spheroids decrease after 6 days in a spheroid-hydrogel model. Error bars represent the mean ± SEM; n=1 independent experiments with 4 internal replicates.

9.7 Appendix Figure 7

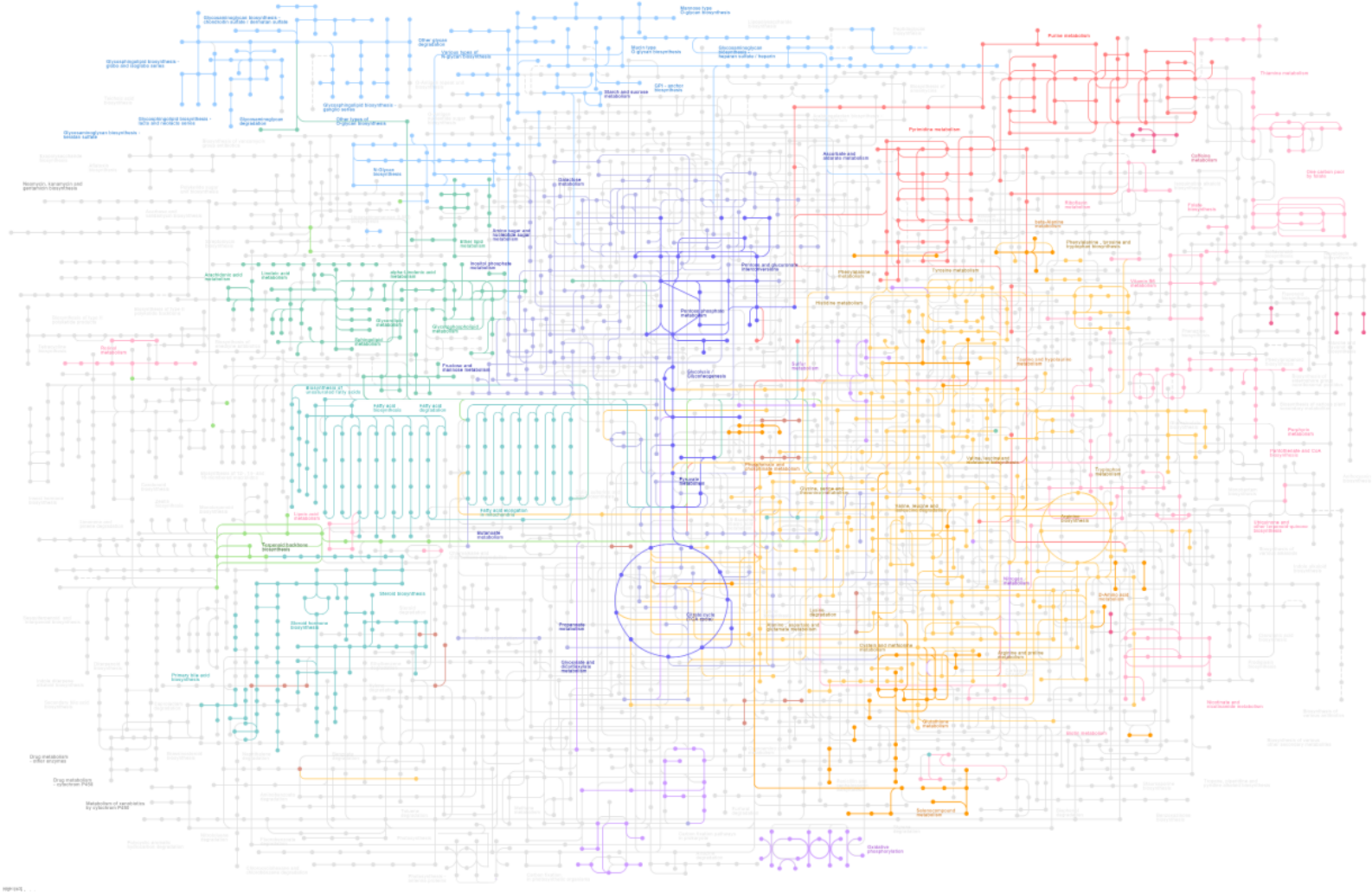


Figure 9.2 Kyoto Encyclopaedia of Genes and Genomes (KEGG) pathway mapping analysis of proteins upregulated by Laminin Subunit α1 (LAMA1) in 2D culture identifies metabolic pathways as an associated pathway. Metabolic pathways components PYGB, AK2, ENO1, NUDT5, ENO2, HSD17B10, SRM, CNDP2, HK1, GANAB, ATP6V1H, CKB, PGLS, LTA4H, PGM1, GSTM3, ADSL, RRM1, GOT2, CTPS1, PAICS, NME1, GLUD1, GNPDA1, MTHFD1, ATP6V1B2, CMPK1, ACO2, TKT, were all identified to be upregulated by LAMA1 in SHH medulloblastoma in 2D culture. Coloured parts of the diagram illustrate the metabolic pathways that were associated with the input proteins. The KEGG pathway diagram was generated as part of the KEGG pathway mapping analysis using the online bioinformatics tool DAVID.

PhD project outputs

This PhD project was funded by the Biotechnology and Biological Sciences Research Council (BBSRC) Doctoral Training Partnership (DTP). It was a 4 year programme, beginning with 3, 7-week research laboratory rotation projects. Between the second and third years, a 3-month professional internship is also undertaken.

Laboratory Rotations

October-November 2018: 'Communication via extracellular vesicles and their microRNA cargo –does the extracellular matrix play a role?' – supervised by Dr Anna Piccinini

November 2018-January 2019: 'Assessing the efficiency of the plasmids pGlux, pGM206 and pGM206 SMAR in transfecting murine precision cut lung slices (PCLS)' – supervised by Dr James Dixon

January-March 2019: 'Investigating Aurora-A kinase activation in medulloblastoma' – supervised by Dr Beth Coyle and Dr Franziska Linke

Publications

Franziska Linke, James E. C. Johnson, Stefanie Kern, Christopher D. Bennett, Anbarasu Lourdusamy, Daniel Lea, Steven C. Clifford, Cathy L. R. Merry, Snow Stolnik, Morgan R. Alexander, Andrew C. Peet, David J. Scurr, Rian L. Griffiths, Anna M. Grabowska, Ian D. Kerr, Beth Coyle, Identifying new biomarkers of aggressive Group 3 and SHH medulloblastoma using 3D hydrogel models, single cell RNA sequencing and 3D OrbiSIMS mass spectrometry imaging, *Acta Neuropathologica Communications*, 11, 6 (2023), https://doi.org/10.1186/s40478-022-01496-4

Louisa Taylor, Philippa Wade, James E. C. Johnson, Macha Aldighieri, Gianpiero di Leva, Ian D Kerr, and Beth Coyle, Drug resistance in medulloblastoma is driven by YB-1, ABCB1 and a seven-gene drug signature, *Cancers,* 15, 4 (2023), doi: https://doi.org/10.3390/cancers15041086

Conference Papers

James E. C. Johnson, Franziska Linke, Catherine L R Merry, Beth Coyle, MBRS-43. ELUCIDATING HOW NOVEL EXTRACELLULAR MATRIX SUBTYPES DIFFERENTIALLY IMPACT THE SURVIVAL OF MEDULLOBLASTOMA SUBGROUPS, *Neuro-Oncology*, Volume 22, Issue Supplement_3, December 2020, Page iii405, https://doi.org/10.1093/neuonc/noaa222.552

James E. C. Johnson, Franziska Linke, Cathy Merry, Beth Coyle, MEDB-24. Tumour secreted extracellular matrix predicts survival and influences migration and cell death in SHH medulloblastoma 3D models, *Neuro-Oncology*, Volume 24, Issue Supplement_1, June 2022, Page i110, https://doi.org/10.1093/neuonc/noac079.398

Poster Presentations

June 2022: International Symposium on Paediatric Neuro-Oncology (Hamburg, Germany)

October 2021: Goodbye Flat Biology (Virtual)

November 2019: Goodbye Flat Biology (Berlin, Germany)

Oral Presentations

November 2022 - Children's Brain Tumour Research Centre Spring Research Seminar Series (30 min)

December 2021 - International Symposium on Paediatric Neuro-Oncology (5 mins)

June 2021 - School of Medicine Postgraduate Research Forum (5 mins)

May 2021 - Children's Brain Tumour Research Centre Spring Research Day (15 mins)

April 2021 - BBSRC DTP Spring School Project Presentations (5 mins)

April 2019 - Children's Brain Tumour Research Centre Spring Research Day (5 mins)

Grant Awards

June 2022: Received the University of Nottingham Graduate School Travel Prize (£600 to attend the International Symposium on Paediatric Neuro-Oncology conference in Hamburg, Germany)

Awards

November 2019 – BBSRC DTP World Crisis Solution Challenge Winner

May 2021 – Third Year Presentation Prize at BBSRC DTP Spring School conference